Simulation of transient states in large hydrodynamic thrust bearings

Piotr Pajączkowski

The work was supervised by professor Michał Wasilczuk from Gdańsk University of Technology. Author is grateful to his contribution into this work. His guidelines, remarks and long discussions helped to make this work better.

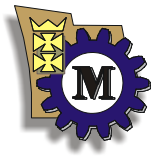

This work was financially and essentially supported by ALSTOM Hydro (Switzerland) Ltd company. Author would like to thank Mr. Andreas Schubert from this company for his time, experience and data that allowed to validate the developed model.

ALSTOM

This research work was supported by the European Union in the framework of the European Social Fund. The system project of the Pomorskie Voivodeship "InnoDoktorant – Scholarships for PhD students, 2nd edition".

HUMAN CAPITAL
NATIONAL COHESION STRATEGY

POMORSKIE
VOIVODESHIP

EUROPEAN
SOCIAL FUND

Special thanks deserves my father. I am grateful for his patience and support that he gave me during my whole life.

Piotr Pajączkowski

Table of contents

Nomenclature **7**

1 Introduction and motivation **9**

2 Current state of knowledge, literature research **11**

2.1 Introduction 11

2.2 Large thrust bearing design 18

2.2.1 Bearing housing arrangement 19

2.2.2 Support systems 20

2.2.3 Auxiliaries 26

2.2.4 Hydrodynamic bearings with polymer coatings 32

2.3 Thrust bearing calculations 35

2.3.1 Hydrodynamic lubrication 35

2.3.2 Generalized Reynolds equation 37

2.3.3 Currently modeled effects 38

2.3.4 Treatment of the thermal effects in the oil film 49

2.3.5 Transient effects on hydrodynamic thrust bearings 52

2.4 Summary 60

3 Goal of the research **63**

4 Calculation model **65**

4.1 Introduction 65

4.2 Fluid Structure Interaction 68

4.3 Structure model 71

4.4 Fluid model 80

4.5 Identification of errors 92

4.6 Model conclusions 94

5 Results of the calculations **95**

5.1 Introduction 95

5.2 Startup simulation of the Kopswerk II thrust bearing 96

5.2.1 Input parameters 96

5.2.2 Comparison with measurements 97

5.2.3 Transient results of the simulation 100

5.2.4 Temperature and velocity distributions on the oil film cross sections 105

5.2.5 Oil film thickness analysis 107

5.2.6 Resulting warm oil mixing coefficient 110

5.2.7 Heat flow through the sliding surfaces and the heat balance 116

5.2.8 Calculated convection coefficients of the pad walls 118

5.2.9 Calculated pressure distributions 119
5.2.10 Conclusions 119
5.3 Influence of chosen parameters on the results of simulation 120
5.3.1 Model validation with DIN bearing calculation guidelines 120
5.3.2 Influence of the boundary condition on the runner 122
5.3.3 Influence of damping coefficients 123
5.3.4 Transient vs. steady state simulation 126
5.3.5 Higher load case 2.43 MPa 129
5.3.6 Influence of the startup time on the bearing deformations 132
5.4 Comparison of the cold and warm startup simulations 136
5.4.1 Input parameters 136
5.4.2 Comparison of the results 137
5.4.3 Conclusions 141
5.5 Comparison of three different support systems 141
5.5.1 Analyzed supporting systems 141
5.5.2 Comparison of the results 144
5.6 Discussion of the results 148
6 Summary and final conclusions 151
6.1 Main conclusions 151
6.2 Further research 152
7 Appendix 155
Bibliography 157

Nomenclature

Latin symbols

a	thermal diffusivity [m^2/s]
a_x, a_y, a_z	secant coefficient of thermal expansion [1/K]
A	area of the sliding surface [m^2]
B	pad radial width [m]
c	specific heat [J/kg K]
$[C]$	structural damping matrix, damping matrix
$d, d_{xx}, d_{yy}, d_{zz}$	damping in specified direction [MN/m/s]
D_{in}	Bearing inner diameter [m]
D_{out}	Bearing outer diameter [m]
E_x, E_y, E_z	Young module [Pa]
F_x, F_y, F_z	structural forces in three spatial directions [N]
$\vec{F}$	applied load vector
G_{xy}, G_{yz}, G_{xz}	Kirchhoff module [Pa]
h_{min}, h_0	minimum oil film thickness [µm]
h_1	maximum oil film thickness [µm]
$h_p,$	pad thickness [m]
$k, k_{xx}, k_{yy}, k_{zz}$	stiffness in specified direction [MN/mm]
$[K]$	structural stiffness matrix, coefficient matrix
L	pad tangential length [m]
$[M]$	structural mass matrix
n	rotational speed [rpm]
n_p, Z	number of bearing pads [-]
$\vec{n}$	normal vector
p	pressure [Pa]
$\bar{p}$	specific pressure [Pa]
P_{loss}	power loss [kW]
$pivot_{rad}$	radial pivot point coordinate factor [-]
$pivot_{tan}, a\_F^*$	tangential pivot point coordinate factor [-]
q, q_{pad}, q_{runner}	heat transfer [W]
$\dot{q}$	heat flux density [W/m^2]
Q_{HS}	hydrostatic system flow [l/min]
r	radius [m]
t	time [s]
t_{step}	time step length [s]
t_{total}	total length of simulation [s]
T	temperature [K]
T_b	bulk temperature of oil [K]
T_{bath}	oil bath temperature [K], cooler inlet temperature
T_{cold}	cold oil temperature [K], cooler outlet temperature
T_w	wall temperature [K]
u, v, w	velocity components in x, y, z spatial directions [m/s]
$\dot{u}, \dot{v}, \dot{w}$	acceleration components in x, y, z spatial directions [m/s^2]

$\vec{u}$	nodal displacement vector, vector of DOF values
$\dot{\vec{u}}$	nodal velocity vector, time rate of DOF values
$\ddot{\vec{u}}$	nodal acceleration vector
U	sliding speed [m/s]
U_x, U_y, U_z	structural degrees of freedom (DOFs) in three spatial directions [m]
x, y, z	spatial directions [m]

Greek symbols

α	convection coefficient [W/m^{2}K]
α_p	bearing pad angle [deg]
$\delta_{pad\ rad}, \delta_{pad\ tan}$	radial and tangential pad deformation [µm]
$\delta_{run\ rad}$	radial runner deformation [µm]
δ_T	thermal deformation [µm]
ΔT	temperature increase [K]
Φ	function of dissipation
$\lambda, \lambda_{xx}, \lambda_{yy}, \lambda_{zz}$	heat conductivities [W/m K]
η, μ	dynamic viscosity of oil [Pa s]
η_{eff}	effective dynamic viscosity of oil [Pa s]
ρ	density [kg/m^3]
$\boldsymbol{\tau}, \bar{F}$	friction torque [Nm]
ν	kinematic viscosity of oil [m^2/s]
$\boldsymbol{v} = u\,\boldsymbol{i} + v\,\boldsymbol{j} + w\,\boldsymbol{k}$	velocity vector ($\boldsymbol{i}, \boldsymbol{j}, \boldsymbol{k}$ are unit vectors) [m/s]
$\nu_{xy}, \nu_{yz}, \nu_{xz}$	Poisson's ratios [-]
ω	rotational speed [rad/s]

Dimensionless quantities

F	Fourier number
$F^*, \bar{W}$	Sommerfeld number, load carrying capacity of the oil film
Nu	Nusselt number
Pr	Prandtl number
Re	Reynolds number
St	Stribeck number

1 Introduction and motivation

Motivation to this work was previous intensive investigation at Design of Machine Elements Department of Mechanical Faculty at Gdansk University of Technology. Development of the design and simulation methods of the large hydrodynamic thrust bearings, especially for large vertical hydro generators, was continuously undertaken for several years. This thesis is a part of further development in this area of research. Transient states are already recognized in the literature as the potential cause of the bearing failures but on the other hand there is lack of the calculation tools that could be used to analyze such problems.

This work was performed with continuous cooperation with ALSTOM Hydro (Switzerland) Ltd company which is a world leader in the area of the design and manufacturing of the hydro generators. Thrust bearings designed and delivered by the company belong to the largest ones in the world. Continuous development, forced by strong competition in the hydro power generation industry, leads to arising difficulties with many key components of the hydro generators. One of them is a thrust bearing that supports the axial component of the load. In case of the vertical machine this load is a sum of the weight of the rotating parts and magnetic and hydraulic thrusts generated by the generator and the turbine and can reach up to 6000 t in the largest machines. The aims of the development are mainly decrease of generated power losses and increase of reliability of the bearing.

The main purpose of this work is development of a simulation model of the thrust bearing that takes into account most of already identified different physical effects that take place during hydrodynamic lubrication and additionally will allow to perform transient analysis of the thrust bearing. The calculation model should be flexible in order to cover many different designs of the thrust bearings that appear in the real machines. This aspect of modeling is especially important in case of hydro generator industry where many different and not standardized bearing designs are present. Flexibility of the developed tool will allow to analyze existing bearings as well as those currently being developed.

Second stage is the validation of the obtained results with the use of measurement data obtained from the large thrust bearing installed on the hydro power plant. Comparison of the measurement data with the obtained results should help to validate developed simulation model. After validation the influence of different parameters is investigated in order to show the advantages of the model and to check its properties.

2 Current state of knowledge, literature research

2.1 Introduction

Thrust bearing is a key component of every large hydro generator and can also be found in many other rotational machineries like pumps, compressors, engines, marine propulsion systems etc. Actually this machine element is present in every rotational device but its particular design can have many different forms. In this chapter a summary of the current knowledge is presented considering hydrodynamic thrust bearings with tilting pads design and calculation tools of the operational parameters. In this work large design and simulations of the thrust bearings for the reversible hydro generator/motor have been taken under investigation. In Figure 2.1 [**1**] the development of hydro projects in the recent years is presented. Sizes of the units and output powers are increasing as well as the supporting bearings themselves.

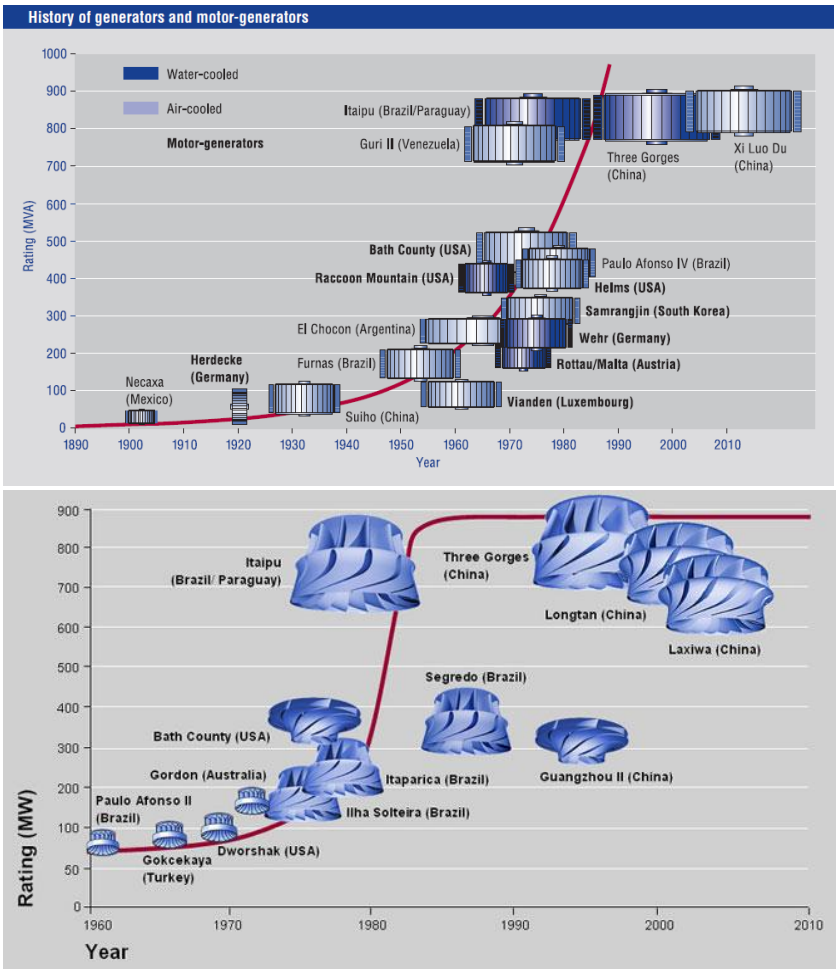

Figure 2.1. Development of the hydro generators in the recent century [1]

In Figure 2.1 one can observe continuous trend of growing sizes of the hydro generators. This trend will be probably followed also in the future since such hydro markets like China, which is already the largest hydro power producer in the world, or Africa are in the growth phase. It allows to believe that in the future challenges for thrust bearings will also increase. Requirements will increase in case of efficiency and reliability at the same time especially. These are conditions that are opposing each other. The balance between them has to be found in order to ensure efficient and safe solution.

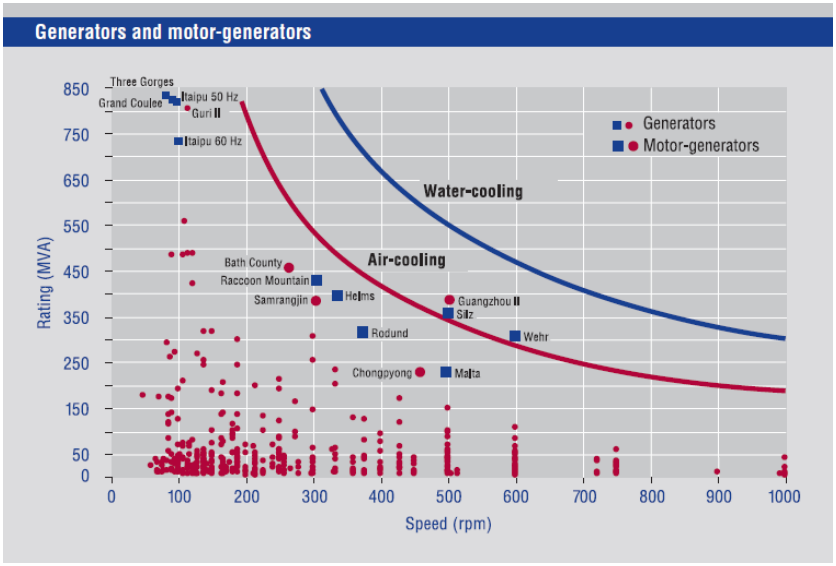

Figure 2.2. Range of the operating parameters of the hydro generators [2]

Parallel to this substantial growth one can notice that there are more and more pump storage power plants built (PSP). These plants are continuously becoming the very important part of the hydro power plants market. Especially in Europe and United States where the demand on the network balancing is getting more important. Mainly due to wind and other modern (unconventional) technologies (solar, biomass, tidal and wave, etc.) power generation. These sources are unpredictable due to their nature and the PSP is easiest and the most efficient way to control the power generation in the network.

Large hydro generators have usually vertical axes of rotation in order to minimize deflections due to the weight, assembly inaccuracies and vibrations. Thus the main load is carried by the hydrodynamic thrust bearing. It is arranged in form of several tilting pads around the shaft. The load is carried from the shaft by the means of the thrust collar and runner. And then through the oil film to the bearing pads and further through the supporting system to the foundation.

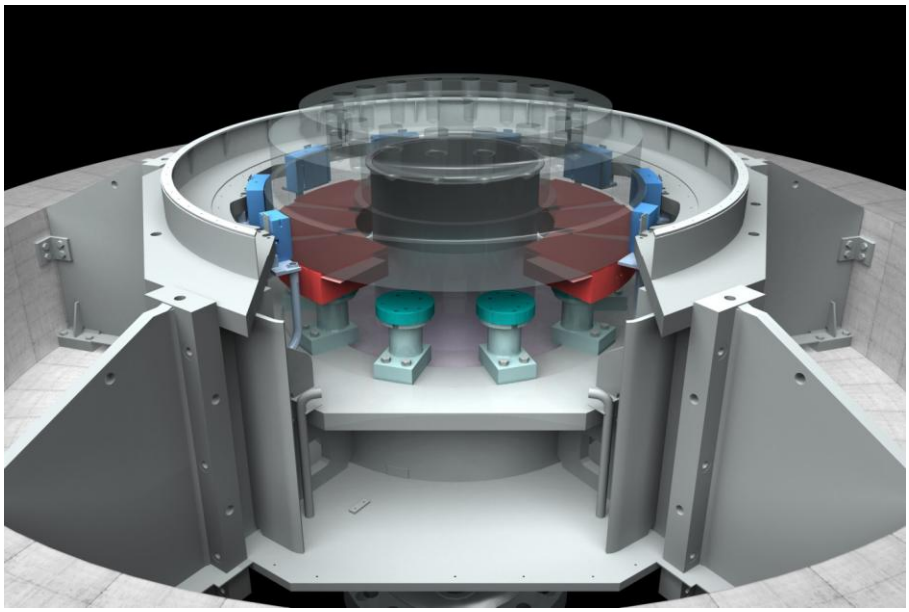

Figure 2.3. Thrust bearing of a large hydro generator unit (ALSTOM Hydro)

A large hydrodynamic thrust bearing of a vertical hydro generator is presented in Figure 2.3. In the figure one can distinguish following components: thrust and guide bearing pads and thrust collar (transparent) attached to the shaft (not visible), bearing support system (supporting disc and spindle support – described further in this chapter) and the housing that transfers the load to the ground and at the same time has the function of the oil tank. In the presented case the thrust bearing is combined with the guide one in order to use the same lubrication/cooling system and other devices. The bearing housing ensures that both loads (axial and radial) are transferred to the supporting foundation. It also has to ensure that the load is carried independently of the thermal state of the system.

The thrust bearing operates close to its operational limits in order to make its design on one hand side efficient and on the other very reliable. Too conservative bearing design leads to unnecessary high bearing power losses which causes further over dimensioning of other elements of the lubrication system (cooling system, oil tank, etc.). For several years the nominal rotational speed of the hydro generators has been increasing so the power losses are getting more important. Units with a rotational speed of 500 or $1000\,rpm$ are not rare. The sliding speed exceeds in these cases $60\,m/s$. The friction losses increase as a function of the rotational speed according to the diagram in Figure 2.4 [**3**]. They can be divided into two main groups. First of them is viscous shear in the oil film (H1 and H2) and the second one is oil mixing and turbulences in the oil volume (H3, H4, H5 and H6).

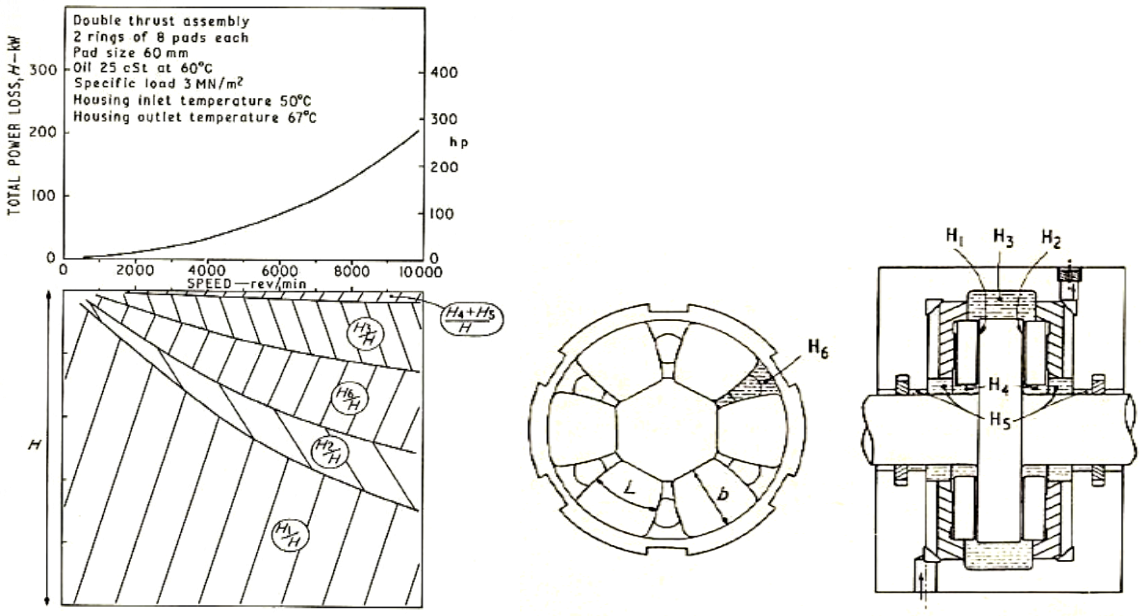

Figure 2.4. Power losses in the double tilting pad thrust bearing [3]

From Figure 2.4 one can see that in case of the low speed bearings the power losses are mainly generated in the oil film. For higher speeds oil mixing losses can reach up to $50\,\%$ of the total. From this diagram one can notice that power losses increase as a function of rotational speed according to the formula (2.1).

$$P_{loss} \sim n^{1.6} \tag{2.1}$$

High power losses lead to higher bearing temperatures and enforce over-dimensioning of the oil cooling system. The volume of the bearing housing (oil tank) also has to be increased due to higher

power losses. Lifetime of the hydro generators is usually predicted to be 50 or more years so even small unnecessary power loss generated in the bearing can cause significant economical waste.

On the other hand too optimistic bearing design (high specific pressure and temperatures) results in low safety margin (oil film thickness). Moreover the bearing has to carry not only the design load but many different situations may occur when the operating conditions are more severe. Thrust load may increase during transient states of operation or due to failure of a certain component of the system either on turbine or generator side. According to the experience of the ALSTOM Hydro company the contractual conditions are formulated in such way that the bearing has to be able to stop the unit safely, without hydrostatic jacking what may occur in case of lack of the power supply from the network. Load rejection during pumping mode means for the bearing even more severe operating conditions. The unit is, in such situation, first stopped within a very short time by the water flow and then accelerated in the opposite direction (turbine mode). Then it is possible to stop the unit mechanically. This emergency situation can take place also without working hydrostatic jacking system what means that there is neither hydrodynamic (at zero speed) nor hydrostatic lubrication. The thermal deformation of the bearing pad and runner, due to their thermal inertia, cannot adapt as quick and thus the oil film gap may have disadvantageous shape. These examples show clearly that during lifetime the bearing may operate under much more severe conditions than the nominal ones.

Therefore both: all possible operating conditions and the limits of hydrodynamic lubrication have to be precisely defined. Beyond them the bearing failure occurs rapidly when the situation becomes unstable [**4**]. In the Figure 2.5 [**5**] the typical envelope of the bearing operating limits is presented.

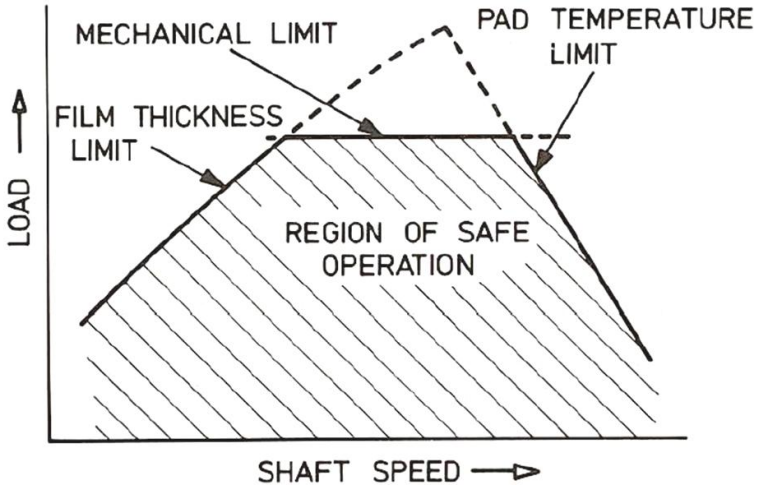

Figure 2.5. Limits of safe operation for tilting pad bearing [5]

The operation field (speed – load) of the hydrodynamic tilting pad bearing is limited in low speed range by the minimum oil film thickness condition. Low speed hydro generators ($10\ m/s$) may have sometimes very large dimensions and weight. In such case high load and low load carrying capacity cause problems with the minimum oil film thickness [**6**].

The load is limited in order to ensure that the fully developed fluid lubrication occurs. The mixed lubrication leads to an increased friction coefficient (power losses) and wear of the bearing sliding surface. Friction coefficient (losses) were investigated by Stribeck [**7**]. From this curve one can notice

that the friction coefficient has its minimum value for a certain Stribeck number. It is a dimensionless parameter and for thrust bearings it is defined in the following way:

$$St = \frac{\mu \cdot \omega}{\bar{p}} \tag{2.2}$$

From the efficiency of operation point of view the bearing should operate exactly in this point of minimum value of friction factor (marked by A on the diagram). In such case the power losses are also minimal since they depend directly on the friction coefficient. In order to ensure safe operation of the bearing it is necessary to define the point of operation at higher value of Stribeck number (marked by B on the diagram). In this way also during emergency situations or transient operation conditions the bearing can also operate safely.

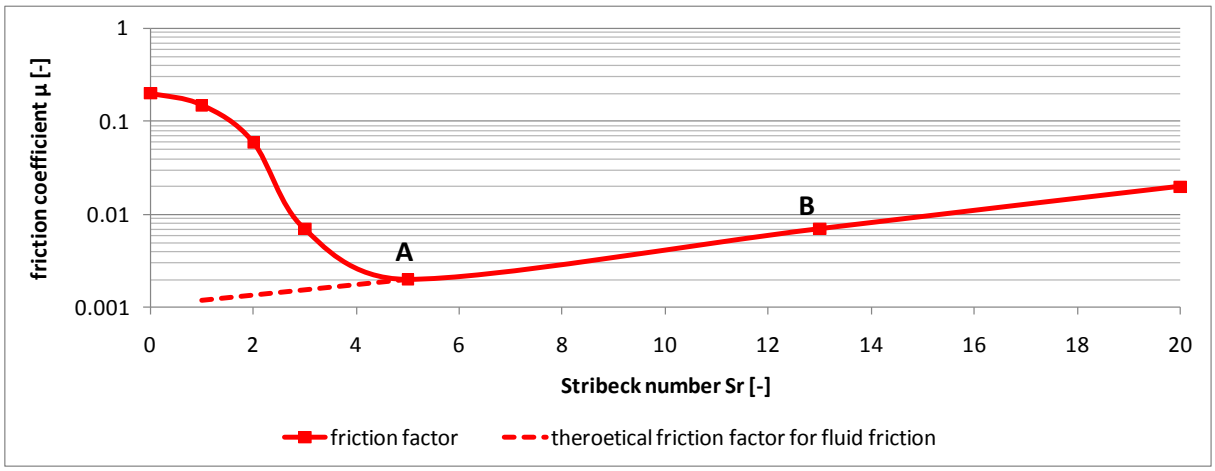

Figure 2.6. Stribeck curve

For the sliding speed equal to zero the friction coefficient μ_f has the highest value. It is the so called static friction coefficient. The dashed line shows the theoretical profile for the fully fluid lubrication under an assumption as if there was no surface roughness on both sliding surfaces of the bearing. Additionally it can also illustrate coefficient of friction in case of hydrostatic lubrication when the sliding speed is very low (or equal to zero) and the parts are still separated by a thick layer of the oil. In case of hydrodynamic lubrication when the oil film thickness is lower than the doubled height of roughness profile of contacting surfaces the boundary or mixed lubrication occurs [**7**,**8**]. For this reason at low speeds the load is the limiting parameter. Higher loads lead to low oil film thickness and thus the friction coefficient and power losses rapidly increase. In this range also excessive wear or seizure may occur.

The hydrodynamic lubrication analyzed in this elaboration takes into account only the fully developed fluid lubrication regime. The parts are treated as completely flat (in standstill) and without any surface roughness profile and/or manufacturing inaccuracies. Usually in case of large babbitted tilting pad thrust bearings it is not allowed to operate in the region of mixed lubrication. The tin based materials are not reliable under such conditions and the situation can become unstable very quickly. Due to much higher heat generation the temperature rises and the strength of material decreases. It is said that the babbitt properties can save the bearing from damage of the runner surface due to its self-lubricating properties in case of lack of oil in the bearing. This attribute of lining material gives a chance to shut down the unit safely and without severe damage of other

components. Nevertheless this is a serious bearing failure and in such case the lining of the pads has to be replaced.

In case of the high speed range the limiting parameter is the temperature of the bearing. In case of laminar flow of the Newtonian fluid viscous heat generation is caused by high velocity gradients and results in high temperatures in the bearing elements, according to the formula (2.3). The strength of lining material is one of the limiters for further increase of the speed and/or load.

$$\tau = \mu \frac{du}{dy} \tag{2.3}$$

If the operational point of the continuous operation is close to one of these limitations it is necessary to assure that none of them is exceeded under any possible operating condition. Therefore it is necessary to predict the operating parameters of the hydrodynamic bearing in a precise way. The tin based sliding materials (e.g. babbitt) have superior sliding properties and low coefficients of friction but are unfortunately subjected to rapid failure, seizure of the bearing even if the limits are only slightly exceeded. Then the material begins to melt without any warning [**9**]. There is no warning because of the character of the lining material but the reason is also a monitoring system. Usually the temperature is measured by the sensor located several tens of millimeters below the sliding surface, so the diagnostic signal is delayed in reference to the actual state [**10**]. Delay of diagnostic is explained in Figure 2.7. When the information (increased temperature) reaches the measuring device it is already too late for any reaction – the failure has already occurred.

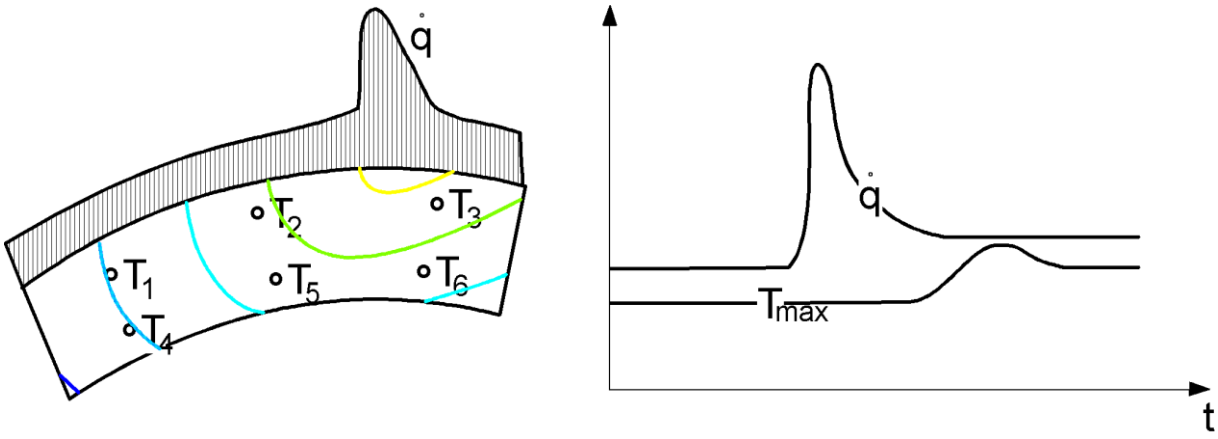

Figure 2.7. Delay of diagnostic information [10]

In the literature [**11**] and manufactures' catalogues [**12**] one can find curves of the yield limit as a function of the temperature for the Babbitt which is the most common lining material used for the large hydrodynamic bearings of hydro generators. At a certain temperature level yield limit is very close to the hydrodynamic pressure in the oil film. In such case plastic deformation of the lining material may occur. According to the manufacturer [**12**] the recent progress in material science and technology caused that the pad lining is not anymore the limiting component of the bearing. It is the lubricant now. High temperatures, over $130\ °C$, accelerate ageing. According to the catalogue values the modern Babbitt has a significantly higher $(30 - 50\%)$ yield limit in comparison to the formerly used tin based materials.

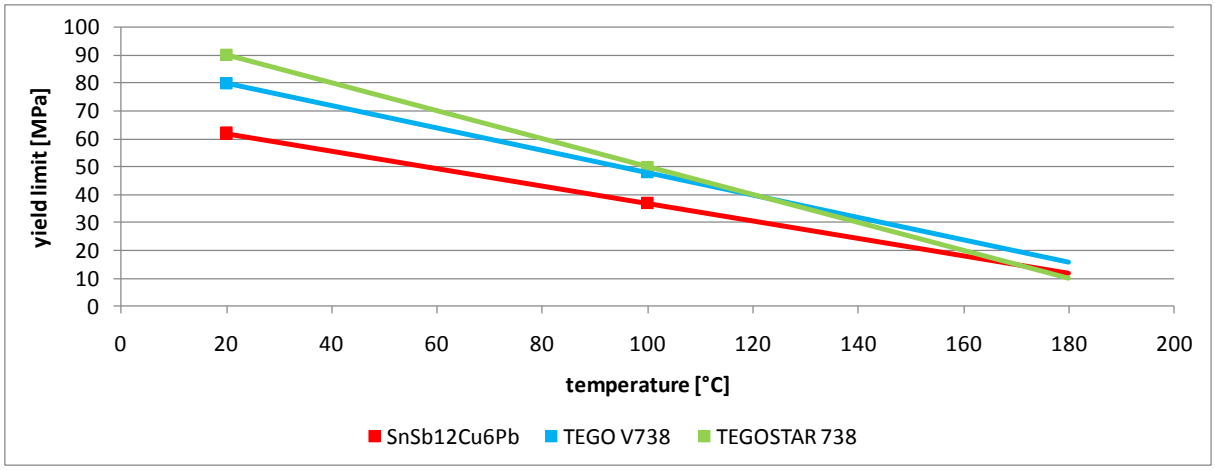

Figure 2.8. Yield limit of the common bearing lining material (Babbitt) and modern material TEGO V738 and TEGOSTAR as a function of the temperature [12]

At this point it is also worth to mention that the melting point for standard whitemetal (SnSb12Cu6Pb) is $183\ °C$ and for modern ones (TEGO V738 and TEGOSTAR) is $235\ °C$. This difference can save the bearing from the seizure in case of critical situations since the catastrophic failure occurs when the pad lining starts to melt. Moreover the higher yield limit increases durability of the lining (continuous operation at the load levels close to the yield limit cause fatigue wear of the material). The hot spot temperature of the sliding surface is often higher than $120\ °C$ while the hydrodynamic pressure obtains values quite close $(10 - 15\ MPa)$ to the yield limit for the conventional lining material $(20 - 30\ MPa)$. This may not lead to babbitt melting and seizure of the bearing but the fatigue strength of the pad lining surface might be decreased. Plastic deformations of the babbitt can also cause disadvantageous profile of the oil film gap. Fatigue cracks may occur. Therefore it is very important to accurately predict the operational parameters of the bearing in a design phase. The thermal peaking during startup or shut down without hydrostatic jacking support (or any other situation where limited load carrying capacity occurs) may lead to bearing seizure. In [**5**] one can also find the information that the maximum allowable operating temperature for babbitted bearing is $130\ °C$ but the failure can occur approximately $30\ °C$ higher due to material limitations. Other materials like copper or polymers (PTFE, PEEK) have their limits much higher and can operate up to 170 or even $200\ °C$. These information confirms the data presented previously.

Improvements in manufacturing technology improved also the strength of the babbitted pads and their resistance to the temperature. The diagram in the Figure 2.9 describes the relationship between the yield limit of the babbitt layer and its thickness. The strength is doubled for the layer thickness $1.5\ mm$ in comparison with $5\ mm$. Fatigue strength decreases for babbitt layers higher than $0.25\ mm$ [**13**]. Therefore it is clear that for modern highly loaded bearings it is necessary to manufacture the pad lining with relatively small thickness. Values between 1 and $2\ mm$ seem reasonable. Smaller thickness does not leave safety margin in case of bearing seizure. In such situation melting Babbitt “plays a role” of a lubricant and allows for a safe shut down without damage of the sliding surface of the runner.

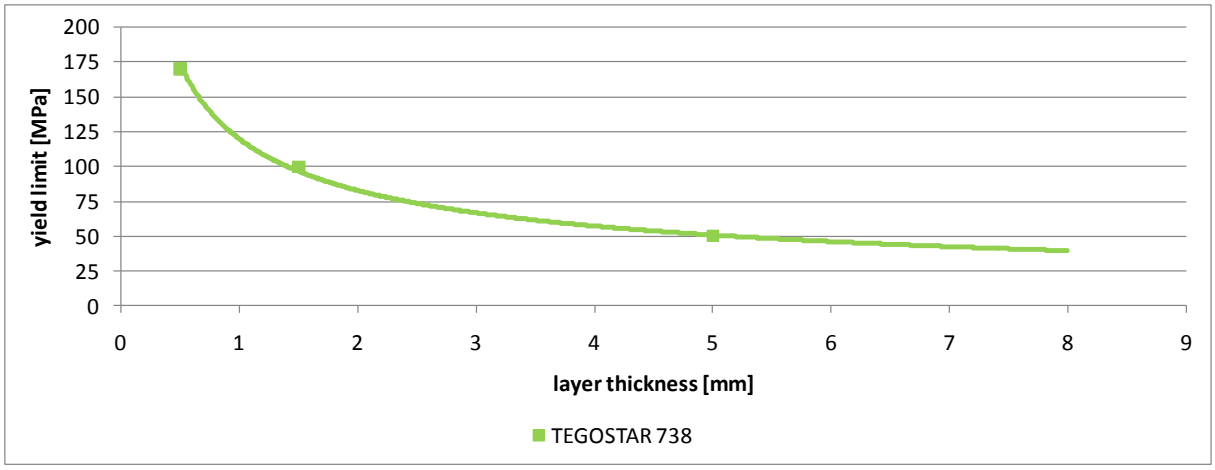

Figure 2.9. Yield limit of the TEGOSTAR 738 lining material at 100°C as a function of the layer thickness [12], marked measurement values

On one hand it is very important to define the limits of operation but on the other during bearing design one has to know the exact values of the operating parameters. Only if these two conditions are fulfilled a balance can be found between safe and efficient operation. According to [**14**] for large bearings the load is additionally limited by the thermal effects that occur during operation. Due to scale effects the load capacity does not increase proportionally to the size of the bearing.

In [**15**] one can find comprehensive comparison between German (DIN 31654) and English (ESDU 83004) guidelines and design criteria for hydrodynamic thrust bearings. Essential operating parameters are analyzed:

- minimum oil film thickness,
- allowable specific pressure,
- maximum allowable temperature.

General conclusion from this publication is that criteria presented in both standards are similar and can be popularized among the society of engineers. Both of them take into account similar parameters and establish similar limit values for them.

For the reasons outlined in this chapter it is very important to develop calculation tools that allow to design thrust bearings with smaller margins of safety. Transient behavior in such situations can be especially important due to decreased load carrying capacity due to lower speed and higher thermal gradients.

In this chapter actual state of knowledge is presented regarding the design and calculation methods of large bidirectional thrust bearings.

2.2 Large thrust bearing design

Large hydro generators have usually vertical axes of rotation since such an arrangement makes the overall design more compact and robust. Deflections of the structure are smaller. This approach leads though to a thrust bearing high load which is also loaded in still stand and during startup and shut down – circumstances where the hydrodynamic action of the oil film is strongly limited. Due to variable axial deformations of the whole unit (elastic and thermal) there is always only one thrust bearing. The axial load consists of two components. First of them, the constant one, is the weight of

the rotational part of the hydro generator. Generally it can be said that the weight of the hydro generator is about $80\ \%$ of the whole unit and the rest is the turbine. Sometimes it is called dead weight. The second component of the axial load comes from the hydraulic thrust which is generated by the turbine. The power (torque) is generated by the tangential component of the force, however there occurs an additional axial component of the force. This part is subjected to variations as a function of the actual power delivered to the network. It may change rapidly in transient (emergency) cases (e.g. power rejection). These variations occur due to changes of the water pressure, speed or even flow direction. They may have both directions (downwards and upwards) and are difficult to predict. There are often experimental investigations made in order to estimate these values.

There may also be an additional thrust load from the magnetic thrust created by the generator. This component is subjected to the assembly inaccuracies and is usually small. It may also have both directions – it may create additional load but it may also reduce the overall load of the thrust bearing. Nowadays there are more and more reversible hydro generators being built. The main reason for this is the increasing demand of the better balancing of the electrical network. Conventional and nuclear power plants cannot be easily and quickly adjusted to demand of the power. For example it takes between 60 and $90\ min$ to start up the steam turbo generator. This means also new challenges to the thrust bearing design and reliability since bidirectional thrust bearings (symmetrically supported pads) have much smaller load carrying capacity [**16**]. One of the main hydro power plants suppliers, ALSTOM Hydro, justifies the increasing amount of the pump storage power plants in the following way [**17**]:

The electricity production has to be balanced at all times with electricity demand. The ever-increasing wind power capacity poses new challenges to grid stability due to its intermittent nature. Pumped storage is increasingly being used to level the output of fluctuating or inflexible power sources, such as wind or nuclear and could in future be applied as a balancing factor for large-scale solar power generation.

Recently asynchronous PSP hydro generators with variable speed are built for example by the ALSTOM Hydro company. This can also mean additional challenges for thrust bearings since they have to operate in a wider range of operational parameters. Nominal operating conditions (rotational speed, thrust load) are not constant but vary within a certain range (e.g. $\pm 20\ \%$).

In this elaboration mainly bidirectional thrust bearings are analyzed. These bearings have more difficulties with load carrying capacity (minimum oil film thickness) and the transient effects have stronger influence on their behavior. Thermal bending of the bearing pad has essential influence on their load carrying capacity. Most of the tools that were developed in the past consider the steady state simulation of the bearings with single direction of rotation.

2.2.1 Bearing housing arrangement

The thrust bearing can be either single or combined with the guide bearing in order to save place and to use common auxiliary devices for both of them. In case of vertical hydro generators bearing is usually fully immersed in oil. In this case the housing has an additional function of the oil tank. The space is then divided in three separate chambers

- cold oil, where the fresh oil is delivered and directed to the bearing pads,

- warm oil, where the warm oil is stored – outlet to the cooling system,
- air chamber, space for possible oil expansion due to temperature increase and air in oil.

The radial ribs in the housing prevent from the circumferential flow of the oil and allow for air separation.

Guide bearing can be combined with the thrust one in the same housing. Sometimes the guide bearing pad can be used to pump the oil through the coolers instead of installing the external pump. In such case the cooler has to be able to dissipate the power losses created by the both bearings together. Such approach is quite often used during design of hydro generators. It reduces number of bearing brackets and auxiliary systems. On the other hand design of both bearings has to be fitted to each other. It can for example lead to over dimensioning of the guide bearing diameter.

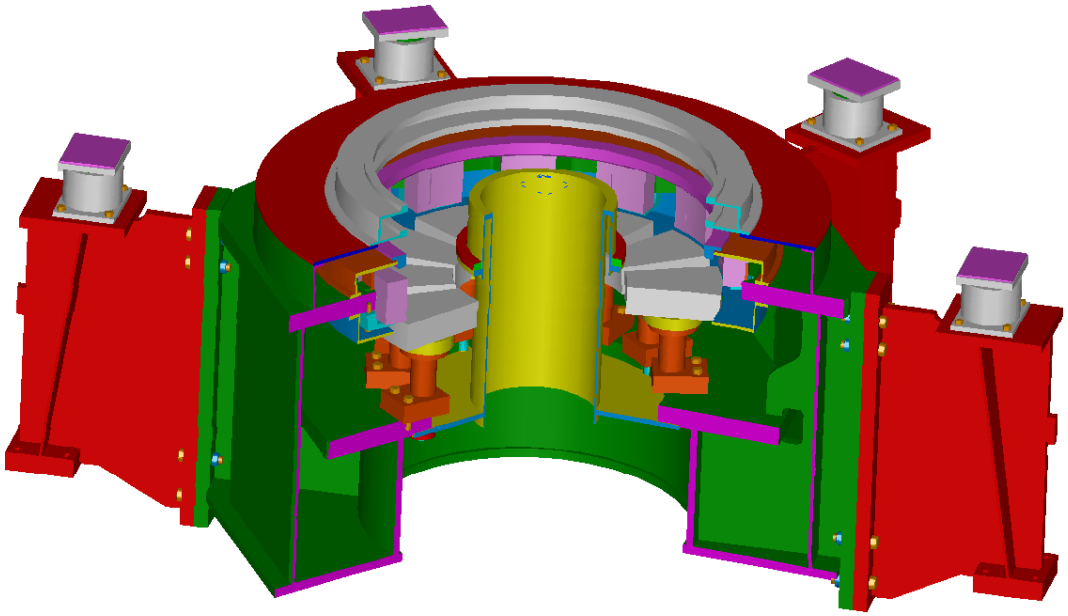

Figure 2.10. Typical combined thrust-guide bearing housing of a large hydro generator (ALSTOM Hydro)

Some bearing manufactures make use of special devices that deliver the fresh oil close to the rotating shaft surface. Among them one can distinguish different oil spray systems or LEG (Leading Edge Groove) technology offered by Kingsbury company.

2.2.2 Support systems

The overall thrust bearing design is similar in most cases and the main differences may occur in design details. One of them is the support system of the bearing pads. Its main function except the most obvious (load transfer from the bearing pad to the ground) is the equalizing of the load among all the bearing pads. Different manufactures have developed their different designs that assure appropriate load distribution. Among them one can distinguish the most popular:

- without any load equalizing,
- mechanical load equalizing,
- additional elasticity in the load chain,
- hydraulic support.

In the literature one can find information about problems with appropriate load equalizing between the pads [**4**,**18**]. For example in [**18**] authors consider problems with hydro generator thrust bearing

with the outer diameter equal to $1.8\,m$. The presented measurement data indicated that the temperatures between the pads varied within the range of $18\,°C$. This suggested that some of the pads carried much higher load than the others. The careful analysis indicated that the warmest pad carried approximately doubled force. This example shows how important it is to ensure precise load distribution. Otherwise the most loaded pad may initiate the process of the seizure of the whole bearing. This happens due to carry over of the melted Babbitt to the following pads and its aggregation on their leading edges. In this way the oil film is broken away and the hydrodynamic lubrication of the next pad is interrupted. Description of such mechanism of bearing damage can be found for example in [**9**].

In case of large thrust bearings it is important to assure that pads are free to tilt in both directions. The tangential tilting is important because of the inclination of the pad and the hydrodynamic pressure generation and the radial tilting compensates thermal and elastic deformations of bearing components (runner and bracket). Pad and runner sliding surfaces remain almost parallel in the radial direction. For this reason in the hydro generators almost only point supported thrust bearings are used. This solution has been patented by Kingsbury in the USA in 1912 [**19**]. Since that time many different supporting systems have been developed but the general function of such bearing remains the same. No load equalizing system can be only proposed in case of a small bearing where the manufacturing tolerances and elastic and thermal deformations are within a small range. In case of large scale units bearing equalizing system is a necessary solution. Since the oil film layer is around several tens of microns thick it is essential to ensure that all the sliding surfaces of the segments lay on the same level or within a very tight range. Otherwise some of the pads will be loaded with much higher forces while others will not carry the load at all.

According to the literature [**20**] mechanical equalizing systems are suitable for small and medium sized thrust bearings. In case of large forces in the equalizing system significant friction between elements may occur what can lead to the insufficient equalizing between pads due to relatively wide hysteresis of the system. Waukesha company has developed a system with rolling elements [**21**] in order to reduce internal friction of the system. This is called HyFilm system. The contact surfaces are manufactured in such way that almost only rolling friction occurs. In this way the hysteresis of the system is reduced and thus the load equalizing works in a more precise way. Similar functionality offers the load equalizing system offered by Kingsbury company [**22**].

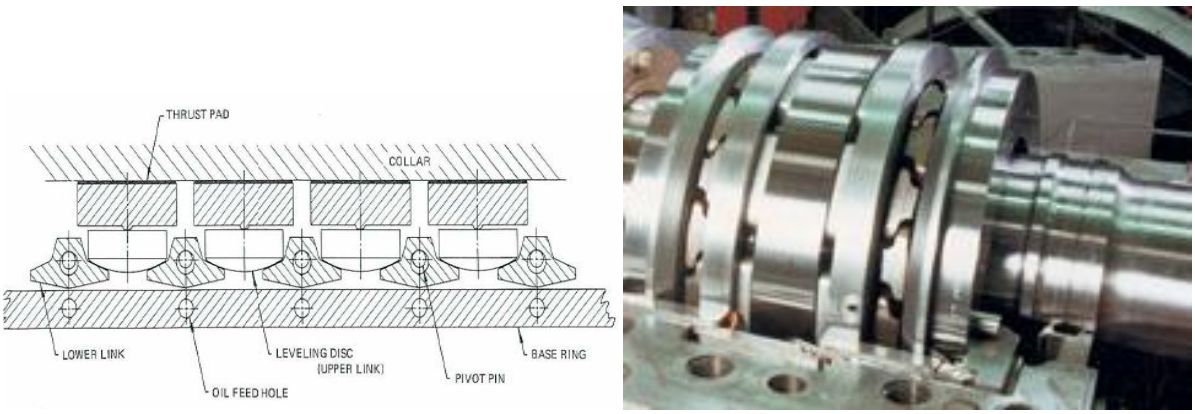

Figure 2.11. Waukesha equalizing shoe leveling HyFilm system [20], gas turbine application [21]

A different approach of the load equal distribution is an additional elasticity in the load chain. Increased elasticity of a support system can give an ability of compensation of the assembly and

manufacturing inaccuracies. Below some of the most common supporting systems that make use of the increased elasticity are presented.

Plate spring design

Plate spring is a solution for small hydro generators with the outer bearing diameter up to $1.2\ m$. It is easy to manufacture and assembly. Its additional advantage is that it does not require much space in axial direction. In a design phase the geometry can be adjusted in order to obtain the required axial stiffness. It should be as small as possible in order to ensure a wide range of axial deflection under the load but on the other hand is has to be large enough to keep the critical axial frequency of vibrations on a relatively high level. In the middle of the spring one can see a sort of bumper. Its role is to limit the deformations and stresses in the spring in case of extremely high loads (e.g. emergency or failure).

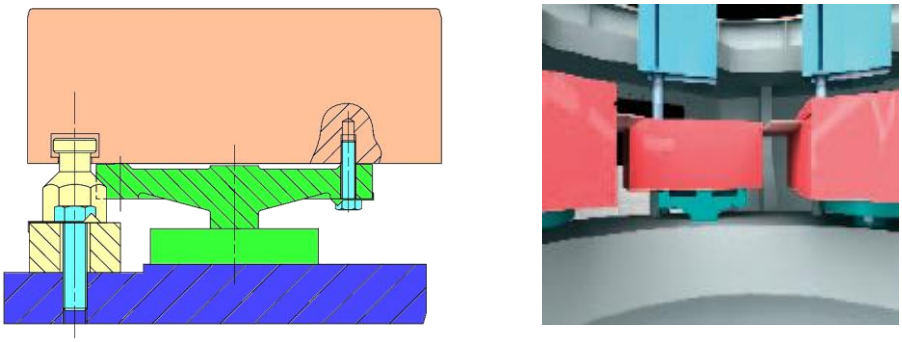

Figure 2.12. Plate spring (ALSTOM Hydro)

Spindle support design

Spindle support is a solution designed for medium and large sized generators. It allows for the adjustment of each of the pads separately during the final assembly of the generator. The lower end is connected with the ground via a thread connection. Its relatively small cross section ensures the required elasticity which can be adjusted during the design process. Inside there is a measurement pin attached to the top of the spindle so the axial deformation can be measured during assembly of the bearing. The deformations of all the spindles are compared with each other and necessary adjustments are made in order to equalize the load.

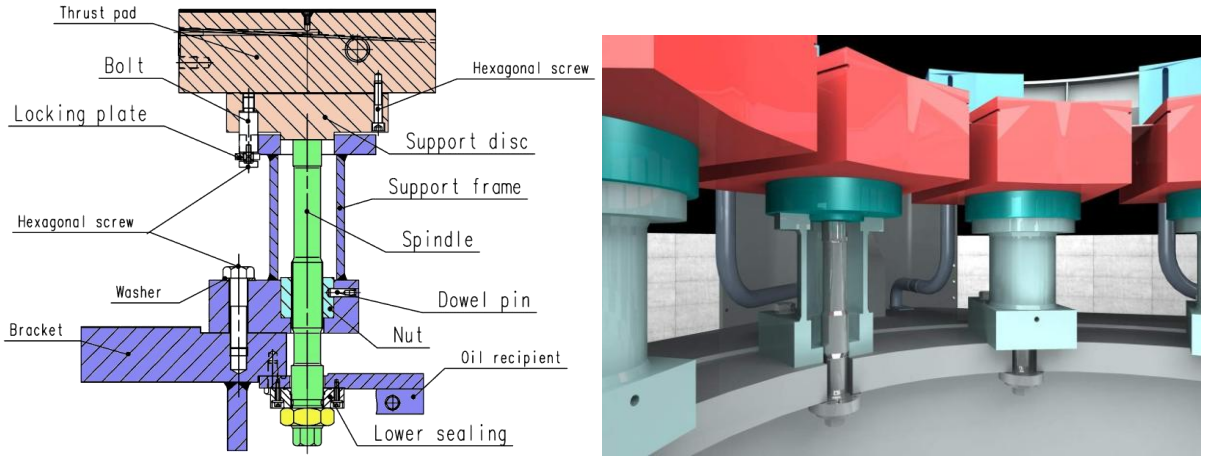

Figure 2.13. Spindle support (ALSTOM Hydro)

The final confirmation of the appropriate load distribution among the pads is made during first mechanical tests of the unit. If the pads are loaded equally the temperatures among the pads should also be equal. Normally there is certain range of tolerance for the measured temperatures. All values should be within the range of $2 - 3\ °C$.

Spring mattress design

Spring mattress design has been invented by H. G. Riest at General Electric Company around 1915 [**23**]. At that time it was designed in form of a thin, washer type ring with one radial gap. Later this design was adopted to segmented thrust bearings. They are used in order to obtain concave elastic bending of the pad and the compensation of the pad thermal crowning. However in early designs the pads were supported by springs from edge to edge, distribution and stiffness of the springs can be adjusted within a wide range during design in order to optimize elastic deformation of the pad [**24**]. Thickness of the pad should be relatively small in comparison with other dimensions in order to increase its elasticity. Otherwise the elastic effects will not be sufficient. According to the literature such bearing design has some advantages over other types but it is complex to analyze and to predict the performance. Thus a flexible calculation tool that allows such investigation is needed. FEM method seems to be perfect for such purpose since the geometry (locations and number of springs) can be varied in a very wide range. Influence of arrangement of the springs has been investigated in [**25**].

For bidirectional bearings spring support has the disadvantage of an additional reaction moment of the support that reduces the tilt angle. The arrangement of the springs has to be symmetrical in order to ensure equal behavior in both directions (center of effort). Since the bidirectional tilt angle is already very small such effect can have a negative influence on the bearing temperature and minimum oil film thickness since the inlet oil gap is smaller and there will be less cold oil entering the oil film. This influence is investigated further in this work.

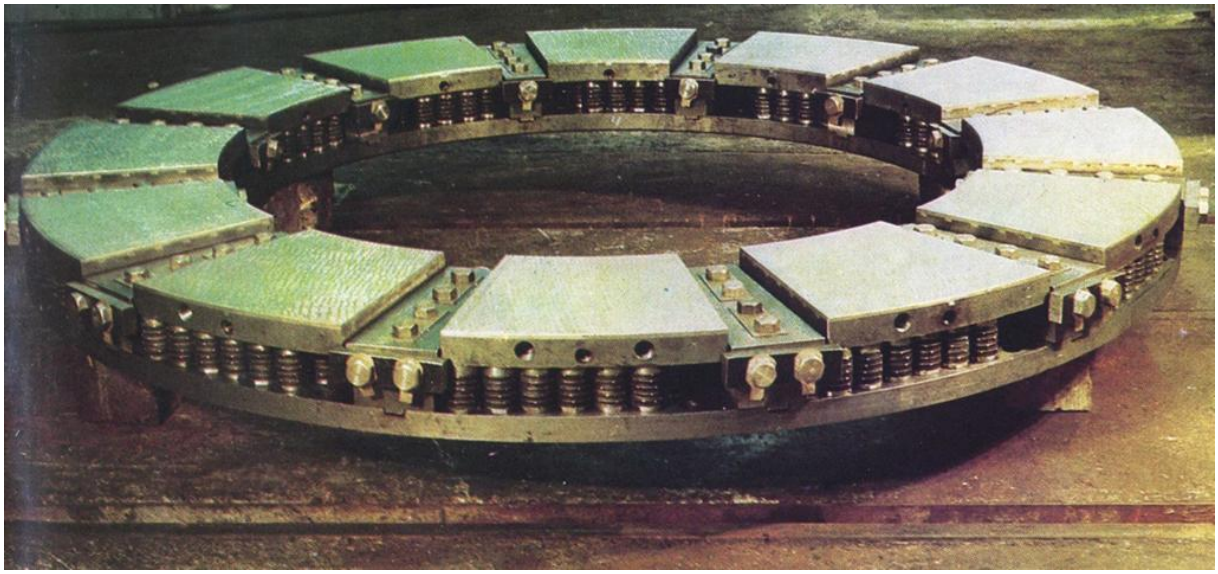

Figure 2.14. Spring bed support system [26]

Mattress of rubber springs

Mattress of rubber springs [**27**] is a similar solution to the spring bed one but rubber discs are used instead of helical springs (see Figure 2.15), although the problems with reaction moments remain still

the same as for the spring mattress solution. In the figure one can notice that the discs are distributed symmetrically, so the bearing can operate in both directions. Additionally in the same figure there is an oil distributor shown that sprays the cold oil on the rotating runner surface. This feature is described more in detail further in this chapter.

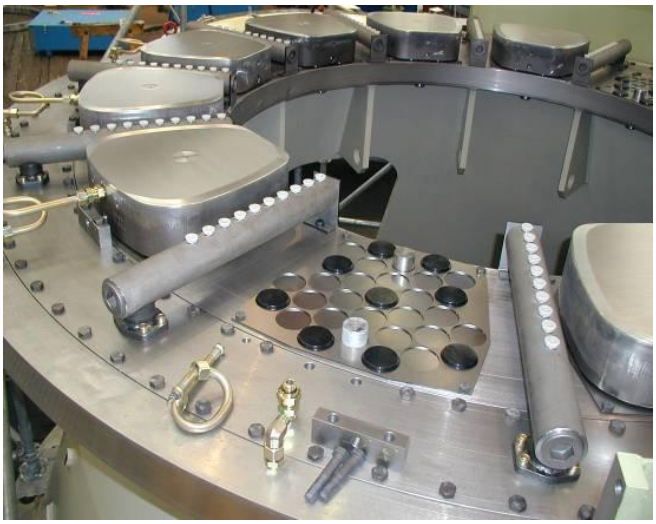

Figure 2.15. Mattress of rubber springs support system [27]

Membrane support makes use of a different approach in order to equalize the load among the pads. The hydraulic connection is made between the pad supports in order to obtain equal reaction on the ground (see Figure 2.16). The connection is realized by the system of bores in the base plate under the membranes. The same reaction forces among the pads means automatically equal load distribution according to the Newton Third Rule.

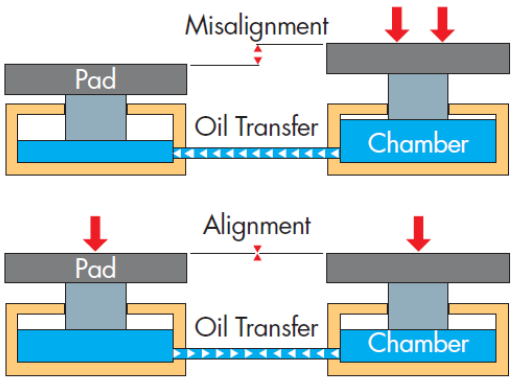

Figure 2.16. Membrane support, principle of operation (ALSTOM Hydro)

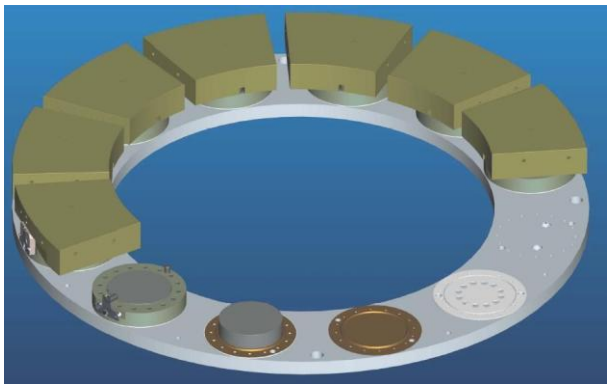

Figure 2.17. Membrane support (ALSTOM Hydro)

Additional advantage of this system, used for large bearings, is that it does neither need assembly nor operational adjustments. Any possible deformation (thermal or elastic) of the bearing bracket or any other element is compensated, within a certain range, by the movement of the membrane. This solution has been used for a long time but recently there has been a new, simplified design developed by ALSTOM Hydro company that made the membrane solution more compact and reliable (see Figure 2.17). The recent development made it compact, reliable and easy to assembly. On the other hand the special tools are needed in order to manufacture the membrane plate.

Elastic compensation of the thermal bending of the bearing pads

As it has been mentioned before deformations of the bearing pads have essential influence on the load carrying capacity. In order to decrease pad thermal crowning Ettles [**28**] proposed elastic compensation of the pad. He proposed to use a disc between the pad and the supporting element. In this way convex thermal deformations can be reduced due to the concave elastic bending of the pad. In such case the pad is supported by the means of a ring, so the hydrodynamic pressure can bend it in opposite direction to the thermal bending. This elastic compensation can be generally used in each type of the bearing pad support system. Thickness of the pad and diameter of the supporting ring need to be carefully designed, with consideration to the operating parameters and size of the bearing, in order to obtain the desirable effect. In the Figure 2.18 the principle of the elastic compensation of the pad thermal crowning is presented. In [**24**] for medium sized pads ($B = 150\ mm$) author proposes ratio $A/B = 0.3$, where A is the diameter of the supporting ring. In case of large bearing pads this ratio should be increased and the deformation should be carefully controlled during design.

In [**18**] one can find a parametric study regarding the performance of the tilting pad thrust bearing of a hydro generator. One of the parameters analyzed in this study is the diameter of the supporting disc. Its influence on compensation of the pad thermal crowning is shown in Figure 2.18. The comparison between the existing and proposed design is given.

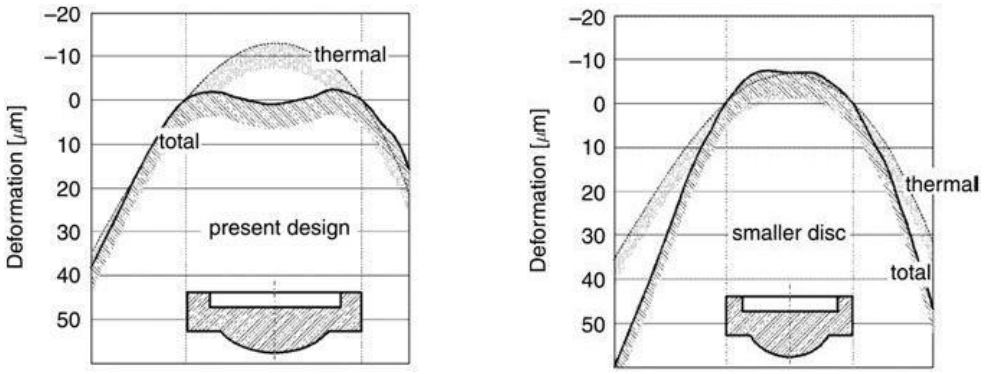

Figure 2.18. Compensation of pad thermal crowning, influence of the supporting disc diameter [18]

Elastic deformation due to its nature is a quick effect connected to the load of the bearing. Inversely the thermal deformation is a long time scale effect. Even if during steady state analysis both effects reduce each other it does not mean that it is the case during transient states. E.g. rapid overload of the bearing can first cause the rapid increase of the elastic deformations while thermal state of the bearing needs much more time to adapt to the new operating conditions.

2.2.3 Auxiliaries

The bearing is equipped with many additional devices that support its main function. The most important ones are described in this chapter.

Hydrostatic jacking system

Since the hydrodynamic effect depends on the relative speed between the pad and the thrust collar in order to prevent wear of the sliding surfaces usually there is additional hydrostatic equipment that supports the bearing during startup and shut down. The additional oil pumped to the oil film assures the lubrication at low rotational speeds and thus the sliding surfaces are always separated.

In case of small bearings, low specific pressures and in case of polymer coated bearing pads there is no need of the hydrostatic assistance. It is enough when before start up the shaft is raised with the use of hydraulic brakes and the oil comes between the collar and the pads. Within the short time the squeeze effect of the oil film can give sufficient lubrication at low speed. In this way design and reliability of the thrust bearing and its design simplicity can be remarkably increased.

In case of any problems with hydrodynamic lubrication (insufficient load carrying capacity) the hydrostatic jacking system may be used permanently in order to increase reliability of the bearing. In such a situation the lubrication system must be equipped with two or three high pressure pumps in order to assure appropriate operation either in case of failure of one of the pumps, lack of power supply or any other reason. Energetic efficiency of the whole hydro generator is not affected in this way since power of the high pressure pump is usually very low (several kilowatts). Additionally it does not operate at rated conditions of the generator.

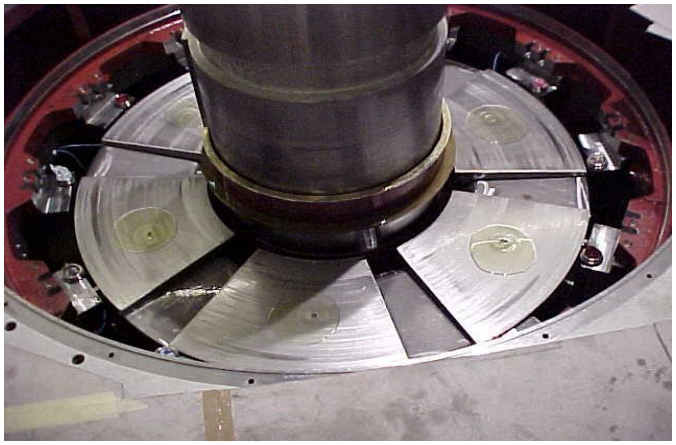

Figure 2.19. Hydrostatic jacking system operation (ALSTOM Hydro)

The hydraulic circuit is equipped with all necessary additional elements like backpressure valves and orifices, so the functionality of the jacking system remains uninfluenced also in case of failure of one (or even more) of the connections. The oil is usually filtered up to $10\ \mu m$. More information about hydrostatic jacking systems can be found in the literature sources e.g. [**9**,**29**].

Cooling systems

In general the cooling systems can be divided into the following groups:

- air cooling,
- water cooling with internal cooler,

- water cooling with external cooler.

For the bearing with relatively small losses and/or allowable higher operational temperature air cooled bearing housing can be proposed, especially in case of small hydro power plants. It makes the whole system compact, independent and robust. The air cooled bearing housing can be realized either with natural or forced convection. Also large hydro generators or pumps with small rotational speeds (power losses) may profit from such simplified cooling methods [**30**]. There has to be just enough oil in the bearing housing to disperse the energy delivered to the system due to the frictional losses.

Internal water cooling systems use the water pipes located in the bearing housing to exchange the heat. It is difficult to predict and control the efficiency of such a system. It can be influenced only by the amount of the cooling water and its temperature (usually cooling water temperature cannot be controlled and additionally it is subjected to variations within a wide range depending on the season). The convection coefficient between oil and the cooling pipes depends strongly on the oil flow in the bearing housing. So it varies with the rotational speed. There is also a danger of water leakage which may require disassembly of the whole bearing.

Figure 2.20. Internal water cooler in the bearing housing (ALSTOM Hydro)

The most up to date solution is external water cooling of the oil. The oil is pumped out from the bearing housing and then through the coolers. The oil can be pumped either with the use of external pumps supplied from the network or with the use of self pumping devices. Self pumping, a technology widely used by ALSTOM Hydro company makes use of viscous pump effects in the bearing housing. Rotation of the shaft is used to pump the oil through the cooling system. This design allows for better control of the dispersed power since both the oil and water flows can be adjusted. In this way constant cold oil temperature can be assured also in transient states. Heat exchange in the coolers is also much better than in case of internal ones due to higher area and better convection coefficients.

Additional advantage of the external water cooling is that the bearing may be equipped with the external oil tank where most of the oil is stored. Thus the bearing housing may have more compact dimensions, which might be important when the large amount of oil is needed in the lubrication system. In contractual requirements it is usually said that, in case of emergency, hydro generator

should run without water cooling for $15\ min$. For this case the whole power loss created by the bearing has to be accumulated in the oil and its temperature should not rise more than $15\ °C$ for safety reasons. Otherwise the oil viscosity might be too low and the temperature too high in order to maintain oil film thickness within the safe range.

Figure 2.21. External water cooler, Kopswerk II 2 PSP power plant

Oil tanks and control of the oil flow

Oil for the bearing lubrication can be stored either in the bearing housing or there may be an additional external tank in the lubrication system. The amount of oil can sometimes be very large in order to ensure an appropriate bearing cooling in case of lack of the cooling water. In such case the bearing has to operate for a certain time ($15\ min$ for example) and the whole power loss has to be dissipated in the oil volume. The time is needed for the safe shut down of the unit and the temperature of the oil must not exceed the assumed value. Another reason for large amount of oil is the oil circulation in the cooling system. The time within which the whole oil is exchanged should not be too short in order to allow the separation of the air that is mixed with oil. Air is usually mixed with oil in the areas of high speeds and where the separation between them is not well defined.

Figure 2.22. External oil tank and coolers, Feldsee PSP power plant

The exchange of the warm oil is usually forced in the bearing housing. It is important to ensure that fresh cold oil is delivered to the oil film inlet area. The bearing housing is arranged a way that rotation of the runner is usually used to enforce the oil flow. This is the so called viscous pump effect. This effect can be obtained by numerous designs. Some of them are described below.

Rotating hole

One of the pumping effects used in order to force the oil flow in the bearing housing is the radial hole made in the runner (see item 22 in Figure 2.23). Due to centrifugal and viscous effects the oil can be pumped in radial direction. The efficiency of such a solution depends on the geometry (number and diameter of the holes, diameter of the thrust block, etc.) and rotational speed of the shaft. In this figure one can also notice that the relatively thin pad lays on the spring mattress. This particular example has been taken from hydro generators catalogue from the ABB company [**31**].

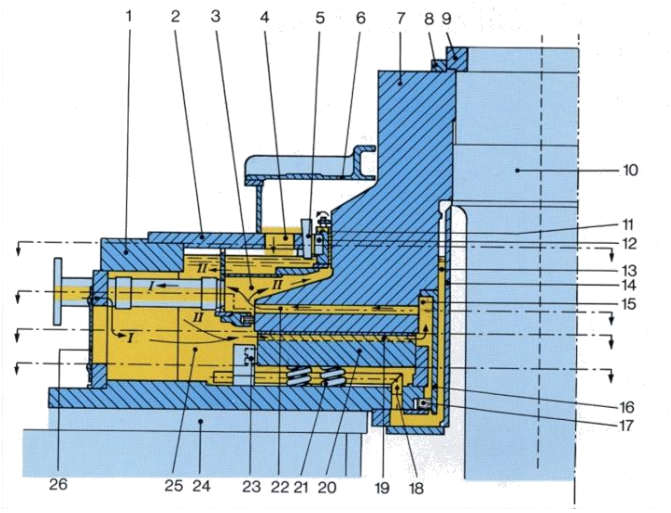

1	Thrust bearing frame	15	Pump oil intake chamber
2	Guide bearing frame	16	Oil seal sleeve
3	Oil-pressure chamber	17	Seal
4	Guide bearing oil return holes	18	Pressure equalizing pipe
5	Adjusting wedge	19	Oil feed slot
6	Bearing cover	20	Thrust bearing pad
7	Thrust block	21	Thrust spring
8	Lock ring	22	Radial pumping duct
9	Thrust collar	23	Pad retaining peg
10	Shaft	24	Bracket
11	Guide bearing pad	25	Oil reservoir
12	Pivot peg	26	Inspection cover
13	Inner oil space	27	Oil pipe from cooler
14	Oil cup	28	Oil pipe to cooler

Figure 2.23. Rotating hole design [31]

Pumping plate

Pumping plate between thrust pads is used in order to separate warm and cold oil in the bearing housing and to deliver cold oil close to the oil film inlet. Additional function is to pump the oil in radial direction. In this way oil circulation in the bearing housing can be controlled. Such cross flow of the oil can cause better oil mixing between the pads and lower warm oil carry over effect.

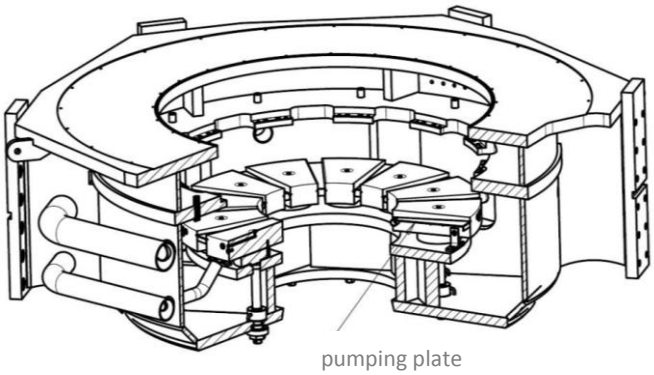

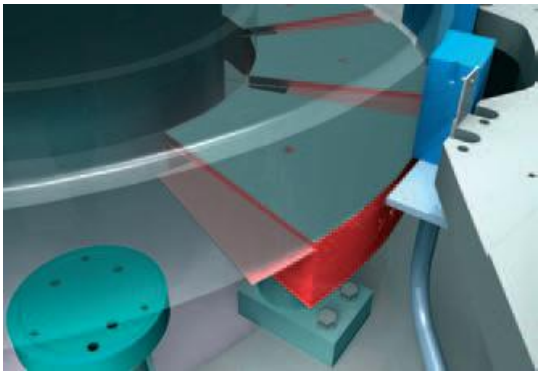

Figure 2.24. Pump plate between thrust pads design and flow (ALSTOM Hydro)

Self pumping pads

ALSTOM Hydro Ltd (formerly BBC) company developed in 1980's a self pumping pads technology [**32**]. At this moment this is a highlight bearing technology of the ALSTOM Hydro company and is used in most of the current projects in case of the combined thrust – guide bearings. This design allows to pump oil through the cooling system with an external cooler and without any external pump. Specially designed guide bearing pads are used instead. Each of the pads has in the inlet area additional so called pumping pockets where the pressure is generated and used for pumping of the oil through the cooling system (see Figure 2.25). Pumping flows from all the pads are then gathered in a common warm oil chamber or ring pipe. Pressure generated in this chamber causes the oil flow through the cooling system. Due to viscous character of such a pump the resistance pressure has to be kept on a relatively low level. For this reason all pipelines and coolers must have cross sections large enough that assure low hydraulic losses. It is also not allowed to install oil filter in such circuit. Main advantages of this technology are lack of maintenance, automatic operation and increase of the pumping flow as a function of the rotational speed of the shaft. In case of bidirectional bearing self pumping pockets need to be manufactured on both sides of the pad.

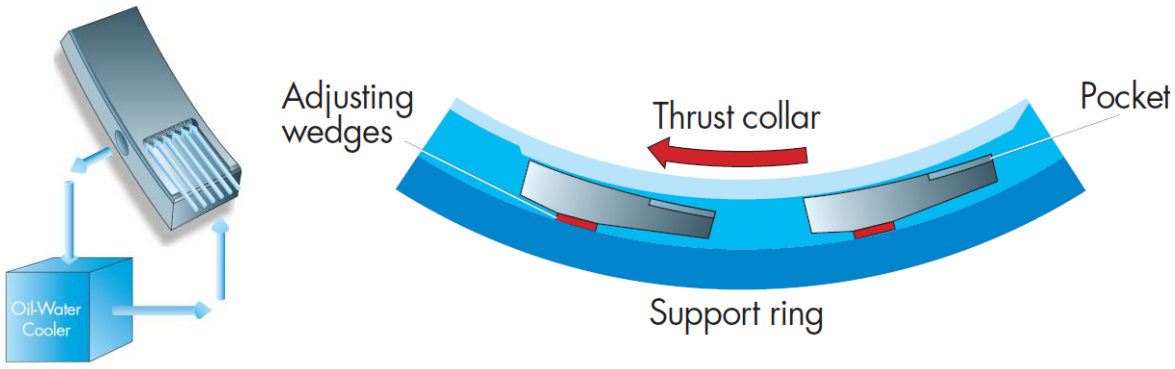

Figure 2.25. Self pumping pad principle (ALSTOM Hydro)

Theoretically it is possible to use similar pumping pockets in the thrust bearing pads but this would reduce the valuable area of the bearing and increase the specific pressure.

External pumps

In case of bearings with high power losses it is possible to install an external pump that ensures circulation of the oil between the bearing housing and the external cooler (see Figure 2.21). Main advantage of such a solution is independence of the oil flow from the rotational speed of the bearing. Hydraulic losses in the cooling system can be also higher so there is no need of using large cross-sections in the cooling system. On the other hand such a system is less reliable so very often the pumps and coolers have to be doubled in order to ensure redundancy of the system. In order to ensure an appropriate function of the cooling system in case of emergency and lack of external power supply an additional sources of power have to be assured. It can be a DC battery or an additional diesel generator. Maintenance of such system is more complicated and expensive. It requires also additional measurement and control devices that monitor its parameters.

Filters and quality of the oil

Oil filtering in case of hydrodynamic bearings is very important since the operational oil film thickness is usually not larger than $20-40\ \mu m$ (depending on the operational conditions). It is always ensured that both sliding surfaces are separated, either due to hydrodynamic or hydrostatic film action. Thus the wear can occur only if particles larger than oil film thickness are being pulled between the bearing parts. Especially bidirectional bearings have low load carrying capacity that results in low oil film thickness. In order to prevent scratching of the sliding surface it is necessary to assure that particles in the oil have smaller dimensions than the minimum oil film thickness. Because of these reasons lubricating oil has to fulfill the following classes of the contamination by the solid particles: SAE class 4 or NAS 1638 class 7 or ISO class --/16/13. These allowable levels of contamination are marked in the following tables (Table 2.1, Table 2.2 and Table 2.3).

Table 2.1. Coding level of contamination by solid particles according to the ISO 4406 standard

	Class	Number of particles per 100 ml larger than			
		> 6 µm		> 14 µm	
		more than	up to	more than	up to
	--/20/17	500000	1000000	64000	130000
	--/19/16	250000	500000	32000	64000
	--/18/15	130000	250000	16000	32000
	--/17/14	64000	130000	8000	16000
→	**--/16/13**	**32000**	**64000**	**4000**	**8000**
	--/15/12	16000	32000	2000	4000
	--/14/11	8000	16000	1000	2000
	--/13/10	4000	8000	500	1000

Table 2.2. Coding level of contamination by solid particles according to the NAS 1638 standard

	Class	Number of particles per 100 ml larger than				
		5 – 15 µm	15 – 25 µm	25 – 50 µm	50 – 100 µm	> 100 µm
	4	4000	712	126	22	4
	5	8000	1425	253	45	8
	6	16000	2850	506	90	16
→	**7**	**32000**	**5700**	**1012**	**180**	**32**
	8	64000	11400	2025	360	64
	9	128000	22800	4050	720	128
	10	256000	45600	8100	1440	256
	11	512000	91200	16200	2880	512

Table 2.3. Coding level of contamination by solid particles according to the SAE 749 standard

Particles size	Class	
	Number of particles per 100 ml	
µm	→ **Class 4**	Class 5
5 – 10	**32000**	87000
10 – 25	**10700**	21000
25 – 50	**1510**	3310
50 – 100	**225**	430
> 100	**21**	41

Remark: Additionally in all classes particles larger than 150 µm are not allowed and water amount cannot exceed 200 ppm ($2cm^3\ H_2O\ /\ 1\ m^3\ oil$).

Water and solid particles accelerate the ageing of the oil since they cause additional wear and corrosion. A properly designed oil filtering system has to fulfill the following tasks:

- filtering solid particles from the oil,
- avoid interruptions between maintenance services,
- assure high operational reliability,
- increase utilization time of the oil,
- maintain parameters of the oil,
- avoid ageing of the oil,
- enable easy maintenance,
- increase durability of the hydraulic system components (decrease of wear).

2.2.4 Hydrodynamic bearings with polymer coatings

In recent years the most of the progress in the hydrodynamic bearings technology has been done in case of the bearing materials. The aim in this field is to design the bearing that operational parameters and reliability are at higher level than for the conventional ones.

Even though the PTFE (*polytetrafluorethylene*) technology has been known for many years, recently there was a visible trend of making use of unconventional materials for the bearing lining. A lot of research work has been undertaken recently [**13**,**33**,**34**,**35**]. The main reason for that is searching for the materials with operational limits beyond these known for babbitted bearings. The power losses of the bearing can be reduced only by the decrease of the bearing size and at the same time increase of the specific pressure. Many different manufactures have already significant experience in use of these new coatings. Among them one can distinguish Michell Bearings [**36**,**37**,**38**,**39**]. It is not easy to cover the steal pad backing with the polymer due to extremely low adhesive forces. Therefore there were several technologies developed which mechanically bind the lining material to the pad backing. The first of them, developed in Russia in 1960's, makes use of a wire mesh soldered to the pad [**6**]. Afterwards the PTFE sheet, under high pressure and temperature, is pressed on this wire and so the stable mechanical connection is obtained.

Figure 2.26. Mesh wire technology [6]

Additional elasticity of the wire mesh bonding layer gives the ability of large deformations under the hydrodynamic pressure. In this way optimum, from carrying capacity point of view, gap shape (pocket) can be obtained [**30**]. This type of bonding allows also for different thermal expansion of both materials – the coefficients of thermal expansion for PTFE is approximately 10 times larger than for steel backing.

Another way of bonding polymer material with the steel pad backing is sintered brass technology. It is used either for PTFE or PEEK (*polyether ether ketone*) lining materials. In this case porous brass layer is sintered to the steel pad backing and later polymer is pressed on it with the use of high pressure and temperature. PEEK filled with carbon fiber attached to the pad backing with the use of sintered bronze layer is a technology used by ALSTOM Hydro company and is called POLYPAD®. Polymer layer is in this case approximately two times thicker than bounding brass. This technology is widely described in [**40**,**41**,**42**,**43**,**44**,**45**].

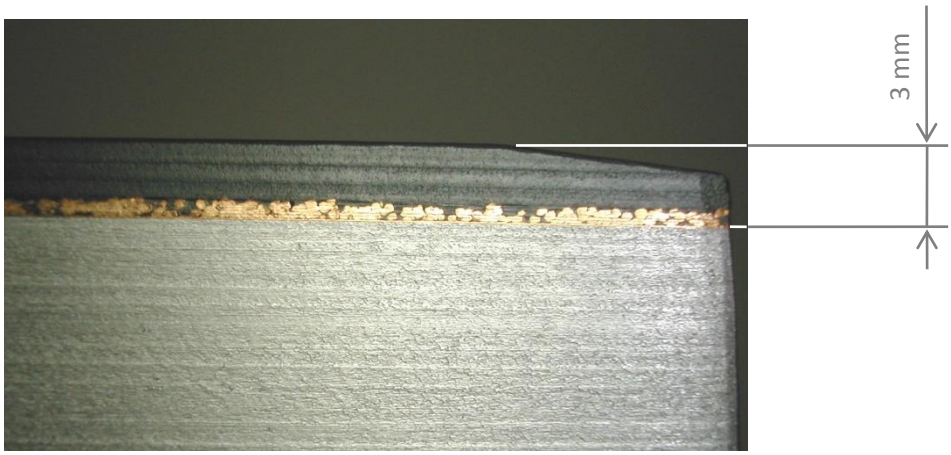

Figure 2.27. Sintered brass polymer bounding technology (ALSTOM Hydro)

In the literature one can also find information about successful implementation of polymer sheets simply laid on the pad backing and mounted only on the trailing edge by the means of screws [**13**,**30**]. These sheets are made of PE-UHMW (polyethylene of ultra high molecular weight). According to literature data, this approach was used only for low speed hydro generators where the main problem is the minimum oil film thickness. This is consistent with physical properties of this material. It has a low coefficient of friction and a high resistance against wear under dry or mixed lubrication conditions. Its disadvantages are a low resistance against higher temperatures ($> 80\,°C$) and low

thermal conductivity. For these reasons it cannot be used in case of bearings with high sliding speeds. In Figure 2.28 one can see a simplified bearing concept with polymer lining. On the pad backing (1) there is located an intermediate plate (2) with mounted polymer sheet of $3\ mm$ thickness (4). The sheet is mounted only by the means of the screws (3) on the trailing edge. Due to acting of hydrodynamic pressure there is no need of additional mounting of the pad lining.

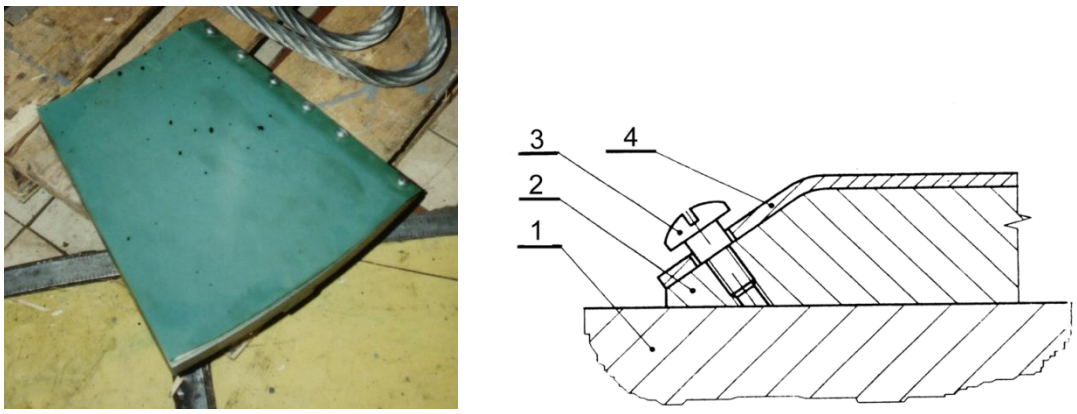

Figure 2.28. Polymer sheet pad lining after [30]

In the literature one can find information that there are hydro generator thrust bearings loaded with specific pressure equal to $11\ MPa$ that worked for 20 years without any substantial wear (maximum reported wear of the sliding surface did not exceed $500\ \mu m$) [**6**]. Such severe operating conditions are only possible with the use of pad lining materials that are able to withstand much higher temperatures than Babbitt. In the described case the pads were coated with PTFE with the use of the technology presented in Figure 2.26.

On the other hand thermal crowning of the pad is significantly lower and can be even totally compensated by the elastic bending of the pad. Thus for the symmetrically pivoted thrust bearing one should take particular care. The thermal bending of the pad coated with thermally insulating material is significantly smaller so the load carrying capacity might not be high enough. The pad inclination, in such case, strongly depends on the thermal deformation. In the Figure 2.29 one can see the comparison of the temperature distribution through the thickness of the conventional and polymer coated pad [**33**].

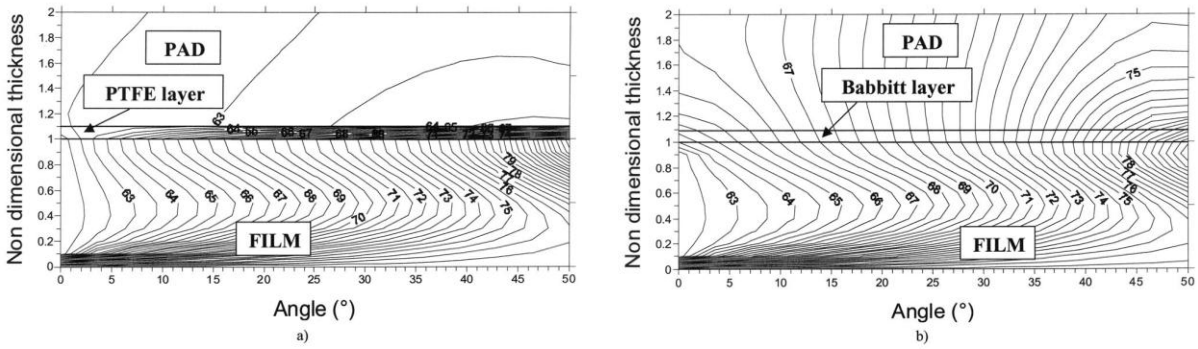

Figure 2.29. Temperature distribution through the thickness of the pad, a) PTFE lined bearing, b) conventional bearing [33]

Long inlet and outlet chamfers of relatively low depth (order of several tens of micrometers) can increase tilting ability of such bearing pad in order to increase load carrying capacity. This practice is

implemented for example by Michell Bearings company [**36**]. It was also investigated by Fillon [**34**]. This design is especially interesting in case of symmetrically supported bearing pads. In such case tilting ability can be significantly improved in this way.

Modern coatings for thrust bearing pads are very promising and forgiving material but care has to be taken during design and implementation of such designs. There are already publications about failures of such bearings [**38**].

2.3 Thrust bearing calculations

2.3.1 Hydrodynamic lubrication

The load carrying capacity of the hydrodynamic bearing is a function of the hydrodynamic pressure distribution in the oil film.

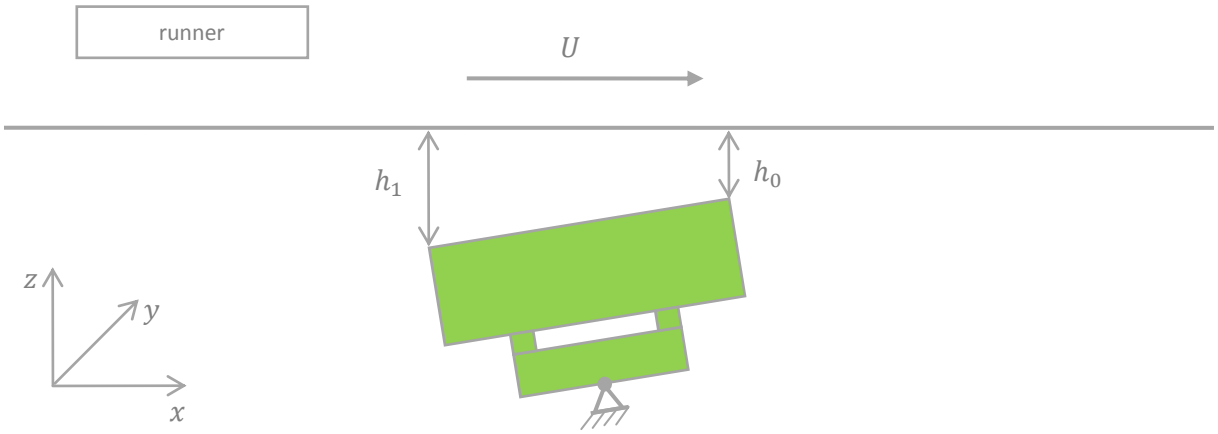

Figure 2.30. Hydrodynamic oil film, coordinates system

In general case the oil flow can be described with the following equations:

Navier-Stokes equation:

$$\rho \frac{d\boldsymbol{v}}{dt} = -grad(p) + \eta \, \Delta \boldsymbol{v} + S \tag{2.4}$$

This is a vector equation and can be written in form of three scalar equations for each spatial direction:

x direction:

$$\rho\left(\frac{\partial u}{\partial t} + u\frac{\partial u}{\partial x} + v\frac{\partial u}{\partial y} + w\frac{\partial u}{\partial z}\right) =$$

$$= -\frac{\partial p}{\partial x} + \eta\left(\frac{\partial^2 u}{\partial x^2} + \frac{\partial^2 u}{\partial y^2} + \frac{\partial^2 u}{\partial z^2}\right) + 2\frac{\partial \eta}{\partial x}\cdot\frac{\partial u}{\partial x} + \frac{\partial \eta}{\partial y}\left(\frac{\partial u}{\partial y} + \frac{\partial v}{\partial x}\right) + \frac{\partial \eta}{\partial z}\left(\frac{\partial w}{\partial x} + \frac{\partial u}{\partial z}\right) \tag{2.5}$$

y direction:

$$\rho\left(\frac{\partial v}{\partial t} + u\frac{\partial v}{\partial x} + v\frac{\partial v}{\partial y} + w\frac{\partial v}{\partial z}\right) =$$

$$= -\frac{\partial p}{\partial y} + \eta\left(\frac{\partial^2 v}{\partial x^2} + \frac{\partial^2 v}{\partial y^2} + \frac{\partial^2 v}{\partial z^2}\right) + \frac{\partial \eta}{\partial x}\left(\frac{\partial u}{\partial y} + \frac{\partial v}{\partial x}\right) + 1\frac{\partial \eta}{\partial y}\cdot\frac{\partial v}{\partial y} + \frac{\partial \eta}{\partial z}\left(\frac{\partial v}{\partial z} + \frac{\partial w}{\partial y}\right) \tag{2.6}$$

z direction:

$$\rho\left(\frac{\partial w}{\partial t}+u\frac{\partial w}{\partial x}+v\frac{\partial w}{\partial y}+w\frac{\partial w}{\partial z}\right)=$$

$$=-\frac{\partial p}{\partial z}+\eta\left(\frac{\partial^2 w}{\partial x^2}+\frac{\partial^2 w}{\partial y^2}+\frac{\partial^2 w}{\partial z^2}\right)+\frac{\partial \eta}{\partial x}\left(\frac{\partial u}{\partial z}+\frac{\partial w}{\partial x}\right)+\frac{\partial \eta}{\partial y}\left(\frac{\partial v}{\partial z}+\frac{\partial w}{\partial y}\right)+2\frac{\partial \eta}{\partial z}\cdot\frac{\partial w}{\partial z} \tag{2.7}$$

Continuity equation (for incompressible flow):

$$div(\boldsymbol{v})=\frac{\partial u}{\partial x}+\frac{\partial v}{\partial y}+\frac{\partial w}{\partial z}=0 \tag{2.8}$$

Energy equation:

$$\rho\, c\,\frac{dT}{dt}=\lambda\,\Delta T+\eta\,\Phi \tag{2.9}$$

$$\Phi=2\left[\left(\frac{\partial u}{\partial x}\right)^2+\left(\frac{\partial v}{\partial y}\right)^2+\left(\frac{\partial w}{\partial z}\right)^2\right]+\left(\frac{\partial u}{\partial y}+\frac{\partial v}{\partial x}\right)^2+\left(\frac{\partial v}{\partial z}+\frac{\partial w}{\partial y}\right)^2+\left(\frac{\partial w}{\partial x}+\frac{\partial u}{\partial z}\right)^2 \tag{2.10}$$

Heat transport equation:

$$\dot{q}=-\int_{(A)}\lambda\,\frac{\partial T}{\partial n}\,dA \tag{2.11}$$

State equation:

$$\eta=\eta(T,p) \tag{2.12}$$

These 7 equations describe the problem of the hydrodynamic lubrication for 7 unknowns: $u, v, w, p, \eta, \dot{q}$ and T thus the mathematical description of the bearing operating parameters in four dimensions (x, y, z, t) is possible.

Additionally the simulation model can be used in order to model turbulent flow around the bearing pad. According to [**46**,**47**] turbulence models can be divided into following groups:

- zero equation (algebraic) models,
- one equation models,
- two equation models,
- Reynolds stress models.

Each of these models adds certain equations to the prior presented system of 7 equations and calculated additional parameters of the flow. Nowadays the most common in use are two equations turbulence models like $k-\varepsilon$ or $k-\omega$. These models add two separate transport equations to the previously defined 7. For example in $k-\omega$ turbulence model first of the two additional unknowns is

kinetic energy per unit mass of fluid arising from the turbulent fluctuations in velocity around the averaged velocity k. The second unknown is the frequency of large eddies ω.

2.3.2 Generalized Reynolds equation

Reynolds presented his theory of the hydrodynamic lubrication in 1886 [**48**]. This approach treats the hydrodynamic lubrication in a simplified way. The most important simplifications are:

- laminar and incompressible flow assumption,
- pressure gradient through the oil film thickness $\frac{dp}{dh} = 0$,
- isothermal flow assumption,
- calculation without influence of the pad and runner deformations.

With these assumptions Reynolds evaluated 2D equation (on $x - y$ plane) from the Navier-Stokes set of equations [**8**]:

$$\frac{\partial}{\partial x}\left(\frac{\partial h^3}{\eta}\cdot\frac{\partial p}{\partial x}\right)+\frac{\partial}{\partial y}\left(\frac{\partial h^3}{\eta}\cdot\frac{\partial p}{\partial y}\right)=6\left[(U_1+U_2)\frac{\partial(\rho h)}{\partial x}+2\frac{\partial(\rho h)}{\partial t}\right] \tag{2.13}$$

Reynolds equation allows for the calculation of the hydrodynamic pressure profile for the infinite width of the bearing pad ($B \to \infty$). So the lateral leakages are neglected and overall load carrying capacity is overestimated.

One of the most significant disadvantages of the Reynolds equation solution is assumption of the constant temperature in the oil film. In a real bearing there are temperature variations that have an influence on the viscosity of the oil. Due to this effect the load carrying capacity of the bearing calculated with the use of Reynolds equation is overestimated in comparison to the measurements. Especially in case of large scale bearings where the temperature influence is more significant. Variable viscosity causes also that centrally pivoted pads are able to create load capacity due to 'shifting' pivot point in the direction of the oil film outlet. Due to constant viscosity across the length of the pad tilt angle is also affected. In the real case load capacity of the oil film decreases from inlet to the outlet thus the pad tilt angle is larger.

Another disadvantage is the assumed oil film geometry. The bearing surfaces are assumed to be flat. So there is no possibility to take into account deformations of the bearing elements. Nowadays it is well known [**14**,**23**] that these deformations, elastic and thermal, have significant influence on the bearing operational parameters. In order to take into account these effects calculation program based on Reynolds equation can be coupled with the procedure that estimates changes of the oil film geometry.

Due to these simplifications the bidirectional (symmetrically supported) thrust bearings may not be calculated since the Reynolds theory predicts zero load carrying capacity for such bearings. Although it is a well known fact that due to the influence of variable viscosity and deformations these bearings generate load carrying capacity and work properly. Due to low tilt angles these bearings operate at higher temperatures and lower oil film thicknesses.

Nowadays this solution does not have any practical importance but is very important from historical point of view. Reynolds equation is solved numerically in order to take into account additional effects like more complicated oil gap geometry or variable viscosity in three dimensions.

Since that time a great progress in case of hydrodynamic lubrication has been performed but there is always need of improvement of the design and optimization of the bearing operational parameters and efficiency. The continuous trend of increasing the specific pressure comes directly form the need of reduction of bearing frictional losses. This is especially important in case of pump storage power plants where all losses are to be taken twice. Once during pumping mode and then during turbine mode.

2.3.3 Currently modeled effects

Steady state calculation

Steady state hydrodynamic calculation tools find the solution (operational point) for given constant operational parameters and are, until now, the most common approach to bearing calculations. Such an approach has consequently been used for the bearing calculation since 1950's and is currently recognized as the standard calculation method. However for large hydrodynamic bearings thermal inertia of the structure may be so huge that the bearing never reaches the equilibrium state. The operational parameters can change before the thermal balance occurs.

Currently used calculation methods for hydrodynamic lubrication can be divided into following groups:

- HD (Hydro-Dynamic),
- THD (Thermo-Hydro-Dynamic),
- TEHD (Thermo-Elasto-Hydro-Dynamic).

In order to simulate, in a realistic way, hydrodynamic bearing operational conditions it is necessary to take into account several physical phenomena. The most obvious part of the model is the hydrodynamic film, which most commonly is calculated with the use of finite differences or finite elements methods that solve generalized Reynolds equation for the flow and energy equation for heat generation. This is HD (Hydro-Dynamic) solution with isothermal flow assumption. Currently used codes take into account oil heating and variable viscosity (as a function of temperature) and thus they are commonly called THD (Thermo-Hydro-Dynamic). In this group of codes temperature field can be treated either in 2 or 3 dimensional way. In the first case temperature may vary only along the length and width of the oil film but remains constant through the oil film thickness. The second approach allows for variations of the temperature field in all three dimensions.

More advanced codes, so called TEHD (Thermo-Elasto-Hydro-Dynamic) use different methods to calculate thermal and elastic deformations of the bearing components (both pad and runner or pad only). Deformations can be calculated either analytically or numerically (also with the use of commercial software). Recent investigations showed that for large bearings runner deformations have to be taken into account due to large influence on the fluid film and consequently on the whole bearing.

The Reynolds theory is still commonly used since it gives reliable results in case of the hydrodynamic pressure profile [**49**]. The influence of other effects (e.g. temperature and viscosity fields) that affect the bearing operational parameters is taken into account usually in the numerical way. The bearing sliding surface is divided in a certain number of nodes (two or three dimensional grid) and the operating parameters are calculated for each of them.

FEM analysis of a thrust bearing has been presented in [**50**]. In this case authors modeled the structural parts of a bearing with the use of 3 dimensional model which was combined with hydrodynamic oil film model built with 2 dimensional fluid elements.

The main disadvantage of these methods is the treatment of the oil film space separately from the space between the pads. As far as effects in oil film are simulated accurately they are based on the boundary conditions that are located on inlet and outlet faces. The significant weakness of this approach is assumption of the oil film inlet temperature. This value is strongly affected by the proportion between cold oil from the bearing bath and warm oil that comes from the preceding pad. This simplification has significant influence on the estimation of the oil film inlet temperature, which is an input parameter in such analysis [**51**]. In this work the author showed an approach to solve the mixing of the oil between the pads in a numerical way. This allows to avoid any assumptions considering the parameters of the oil film inlet like temperature and velocity profiles or pressure value.

Heat transfer effects

The easiest approach to the heat transfer analysis in the oil film is the assumption of the isothermal oil flow [**52**]. The temperature value is either assumed a priori or evaluated based on the overall heat balance in the whole bearing. This approach does not however take into account variations of the viscosity as a function of temperature. The so called effective viscosity is assumed once for each iteration for the whole oil film area. Constant viscosity assumption does not give good agreement with measurements since it has an influence on the tilt angle of the pad.

Assumption of the adiabatic oil flow means that both sliding surfaces are adiabatic boundaries and no heat transfer through them is possible. This assumption is made in all bearing calculation programs that assume two dimensional temperature filed in the oil film. Constant oil film temperature means automatically no heat flow in this direction. In Table 2.4 there is comparison of the heat flow rates for different bearings [**53**]. Heat balance for the oil film volume is given as a sum of all heat flows on the all oil film boundaries (the pad and the runner sliding surfaces, lateral surfaces and the oil film inlet and outlet).

Table 2.4. Heat flow rates for different thrust bearings, comparison of the temperature increase between calculation and measurement [53]

No.	Load	Speed	Calculated ΔT	Measured ΔT	Heat flow			
					Side	Pad	Runner	Groove
	[MN]	[rpm]	[°C]	[°C]	[%]	[%]	[%]	[%]
1	3	95	15.7	16.5	36	27	16	21
2	4	360	44.5	45	73	14	12	4
3	4	257	34.7	35	78	14	9	1
4	7.9	257	45.2	41	53	17	12	4
5	9.6	95	24.9	24	14	28	17	40
6	12	200	38.7	41	84	12	7	0
7	20.5	90	27	33	18	30	11	43
8	37	450	15.5	15.5	32	27	25	13

According to this comparison it is clear that adiabatic oil film assumption can lead to high inaccuracies since the heat flow through both sliding surfaces can, for certain conditions, exceed 50% of the total power loss (heat generated in the oil film). On the other hand such an assumption leads to overestimated oil film temperatures.

The most advanced calculation models take into account thermal flow through the sliding surfaces of the pad and the runner. This allows not only for more appropriate calculation of the temperature field distribution in these elements but also for calculation of thermal inertia effects. The power loss created due to the friction in the oil film is divided into three components. For high speed thrust bearings the main part (approximately $90-95\ \%$) is taken away with the oil flow. This is due to high Prandtl number of the lubricant (approximately equal to 650) and a very high intensity of the oil flow. The thermal boundary layer is much thinner than the velocity boundary layer. The rest of the heat is transported, by the means of convection and conduction, through the bearing sliding surfaces – pad and runner.

Realistic analysis of the heat transfer in the bearing structure is a complex problem. Heat is transported by the means of conduction and convection.

Conduction of heat is described by the Fourier law which for one dimensional transient case can be written in form of the heat diffusion equation:

$$\frac{\partial^2 T}{\partial x^2} = \frac{1}{a}\frac{\partial T}{\partial t} \tag{2.14}$$

where a is thermal diffusivity and is defined as:

$$a = \frac{\lambda}{\rho\, c} \tag{2.15}$$

Heat conduction occurs in all structural parts of the bearing. In case of heat transfer in the oil one cannot speak about conduction but rather convection due to the very intensive flow of the oil. Typically convection can be divided into two main groups: natural and forced [**54**,**55**]. In case of the hydrodynamic lubrication only the second one occurs.

Convectional heat transfer can be calculated by:

$$q = \alpha \cdot (T_{wall} - T_{bulk}) \tag{2.16}$$

In case of the convectional heat transfer rate the main difficulty is estimation of the convection coefficient α. Just in one dimensional case it is a function of several parameters:

$$\alpha = f(\lambda, x, \rho, c, \mu, u_\infty)$$

Convection coefficient depends on the relation between thicknesses of the velocity and temperature boundary layers. The velocity field of the fluid, the velocity boundary and character of the flow (either laminar or turbulent) layer can be described by the dimensionless Reynolds number Re.

$$Re = \frac{\rho \cdot U \cdot L}{\mu} = \frac{inertial\ forces}{viscous\ forces} \tag{2.17}$$

where the Reynolds number is defined as:

$$Re = \frac{R^2 \cdot \omega}{\nu} \tag{2.18}$$

According to the boundary layer theory [**56**,**57**,**58**] the velocity boundary layer may have significant thickness.

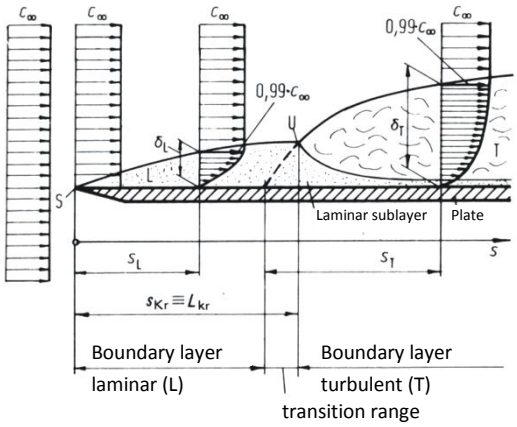

Figure 2.31. Velocity boundary layer thickness [58]

According to the one dimensional boundary layer theory its thickness is a function of the length and can be estimated according to the following formulas, respectively for laminar and turbulent flow regime:

$$\delta_L = 5 \cdot \sqrt{\frac{s_{cr} \cdot L_{cr}}{Re_{cr}}} \sim s_L^{0.5} \tag{2.19}$$

$$\delta_T = 0.37 \cdot \sqrt[5]{\frac{s_{cr}^4 \cdot L_{cr}}{Re_{cr}}} \sim s_T^{0.8} \tag{2.20}$$

The growth of the turbulent velocity boundary layer is much faster ($\delta_T \sim s_T^{0.8}$) than that of the laminar one ($\delta_L \sim s_L^{0.5}$).

For the disc with outer radius R which rotates in the oil the thickness of the turbulent velocity boundary layer can be evaluated with a following form (verified experimentally):

$$\delta = \frac{0.526}{\sqrt[5]{Re}} \cdot R \tag{2.21}$$

Critical Reynolds number (laminar – turbulent transition) is in this case:

$$Re_{cr} \approx 3 \cdot 10^5 \tag{2.22}$$

For the thrust bearings used for hydro applications this velocity boundary layer has thickness of several tens of millimeters. In the Figure 2.32 the boundary layer thickness is shown for a given range of rotational speeds and radii. Curves are limited to the turbulent range only since only this flow regime seems to exist in the real bearing housings (between the pads). The development of the boundary velocity layer depends on the distance between the pads. If it is shorter than the defined sum of the lengths ($s_{cr} + s_T$) in Figure 2.31 then its thickness does not reach the fully developed value.

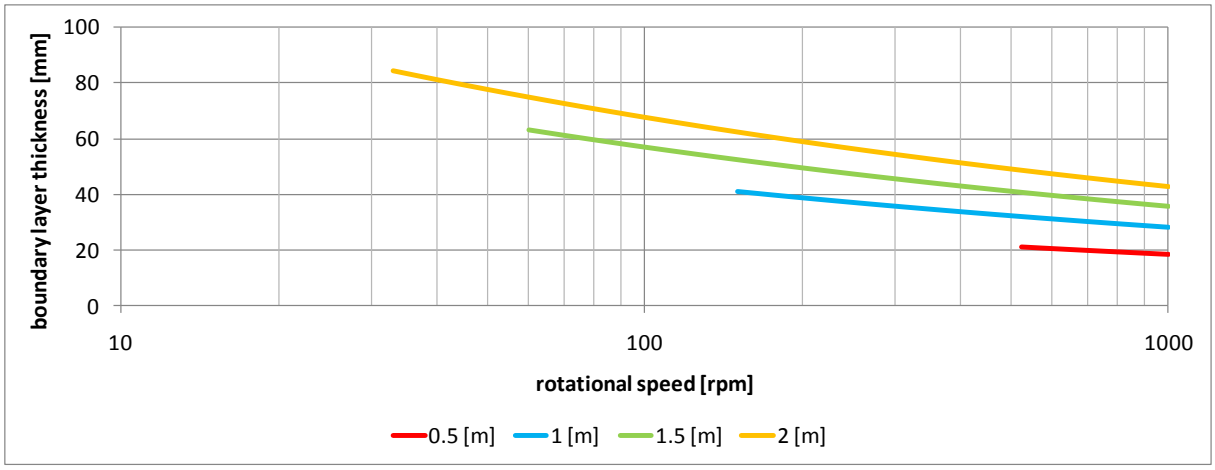

Figure 2.32. Turbulent velocity boundary layer for different runner radii according to [58]

The ratio between thicknesses of the velocity and temperature boundary layers is defined by dimensionless Prandtl number Pr.

$$\mathrm{Pr} = \frac{\nu}{a} = \frac{c \cdot \mu}{\lambda} = \frac{viscous\ diffusion\ rate}{thermal\ diffusion\ rate} \tag{2.23}$$

Pr is a physical property of the fluid and varies from 10^{-2} for liquid metals up to 10^{5} for liquids with very complex molecular structure e.g. oils made of long-chain hydrocarbons. High value, like in case of the oils, means that thermal boundary layer is much thinner than the velocity boundary layer. Heat convection is more intensive than heat diffusion (most of the heat is taken away with passing by fluid) [**55**].

For ISO VG46 oil at the temperature 40 °C:

$$\mathrm{Pr}_{VG46} = \frac{2113.5 \cdot 0.0398}{0.123}$$

$$\mathrm{Pr}_{VG46} = 683.88$$

Finally the convection can be defined by the dimensionless Nusselt number Nu which is a function of the two previously described dimensionless numbers Re and Pr.

$$Nu = f(Re, Pr)$$

$$Nu = \frac{\alpha \cdot L}{\lambda} = \frac{convective\ heat\ transfer}{conductive\ heat\ transfer} \tag{2.24}$$

$L\ [m]$ is the characteristic length of the body, e.g. length of the plate, diameter of the cylinder, etc.

The Nusselt number is inversely proportional to the thickness of the thermal boundary layer:

$$Nu = \frac{L}{\delta_t} \tag{2.25}$$

For example for laminar incompressible case of the flow Nu is defined in the following way:

$$Nu = 0.332\ Re^{1/2} Pr^{1/3} \qquad \text{for} \qquad 0.6 \leq Pr \leq 50 \tag{2.26}$$

or

$$Nu = \frac{0.3387\, Re^{1/2} Pr^{1/3}}{(1+(0.0468/Pr)^{2/3})^{1/4}} \qquad \text{for} \qquad Pr > 100 \tag{2.27}$$

From this brief summary on the boundary layer theory one can see that convection effects can be analyzed in an analytical way. On the other hand, hydrodynamic lubrication is a situation where viscous heat generation plays a key role. Thus the thermal boundary layer is strongly influenced by this heat generation and does not look like the thermal boundary layer in case of normal forced convection. Heat is not only transported but also generated in the boundary layer. In this case it's thickness is mainly defined by the minimum oil film thickness. It is also worth to mention that the direction of the heat flow depends on the position. There is a high temperature difference between inlet and outlet of the oil film. In the inlet area oil film is cold and pad due to heat conduction (in its volume) warm so the heat goes into the oil film. One can observe the opposite situation one can observe in the outlet area where to oil has highest temperature and heat flows into the pad and runner. From this point of view it seems that the temperature field distribution (and viscosity) in this layer should be estimated numerically.

On the other hand it is clear that in the oil film the boundary layer is far different and in most cases it is laminar due to low oil film thickness. However for the journal bearings authors [**59**] allow possibility of the turbulent oil film velocity field, especially in the inlet zone where the oil film thickness has its highest values. This effect is also known from the rapid fall of the bearing temperature with the increase of speed which is explained by the transition of the flow regime from laminar to turbulent (Figure 2.33 after [**60**]). Measurements taken for the $17\ inch$ thrust bearing indicate transition from laminar to turbulent flow regime for the sliding speed of approximately $60\ m/s$. Such values are within the range of high speed hydro generators that are being built nowadays. Such effects were also confirmed by other researchers [**61**,**62**]. Measurements presented by Mikula for tilting pad thrust bearings also indicate that such effects are possible for thrust bearings.

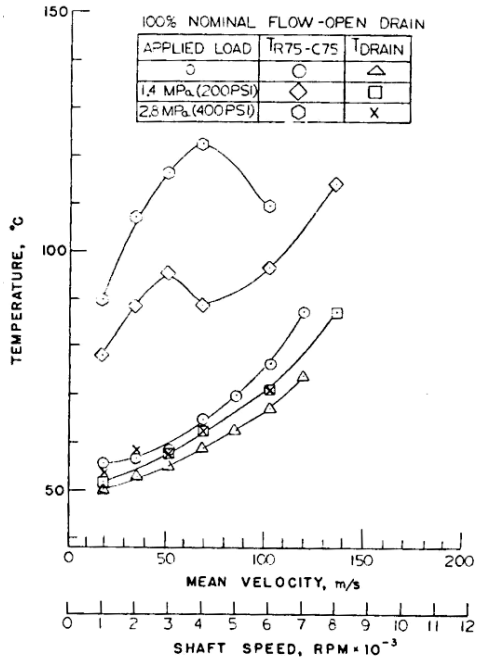

Figure 2.33. Decrease of the bearing temperature due to turbulent oil flow regime in the oil film [60]

Warm oil carry over effect

The importance of the effects between the pads has been indicated in [**63**]. The bearing pads are arranged in such way that the outlet of the preceding pad is located close to the inlet of the following one. The space between the pads is usually as small as possible in order to increase the area of the bearing. The surface covered by pads is approximately equal to $80\ \%$ of the runner area. Due to this reason warm oil that comes out from the preceding pad goes directly into the inlet of the following one. This effect increases inlet temperature T_{in} in reference to the cold oil temperature T_{cold} (see Figure 2.34). Estimation of the oil film inlet temperature has significant influence on the remaining part of the calculation since it is a sort of reference level for the oil film. Appropriate estimation of this temperature has influence on the overall accuracy of calculation.

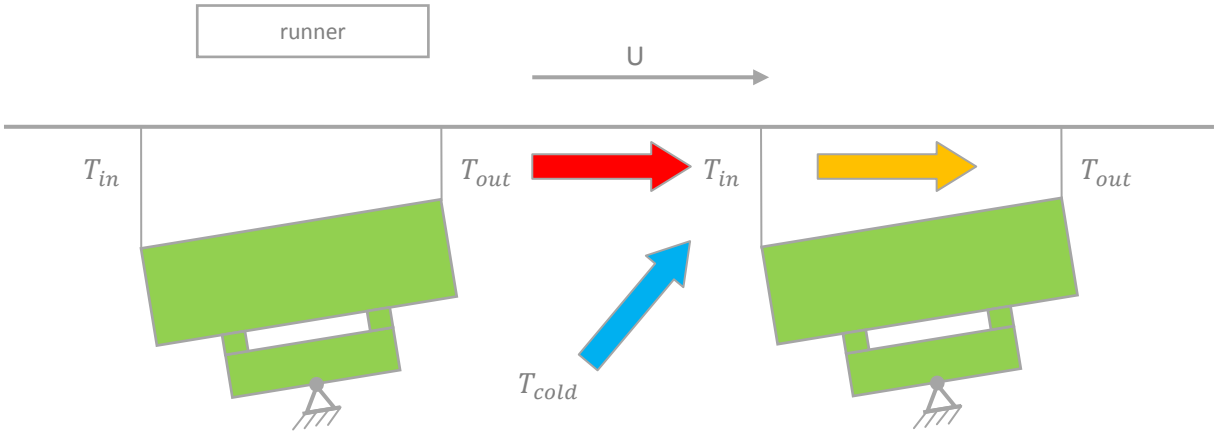

Figure 2.34. Warm oil carry over phenomena after [14]

The ratio between T_{out} and T_{cold} depends on many factors. Among them we can distinguish the most important ones:

- distance between the pads,
- sliding velocity,
- way of delivering the cold oil from the cooler (LEG (Leading Edge Groove), distributors, etc.),
- specific load of the bearing, tilt angle, pivot position.

Ettles [**14**,**64**] introduced warm oil mixing factor k that allows to estimate oil film inlet temperature T_{in} with the use of the iterative formula (2.28).

$$T_{in} = T_{cold} \cdot \left(\frac{1-k}{1-0.5\,k}\right) + T_{out} \cdot \left(\frac{0.5\,k}{1-0.5k}\right) \tag{2.28}$$

The mixing factor k can be estimated with the use of the diagram in the Figure 2.35 which is based on measurements. In this analysis the only parameters taken into account were sliding speed and distance between the pads. Oil film inlet temperature T_{in} has to be estimated in an iterative way since oil film outlet temperature T_{out} also depends on it.

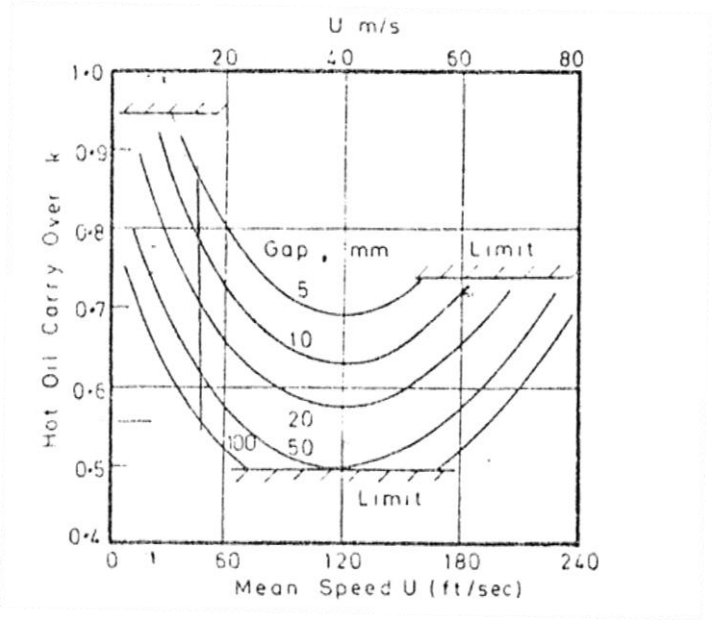

Figure 2.35. Warm oil carry over factor according to [14]

From this diagram (Figure 2.35) one can notice that the distance between the pads and the sliding speed are the key components for the warm oil carry over effects. Thus the mixing has to be considered for each bearing design separately.

There were attempts to decrease the hot oil carry over by mounting scrapers on the outlet of the pad that "scratch" the warm oil layer from the runner surface. For example in [**65**,**66**] one can find an example of such device mounted between the tilting pads of a journal bearing. In this case scraper is combined with oil injection. The results of such methods remain controversial since the hot oil layer is very thin. The thermal boundary layer on the runner is very thin and does not exceed $0.5\ mm$ (high Prandtl number for the oils). These "devices" may work properly after mounting them in the bearing housing but wear of the sliding surface may reduce their efficiency after certain time of operation. They can also produce additional power loss and cause warming up the boundary layer on the sliding surface. The runner surface itself is also warm ($70 - 80\ °C$) and due to rotation has a constant (or almost constant) temperature in the tangential direction so it causes warming up of the oil layer also between the pads and behind the scraper.

Warm oil carry over effect can be potentially reduced by directed lubrication devices mounted in the space between the pads but according to the literature and common knowledge these attempts do not allow to influence the operational parameters of the bearing in a significant way [**51**]. The main reason of the lack of the influence is the oil bath in the bearing housing. Therefore the oil flow from the injecting hole cannot "reach" the sliding surface of the runner and there is no influence on the mixing of the warm oil between the pads. Thrust bearings of large hydro generators are immersed in oil bath in order to assure their safe operation and to fulfill contractual requirements.

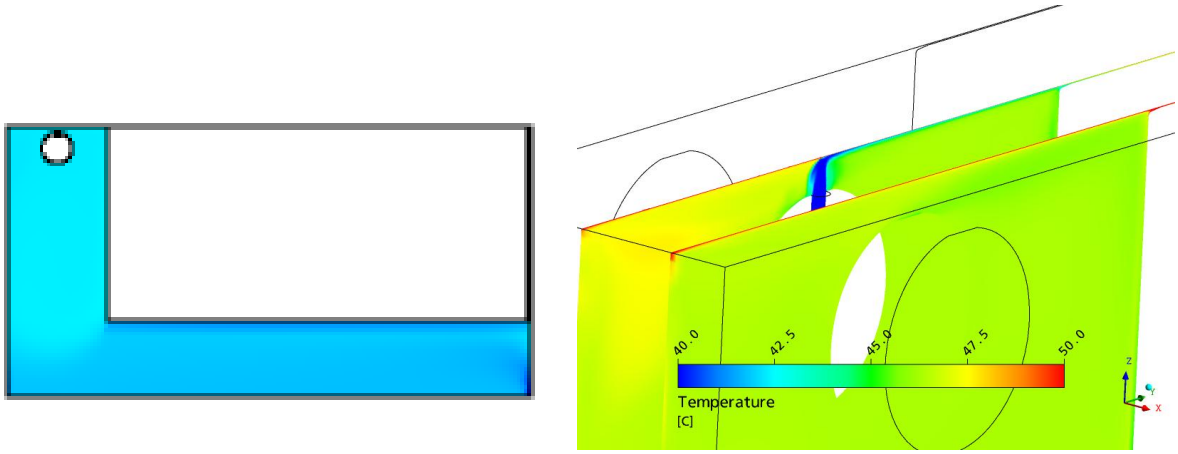

Figure 2.36. Oil injecting on the runner sliding surface, CFD simulation [51]

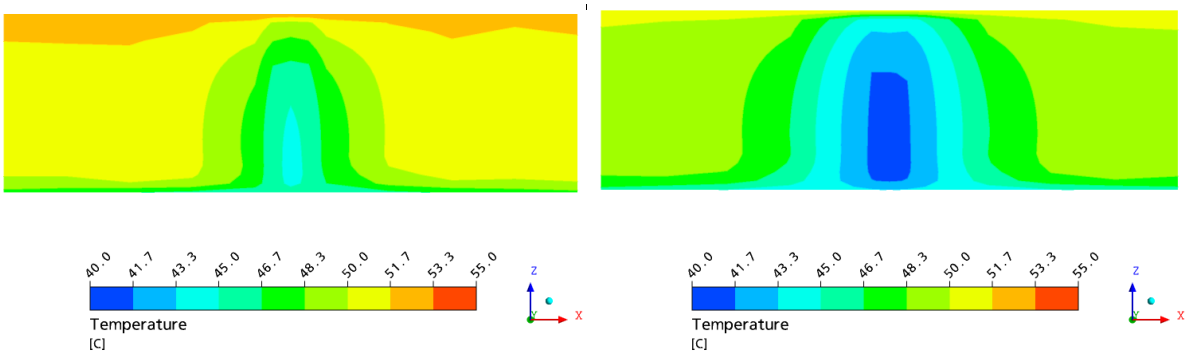

Figure 2.37. Oil injecting on the runner sliding surface, influence of the oil flow (330 and 660 l/min) on the oil film inlet temperature distribution [51]

In Figure 2.37 one can see the influence of the injected oil flow on the oil film inlet temperature. Increase of the injected oil flow from 330 to $660\ l/min$ results in change of the average oil film inlet temperature from 49.4 to $46.2\ °C$. There remains always a thin layer of the warm oil close to the runner sliding surface. Also in the radial direction influence on the oil film inlet temperature has only local character. Space between injection points remains almost not influenced at all.

The aim of all these attempts is to decrease the oil film inlet temperature – to make it possibly close to the cold oil temperature. Thus the best way to reduce warm oil carry over effects is “dry” bearing housing with oil presence only in the oil film. Together with directed lubrication methods one can assure delivery of the cold oil directly to the oil film inlet without negative influence of any mixing effects.

The above results lead to an idea that oil supply could be realized not with the use of injection holes but with sort of an oil knife (or several knives). Such linear oil injection would deliver cold oil not only on several spots on the leading edge but on its whole radial length.

Deformations of the pad and runner

It is well known that the pad elastic and thermal deformation has essential influence on the bearing performance [**14**,**28**]. Tanaka [**59**] indicated that in order to predict the load carrying capacity of the thrust hydrodynamic bearing the thermal and elastic deformation of the runner has to be taken into account. Otherwise the oil film thickness profile could be overestimated. For this reason it seems

necessary to include this effect in a modern calculation tool for the hydrodynamic thrust bearing. In Figure 2.38 visual demonstration of the expected shape of the deformations and tilting of the pad is shown (for counterclockwise direction of rotation).

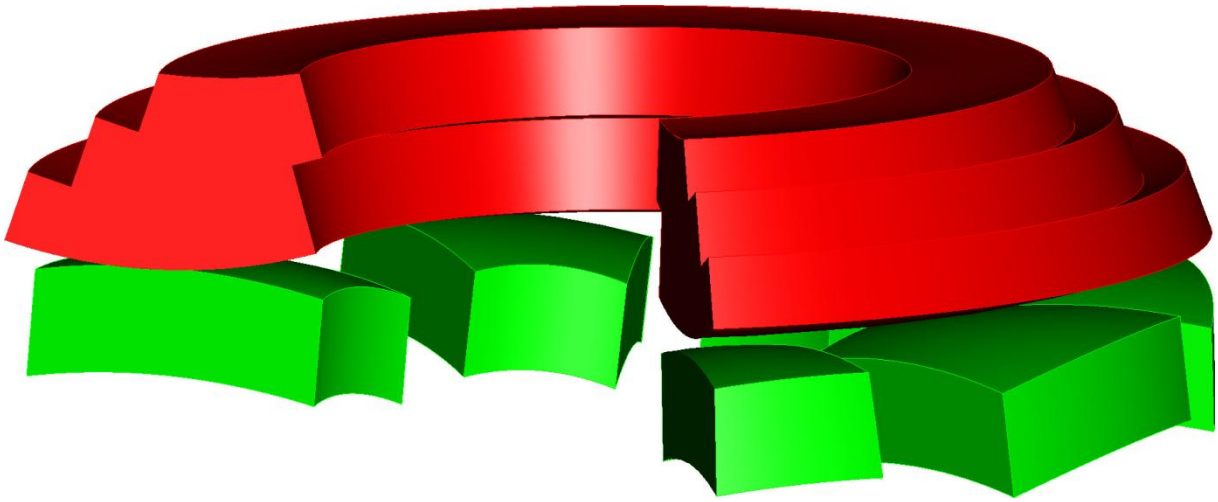

Figure 2.38. Graphical representation of the possible deformations of the bearing elements

Both analytical and numerical (FEM) approaches are used in order to estimate deformations of the bearing elements.

The analytical estimation of the deformations assumes their shape (sphere for the pad and torus for the runner surface). Since the elastic deformation is very small the deformation is based mainly on the distribution of the temperature field in the bearing elements. The main unknown for such calculation are the thermal boundary conditions. Many researchers propose their own assumption of convection coefficients on the walls of the pad and runner that are not connected with the oil film. The assumed values vary in a certain range and may have an influence on the obtained temperature field distribution and further on the deformation of the element. Until now it is not clear what the real conditions on these surfaces are. According to [**67**] these coefficients of free walls of the pad may vary within the range $1 - 10\ kW/m^2\ K$ depending on the bearing arrangement. Additionally it is very probable that these coefficients have different values at different walls of the bearing pad.

Runner boundary condition is also essential for the appropriate estimation of the thermal deformation of its sliding surface. This input parameter has a significant influence on the temperature distribution and further on the resulting deformation. The estimation of the temperatures on the cylindrical walls that rotate in oil and air is very difficult. It may vary for different bearings due to design and operational conditions like rotational speed or oil temperature in this area. The estimation of these temperatures (boundary conditions) can be most easily done with the use of the measurement data.

Until now many researchers have not been taking deformation of the runner surface into account regardless the fact that it may have significant influence on the obtained results of the simulation. Deformations play a significant role for large sized bearings like the ones made for vertical hydro generators. Ettles [**14**] showed that there is a significant influence of the scale factor on the bearing deformations. He demonstrated that linear a increase of the bearing dimensions leads to more

severe operating conditions at the same specific load level, which means that operational limits of the large hydrodynamic bearings are much lower than for smaller ones (see Figure 2.39).

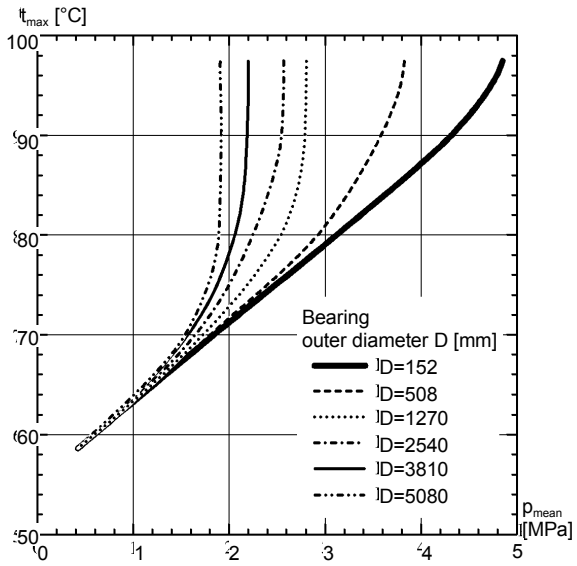

Figure 2.39. Scale factor influence on the bearing load carrying capacity [14]

These deformations are even more important for centrally pivoted pads which was shown by Raimondi [**16**]. He showed that centrally pivoted pads need certain amount of thermal deformation in order to generate load carrying capacity. It is well known that such bearings have zero load carrying capacity according to the Reynolds theory but on the other hand they work properly in many machines. The optimal relative deformation according to Raimondi is within the range between 0.6 and 0.9. This shows that it is essential to decrease the pad thermal deformation in order to increase the load carrying capacity of the bearing. There are several ways to obtain this effect [**14**]. On the other hand side this deformation (due to compensation) may not be too small. This shows how important it is to optimize deformations for each specific case during design of the new bearing.

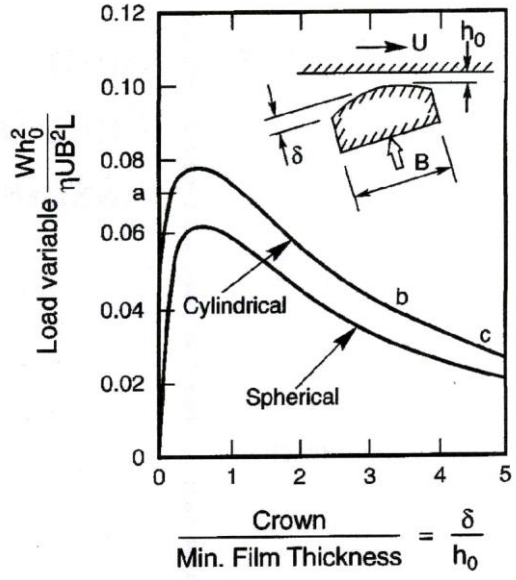

Figure 2.40. Influence of the relative pad deformations on the load carrying capacity of the centrally pivoted pad [16]

The thermal deformations of the pad depend on its size. According to the following formula one can see that in order to obtain similar thermal deflection for larger bearings it is necessary to increase the pad thickness not linearly with the geometrical scale factor. For this reason larger bearings have lower allowable operating specific pressures than the smaller bearings.

$$\delta_T = \frac{B^2 \cdot \lambda \cdot (T_{max} - T_{min})}{8 \cdot H} \tag{2.29}$$

For optimum load carrying capacity (marked by 'a') of a bidirectional thrust bearing the δ_T should be approximately equal to the minimum oil film thickness h_0. As the h_0 may vary for different operational conditions it is necessary to assure during design of the bearing that this ratio remains close to unity. At the same time one can notice a rapid decrease of the load carrying capacity of the pad for higher values of the deformations. This may occur for example during startup when the sliding surface reaches its operating temperature very quickly and the backing of the pad remains cold (marked by 'b'). The process may become also unstable since the decreased minimum oil film height leads to higher temperatures and higher thermal distortion of the pad (marked by 'c'). Finally the seizure and plastic flow of lining material may occur as in the case shown in Figure 2.41. The damaged area located in the middle of the pad indicates that the pad was distorted heavily during operation.

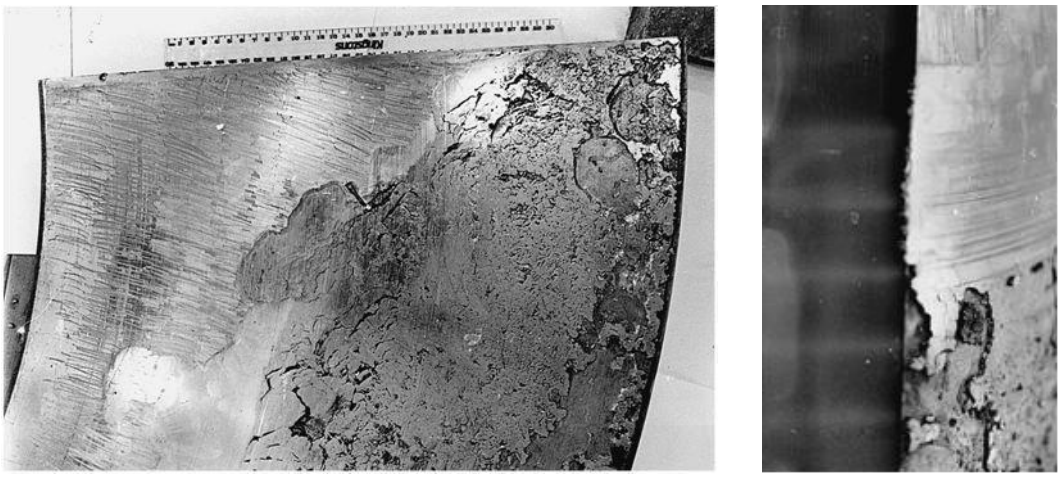

Figure 2.41. Damaged sliding surface due to overload and loss of the load carrying capacity [4]

2.3.4 Treatment of the thermal effects in the oil film

Isothermal oil film solution

One of the rather conservative calculation methods is the one defined in the German Standard DIN. The main assumptions made in this method are similar to those made by Reynolds. Additionally heat balance is taken into account in order to estimate average oil bath temperature. The, so called, effective viscosity is evaluated but the calculation is still treated as an isothermal one. Since the viscosity is assumed to be constant it is not possible to calculate with this method centrally pivoted bearings. Nevertheless it is a standardized method and some rough approximation of bearing operational parameters can be made. In Figure 2.42 there is diagram presented that allows for the estimation of the load carrying capacity of pivoted bearing pads. This method is based on numerical solution of the Reynolds equation for a finite width of the bearing pad B.

For a given pivot tangential position and B/L ratio it is possible to estimate the load carrying capacity F^*. According to this result one can calculate the minimum oil film thickness h_0 with the use of the following formula. Where Z stands for number of bearing pads.

$$F^* = \frac{F \cdot h_0^2}{U \cdot \eta_{eff} \cdot L^2 \cdot B \cdot Z} \tag{2.30}$$

Additionally single value of effective viscosity η_{eff} has to be evaluated from the heat balance equation. It is based on power loss calculation in the oil film part.

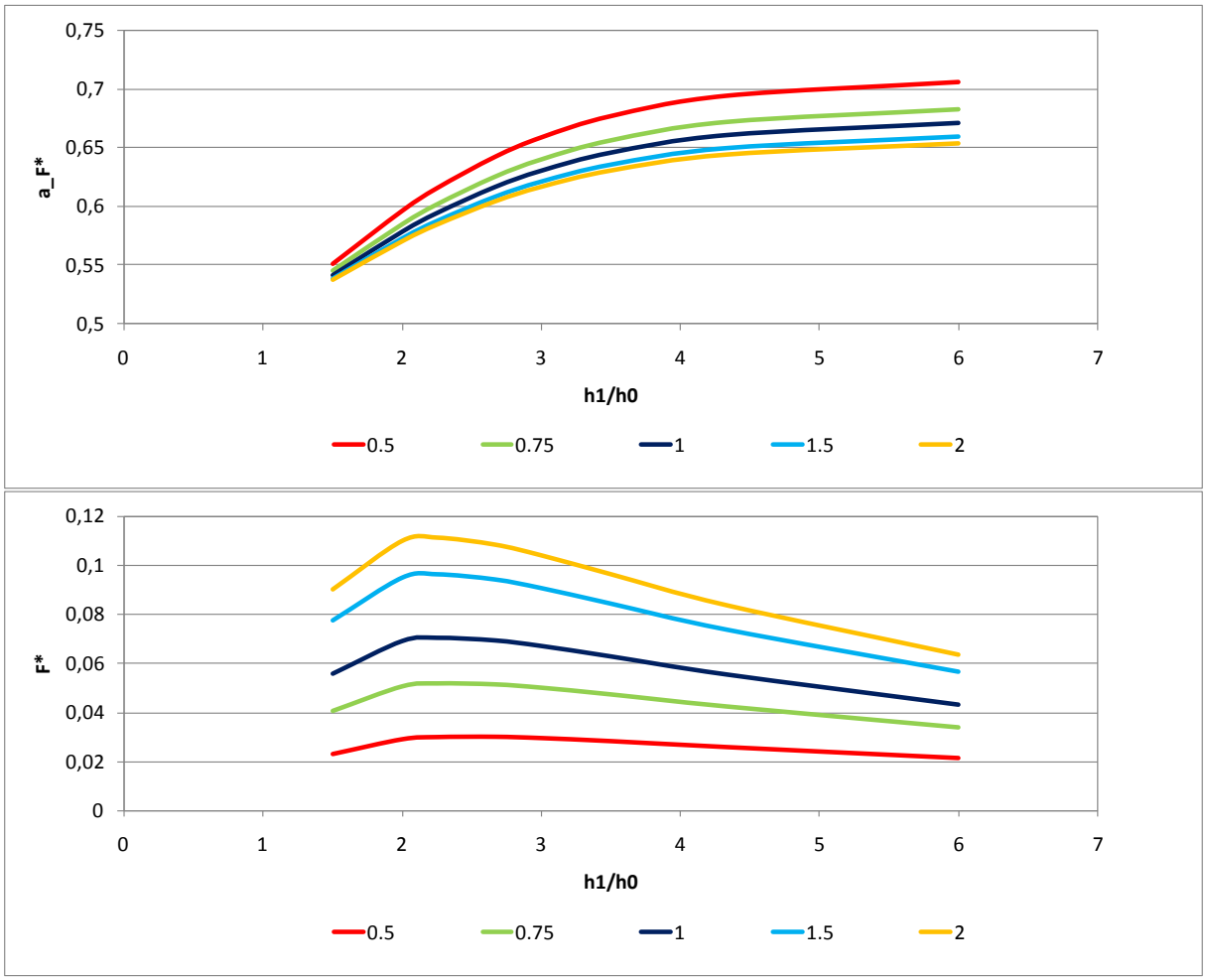

Figure 2.42. Support position (top) and load carrying capacity (bottom) for different tilt parameters and B/L ratios [52]

The theoretical optimum of the load carrying capacity for all B/L ratios is obtained for tilt parameter $h_1/h_0 = 2.18$.

In order to validate the fundamental functionality of the developed model a comparison with DIN results has been performed in Chapter 5. In order to analyze similar flow cases the model has been simplified and in first stage of validation isothermal (constant viscosity) simulation has been performed without the influence of deformations. With such degenerated model comparisons of load carrying capacity are performed for different pivot point positions. It is done in order to check if the tilt angles (balance of the pad, pressure field) calculated by the FSI model are estimated correctly.

2D and 3D temperature field in the oil film

The temperature distribution in the oil film can be treated either as a two or three dimensional problem. The 2D temperature field is a simplification of the physical phenomena with an assumption that the thermal conductivity of the oil is very large (approaches ∞) and the oil film thickness very small. In such case the temperature field may vary only in two directions (radial and circumferential). Temperature is averaged across the oil film thickness. Since there is no thermal gradient across the oil film thickness the heat flow in this direction is also neglected. Thus the sliding surfaces are treated as the adiabatic boundaries. In case of 3D analysis the variable temperature has influence on the physical parameters of the lubricating oil and shape of the velocity field. The most important is the varying viscosity. For example in [**68**] it is stated that this influence is much more important than variations of the density as a function of temperature. In [**67**] one can find a detailed comparison between isothermal, 2-dimensional and 3-dimensional treatment of the temperature field. Authors presented influence of the calculation model on the bearing operational parameters (load capacity $\overline{W}$, friction torque $\overline{F}$ and increase of the temperature $\Delta T = T_{max} - T_{in}$). The analysis was performed without influence of neither elastic nor thermal deformations of bearing elements but due to small dimensions ($R_{in} = 0.16\,m$) most probably this influence would be negligible. An example diagram of this analysis is shown in Figure 2.43. Operational parameters are presented as a function of the rotational speed and minimum oil film thickness.

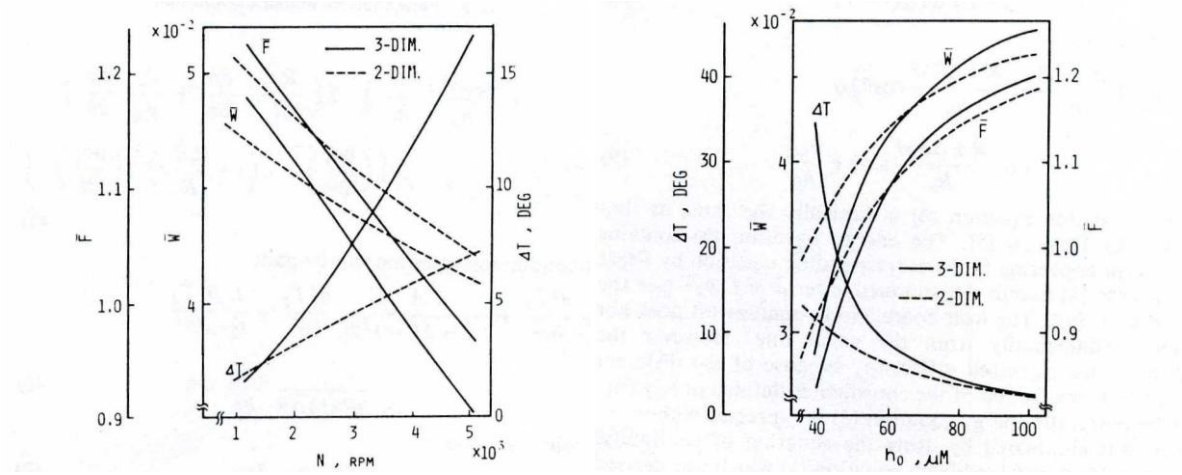

Figure 2.43. Bearing operational parameters as a function of rotational speed and minimum oil film thickness [67]

The authors stated that the agreement between 2D and 3D analysis can be obtained only on one of three results ($\overline{W}$, $\overline{F}$ or ΔT) for a particular speed or minimum oil film thickness. For other two results there is discrepancy in such point. For this reason 2D analysis cannot substitute 3D one. It means that agreement is coincidental at the cross points of the parameter curves.

The authors also analyzed the influence of the pivot point position on the bearing performance. For each model maximum load capacity was found for different tangential pivot positions ($isothermal = 0.395$, $2D = 0.407$, $3D = 0.388$). The pivot position in this case is defined from the trailing edge. Significant discrepancies can be observed for ΔT for pivot point positions closer to the center of the pad. For middle supported pads these differences can be even higher. It means that the optimization of the bearing design with each of three methods gives different results (see Figure 2.44).

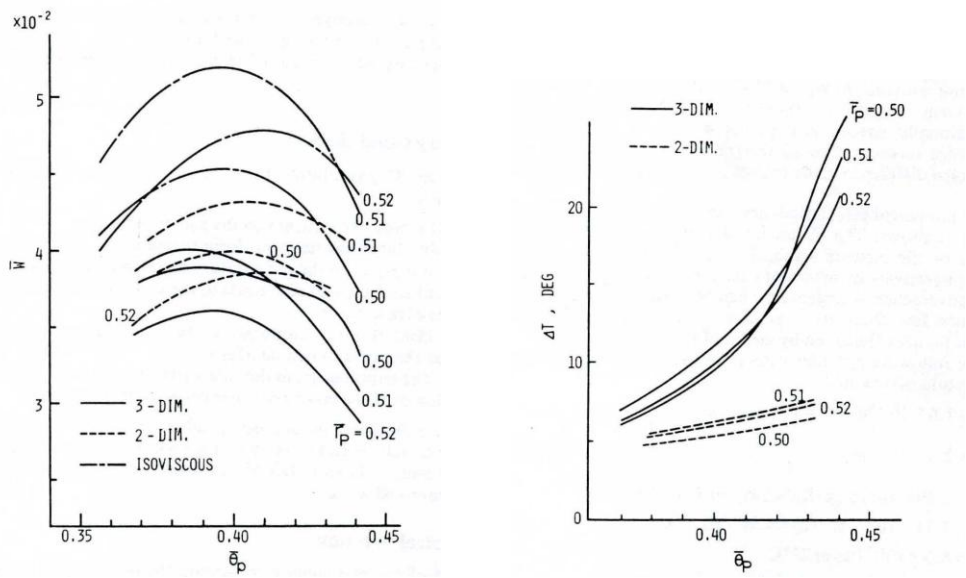

Figure 2.44. Load carrying capacity and temperature raise for different pivot point tangential positions [67]

The main conclusion is that the temperature distribution through the oil film thickness plays an important role in case of hydrodynamic lubrication and thus it should not be neglected. 2D treatment of the oil film temperature leads to underestimated maximum temperature (what is especially connected with seizure) and overestimated minimum oil film thickness. In real bearings it results in smaller safety margin than the calculated one. Such influence can be noticed especially in case of high speed, heavily loaded bearings. Thus 3D analysis allows to design bearings with better accuracy and closer to its operational limits.

2.3.5 Transient effects on hydrodynamic thrust bearings

Transient behavior in case of the large hydrodynamic bearings is a very interesting and important phenomena. Especially during startup of the generator certain conditions may occur that have an essential influence on the operating parameters of the bearing or may even lead to the bearing damage. According to the literature research [**69**,**70**,**71**] transient thermal effects that occur during operation are the most important. In case of large bearings thermal inertia is very large and thus the stabilization of thermal effects may occur long time after the change of operating parameters (e. g. several hours). Ettles writes [**72**]:

Although the importance of thermal transients is recognized at the operations level, the choice of dwell times is arbitrary or empirical. In dealing with practical bearing assemblies there is no guidance available, other than intuition and experience, as to the time scale of thermal "events" resulting from, say, a change of load or speed.

Transient effects that occur during lifetime of the hydro generator that affect the thrust bearing:

- startup,
- shut down,
- runaway and over speed,
- changes of the hydraulic thrust load due to output power variations or other reasons,
- changes of the cold oil temperature due to the cooler operation,
- other disturbances that occur due to improper operation of the machine (hydrostatic jacking system malfunction, etc.).

Startup of a thrust bearing is usually performed with assistance of the hydrostatic lubrication system which generates the pressure outside the bearing with the use of volumetric pumps. Only small bearings with low specific pressure values can be started without hydrostatic jacking system. Also in case pad lining materials with low friction coefficient the bearing can be also started without hydrostatic jacking. Those materials can be PTFE or PEEK for example. Such approach makes the bearing design simpler and more robust since some auxiliaries can be omitted. On the other hand bearing sliding surfaces are subjected to wear during start-up and shut-down when mixed lubrication occurs because of weaker hydrodynamic effects.

Over speed and runaway factors with reference to the nominal speed for different types of turbines are presented in the Table 2.5. Overspeed may occur during shutdown when the electric power is cut off from the generator and the guide vanes close slowly in order to prevent high pressure variations in the penstock (water hammer effect). Runaway is an emergency situation when the electric power is cut off from the generator and the guide vanes remain open. Increase of the speed means in general higher dissipation of the power in the oil due to higher velocity gradient in the oil layer but on the other hand heat exchange due to better convection rate is also greater so the final influence is difficult to predict. Also laminar-turbulent transition may occur during the runaway [**62**]. This effect, well known in case of some bearings, may even cause the decrease of the bearing temperature in a certain range of sliding speeds.

Table 2.5. Overspeed and runaway factors (ALSTOM Hydro)

No.	Turbine type	Over speed	Runaway
1	Pelton	< 1.1	1.8
2	Francis	1.4 – 1.6	2
3	Kaplan	1.4 – 1.6	2.2 – 2.6
4	Bulb	1.6 – 1.8	2.7 – 3.4
5	PSP (pump storage)	> 1.5	1.5

Load and rotational speed are two main factors for the hydrodynamic bearing that define the point of operation for the whole assembly. An example of a registered hydro generator startup is presented in Figure 2.45. At the top diagram three pad temperatures and two oil bath temperatures are given. In the bottom diagram measured oil film thickness on the leading and trailing edge is presented. Both thicknesses were measured by distance sensors mounted on the average diameter of the bearing pad. Measurement was taken every $10\ min$. One can notice that stabilization of the temperature values takes approximately $2\ hr$. In case of distance measurements stabilization takes much more time (approx. $5\ hr$). Both distance sensors indicate interesting behavior after startup. After rapid initial increase both of them decrease. This drop is probably caused by turning off of the hydrostatic jacking system. Afterwards very slow relaxation and finally stabilization occurs. Most probably this behavior is caused by thermal effects in bearing elements. Directly after startup increased thermal crowning could cause lower load carrying capacity and lower oil film thickness.

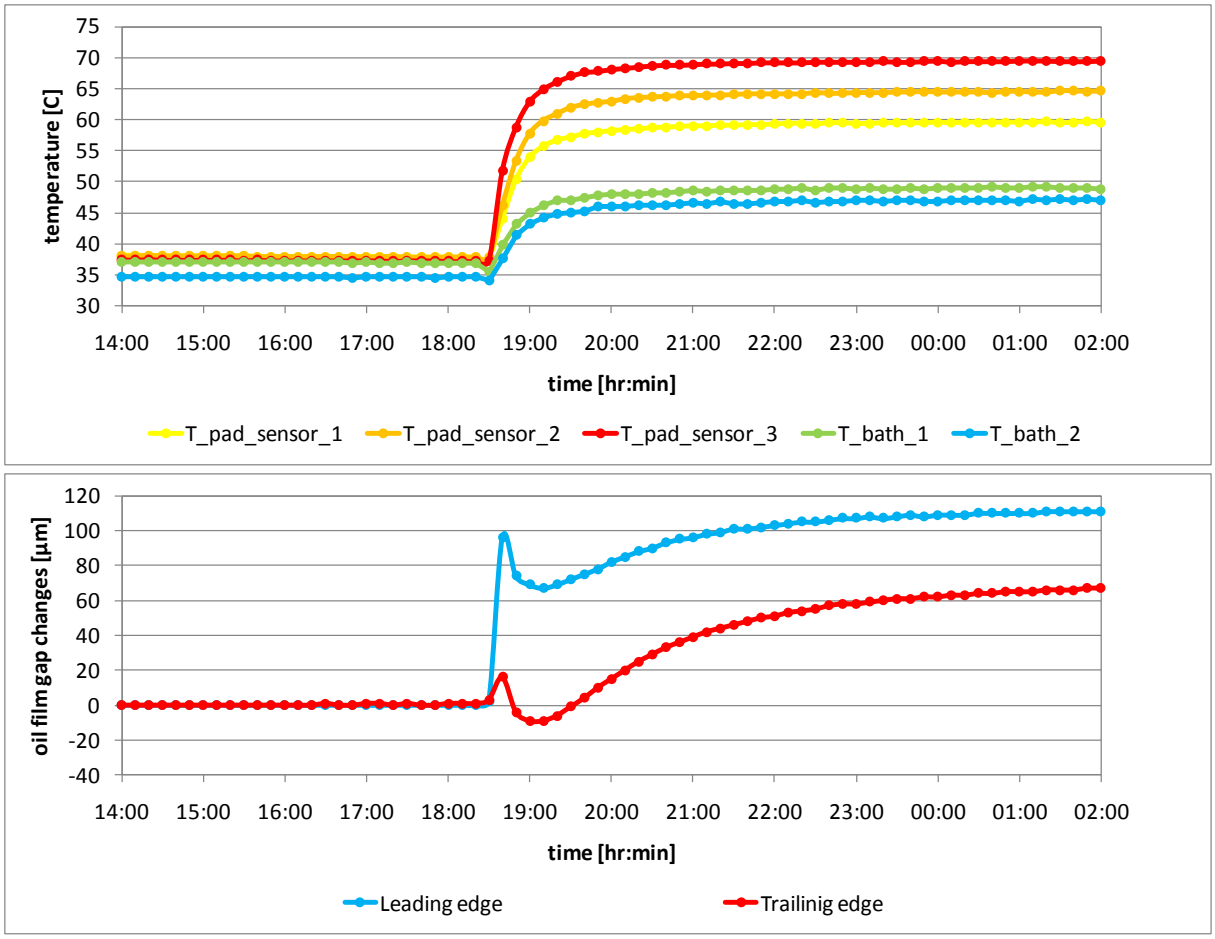

Figure 2.45. Measured changes of the bearing temperature and oil film thickness taken during startup of a hydro generator (ALSTOM Hydro)

According to the literature knowledge there are now calculation tools available that allow for transient thrust bearing simulations [**59**] but they do not treat the bearing calculation in a complex way and are based mainly on the analytical approach in order to simplify the calculation models. In this paper author indicated also that there is still need of development of transient state calculation tools.

Ettles showed [**9**] that the disadvantageous startup conditions may lead to the bearing seizure due the thermal peaking effects (Figure 2.46).

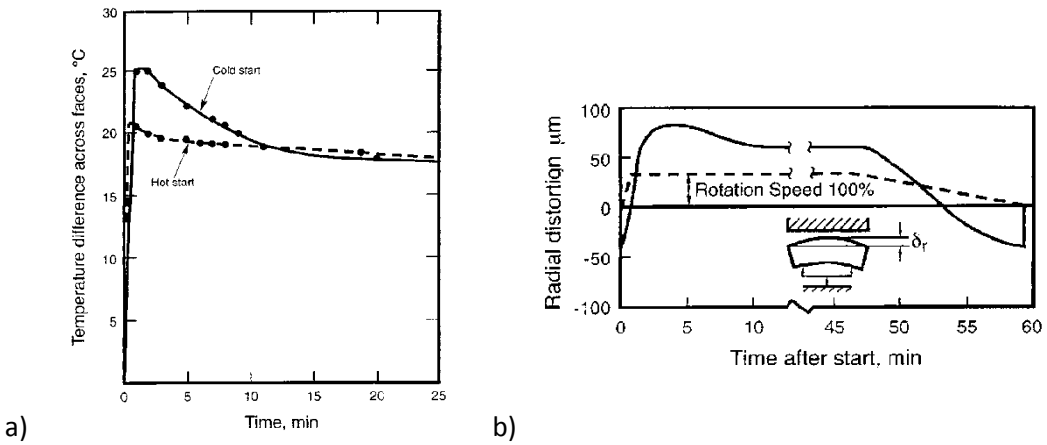

a) b)

Figure 2.46. Transient behavior of the pad during startup after [9], a) measured thermal gradients, b) measured radial deformations of the pad [73]

This phenomena occurs during startup when the sliding surface reaches its operating temperature very quickly and the pad backing still remains cold. In case of the large thrust bearing the time between the startup and stabilization of thermal parameters may take several hours.

Ettles proposed a transient model [**72**] to take into account variations of parameters during operation. In this case instead of tilting pad he analyzed 2 dimensional cantilever bearing pads that are bended due to acting hydrodynamic pressure and thermal gradient. Since the proposed model was 2 dimensional the influence of the runner surface deformation was not taken into account. Also rather than pad tilting the oil film inclination is created by elastic bending of the cantilever.

As a result of transient thermal analysis the author expected low frequency cyclic behavior (bearing natural thermal frequency). For example he expected more efficient oil film gap shape in transient state than in steady state. The result of this investigation was that no oscillatory behavior is apparent. Author indicated also that no such oscillatory behavior ever occur in practical bearing assemblies.

In order to analyze transient thermal behavior Ettles used a finite differences method in the bearing pad, runner and the oil film.

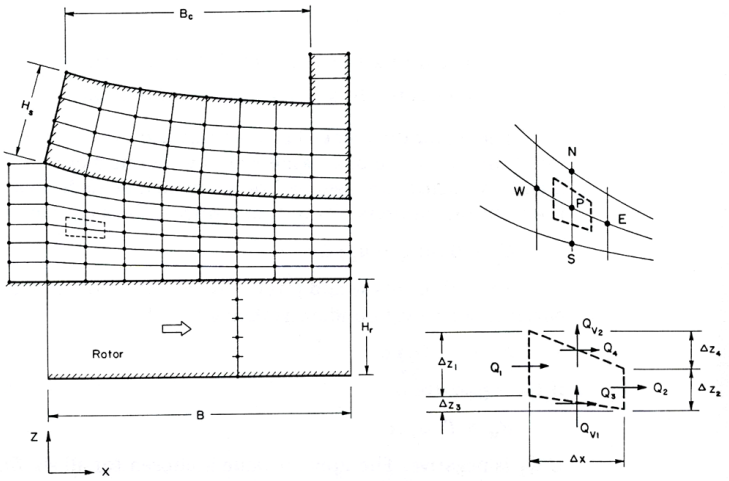

Figure 2.47. Transient 2D model of a cantilever bearing [72], finite differences grid and control volume

An example of the steady state results of the performed analysis is shown in the Figure 2.48. The model is able to predict the reverse flow in a oil film if the inclination h_1/h_0 is high enough.

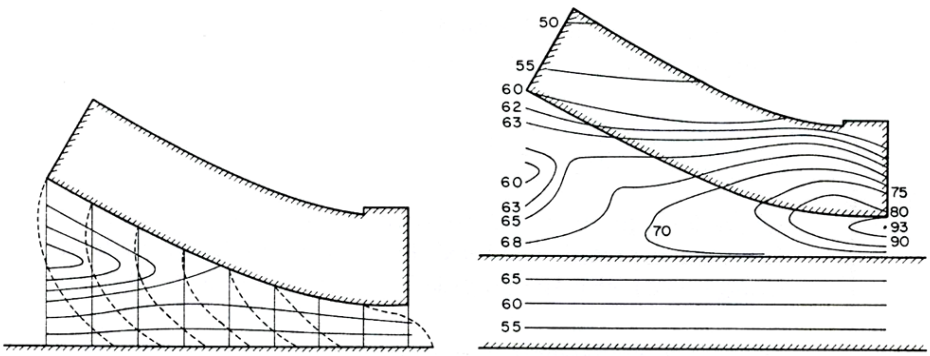

Figure 2.48. Results of analysis, velocity (with reverse flow region) and temperature fields [72]

Ettles introduced a dimensionless Fourier number F in order to estimate the timescale of the thermal peaking. It is directly related to the thickness of the pad according to the following formula [**71**] and allows to describe the transient thermal effects in the bearing pad regardless of the bearing design or dimensions.

$$F = \frac{k}{\rho c}\frac{t}{H^2} \tag{2.31}$$

As a transient change of operational parameters author took under investigation sudden doubling of the bearing load at constant speed. In the Figure 2.49 results are presented as a function of time. Asymptotic values, taken from steady state solution, are also marked. These results come from steady state calculation. Deflection of the pad reaches its maximum for $F = 0.2$ what corresponds with real time value $t = 12.6s$ (pad thickness $H = 30mm$). Further investigations showed that the maximum of thermal deformation occurs for $F = 0.1$. Autor showed also that Fourier timescale is independent from size of the bearing (thickness of the pad). This effect illustrates the Figure 2.49 where maximum of thermal deformations (d/d_{max}) always takes place for $F = 0.086$.

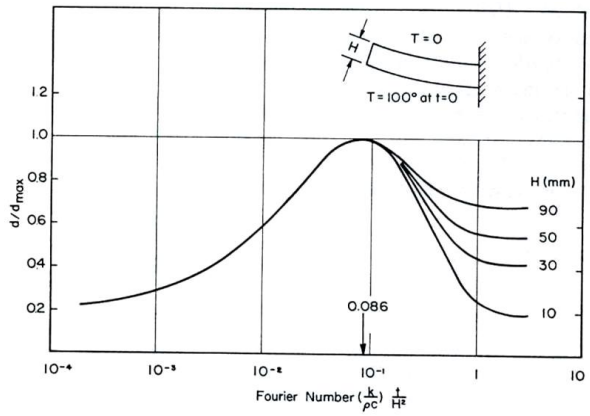

Figure 2.49. The effect of thickness on the thermal deflection [72]

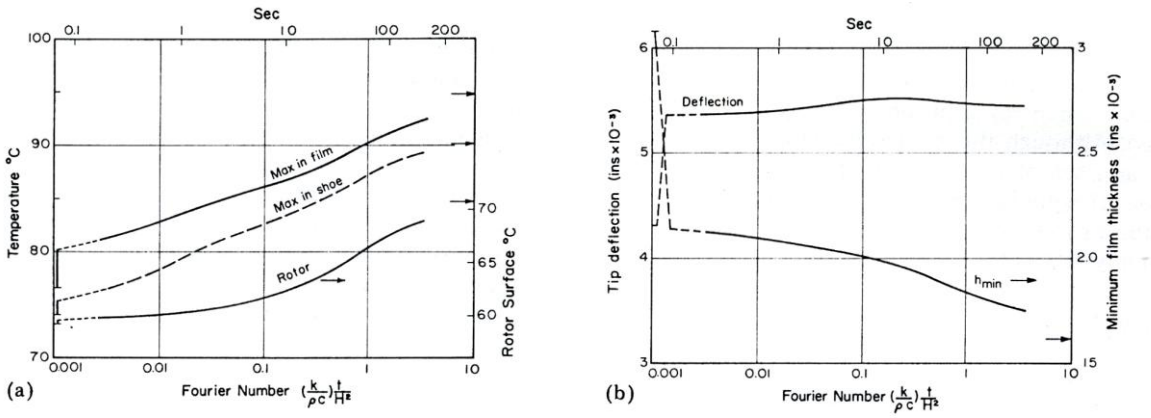

Figure 2.50. Results of analysis, a) temperatures, b) minimum oil film gap and pad deformation [72]

A very interesting conclusion is that thermal equilibrium of the temperature field in the bearing pad may be obtained for a Fourier number of at least 10. This means that large hydro generator bearings, often with pad thicknesses between $200 - 300\ mm$, require a long operation time to obtain thermal balance. In case of PSP power plants operational parameters would most probably change before such an equilibrium occurs. In case of these hydro generators output power is varied simultaneously (adjusted to the network demand). From this point of view it is doubtful that large bearings ever

achieve the thermal steady state since the operating conditions would rather change earlier. In the diagram in the Figure 2.51 one can observe time to thermal peaking ($F = 0.1$) and steady state operation ($F = 10$) as a function of thickness of the pad.

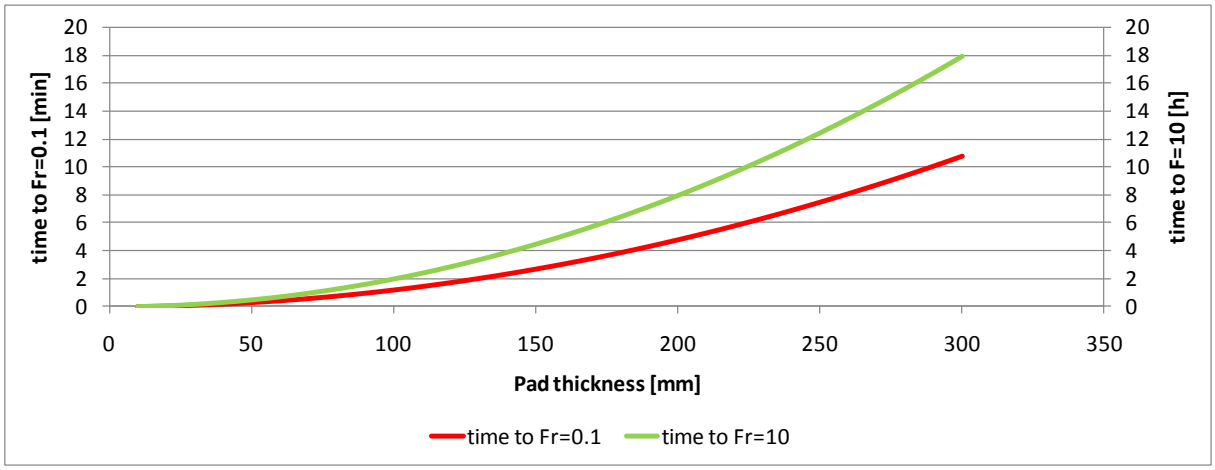

Figure 2.51. Time to maximum deflection of the pad and thermal balance of the temperature field as a function of thickness of the bearing pad

Estimation of the time constant F may help to adjust the time with the hydrostatic jacking operation. According to [**9**] this time should be longer than the thermal peaking time value. This second one occurs approximately for the time constant $F = 0.1$. One can notice that this time linearly depends on the thickness of the pad. Which is one of the main parameters that describe the scale of the bearing design. It is quite strongly connected to the other bearing dimensions. According to the catalogue data (Glacier, Kingsbury, Waukesha) the thickness of the pad equals approximately $H = 0.3B$, where B stands for width of the pad. After [**30**] catalogue values for pad proportions are presented in the Table 2.6.

Table 2.6. Geometrical proportions of the thrust bearing pad according to leading bearing manufactures [30]

Parameter	Company		
	Glacier	Kingsbury	Waukesha
number of pads	7 8 10	6 8	6 8
length / width (L/B)	1	1.33 1	1.33 1
thickness / width (H/B)	~ 0.3	~ 0.33	~ 0.33

In [**9**], Ettles showed a procedure to calculate bearing operational parameters with the use of steady state tool for different rotational speeds as a way to estimate bearing operational parameters. This approach unfortunately leads to an overestimated load carrying capacity of the bearing since the thermal peaking is not taken into account. This behavior may be essential for the thrust bearing operation conditions. In winter when the temperatures are significantly lower it can even lead to a bearing damage (as shown by several examples in [**9**]). There is a common rule that the hydrostatic jacking system is turned off at certain rotational speed, for example at $75\ \%$ of nominal speed. If the start up procedure takes less time than the development of the temperature field the bearing has to operate without hydrostatic jacking assistance during the most difficult phase of operation. This is quite common, since the hydro generators are brought to the operation as quickly as it is possible

and the development of the temperature field takes longer time in case of large sizes of bearing pads.

In order to take all interacting effects into account the fully transient model of the bearing has to be developed. It should take into account inertia effects of the temperature field in the bearing elements. Also input operational parameters have to be treated in a transient way. For example rotational speed, hydrostatic jacking system status, cold oil temperature etc. Ettles [**9**] indicates that transient effect may be very important for the operating conditions if the bearing sizes are large enough. Pad thermal peaking that occurs especially during so called cold startup shown in that paper is a quite common effect. The sliding surface reaches high temperature a few seconds after startup while the pad backing remains cold for a long time. This delay results in higher temperature gradients through the pad thickness and finally in significant thermal distortion of the pad.

Start up simulation would be a useful tool in these cases that would help to simulate the bearing behavior under various conditions. In order to calculate the fully transient behavior of the thrust bearing structural and thermal inertia and damping properties have to be taken into account.

Structural effects:

- inertia,
- stiffness,
- damping.

Thermal effects:

- thermal capacity (specific heat and density),
- thermal conduction, development of the temperature field,
- thermal deformations according to the actual shape of temperature field.

Fillon [**69**,**70**,**71**] analyzed transient thermal behavior of the tilting-pad journal bearings. He showed that the startup time has a significant influence on the bearing assembly due to decreasing operational clearance during startup. Different load cases have been analyzed and compared with the measurement data. The journal diameter was $100\ mm$ and its length $70\ mm$.

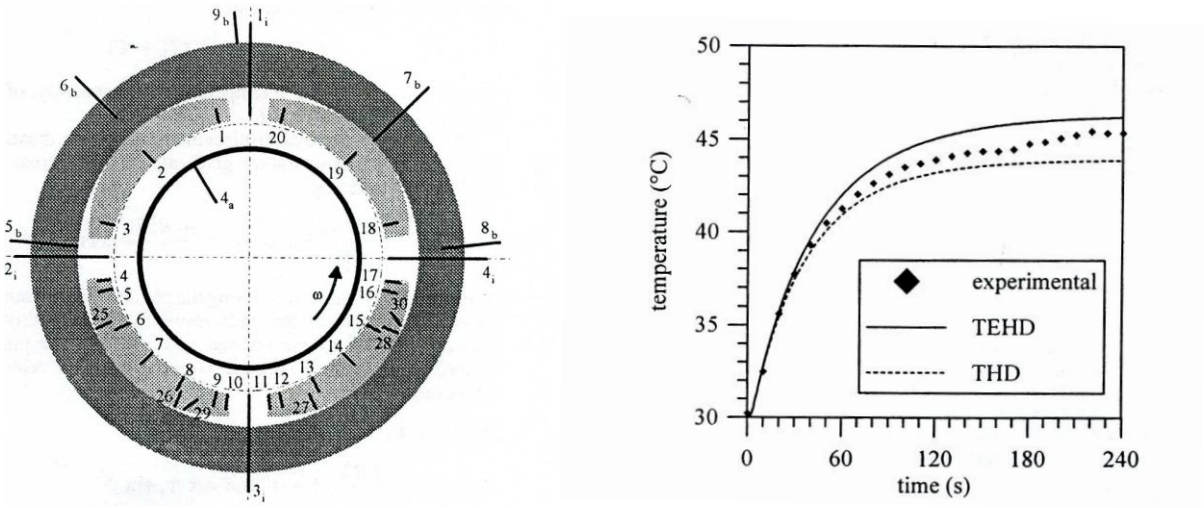

Figure 2.52. Tilting pad journal bearing and calculated and measured temperature profiles at the half of the pad as a function of time [69]

In that work it has been shown that rapid acceleration of the shaft can cause bearing damage. If the startup is too rapid seizure may occur due to thermal expansion of the bearing pads and the shaft. When the bearing is accelerated very quickly there is not enough time for thermal expansion of the housing and the bearing clearance decreases until zero where metallic contact occurs. As an example authors performed a startup simulation from 0 to $10000\ rpm$ within $5\ s$. In the Figure 2.53 one can see the results of this simulation. Approximately after $50\ s$ minimum oil film thickness is very low (approx. $2-3\ \mu m$) and the temperature reaches $150\ °C$.

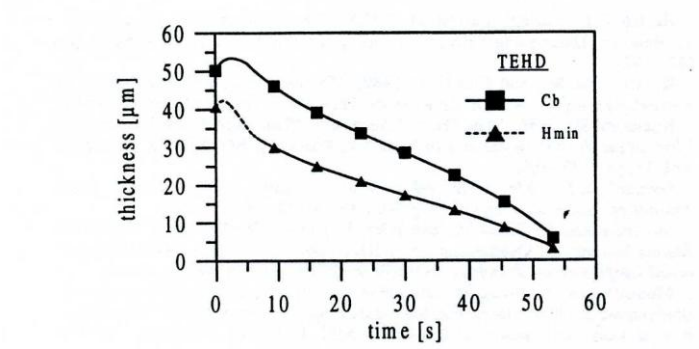

Figure 2.53. Radial bearing clearance Cb and minimum oil film thickness Hmin as a function of time [70]

Main conclusions from these investigations considering transient effects for hydrodynamic bearings can be summarized in the following points:

- time scale of thermal transients is significantly larger than that for other effects (up to 3 orders of magnitude),
- heat transfer has to be taken into account in order to obtain realistic results, otherwise thermal transients are not calculated properly,
- thermoelastic deformations of the bearing elements have to be taken into account in order to obtain good agreement with experimental data.

It seems that from the thrust bearing operation point of view the most important transient effect is the thermal expansion of the bearing elements and the influence of these effects on the bearing overall performance. Large bearings of the hydro generators are usually not loaded by any dynamic forces. From this point of view the most interesting transient aspect of the analysis is the startup of the bearing. During this state the thermal gradients are most significant and therefore also thermal distortions of the bearing pad and runner. These effects have an essential influence on the bearing load capacity and adverse startup conditions may finally lead to bearing seizure.

The transient simulation tool might also be a great help in case of a bearing failure investigation. It usually happens under undefined conditions when many cumulating problems lead to seizure. It can be a rapid startup [**9**] from the extremely cold initial condition or shut down with malfunction of the hydrostatic jacking system [**74**]. In this paper the advantages of the developed transient calculation tool have already been proven. Authors analyzed the case of the thrust bearing seizure during shut down.

A different approach to the transient simulation of a thrust bearing was presented by the author in [**75**]. In that research the author analyzed thermal and elastic deformations of the bidirectional thrust bearing pad (outer diameter $2.755\ m$). It has been said that the Francis pump/turbine is subjected to two or three startups per day. The reason for the investigation was a damage of the

Babbitt surface (wiping) during commissioning. Failures occurred during winter months (from October to January) when the temperatures were the lowest. A FEM model of the pad was thermally loaded by the temperatures taken from measurements (17 sensors close to the sliding surface and 13 close to the bottom surface). Temperature profiles were applied as loads for the thermal analysis of the pad deformations. According to the measurements stabilization of the temperature field has been obtained after 18 minutes of operation. This combined method (based partially on measurements) showed significant pad thermal distortions and their influence on bearing operation. The comparison between warm ($T_{cold} = 39°C$) and cold start ($T_{cold} = 15.5°C$) of the bearing has been presented. Deflection of the bearing pad for warm start was $0.08\ mm$ and for the cold start $0.17\ mm$. The deflections are almost doubled! Performed analysis gave valuable conclusions that caused modification of the startup procedure. It has been made obligatory to warm up the oil bath and submerged bearing pads up to $45\ °C$ prior to startup.

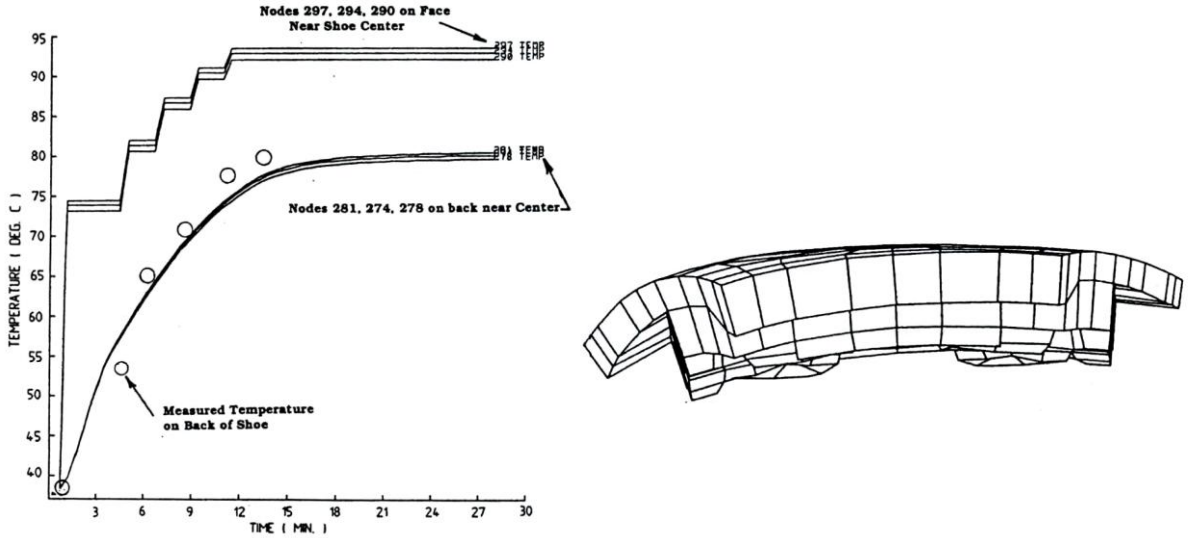

Figure 2.54. Temperature profile as a function of time and thermally deformed thrust bearing pad [75]

Even such simplified, based on measurement data analysis can give some interesting data considering thermal deflections of the bearing pads but does not give any information about general state of the bearing and its operational parameters. In order to obtain such results parallel simulation has to be performed which can give the full view.

2.4 Summary

Even though a great progress occurred within recent years there is still a need for development of both simulation and measurement techniques because of increasing requirements of the accuracy of the prediction of the bearing behavior. The operational parameters are approaching the limits of the range of operation in order to increase the efficiency and limit the costs. Thus safety margin is getting smaller and the point of operation has to be defined in a better way. The transient bearing calculation techniques are getting more and more important since on one hand the computation times are shorter than a couple of years before and on the other hand it is more and more important to know where the real operating limits for the hydrodynamic bearings are, not only for steady state condition but also during transient phases after change of operational parameters.

In a summary of the current state of knowledge one can also try to define which components or effects of the hydrodynamic lubrication should be taken into account. According to the experience of

many researchers the new simulation tool should first of all allow for 3D temperature field in the oil. Only in this way realistic results can be obtained. The isothermal and 2D solution leads to the overestimated load carrying capacity. The turbulent oil mixing between the pads and hot oil carry over effect are also very important due to their major influence on the oil film inlet temperature and finally on the maximum temperature in the oil film. One of the most interesting components is also realistic treatment of the heat exchange between the oil and the surfaces of the pad and runner. If the convection coefficients on the walls could be calculated in the model there would be no need to input them as boundary conditions. In this way temperature field distribution and further thermal distortions of these elements can be obtained. Taking into account these effects allows for accurate estimation of the oil film gap profile.

Taking into account the geometry of the bearing housing and the heat exchange on the remaining pad surfaces may increase the accuracy of the obtained results due to the lack of additional assumptions for the boundary conditions in the model.

Transient bearing operation requires transient simulations in order to estimate real bearing condition. Modern pump storage power plants are simultaneously adjusted, within the whole power range ($0 - 100\ \%$), in order to cover variable network demands. Sometimes mode of operation may be switched, form pumping to generating, within a few minutes. These generators may work also within short periods of time so the bearing never reaches the thermal steady state conditions.

According to the literature currently used calculation software does not allow for the transient simulations of the real bearing. There were approaches to estimate the state of the bearing during startup with steady state tools. The only changed parameter was speed. This approach is allowable only for very slow startup when there is enough time for equalization of the temperature field. This condition can only be fulfilled either for a very small bearing (small time constants for the temperature effects) or for the extremely slow startup (several hours for the large bearing). None of these conditions is fulfilled in case of large hydro generators. Their dimensions can reach up to several meters of diameter and usually they are brought to the operation rapidly (within a couple of minutes and sometimes even less).

The next step of bearing simulations could be taking into account transient effects. Such model could simulate for example warming up after startup of the bearing, variable operational conditions (variable speed or load) or even change of the direction of rotation. In Chapter 2 it has been shown that increased temperature field gradients can cause increased thermal deformations of bearing components and that they have an essential influence on the load carrying capacity of bidirectional bearing pads.

Taking into account oil flow around the bearing pad gives also a possibility to simulate convection heat transfer on the remaining walls of the bearing pad. There is no need to assume convection coefficients on these walls. This approach allows also to take into account different oil supply systems and bearing housing arrangements (flooded and direct lubrication), LEG (Leading Edge Groove [**76**]) oil supply or pumping plate for example.

Hydrostatic jacking chamber with assumed oil flow (not pressure) can also be modeled in order to simulate real startup conditions. The hydrostatic pressure is calculated according to the external load

and the oil film geometry. More realistic initial condition for startup simulation allows to follow the whole startup procedure in a more precise way.

With the use of a structure model heat transfer through the bearing parts could be calculated. This ability gives two main advantages to the whole bearing model. First the realistic boundary condition for the oil film sliding surfaces can be applied. Neither adiabatic nor isothermal oil film assumption has to be made. The temperature field in the bearing elements can be simulated as a function of time, so the transient bearing behavior, thermal bending of the bearing pad and runner or variable operating conditions (startup, variable load, shut down) can be included.

3 Goal of the research

The literature research presented in the previous chapter, the analysis of the most current knowledge and operational experience based on numerous bearing failure investigations lead to the conclusion that the transient effects sometimes play the major role in the bearing operation performance. It is especially important for the bearings of PSP hydro generators that work under variable conditions and at the same time have limited load carrying capacity due to symmetrically supported tilting pads. On the other hand there are a few simplified simulation models that allow for transient simulations that additionally do not treat bearing operation in a complex way. These facts indicate that there is need to create a more complex simulation tool that would allow to analyze bearing operating parameters and physical effects in a detailed way.

According to this previous research and experience purpose of the research can be formulated in the following form:

The goal of the research is to develop, verify and demonstrate functionality a bearing calculation tool that allows for transient simulations and additionally takes into account most of the major effects that take place during hydrodynamic lubrication.

In order to realize this purpose there has to be an appropriate bearing model built and validated with measurement data. The target is to take into account most of the effects identified by other researchers that occur during hydrodynamic lubrication. The simulation tool should be possibly close to the physical phenomena. The assumptions for this calculation tool were made in the summary of the literature research (Chapter 2) of this elaboration.

Further part of this work is mainly focused on proving the proposed thesis with the use of modern simulation techniques. In order to do so the combined Finite Elements Method (FEM) and Computational Fluid Dynamics (CFD) calculation methods are used. The combination of these two methods is called Fluid Structure Interaction (FSI). A decision was taken to use a commercially available software because of several reasons. First of all these are modern calculation tools that are being constantly developed. Thus continuous improvement of the developed model can be assured in the future. Additionally automatic treatment of boundary conditions and other effects like viscous heat generation, warm oil mixing or turbulence transition allows to simulate bearing operation in a similar way like it takes place in reality.

The work is mainly focused on the development of the temperature field in the bearing elements as a function of time. The developed model is presented in Chapter 4 and the obtained results, together with a comparison with measurements are placed in Chapter 5. The transient state of bearing operation is based on the startup procedure that has been performed during unit commissioning in the power plant. This gave first the possibility to validate the obtained results and additionally to check the performance of the real bearing.

4 Calculation model

4.1 Introduction

Calculation model of the trust bearing is built with the assumptions made in the previous chapters. It is prepared in form of a sector shaped pad (see Figure 4.1) that is totally immersed in the oil and supported on a supporting structure (different systems can be applied). Load is transferred from the rotating runner through the oil film to the bearing pad and the support. Rotational repeatability of the system is used so the model can be limited to a single sector.

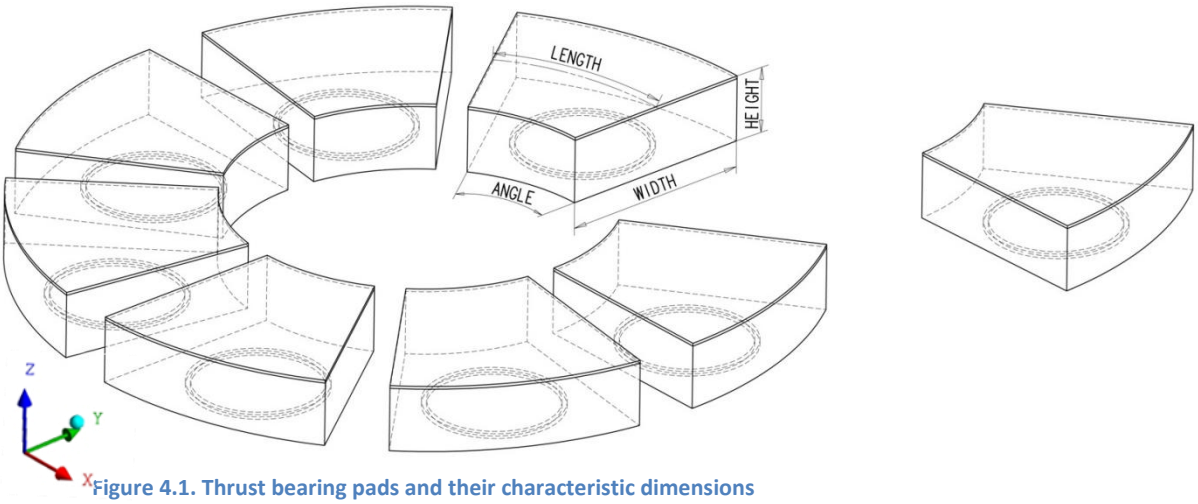

Figure 4.1. Thrust bearing pads and their characteristic dimensions

In order to resolve hot oil mixing in the bearing housing a space between the pads is also modeled in the fluid model (see Figure 4.2). In this way a connection between outlet and inlet oil film temperatures is created.

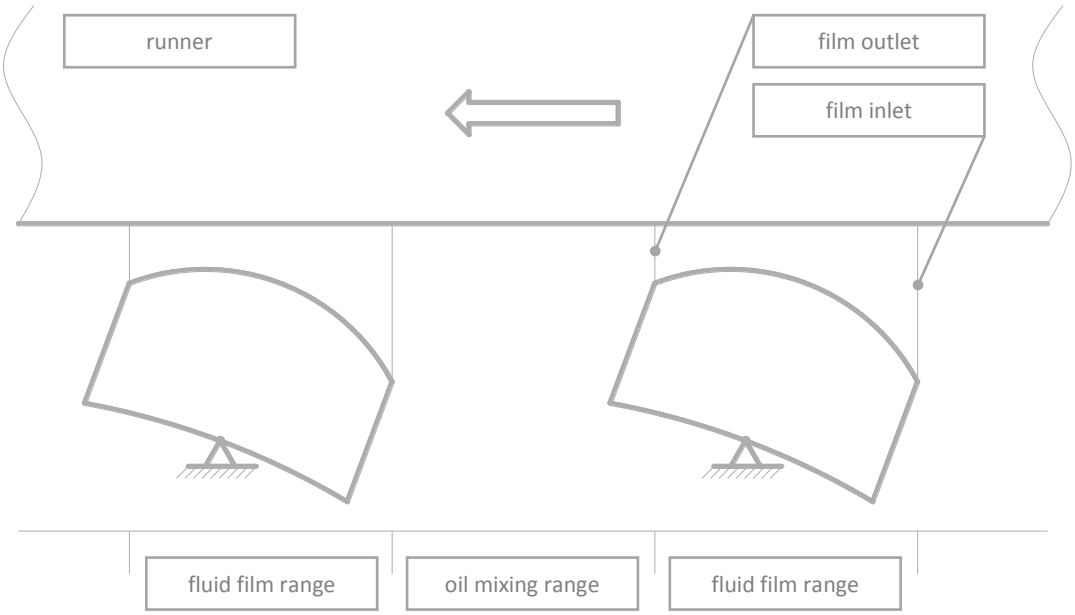

Figure 4.2. Film inlet and outlet boundary condition, oil mixing between the pads

Usually oil film inlet temperature is obtained with the use of additional oil mixing models/factors [**14**,**77**] and has large influence on the other bearing parameters because they all are strongly coupled. Increased inlet temperature causes higher temperatures in whole oil film and, at the same

time, decreases viscosity. It leads to lower oil film thickness and finally to higher heat generation. As a result different bearing parameters (e.g. oil film thickness, sliding surface temperature, power loss, etc.) are obtained than those for the lower inlet temperature. In order to avoid such an assumption/calibration oil mixing and warm oil carry over effects have to be calculated in the bearing model automatically. This approach forces one to model two completely different elements at the same time: oil film and oil surrounding the pad. The most obvious difference between them are dimensions that can vary several orders of magnitude. Oil film thickness is usually measured in microns (minimum oil film thickness usually varies within the range of several tens of microns) depending on the other bearing dimensions – smaller values are usually obtained for small and heavily loaded bearings) while other bearing dimensions are measured in meters (e.g. outer bearing diameter of a hydro generators D_{out} varies approximately within a range from 1 up to $6\ m$ [**78**,**79**]. As a consequence of this mesh aspect ratios are of very high values. This causes numerical problems with convergence. Very fine mesh in the fluid film region can be however treated as a boundary layer, where two walls are very close to each other. In the boundary layer high aspect ratios are allowed but development of the mesh into remaining space has to be gradual. There are not allowed steps of element sizing – so called expansion ratios, larger than 1.5 [**47**]. The expansion has to be done in order to limit the number of nodes the fluid domain and so the computation times.

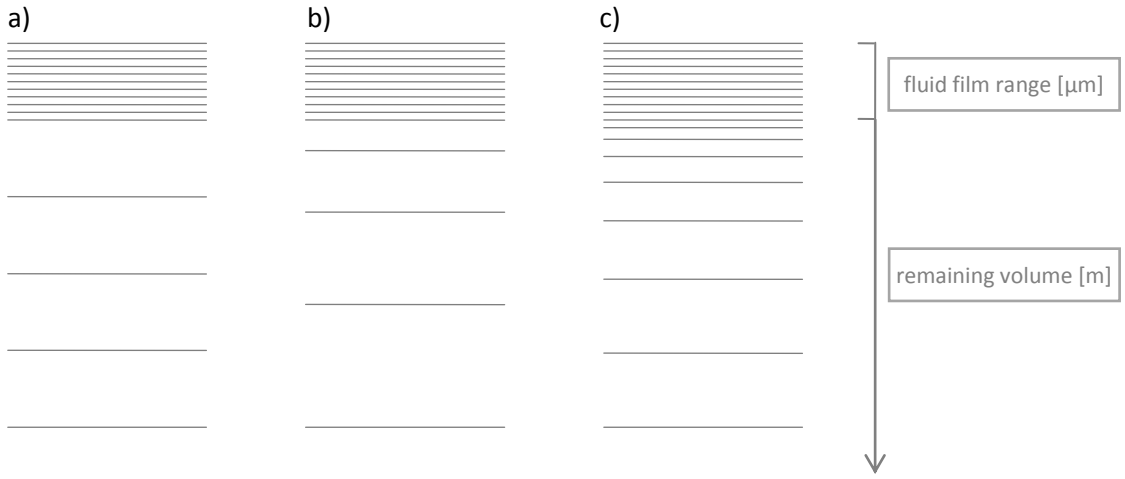

Figure 4.3. Mesh expansion possibilities: a), b) not allowed, c) allowed

The second, maybe not so obvious, difference is the flow regime in both parts. For the whole bearing housing we obtain most likely turbulent flow while in the oil film we get usually (but not always) laminar flow. Proposed complex model has to give an ability to calculate these two separate regions at the same time. There has to be either the ability of calculating two different regions at the same time or calculation of the turbulence transition between laminar and turbulent flow regime. The used SST (Shear Stress Transport) turbulence model is the most current one among available turbulence models. This model makes use of the so called wall functions. The grid resolution can in this way be reduced at the wall boundaries. It is described in more detail further in this chapter.

In this chapter the proposed numerical models (FEM + CFD) are presented that allow the transient simulations of hydrodynamic thrust bearings. Startup simulation is mainly considered. Methods and parameters are described and detailed explanations are given.

The bearing model described in this elaboration is based on, unless other specified, the Kopswerk II pump-storage power plant design which is located in Austria [**80**] (see Figure 4.4). This is a very

modern PSP hydro power plant with a separate Pelton turbine and attachable pump which is located in the lower part. The pump can be attached to the main shaft by the means of the fluid coupling – hydraulic torque converter [**81**]. During acceleration of the attached pump shaft (which takes approximately $8\ s$) additional thrust force of 200 t is produced and has to be carried by the thrust bearing. Hydraulic thrust from the attached pump is carried by the separate thrust bearing.

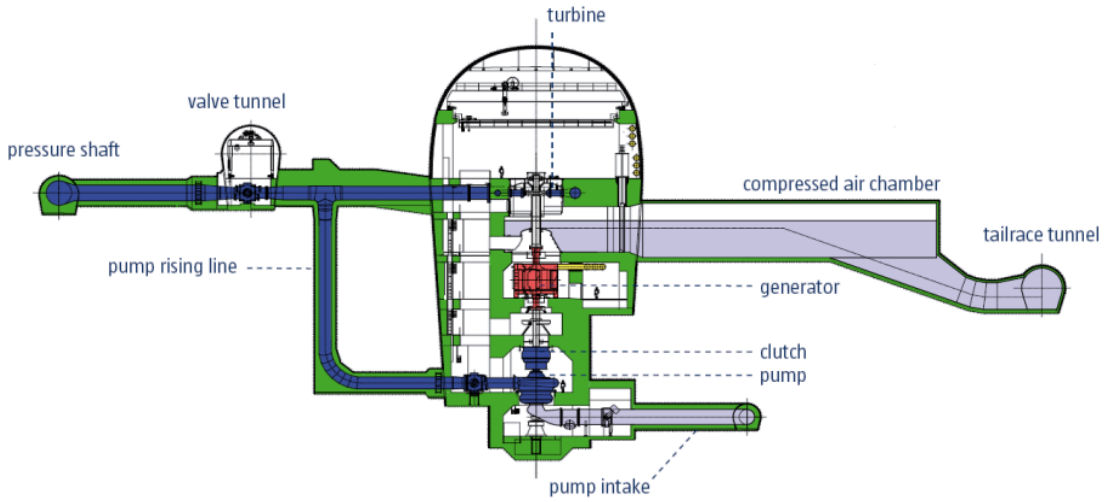

Figure 4.4. Kopswerk II hydro power plant [80]

This power plant is taken under consideration because of several reasons. First of all it has a Pelton turbine with precisely defined constant thrust load. This type of turbine has no additional axial load that comes from the water thrust and the weight is the only component. Thus it is easier to define the load for the simulation. Otherwise the load profile should be applied as a function of time. Geometrical parameters of the described thrust bearing are listed in Table 4.1.

Table 4.1. Parameters of the analyzed thrust bearing

No.	Parameter	Symbol	Value	Unit
1	Outer diameter	D_{out}	2.3	m
2	Inner diameter	D_{in}	1.3	m
3	Pad angle	α	24	deg
4	Pad width	B	500	mm
5	Pad length	L	377	mm
6	Pad thickness	H	170	mm
7	B/L ratio	B/L	1.326	-
8	Radial support position	$pivot\_rad$	0.53	-
9	Tangential support position	$pivot\_tan$	0.5	-
10	Nominal speed	n	500	rpm
11	Average sliding speed	U	47.12	m/s
11	Load	F	3512	kN
12	Specific pressure	p	1.53	MPa
13	Cold oil temperature	T_{cold}	36	°C
14	Oil grade	ISO	$VG46$	-
15	Oil dynamic viscosity	μ	0.0398	Pa s

The other reason of taking this bearing into account is the lack of the additional guide bearing in the housing. Guide bearings have influence on the runner temperature field and its deformations, overall power dissipation in the tank and the oil flow. Since there is no guide bearing in the analyzed simulation model measurement data should come also from a thrust bearing without a combined guide bearing.

4.2 Fluid Structure Interaction

FSI (Fluid Structure Interaction) allows to simulate interaction between two physical fields (structure and fluid) as it takes place in the real world. According to [**47**] this type of coupling is intended to the use of the following typical applications:

- biomedical applications,
- aerospace applications,
- automotive applications,
- fluid handling applications,
- civil engineering applications,
- electronics cooling.

Two models have to be created (see the next chapters for a more detailed description) in order to simulate both fields. Both of them have been created in form of APDL (ANSYS Parametric Design Language) macros. They are fully parameterized thus any geometrical changes can easily be introduced. The geometrical interface between them has to be exactly the same so they can communicate with each other and exchange the information. There are two types of coupling possible: mechanical and thermal. In case of bearing simulations both of them are needed due to combined nature of the physical processes that occur in the bearing. Heat generation produces temperature gradients in bearing elements, what in consequence causes their thermal deformations (thermal bending of a bearing pad). This effect changes the oil film gap shape and operational conditions of the whole bearing (load carrying capacity for example). Bearing deformations are also an essential parameters for bidirectional bearings in order to obtain any load carrying capacity [**28**]. According to [**47**] the analysis has to fulfill following requirements:

- must be three-dimensional,
- the ANSYS model must be single-field and the elements involved in load transfer must be 3-D with either structural or thermal DOFs,
- only surface loads are transferred. Valid surface loads are displacement, temperature, force and force density, heat flow, and heat flux,
- only two field solvers, one ANSYS and one CFX, can be coupled, a given analysis can have only one coupling between two field solvers, but it can have multiple load transfers,
- the ANSYS field cannot be distributed, but the CFX field can use CFX's parallel processing capabilities. A CFX field being solved using parallel processing is still considered a single field solver,
- the analysis must be a batch run,
- only the single frame restart is supported,
- ANSYS allows static and transient analyses; however, CFX allows only transient analyses.

Block scheme of the simulation process:

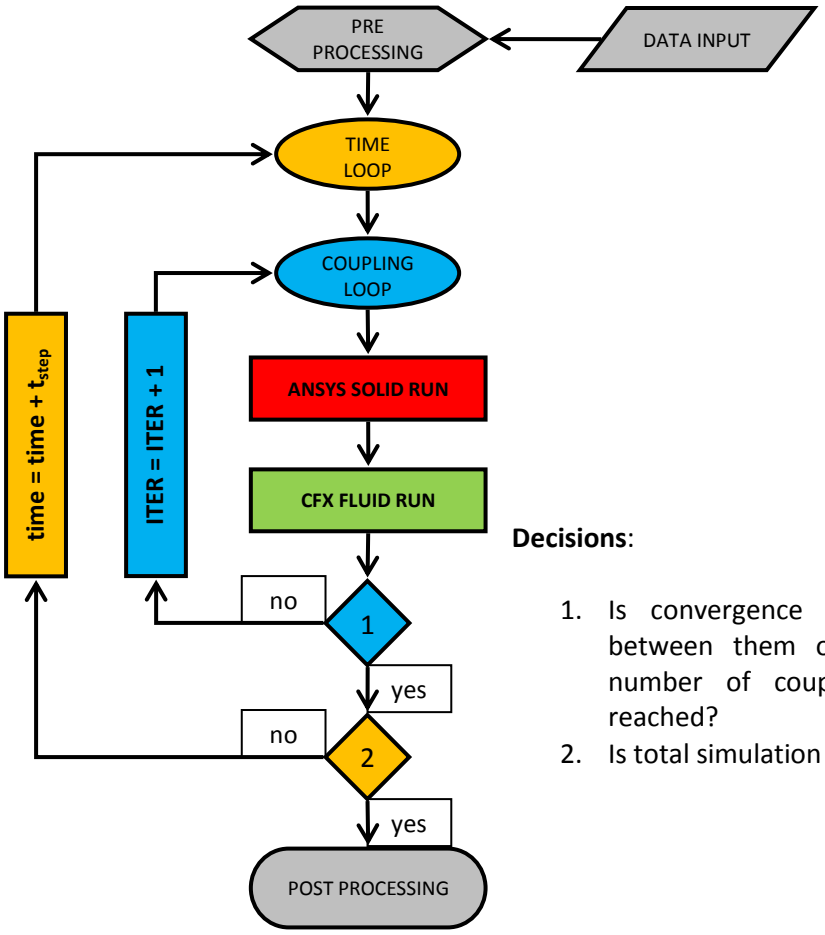

Decisions:

1. Is convergence of both solvers and between them obtained or maximum number of coupling iterations (ITER) reached?
2. Is total simulation time t_{total} reached?

Figure 4.5. Computation process

The great advantage of the ANSYS and ANSYS CFX software is ability of two directional FSI interaction. It allows to simulate influence of the fields on each other as it takes place in reality. Boundary parameters (nodes locations, nodal forces, temperatures and heat fluxes) are updated during simulation for each coupling iteration. Two separate regions of information exchange need to be created – pad surface and runner sliding surface. Information is exchanged in the way presented in Figure 4.5 in a coupling loop.

The information is exchanged in two processes, for structural and thermal coupling separate as shown in the graphs (Figure 4.6 and Figure 4.7), for each coupling iteration. There are up to five coupling iterations allowed in a single time step t_{step} in order to avoid long computational times in case of convergence problems. Sometimes also the convergence oscillates around a certain residuum value and does not decrease. For such difficult cases it is allowed to further go on with simulation while the better convergence can be obtained in the next time steps.

For structural task:

Figure 4.6. Structural coupling information exchange

Elastic and thermal deformations as well as displacements are calculated in ANSYS software with the use of FEM algorithms.

For thermal task:

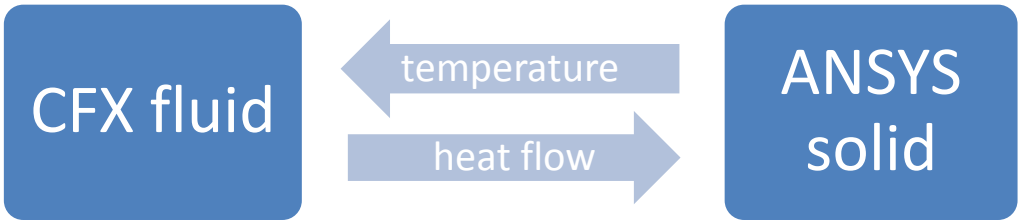

Figure 4.7. Thermal coupling information exchange

Heat conduction and temperature field distribution are calculated in a structural model and boundary temperatures are then transferred to the fluid model as boundary conditions. After fluid solver run heat fluxes with profile preservation (value and distribution) are applied to the structural model as boundary conditions.

Meshes of both models do not have to correspond to each other due to sophisticated interpolation procedures offered by ANSYS software. They may have different mesh densities so each can be adjusted to the requirements of the model. It is only necessary to assure that the meshes geometrically complement each other. Mapping from one grid to another is performed in a way presented in Figure 4.8 [**47**]. This allows to create coarse mesh for the structural model, while calculated deformations and expected temperature fields are relatively simple. Solid model is also built with the use of 20-node elements with square shape functions. Thus the mesh does not have to be very fine. On the other hand fluid mesh has to be fine enough to calculate properly boundary layers (velocity and temperature) in order to evaluate convection effects in the oil film and other regions.

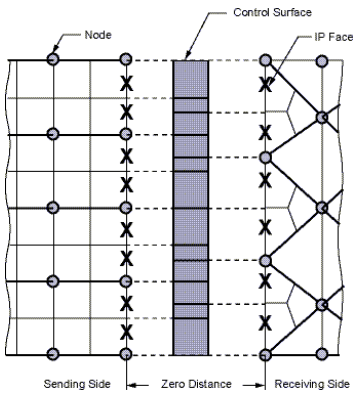

Figure 4.8. Mapping between the grids [47]

In order to configure FSI coupling several special commands are required to specify coupling parameters. They allow to configure every aspect of the coupling like:

- order of simulation (parallel or serial),
- relaxation factors for all fields,
- structural and thermal regions of exchange of information,
- time step and total time of simulation,
- number of coupling iterations.

ANSYS (structural model) and ANSYS CFX (fluid model) are run in a serial mode in order to supply the most recent parameters to each solver. This option is advised for strongly coupled fields like FSI for example. In the Figure 4.9 both options (parallel and serial) of running the solvers are presented. Parallel connection is faster but in serial mode solvers work always with the most current results. Thus this second option should be used in case of strongly coupled fields (like FSI for example).

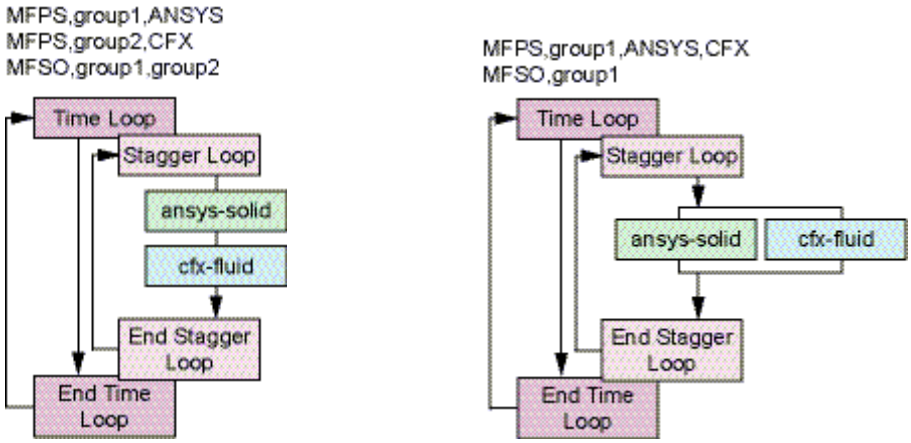

Figure 4.9. Serial or parallel solution order [47]

FSI coupling offered by ANSYS software has been presented in this chapter with a brief description of the methods and configuration parameters needed to perform a simulation. From the initial recognition this FSI seems to be an appropriate tool for the hydrodynamic bearing simulations. The purpose of further investigations is to build calculation model and to verify it with measurement data in order to prove or deny applicability of the presented approach.

4.3 Structure model

The structural model has been built with the use of ANSYS software. It is written in form of a APDL (ANSYS Parametric Design Language) macro (see APPENDIX) and enables either steady state or transient calculations. Three dimensional 20-node coupled field solid elements named SOLID226 are used in the model. The coupled field capability allows to solve at the same time both tasks: structural (stresses, elastic and thermal deformations) and thermal (heat conduction). For this reason each node of the element has four DOFs (Degrees Of Freedom): three displacements in spatial directions U_x, U_y, U_z and temperature T. A significant effort has been made in order to prepare both bearing parts with the use only of hexahedral finite elements in order to increase accuracy (convergence) and decrease the overall number of elements. Thus the overall simulation time could also be reduced.

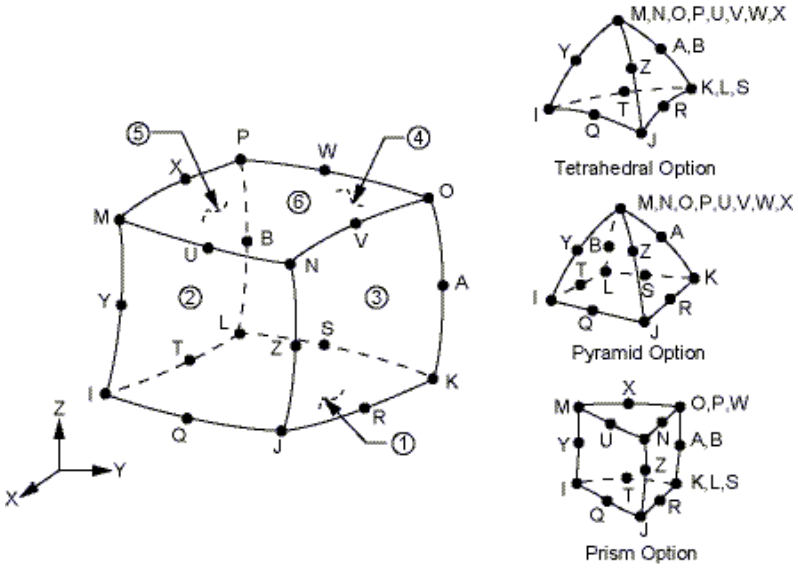

Figure 4.10. Finite element for solid model discretization [47]

The geometrical parameters were taken from the documentation of Kopswerk II hydro generator as listed in Table 4.1. In Figure 4.11 both bearing elements and design details are presented.

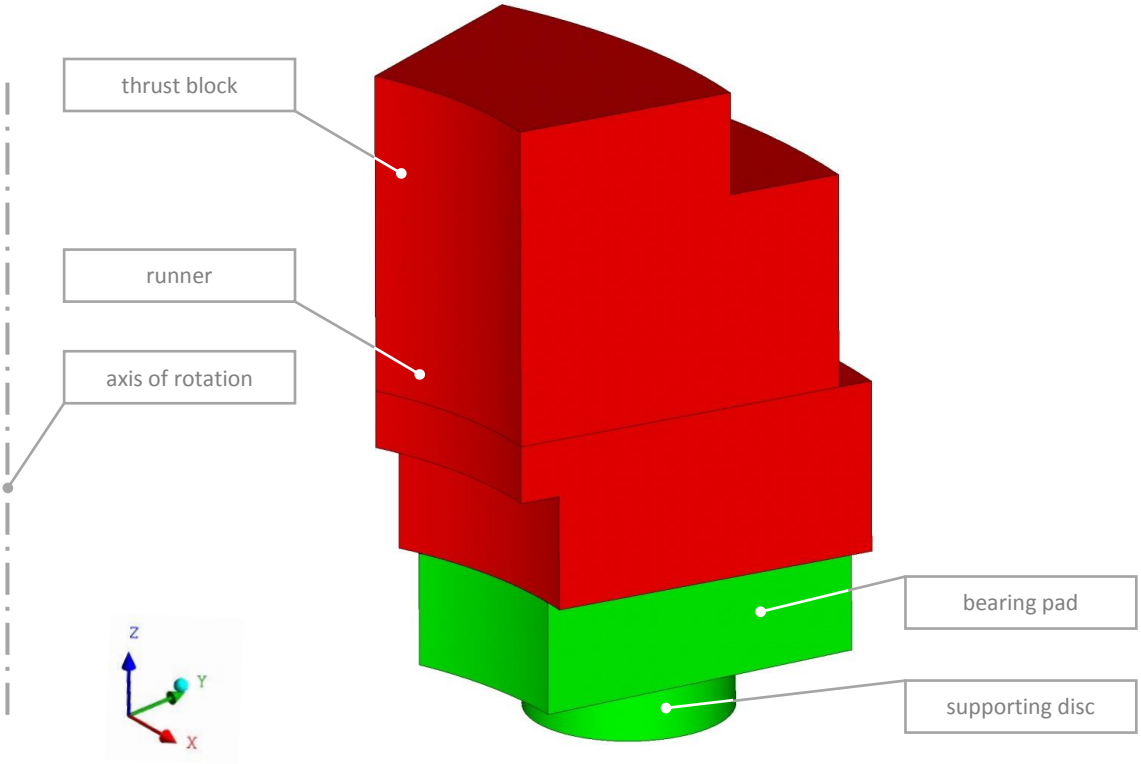

Figure 4.11. Structural model

Material properties of the analyzed thrust bearing are presented in Table 4.2. A standard elastic isotropic material has been used in order to model elastic and thermal deformations of the bearing structural elements.

Table 4.2. Material properties of the structural model

Structural

No.	Parameter	Symbol	Value	Unit
1	Young module	E_x, E_y, E_z	2.1e11	Pa
2	Poisson's ratio	$\nu_{xy}, \nu_{yz}, \nu_{xz}$	0.3	-
3	Kirchhoff module	G_{xy}, G_{yz}, G_{xz}	0.8e11	Pa
4	Density	ρ	7810	kg/m^3

Thermal

No.	Parameter	Symbol	Value	Unit
1	Heat conductivity	$\lambda_{xx}, \lambda_{yy}, \lambda_{zz}$	50	W/mK
2	Specific heat	c	470	J/kgK

Structural-Thermal coupling

No.	Parameter	Symbol	Value	Unit
1	Coefficient of thermal expansion	a_{xx}, a_{yy}, a_{zz}	12e-6	1/K

The structural model consists of two separate parts: runner (connected to the shaft) and pad. There is no connection between them so the whole applied load from the runner can be transferred to the support through the fluid model only.

The pad is supported by a disc with ring in order to compensate for the thermal deformations with elastic deformations [**28**]. In reality the disc is supported by adjustable an spindle (Figure 4.12) but this part is not modeled in the model. This simplification is not significant since stiffness of the spindle has only influence on the natural frequencies of the bearing axial vibrations and these effects are not considered in the presented model. The calculation of the bearing film stiffness is still possible since it takes into account only the load ΔF and minimum oil film thickness Δh_{min} according to Formula (4.1).

$$k_z = \frac{\Delta F}{\Delta h_{min}} \tag{4.1}$$

The disc is only supported on the point and is free to tilt in both directions (tangential and radial) as it is in the real bearing of Kingsbury's type [**82**]. All structural DOFs (U_x, U_y and U_z) are locked for that point. Bottom surface of the pad is additionally supported by the means of damping elements in order to increase stability and to limit velocity of the displacements. They are of little importance since analyzed thermal effects are of several orders of magnitude slower than dynamic pad movements. In order to equalize timescales of both phenomena and to increase the length of time steps such artificial modeling is needed. All six surfaces of the pad are loaded by the pressure and heat flux which is sent by the fluid model. Additionally the supporting disc is supported in tangential direction in order to avoid pad rotation around the vertical axis.

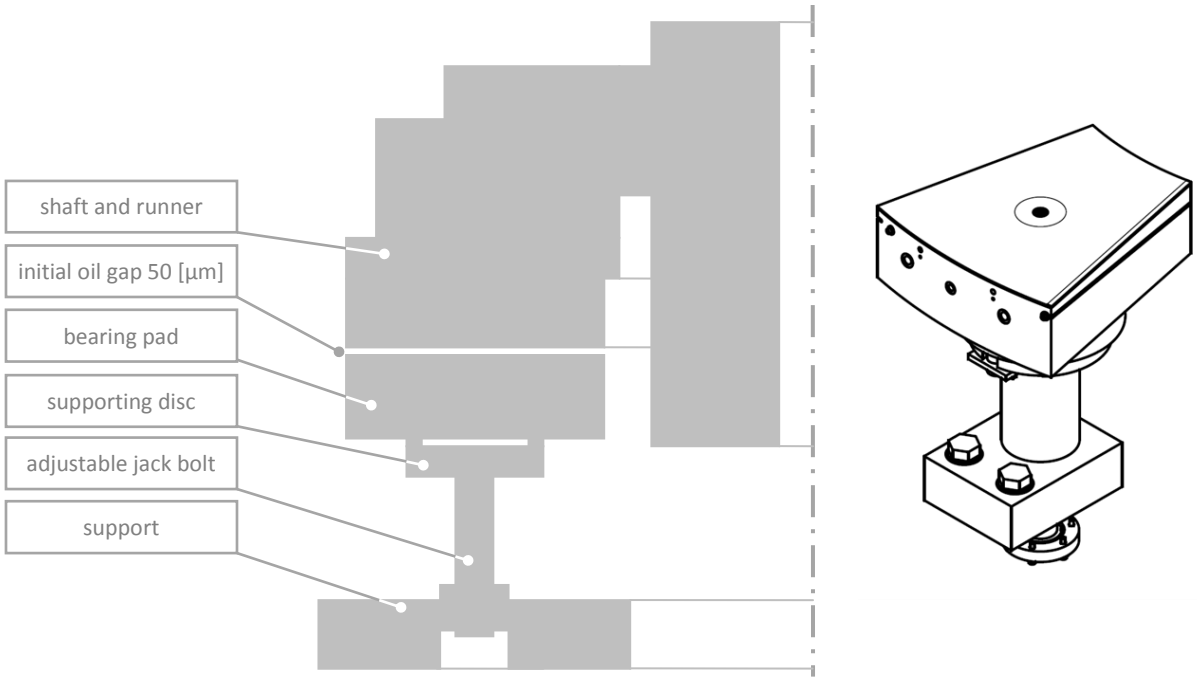

Figure 4.12. Support system of a thrust bearing, sketch and 3D model of the real thrust pad, initial gap between pad and runner is set to 50 µm

The modeled part of the supporting system is presented in Figure 4.13. The bearing pad is supported by the means of a disc with machined ring support. Additionally the disc is locked against rotation around its axis. In this way, the behavior of the pad is similar to the real bearing. Machined geometrical features in the sliding surface (chamfers and hydrostatic jacking chamber) are exaggerated in order to make them visible in the figure.

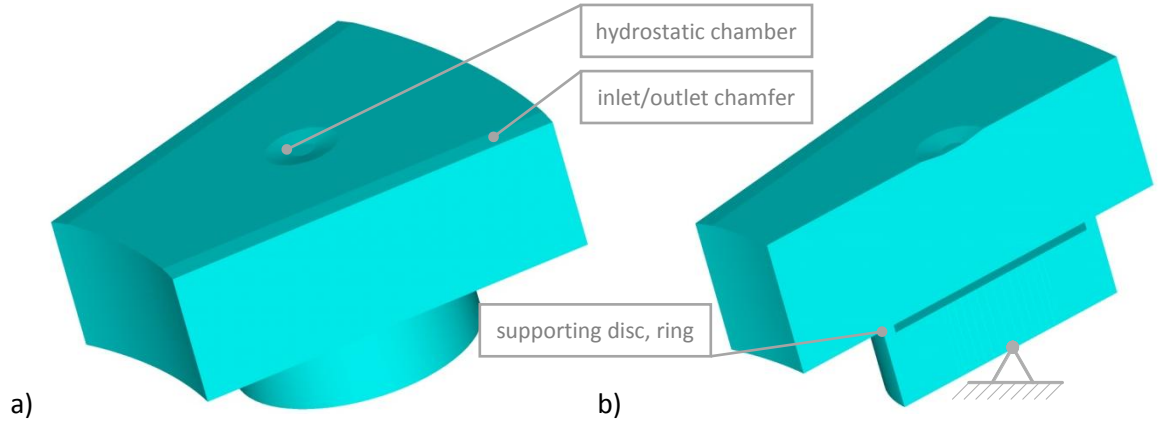

Figure 4.13. Modeled part of the support system, a) view, b) radial section

The top surface of the runner is supported in a way that only axial movements are allowed (U_x and U_y DOFs are locked). This is another consequence of modeling only a single pad instead of the whole bearing. Uniform load on all bearing pads indicates also that the shaft axis has to remain vertical at all times. On the same surface axial load is attached in form of nodal forces and additional damping elements to increase numerical stability. Otherwise the runner would move like a “rigid body” at the beginning of the simulation because it is not supported in axial direction at all and is free to move. The pad does not “know” that there is a runner located above. The only contact to the supported bearing pad can be obtained through the oil film load carrying capacity which is extremely low at the

beginning of the simulation. The runner movement downwards and fast acceleration would cause a larger displacement in the first few time steps than the initial gap between both bearing elements (set as equally to $50\ \mu m$ – see Figure 4.12). Additional mass elements are located on the top runner surface to increase the mass and in this way simulate appropriate inertia of the whole rotor. Rotating mass attached to the runner (shaft, turbine and generator) is modeled in this way.

Two radial cross sections of the runner are coupled in order to simulate periodicity and all runner nodes are coupled in circumferential direction to obtain an axis symmetrical temperature field which can be expected due to fast rotation of the runner. Time constant for the heat flow is much larger (1000 times) than the movement of the shaft due to rotation. Thus there is not enough time for the temperature variations as the shaft changes its position in tangential direction. Such an assumption has also been made by many researchers that analyzed the temperature field in the runner [**14**]. Mechanical coupling of both runner sections and thermal coupling of all nodes in circumferential direction is presented in Figure 4.14. Structural DOFs ($\mathrm{U_x}$, $\mathrm{U_y}$, $\mathrm{U_z}$) of the nodes between two coupled surfaces are not coupled (only sides A and B) but in case of temperatures all nodes in circumferential direction are equalized (all nodes). The difference between thermal and structural coupling is presented in Figure 4.15.

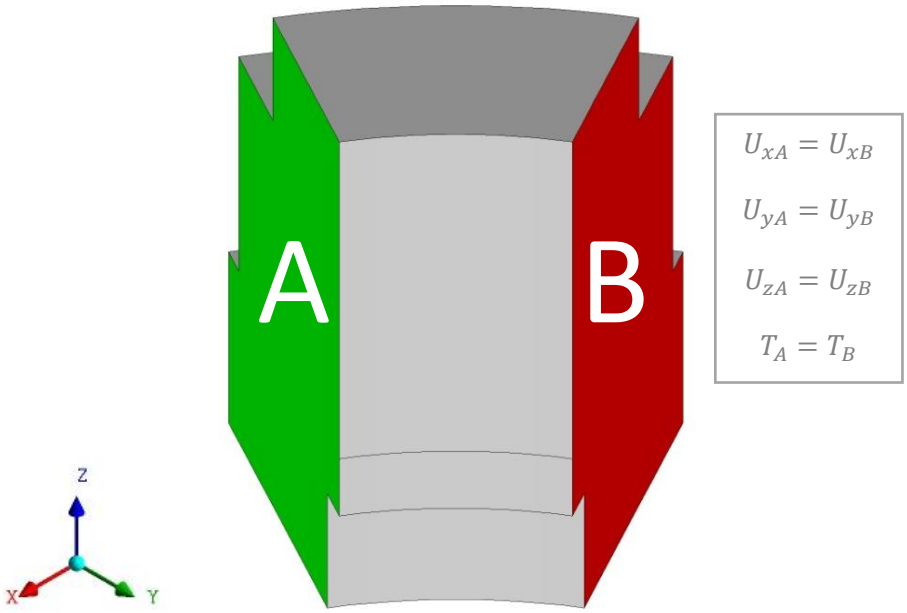

Figure 4.14. Runner circumferential coupling of the runner sections

Additional coupling of the temperature field can be presented, in a simplified way, in the Figure 4.15. U symbolizes all node movements in three spatial directions (x, y and z). Nodes in other sections (e.g. C, D and so on) are free to move since they are not coupled with the nodes that belong to the radial sections A and B.

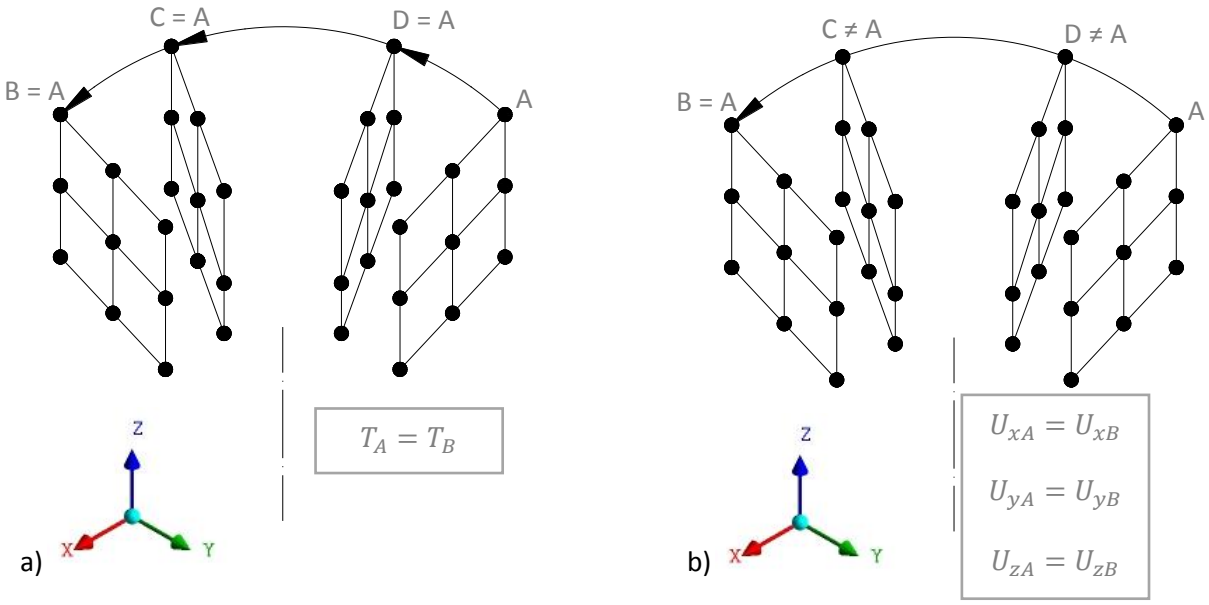

Figure 4.15. Runner sliding surface circumferential coupling, a) thermal, b) structural

Side walls of the runner are not connected to the fluid model so the convection boundary conditions have to be assumed. For the part that works in oil convection coefficient $\alpha = 350\ W/m^2K$ and bulk temperature $T_b = T_{cold} + 12\ °C$ were assumed. For the part that rotates in oil coefficient $\alpha = 10\ W/m^2K$ and bulk temperature $T_b = T_{cold} + 12\ °C$ were assumed according to measurements of the warm oil temperature in the bearing housing of several thrust bearings. Influence of these boundary conditions is presented in Chapter 5.

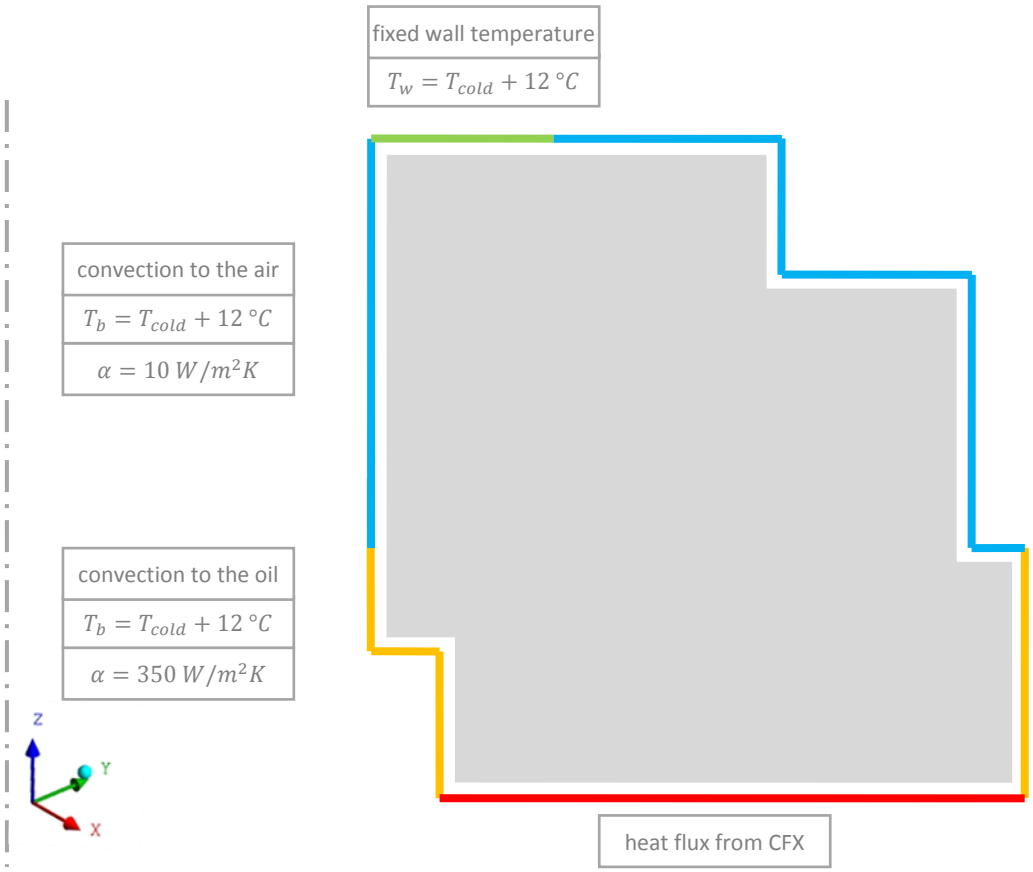

Figure 4.16. Thermal boundary conditions applied to the runner

The structural boundary conditions for the runner take the not modeled part of the rotating mass into account that is attached to the runner in case of real hydro-generator. Main components of this weight are generator and turbine. In order to model this additional concentrated weight, MASS21 elements have been used. In this simplified way realistic inertia in axial direction of the bearing shaft can be taken into account. The axial load for the bearing comes only from the weight of the rotating components of the hydro generator since the Pelton turbine does not generate any hydraulic thrust. Thus the value applied to the runner remains constant during the whole simulation. Additional damping applied to the runner surface has a similar purpose like the one applied to the pad – stabilization of the structural movements and numerical effects.

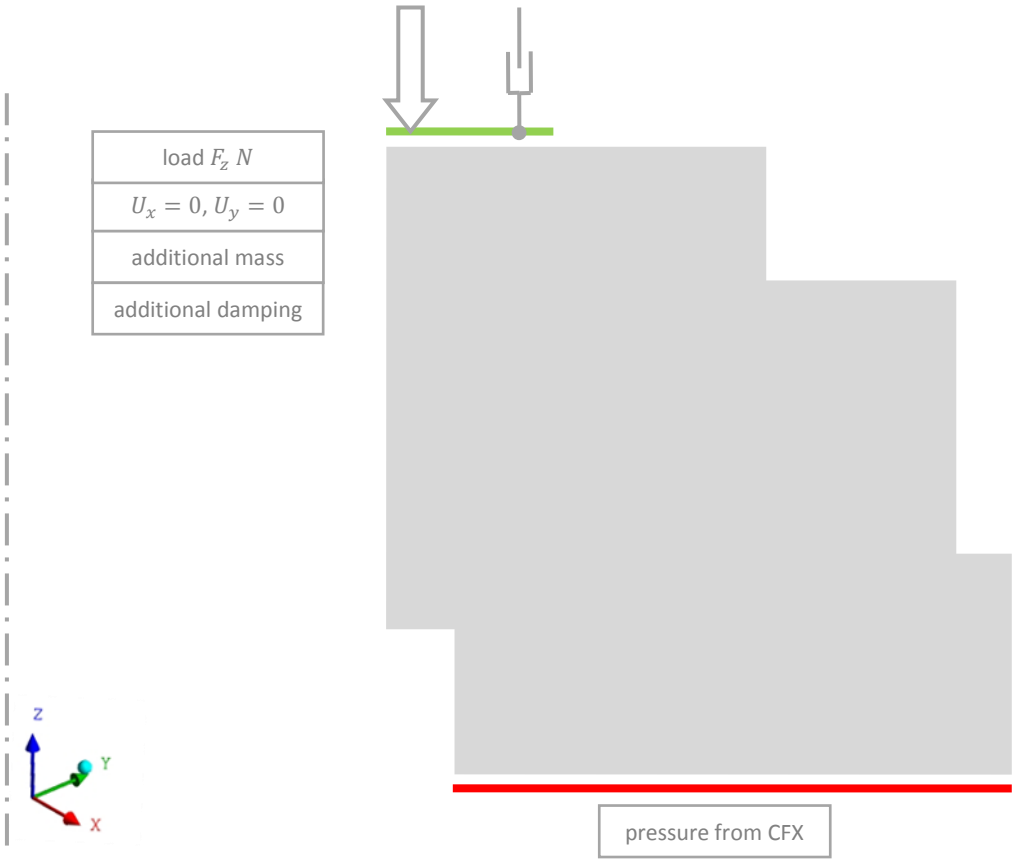

Figure 4.17. Structural boundary conditions of the runner

In order to obtain numerical stability, mainly at the beginning of calculations, both parts of the structure model are additionally supported by sets of spring-damper elements called COMBIN14. Spring stiffness was assumed equal to zero and damping coefficients are adjusted in order to obtain stability but not to influence the results. In practice the bearing elements have to find an equilibrium position within not more than 30 time steps. This means that their values must vary with the length of time steps and also have to be adjusted for different bearing sizes and/or load cases. In this time the solution goes gradually from initial conditions defined by simulation input (50 μm parallel oil gap) to the calculated initial conditions (hydrostatic jacking system working, no rotational speed). Relatively small damping coefficients values do not influence the remaining solution phases (bearing startup and approaching the thermal steady state conditions) due to smaller velocities of movements. Too small damping results in element oscillations and too large damping causes a slow response of the bearing elements to the applied load (force, rotational speed).

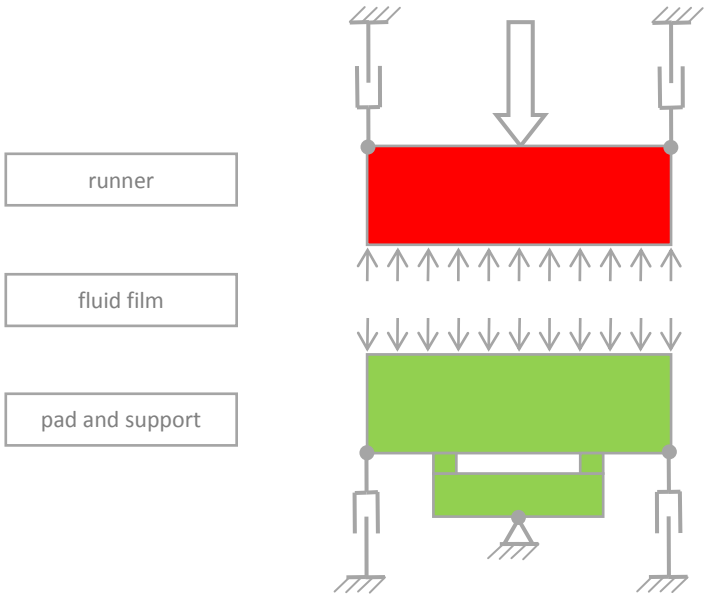

Figure 4.18. Damping elements attached to the runner and pad

Dynamically the model can be described as a second order system for structural effects

$$[M]\vec{\ddot{u}} + [C]\vec{\dot{u}} + [K]\vec{u} = \vec{F} \tag{4.2}$$

and as a first order system for thermal effects

$$[C]\vec{\dot{u}} + [K]\vec{u} = \vec{F} \tag{4.3}$$

where:

$[M]$	structural mass matrix
$[C]$	structural damping matrix, damping matrix
$[K]$	structural stiffness matrix, coefficient matrix
$\vec{\ddot{u}}$	nodal acceleration vector
$\vec{\dot{u}}$	nodal velocity vector, time rate of DOF values
$\vec{u}$	nodal displacement vector, vector of DOF values
$\vec{F}$	applied load vector

Additional damping is added in order to obtain numerical stability and to allow longer time steps (decrease the total computation time). The damping coefficients, both for pad and runner, have to be adjusted in order to support bearing elements (reduce the velocity of movements) but in a way that there will not be any influence on the obtained solution. This can be done during initial condition calculation when the elements should find their equilibrium positions within $20 - 30$ time steps. Damping elements are divided into two parallel sets c_1 and c_2 both for pad and runner and have unequal damping coefficients. They can be activated independently. This approach gives the possibility to use stronger damping forces during initialization of the simulation and smaller damping during calculation, so the solution will not be affected. The proportion between sets has been found after a series of numerical experiments. Set c_1 is active only during the initial search for balance of

bearing elements and then is not active anymore. The movements of elements due to bearing acceleration and thermal expansion are not damped thus the transient results are not influenced.

$$c_{total} = c_1 + c_2$$

$$d = 0.8$$

$$c_1 = d \cdot F_1$$

$$c_2 = c_{total} \cdot (1 - d)$$

In case of this model damping force depends linearly on the velocity difference of both ends of the damping element. For each damping element one end is attached to the model and the second one is not allowed to move at all. Thus the damping force depends only on the velocity of the supported element. The damping force for the single damping element can be evaluated as follows:

$$F_{total} = c_{total} \cdot \dot{\vec{u}}$$

$$F_{total} = c_1 \cdot \dot{\vec{u}} + c_2 \cdot \dot{\vec{u}}$$

$$F_{total} = F_1 + F_2$$

For the real startup simulation $c_1 = 0$ the damping force is equal to 20 % of the one at the beginning of the simulation

$$F_{total} = F_2$$

The total damping force for the whole model is simply the sum of all damping forces of all damping elements attached either runner or pad.

$$F_{damping} = \sum_{i=1}^{n} F_{total}$$

The phases for both damping sets can be shown in Figure 4.19. In the background there is also rotational speed shown in order to locate in time the damping coefficient variations.

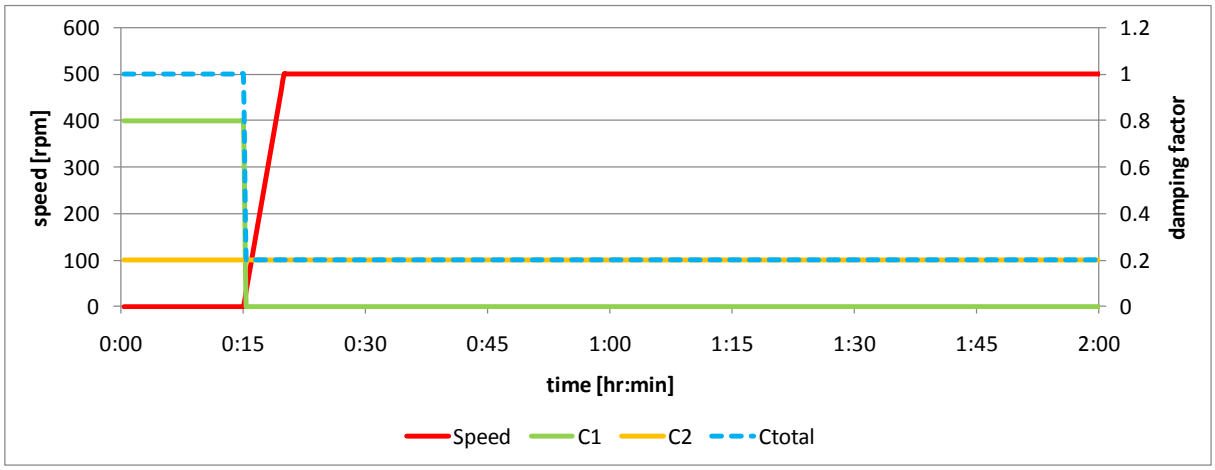

Figure 4.19. Damping sets c_1 and c_2 during startup simulation

When constant damping is specified during whole the simulation either it is not possible to find initial balance (damping too small) or solution is affected during startup (damping too large). Large damping during startup causes overload of the bearing up to 30 % and in this way thermal effects occur much faster than it could be expected for the real bearing (not overloaded one). Comparisons of warming up of the bearing after startup for different damping coefficient configurations (constant and variable) are shown in Chapter 5.

4.4 Fluid model

The fluid model has been built with the use of ANSYS CFX computational package. It is fully parametrical and can be used for any bearing simulation with similar design. Also different design changes can be introduced to the model. The APDL macro that creates the geometry and mesh is attached to this elaboration in APPENDIX. Geometrically it fits perfectly to the structural model thus they complement each other and fill the space in 100% without neither gaps nor interferences.

Physical fluid flow can be mathematically described by partial differential equations that are given in Chapter 2. Numerical solution of the flow is obtained by dividing the volume of interest into a large number of control volumes (elements or cells) and solving sets of algebraic equations instead of partial differential equations. Sets of algebraic equations can be solved with the use of different solution algorithms [**46**].

The grid is made of 8-node elements and the task is solved with so called RANS (Reynolds Averaged Navier-Stokes) equations with the use of FVM (Finite Volumes Method). Reynolds-averaged equations are temporal average of the turbulent flow. Also transient flows can be analyzed in this way but temporal averaging of the flow must not affect the physical unsteadiness of the analyzed case. Time scale of the turbulence effect should be much smaller than the time scale for the mean unsteadiness. Additionally the software gives an opportunity for FSI (Fluid Structure Interaction) simulations where the fluid flow interacts with the surrounding structure. This interaction works in both directions of the coupling. This ability is essential for bearing simulations while both physical fields (fluid and structure) are strongly coupled. In other words effects on one side have a strong influence on the second.

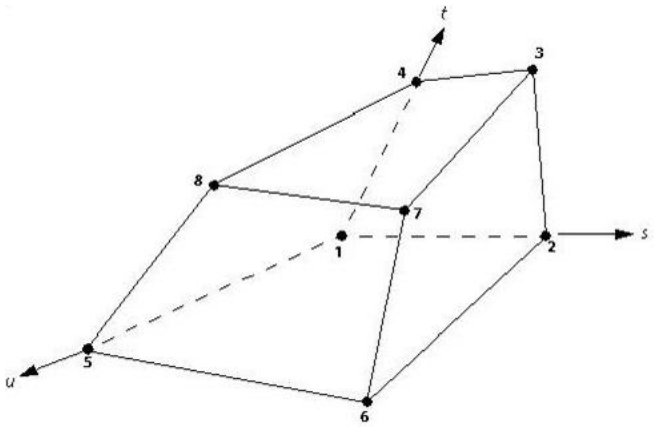

Figure 4.20. Hexahedral finite 8-node element for fluid model discretization [47]

The fluid model consists of both hydrodynamic oil film and oil bath surrounding the bearing pad on all the remaining walls. This allows to simulate heat flow in the segment without any additional assumptions on the pad walls, since boundary conditions are calculated and updated the during

simulation. Convection film coefficient α is a property of a fluid velocity field in the boundary layer and heat conduction coefficient of the fluid. For a given temperature difference between the wall T_{wall} and the fluid T_{bulk} the heat flux $\dot{q}$ can be calculated with the use of formula (4.4). The temperature and the velocity fields depend as well on time and location coordinates, so the convection coefficient and heat flux rate are subjected to the variations.

$$\dot{q} = \alpha \cdot (T_{wall} - T_{bulk}) \tag{4.4}$$

For the turbulence modeling, SST (Shear Stress Transport) turbulence model is used. Since in CFX ANSYS package there is no possibility of simulating two regions with different turbulence models, the transition of turbulence has to be simulated in order to calculate two different flow regimes, laminar (fluid film) and turbulent (bearing housing), at the same time. Such automatic treatment is very helpful because before simulation it is difficult to predict the location of the turbulent flow regions.

The SST turbulence model is based on the $k-\omega$ one. It belongs to the group of two equation turbulence models. They are currently the most popular turbulence models among these available in CFD packages. The use of SST turbulence model allows to simulate boundary layers in a precise way without generating very fine meshes. Instead of resolving the velocity boundary layer the profile is assumed with the use of the wall functions [**46**,**47**]. Moreover laminar regions (e.g. oil film layer) are automatically treated as laminar flow whereas the turbulent regions (e.g. space between the pads) have turbulent flow regime due to consideration of the turbulence transition. This way it can be ensured that each region has an appropriate flow regime and there is no need to calculate them separately.

k – equation:

$$\frac{\partial(\rho k)}{\partial t} + \nabla(\rho U k) = \nabla\left[(\mu + \frac{\mu_t}{\sigma_k})\nabla k\right] + P_k - \beta'\rho k\omega \tag{4.5}$$

ω – equation:

$$\frac{\partial(\rho \omega)}{\partial t} + \nabla(\rho U \omega) = \nabla\left[(\mu + \frac{\mu_t}{\sigma_\omega})\nabla \omega\right] + \alpha\frac{\omega}{k}P_k - \beta\rho\omega^2 \tag{4.6}$$

In Table 4.3 assumed material properties of the ISO VG46 oil are listed.

Table 4.3. Material properties assumed for the ISO VG46 oil

No.	Parameter	Symbol	Value	Unit
1	Thermal diffusivity	α	$f(\mu_o, T)$	m^2/s
2	Nominal dynamic viscosity at 40°C	η_o	0.0398	Pa s
3	Nominal kinematic viscosity at 40°C	ν_o	$4.59 \cdot 10^{-5}$	m^2/s
4	Heat conductivity	λ	0.123	W/m K
5	Specific heat	c	2113.5	J/kg K
6	Density	ρ	867	kg/m^3

Viscosity is modeled as a function of the local temperature with the use of Sunderland formula according to [**47**]:

$$\mu = \mu_o \cdot e^{c2\cdot\left(\frac{1}{T}-\frac{1}{c1}\right)+c3\cdot\left(\frac{1}{T}-\frac{1}{c1}\right)^2} \tag{4.7}$$

The symbols used are explained in Table 4.4.

Table 4.4. Viscosity properties assumed for the ISO VG46 oil

No.	Parameter	Symbol	Value	Unit
1	Dynamic viscosity	μ	$f(\mu_o, T)$	Pa s
2	Nominal dynamic viscosity at 40°C	μ_o	0.0398	Pa s
3	First viscosity coefficient	$c1$	313.16	K
4	Second viscosity coefficient	$c2$	3140.832	K
5	Third viscosity coefficient	$c3$	-946242.894	K^2

Dynamic viscosity of oil evaluated with the use of Sunderland formula [**47**] and presented input parameters can be shown as a function of temperature in the diagram in the Figure 4.21. This curve is defined in the CFD program and local viscosity values are updated for each node as temperature changes occur.

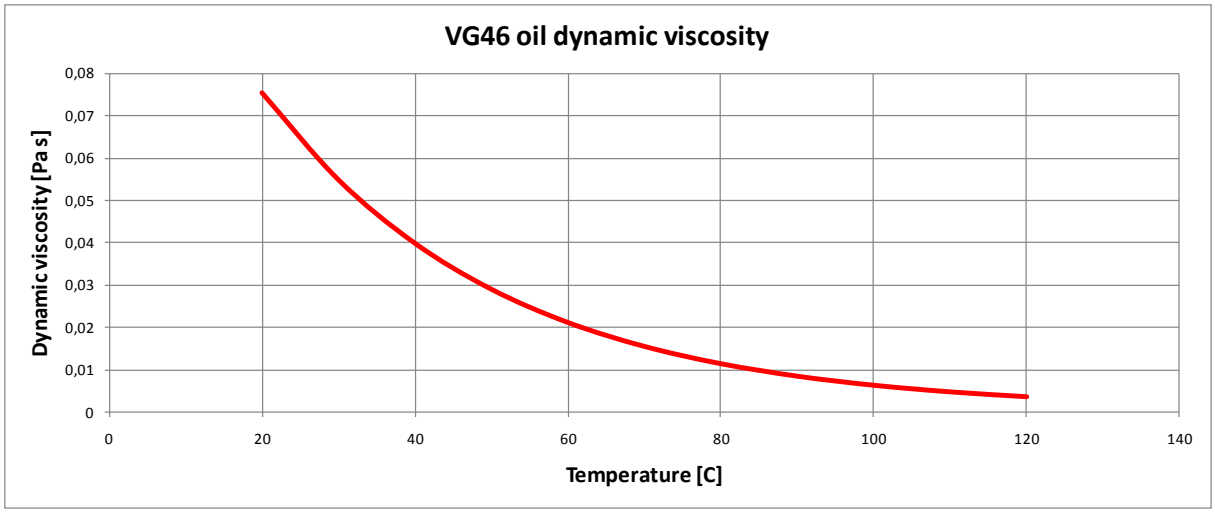

Figure 4.21. Dynamic viscosity of the ISO VG46 oil according to the Sunderland formula.

The remaining oil parameters (density, heat conductivity, specific heat, etc.) are assumed to be independent of temperature. It is assumed that the influence of these variations is small what is consistent with current knowledge in this matter [**30**,**68**]. None of these parameters can vary as a function of pressure, due to the very small influence on their values within the expected range of pressure (up to 20 MPa) [**8**,**83**,**84**,**85**].

The Total Energy flow model is used for fluid calculations. According to the CFX Best Practice Guidelines [**46**]:

"This models the transport of enthalpy and includes kinetic energy effects. It should be used for gas flows where the Mach number exceeds 0.2, and high speed liquid flows where viscous heating effects arise in the boundary layer, where kinetic energy effects become significant. The selection of the Total Energy model has implications for whether the fluid is modeled as compressible or incompressible."

According to this statement, the Total energy flow model seems to be a perfect choice for the bearing calculation tool since the viscous heat generation in the oil film has the most significant influence on other effects. It includes high-speed energy effects and the viscous work term in the energy equation. These capabilities are essential for an appropriate estimation of the viscous forces in the oil film.

The flow is modeled as incompressible and without hydrostatic pressure component. These assumptions may have influence on the solution since in the real bearing the air mixed in the oil can change its physical properties (e.g. viscosity, density, etc.)

Relatively long time steps are averaging the solution of the flow. Thus it is treated as the steady state flow around the pad. In the described bearing analysis it is not the intention to resolve unsteadiness of the flow around the bearing pad since the time scale of the thermoelastic effects is several orders of magnitude higher.

Discretization of the flow volume is an important step during numerical analysis of the flow. The grid of the model has been prepared with care in order to assure good accuracy of the obtained results. The main parameters of the generated mesh are presented in Table 4.5.

Table 4.5. Mesh parameters of the fluid model

No.	Parameter	Value
1	Number of Nodes	108010
2	Number of Hexahedra Elements	95120

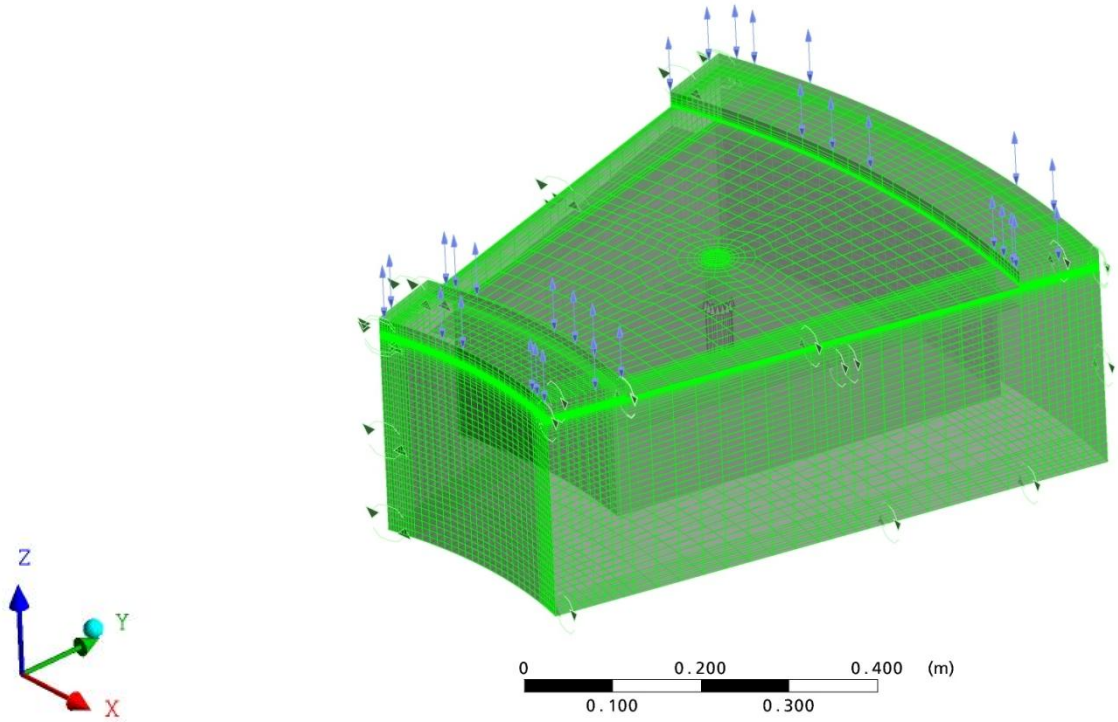

Figure 4.22. Fluid model mesh (108010 nodes and 95120 elements)

The density of the mesh is increased close to the sliding surface in order to calculate boundary layer at the rotating surface with sufficient accuracy. The fluid film thickness is divided into ten element

layers while in radial and tangential direction it has 20 divisions. At the same location as the support point of the bearing ($pivot_{rad} = 0.53$, $pivot_{tan} = 0.5$) is the conical hydrostatic jacking chamber located. There are two reasons to model this part of the bearing. First of all it gives an opportunity to simulate the real bearing startup, from hydrostatic jacking conditions and no rotational speed up to nominal hydrodynamic conditions. The second reason is that the hydrostatic jacking chamber deforms in a significant way the hydrodynamic pressure profile and thus affects the load carrying capacity. With no hydrostatic jacking chamber the simulated bearing parameters would be more optimistic than for the real bearing.

Hydrostatic jacking chamber and inlet and outlet chamfers are presented in the Figure 4.23. The chamfers are located on both sides since the bearing has to work in both directions. They help to tilt the pad at the beginning of startup (when the pad is parallel to the runner) and also increase the numerical stability of the fluid model. The initial oil film thickness, which is equal to $50\ \mu m$, is also visible in the Figure 4.23.

a) 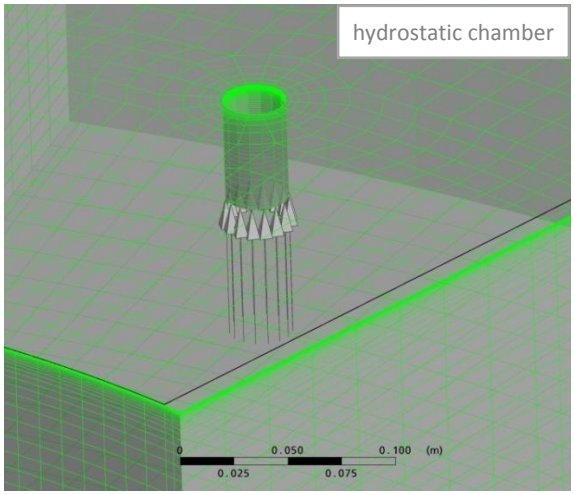

b) 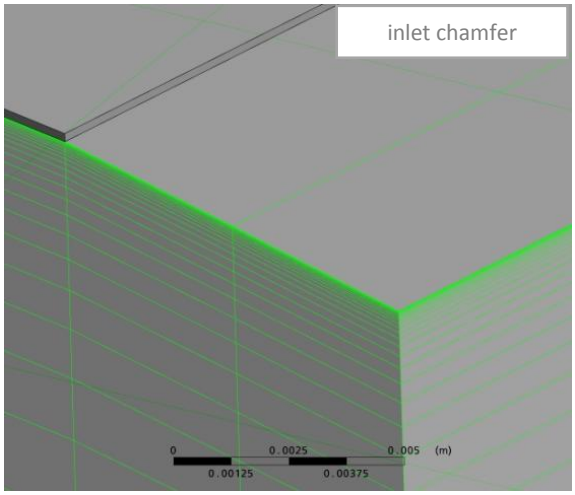

Figure 4.23. Fluid mesh details, a) hydrostatic jacking chamber, b) inlet and outlet edge chamfer

Boundary conditions define the flow conditions on the surfaces where user knows or assumes certain parameters (e.g. velocities or temperatures). In CFX software there are several possibilities to apply on the boundary surfaces. They can be divided into the following groups:

- inlet,
- outlet,
- opening,
- wall,
- symmetry.

Additionally many different domain interfaces are allowable – translational or rotational periodicity for example.

In the following points the applied boundary conditions have been described.

Walls:

All six sides of the pad are grouped in this area. All variables (pressures, displacements, temperatures and heat fluxes) are calculated in the coupling of two separate solvers. It means that there is no need for additional assumptions regarding the pad surface. Results are then converged on the common areas. The wall is modeled without any slip whereas some authors indicate that there is the possibility of lubricant slip in the hydrodynamic layer [**86**]. This effect is not taken into account since it can be significant only at very high pressure flows. Wall velocity is equal to zero relatively to the mesh motion calculated by the structural solver.

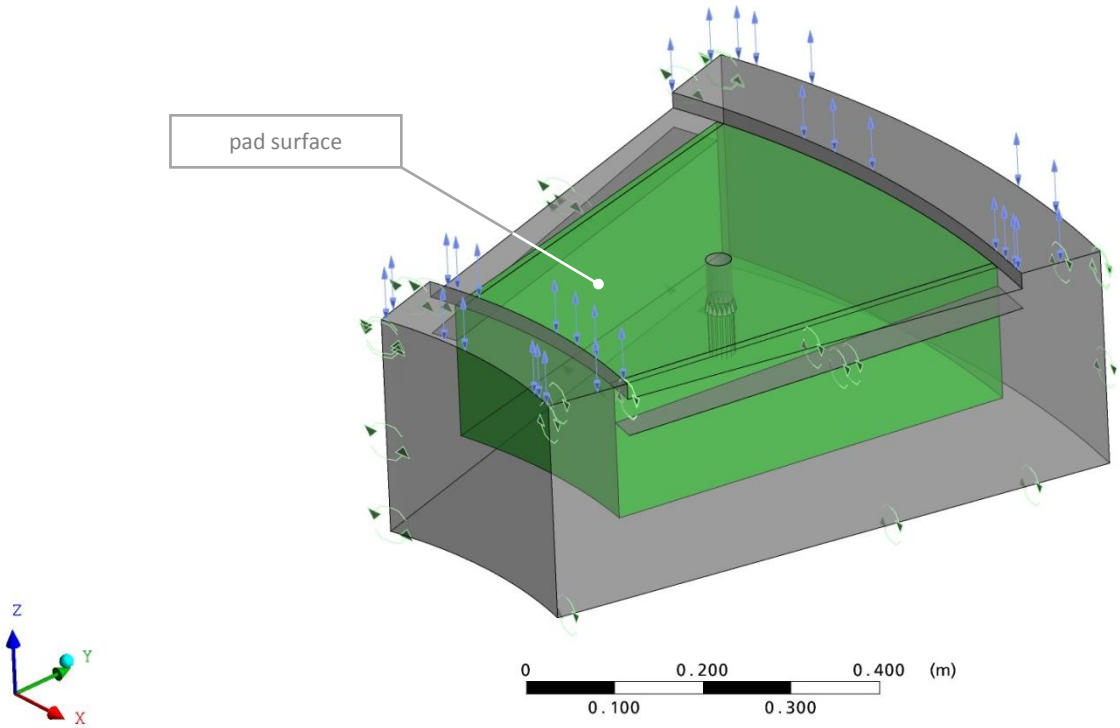

Figure 4.24. Pad boundary condition

The runner surface is modeled as a rotating wall around the z axis with given rotational speed $\omega\ rad/s$ with no slip assumption. Similarly as the pad surface, the sliding surface is connected to the structure model in order to exchange information. It "sends" pressure and heat flux (both with profile preservation) and receives as a boundary condition mesh displacement and temperature profiles. All coupling information is updated for each coupling iteration since solvers run in a serial mode. Also parallel run mode is possible but it is not recommended for strongly coupled fields since solvers may not receive the most up to date results.

None of the two cylindrical runner surfaces are connected to the structural model. Instead, they have adiabatic heat flow assumption and unspecified mesh motion because they connect the moving sliding surface with the stationary opening surface. They allow for an offset between oil film and the opening surface. Rotational speed can be varied as the simulation goes on. An example of the rotational speed variations during startup and shutdown is shown in Figure 4.25. The cold oil temperature T_{cold} is not subjected to any changes in order to simplify the interpretation of the obtained results.

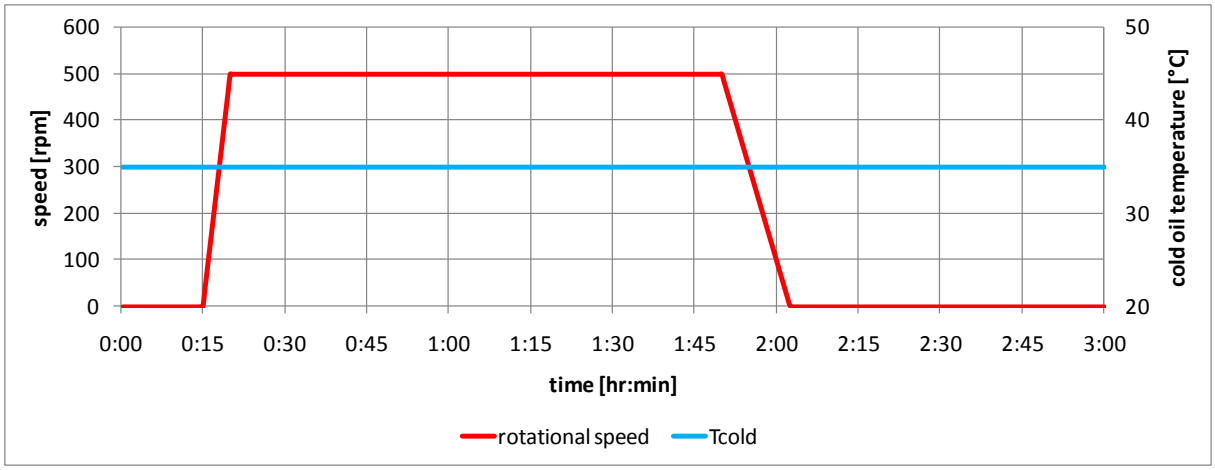

Figure 4.25. An example diagram of input parameters as a function of time

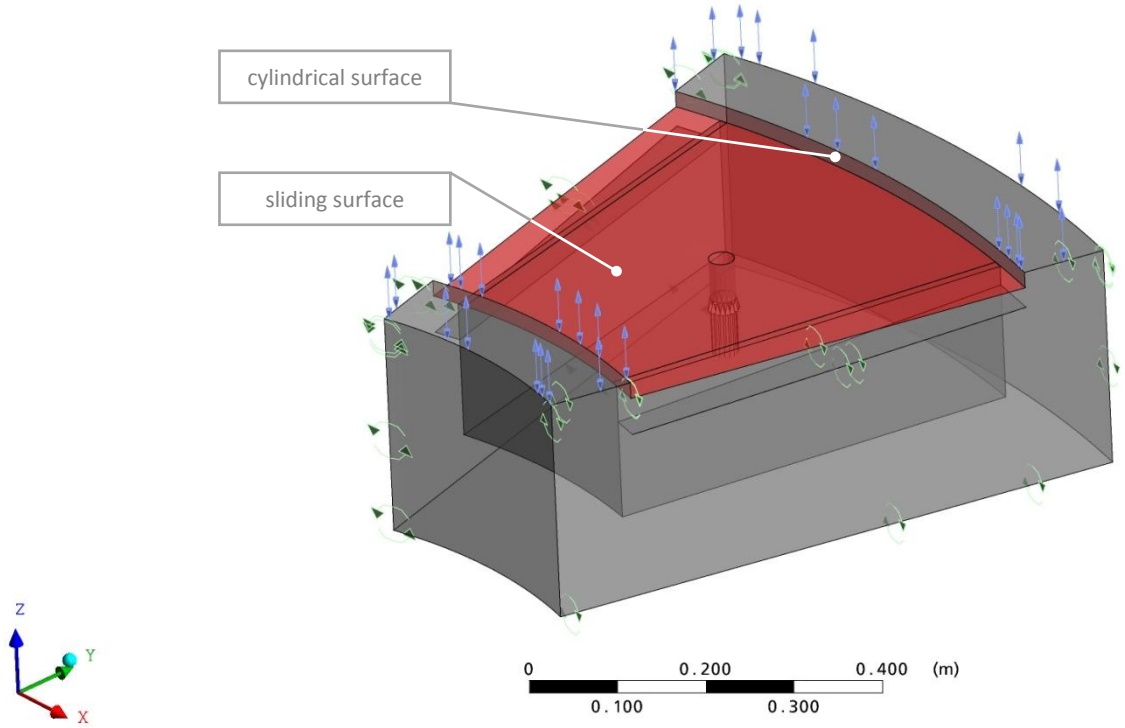

Figure 4.26. Runner boundary condition

All remaining walls in the fluid model are stationary with adiabatic heat flow assumption. In this way heat delivered to the oil due to friction losses can be taken away either by the oil flowing through the two opening rings at the top of the model or through the sliding surfaces of the bearing elements.

In order to decrease the density of the grid, so called automatic wall functions are used in the fluid model. The purpose is to use a smaller number of points in the velocity boundary layer. The velocity profile in the near wall region does not need to be resolved with numerical model but is bridged with an assumed logarithmic velocity profile. In this case the first node from the wall can be located slightly above the logarithmic layer (see Figure 4.27) – already in the turbulent part of the boundary layer. The great strength of the modern CFD simulation programs are the scalable wall functions – the mesh does not need to be exactly fitted to the resolved velocity field. This was a significant disadvantage of the standard wall functions used in previous programs [**46**]. In these early wall

functions versions, the grid had to be almost exactly fitted to the expected velocity field. This is especially difficult since the velocity profile is not known during generation of the mesh.

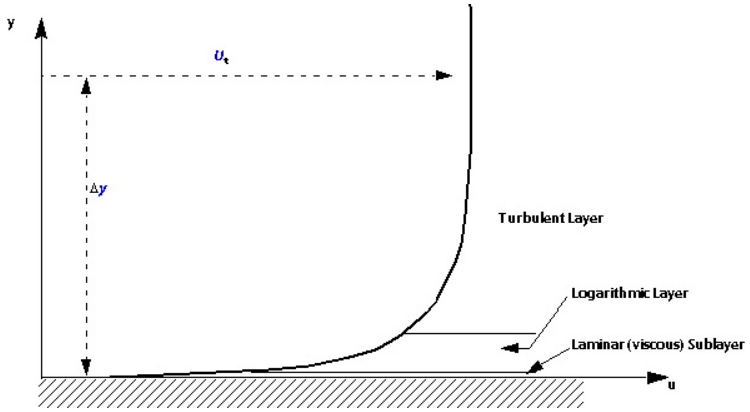

Figure 4.27. Velocity boundary layer in the fluid model [47]

In order to model the bearing housing the bottom and side walls are introduced to the model. They have an adiabatic heat flow boundary condition. Velocity in all directions is set to zero without any slip assumption. Bearing housing is modeled rather symbolically by two cylindrical walls and the bottom below the pad. In reality the bearing housing can be much more complex but the character of the flow remains similar. Due to modeling of the housing the cooling of the pad can be simulated in a realistic way.

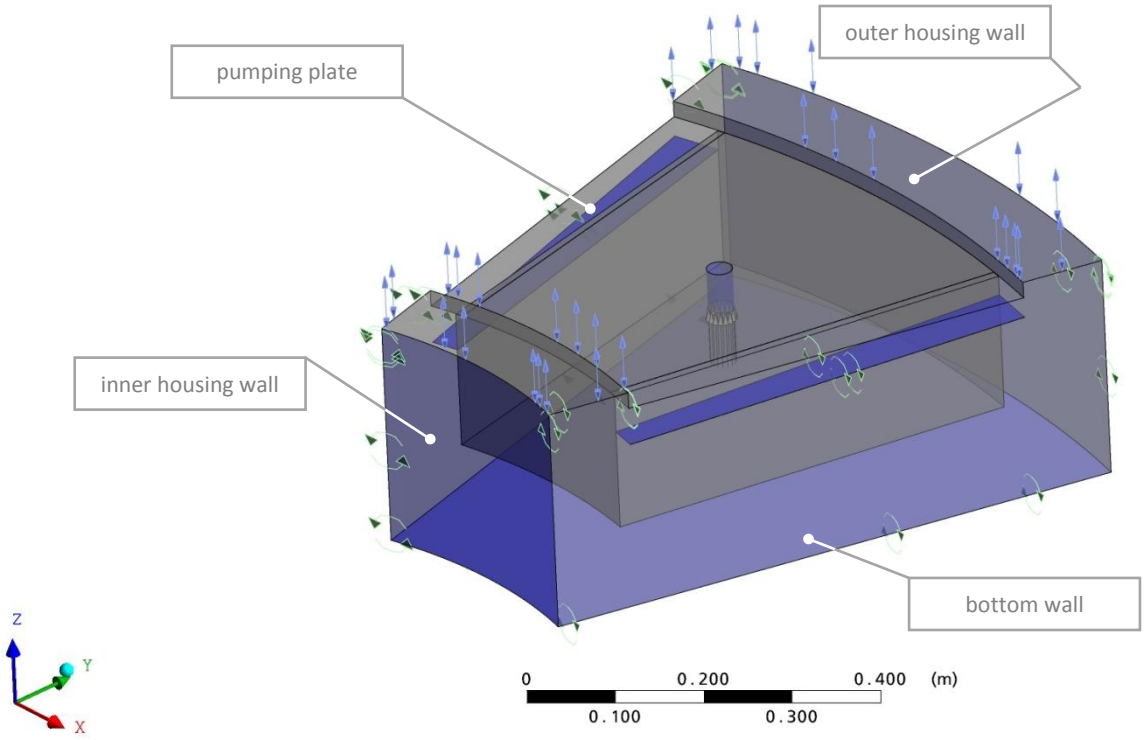

Figure 4.28. Wall boundary condition

A pumping plate located between the pads close to the runner surface is also modeled since it is also part of the analyzed bearing design. Its purpose is to pump oil in radial direction with the use of centrifugal and viscous forces. Therewith better oil exchange in bearing the housing is obtained. The plate is modeled as a thin rib in the oil model without any thickness. Heat conduction through the rib is neglected. The narrow channel between the pads allows to obtain higher flow speed in radial

direction so the mixing effects are more intensive. Therefore the oil temperature on the inlet to the oil film should be lower. Through modeling this design detail flow around the pad is modeled in a more realistic way.

The pipe that joins hydrostatic jacking the system inlet with the chamber is also modeled as a wall. It is not connected to the structural model since the inlet has the stationary mesh movement condition. It connects stationary inlet with varying its position sliding surface. The movement of the pipe is unspecified and is a result of movements of both ends. This wall has also an adiabatic thermal boundary condition since it is hard to predict its temperature when the hydrostatic system is not working anymore. It can be assumed that oil in the pipe and its walls have similar temperatures thus there should be not heat transfer between them.

Periodicity:

To limit the model size only one single pad is modeled. This assumption is correct if all pads in the whole bearing are loaded with equal forces and the runner sliding surface is parallel to the bearing plane. The rotational periodicity around the z-axis has been set. The mesh is exactly the same on both walls (equal number of nodes and their positions) so direct 1:1 connection is possible. The nodal values are simply connected and kept equal to each other on both sides. There is no need for additional interpolation of their values. This approach allows to save computational time and increases accuracy but requires an appropriate (symmetrical) mesh. Nodes have to be located exactly at the same positions on both coupled sides. The connected surfaces (periodic 1 on the inlet side and periodic 2 on the outlet side) are shown in Figure 4.29.

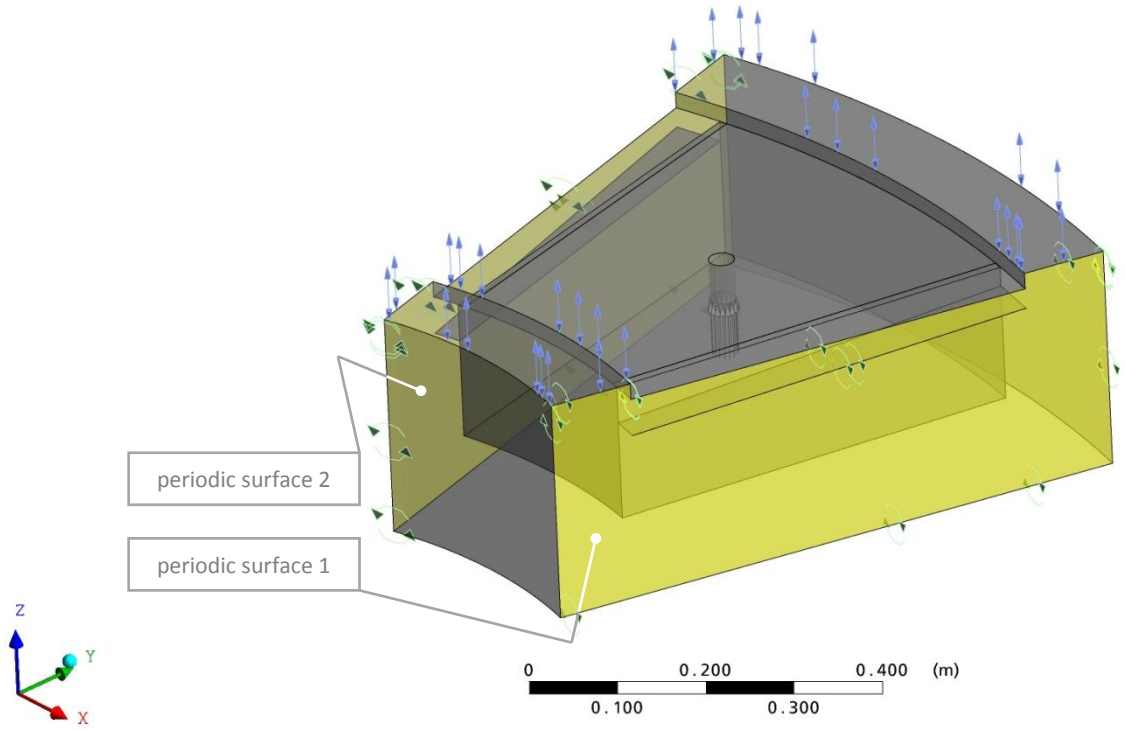

Figure 4.29. Periodicity boundary condition

All nodal values (pressure, temperature, velocity components, mesh movement components etc.) are transferred in this way. Connection of the nodes in case of rotational periodicity condition is presented in Figure 4.30.

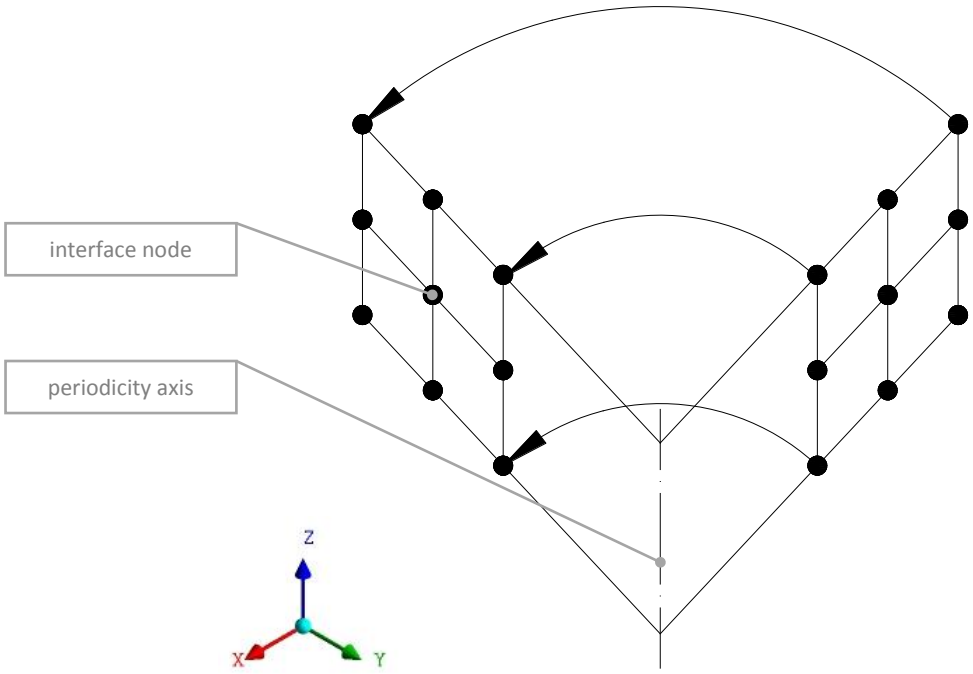

Figure 4.30. Principle of the rotational periodicity boundary condition

Opening:

An opening boundary condition allows the fluid to enter and exit the modeled domain depending on the behavior of the flow. It is modeled above the sliding surface in order to locate this boundary condition further away from the high velocity field gradients regions. Additionally in such way this boundary condition can be modeled as stationary whereas sliding surface of the runner can still move in any direction.

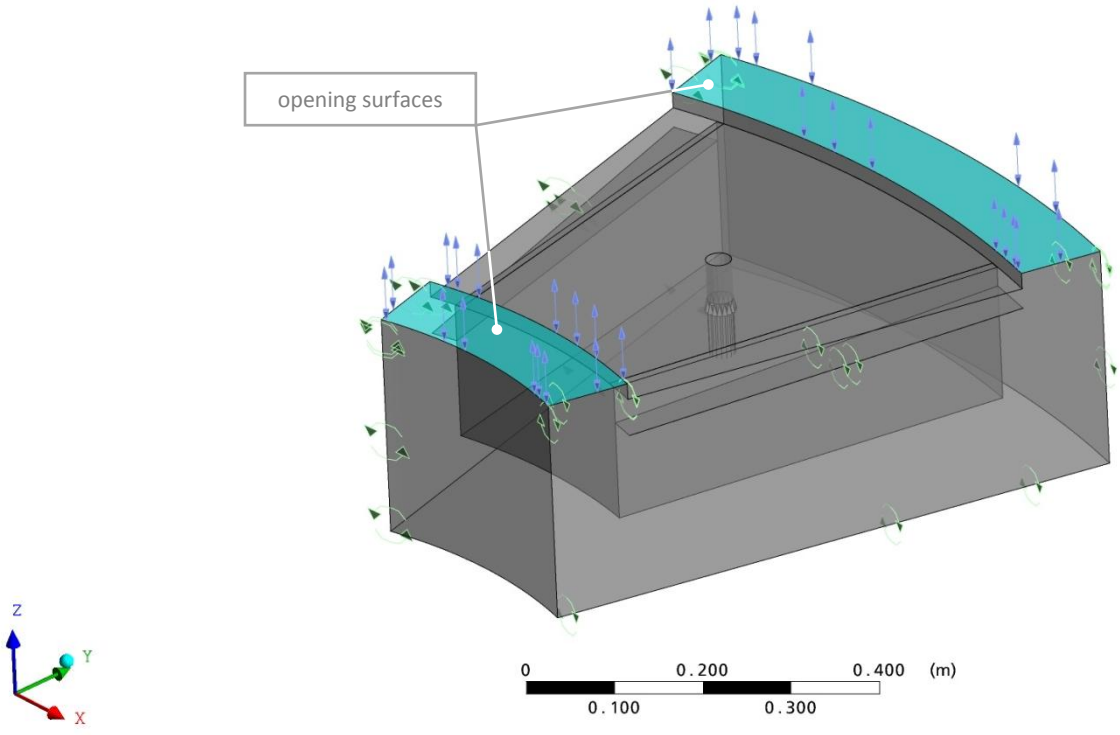

Figure 4.31. Opening surfaces of the fluid model

It is recommended to apply the opening (as well as the inlet and the outlet) boundary conditions on the stationary surfaces [**47**]. Thus there is a sort of extension between moving sliding surface of the runner and the stationary opening.

The temperature of the oil that enters the domain is assumed to be equal to the T_{cold} and the temperature of the oil that leaves the domain is calculated during the simulation. This is the so called oil bath temperature T_{bath}. The opening boundary condition allows to model the heat exchange in the bearing housing as it would take place in the real bearing. Thus T_{cold} has to be assumed (temperature of the oil that comes from the cooling system) and T_{bath} is calculated (result of the oil mixing in the bearing housing) as the average oil temperature in the whole fluid model volume.

Inlet:

The hydrostatic jacking system inlet is located at the stationary end of the pipe. A certain mass flow Q_{HS} $[\mathrm{l/min}]$ can be assumed to simulate real output of the supplying pump. The jacking pressure has to be calculated depending on the resistance that acts on the flow. The Q_{HS} can be modified during the simulation process in order to follow the changes in the real bearing. An example diagram with Q_{HS} variations is shown in Figure 4.32. It describes three hours of system performance ($30\,min$ operating, two hours standby and then operating again). Normally hydrostatic jacking is turned off when the rotational speed is larger than $80\ \%$ of the nominal speed.

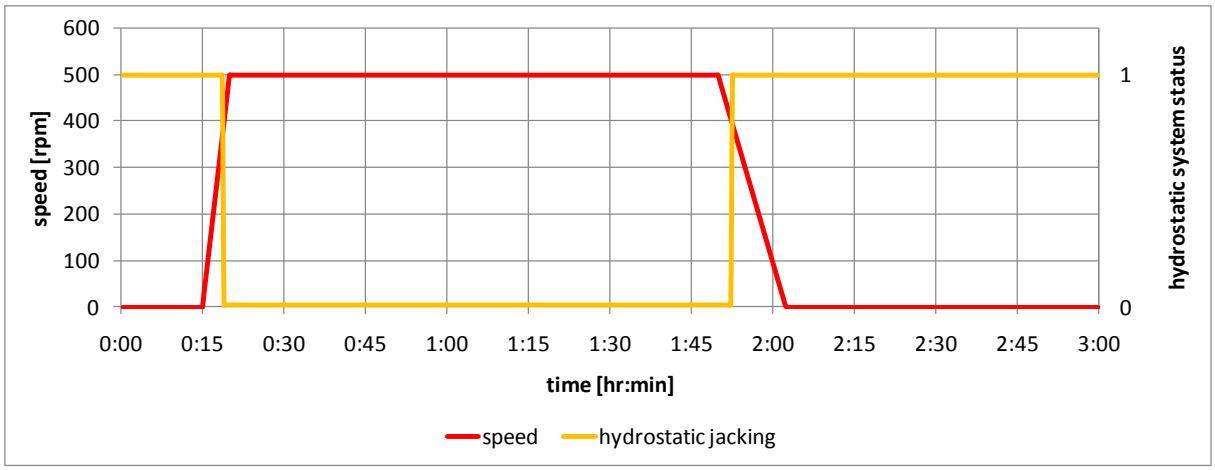

Figure 4.32. Example performance of the hydrostatic jacking system performance as a function of time

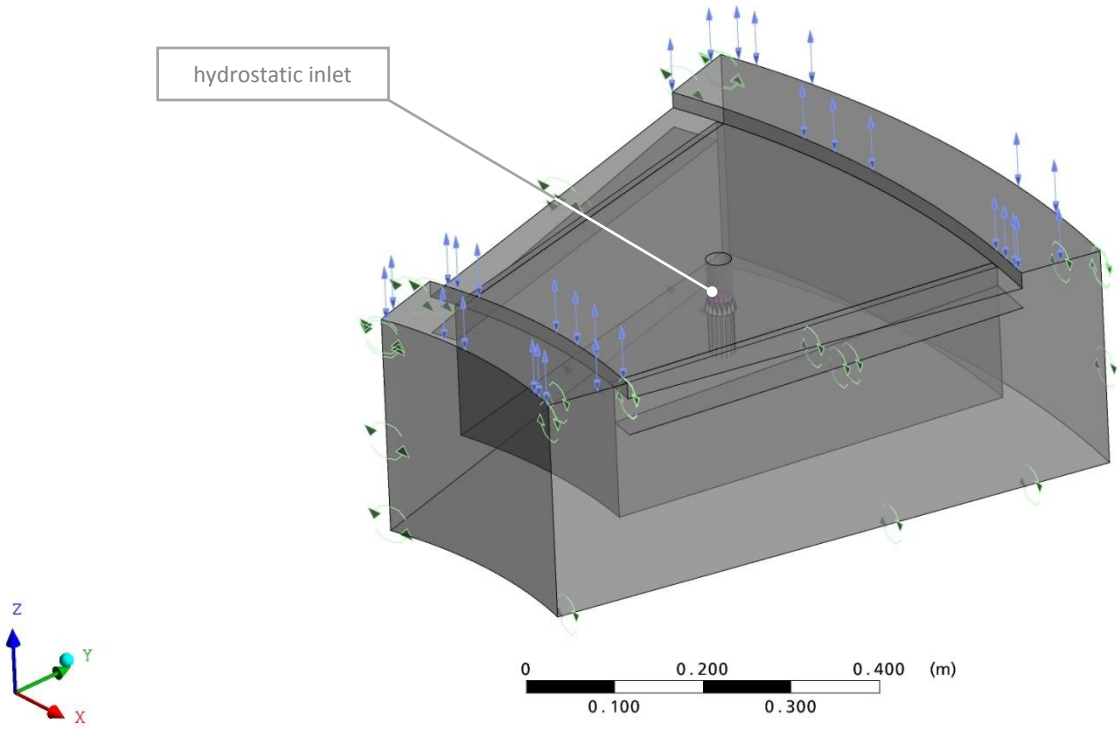

Figure 4.33. Hydrostatic jacking system inlet

Initial conditions

Since the model is provided for transient simulations the initial condition is of high importance due to not only stable startup of the simulation but also an appropriate process of change of parameters as a function of time (influence of initial conditions). Usually, the temperature initial condition is a constant temperature for all bearing elements and equal to T_{cold}. A calculation of the initial condition the hydrostatic jacking mode without rotational speed can be treated. In this way real hydrostatic oil gap shape can be calculated. Bearing works for 15 min of a real time in a hydrostatic jacking mode and after this initial calculation the startup procedure can be performed.

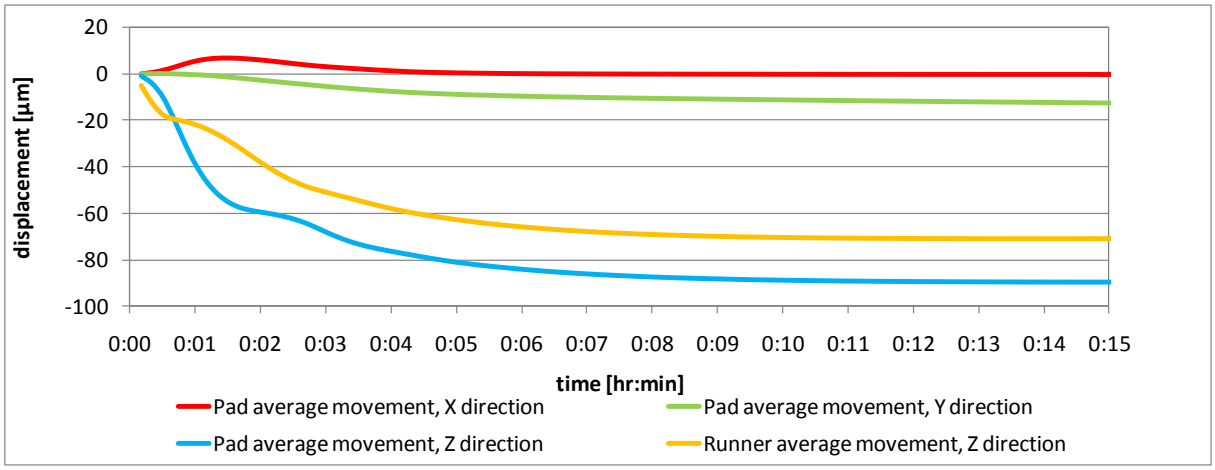

Figure 4.34. Evaluation of the initial condition – bearing parts movements

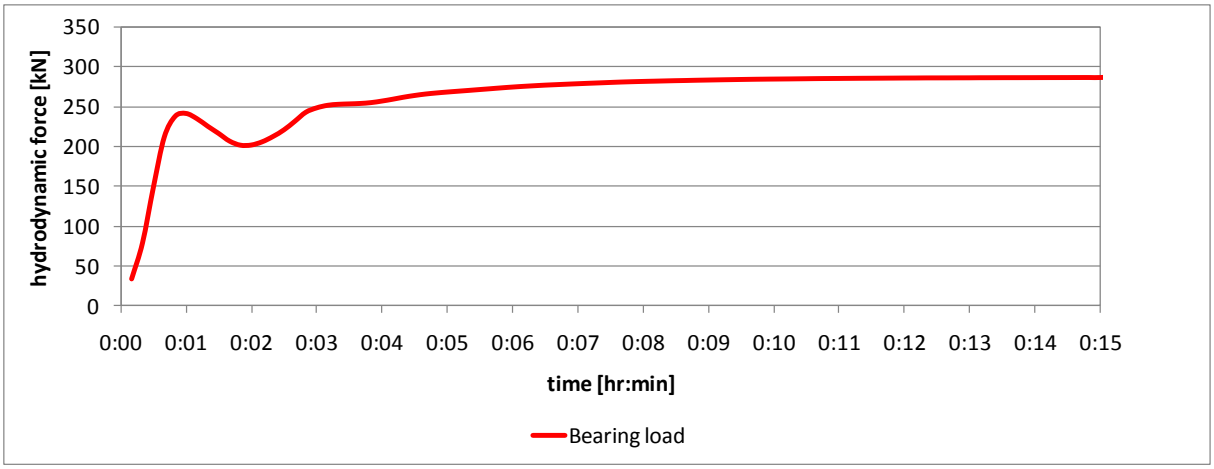

Figure 4.35. Evaluation of the initial condition – bearing load

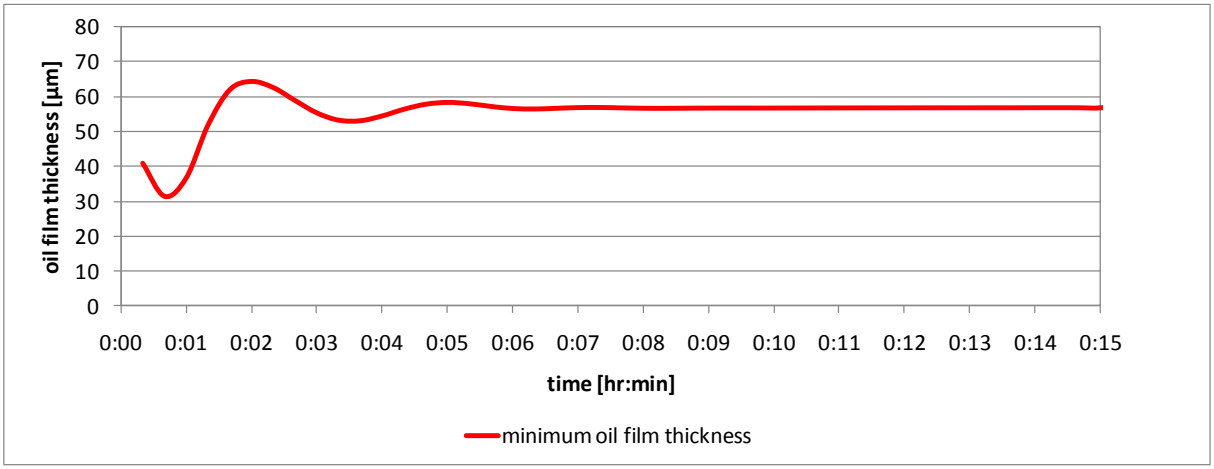

Figure 4.36. Evaluation of the initial condition – oil film gap

Structural initial condition has to be calculated in the first time steps due to lack of knowledge during definition of the model. Also in hydrostatic jacking mode, the oil film gap is not flat as it is defined at the beginning and is different than the initial guess of $50\ \mu m$. The initial calculation allows to find the realistic start point (oil film geometry) prior to real startup simulation.

4.5 Identification of errors

Every simulation is subjected to certain errors that have influence on the final result. CFD methods which solve RANS (Reynolds Averaged Navier Stokes) equations are based on the assumption that the turbulent flow can temporarily be averaged by the steady state solution. This can be done if physical unsteadiness of the flow has a significantly longer time scale than the time scale of the turbulences. Nevertheless all obtained results are within a certain range of tolerance.

According to [**46**] CFD simulations are subjected to many errors and uncertainties. Among them one can distinguish the following ones:

- model uncertainty,
- discretization or numerical error,
- iteration or convergence error,
- round-off error,
- application uncertainty,

- user error,
- code error.

Spatial discretization errors result from the numerical order of accuracy of the discretization scheme and from the grid spacing. The recommended second order scheme is used for each solver. It means that in the cells parameter change (e.g. velocities or temperature) is linear.

During development of the model several different time step lengths have been checked. It has been finally decided to use a standard time step length of $20\ s$. This is the maximum length for which a stable solution in the whole analyzed time range covered by the simulation is assured. Two times shorter time steps give almost exactly the same results but the simulations are much more time consuming.

Mesh density (spatial discretization) was adjusted in order to obtain convergence rates below the allowable limits and smooth fields of the resulting parameters. It was not possible to check the grid sensitivity due to lack of computer resources. Convergence stability of both the normalized residuals and important physical parameters (temperatures, pressures, velocities, lift forces, etc.) indicate good quality of the obtained results.

Convergence is a way of judging the quality of the obtained numerical solution. It is measured by the means of residuals. These are three dimensional fields that indicate the local imbalance of each conservative control volume equation. Most commonly they are normalized in order to make them consistent with generally used convergence criteria. According to [**47**] residuals $[r]$ are normalized for each solution variable ∅ with the use of Formula 4.8.

$$[\tilde{r}_{\emptyset}] = \frac{[r_{\emptyset}]}{\alpha_p \cdot \Delta\emptyset} \tag{4.8}$$

where $r_{\emptyset}$ is the raw residual control volume imbalance, α_p is representative of the control volume coefficient and Δ∅ is a representative range of the variable in the domain.

The most important advantages of normalized residuals are:

- residuals are independent of time step choice,
- residuals are independent of the initial guess.

Levels for convergence judging can be divided into the following groups:

- 5e-4 is very poor, global balances will be poor and quantitative data is largely unreliable,
- 5e-4 is loose convergence, but good enough for most engineering applications,
- 1e-4 is good convergence, often sufficient for most engineering applications,
- 5e-5 is tight convergence, it is often not possible to achieve this level of convergence,
- 1e-5 or lower is very tight convergence, sometimes required for geometrically sensitive problems,
- 1e-6 to 1e-7 is machine round-off.

The influence of several arbitrary assumed boundary conditions applied to the runner (T_b and α) is also investigated in Chapter 5.

4.6 Model conclusions

Detailed model of the bearing has been presented with certain particular design features but it is also possible to build similar model for different dimensions, geometry or even design solutions. Also fluid model can be modified when needed. For example cavitation effects (vapor formation) in low pressure regions can be taken into account. It may be important in case of high speed bearings due to divergent gap at the oil outlet edge. In the future it should also be possible to simulate the bearing with both air and oil together, so the boundary conditions could be placed even further from the bearing oil film. This is all due to the very large degree of flexibility of the FE and CFD methods. It is already possible for steady state bearing analyzes but the short time stepping and large mesh resolution require extremely long times of computation that cannot be accepted.

The model gives a lot of important information about the bearing state in transient and in steady state as well. Parameters that are results of simulation can be divided into following groups with different degrees of importance:

Essential bearing data:

- oil gap shape, minimum oil film thickness,
- inclination of the pad,
- pad elastic and thermal deformations,
- runner bending and thermal deformations,
- transient deformations of the bearing elements,
- sliding surface temperature profiles,
- temperature field distribution in bearing structure,
- sensor temperatures for comparison with measurements,
- pressure profiles on sliding surface in hydrostatic and hydrodynamic mode.

Secondary bearing data:

- heat flow through the bearing sliding surfaces,
- oil and heat flow through the oil film inlet and outlet windows,
- convection coefficients calculated on bearing sliding surfaces and other surfaces of the bearing pad,
- power losses generated due to friction forces in the oil film and mixing,
- circulation of the oil in the bearing housing,
- temperature of the oil surrounding the pad.

The computation takes approximately 8 minutes per time step in case of 5 coupling iterations with the use of Intel Core2Duo® processor with 2.53 GHz frequency and equipped with 4 GB RAM memory. Since a single time step is set to 20 seconds it is necessary to perform a large amount of time steps in order to calculate reasonable real time length. For bearing startup, for example, it is necessary to compute at least 2 hours of bearing operation to obtain steady state values. It means that there have to be 360 time steps performed which takes approximately 5 days. More difficult tasks like bearing calculation with increased specific pressure require even shorter time stepping and automatically longer times of computation.

5 Results of the calculations

5.1 Introduction

In this chapter results obtained with the use of the different versions and configurations of the model described in Chapter 4 are presented. Comparison and validation of the model with measurement data is also presented as well as the influence of certain parameters on the results.

The bearing elements deform in a way similar to the one presented in Figure 5.1 due to thermal gradients. The oil gap is the difference between them. In case of thrust bearing the load has to be always equalized by the hydrodynamic pressure. In the Figure 5.1 a possible deformation of both bearing parts is presented. The distance between both parts defines the resulting oil film profile.

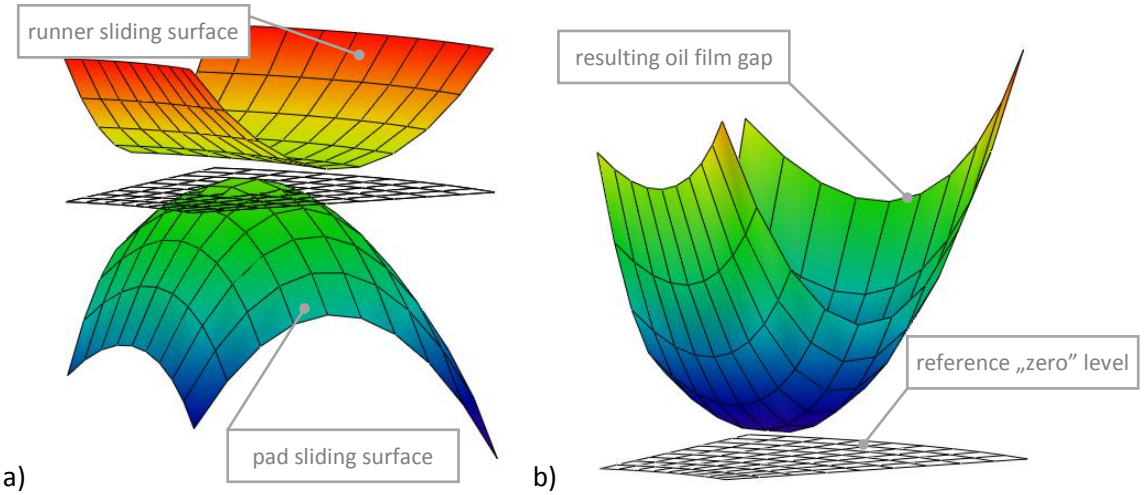

Figure 5.1. Oil film geometry, a) approximate deformations of the bearing elements, b) the resulting oil gap profile

Pad tilt angles and deformations are defined for both directions (radial and tangential) as presented in Figure 5.2.

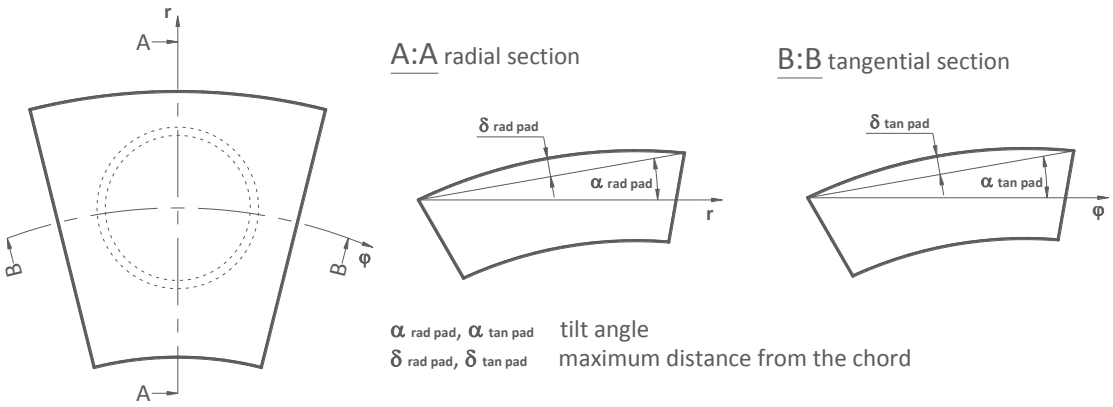

Figure 5.2. Definition of the pad deformations and tilt angles

Runner sliding surface due to rotational symmetry of the temperature field is deformed only in radial direction. Definition of its tilt angles and deformations is given in Figure 5.3.

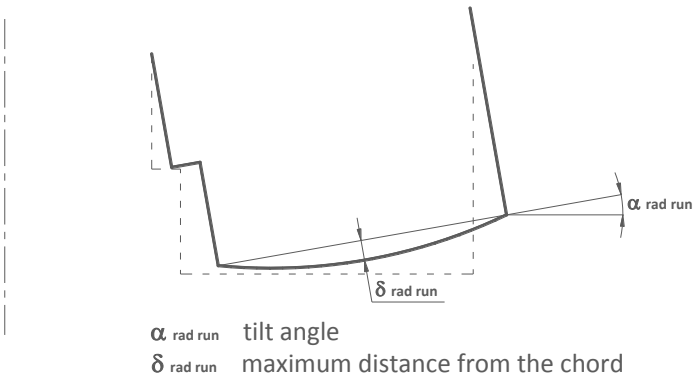

Figure 5.3. Definition of the runner deformations and tilt angles

The radial inclination of the oil film is the difference between the tilt angles of both the pad and the runner. In case of point supported pads both surfaces should be almost parallel in this direction.

5.2 Startup simulation of the Kopswerk II thrust bearing

During commissioning of the Kopswerk II units several detailed measurements have been performed. Comparison with measurement data taken during calorimetric run is presented. It consists of the start-up of the machine followed by continuous operation under stable conditions in order to obtain steady state working conditions which were mainly expressed by constant bearing temperatures. Calorimetric run is performed in order to measure all losses of the unit during operation and thus to calculate its overall efficiency. This measurement is made in the steady state condition so after startup the unit has to run for several hours in order to stabilize all important parameters. This case was taken for the comparison with the simulation of the startup procedure.

5.2.1 Input parameters

Input parameter for the simulation were rotational speed, cold oil temperature and hydrostatic jacking system performance.

During measurements operational parameters of the bearing were also monitored. These measurements are presented in Figure 5.4.

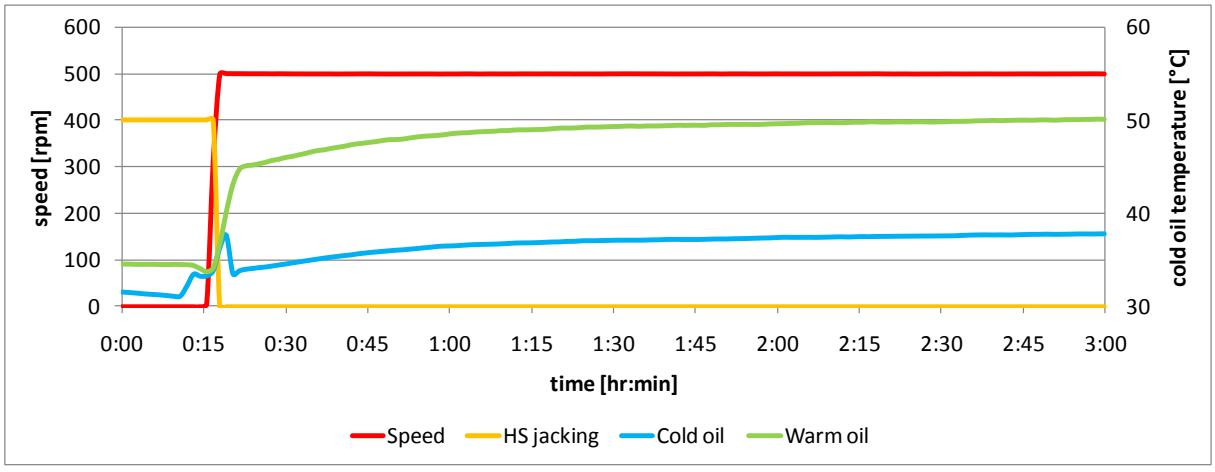

Figure 5.4. Operation parameters registered in the Kopswerk II power plant during startup

Assumed operational parameters for the simulation were adjusted as close as possible to the measured ones (Figure 5.5). The cold oil temperature was set at a constant level and equal to the final cold oil temperature $36\ °C$. The reason of such an approach is the simplification of the input

data supplied to the model. In the design phase there is no information regarding the cold oil variations during operation. That is why this parameter is assumed to have a constant value. The rotational speed of the unit is equal to zero at the beginning of simulation so the bearing works in a hydrostatic mode. After $15\,min$ of operation the speed begins to increase and within $3\,min$ it reaches the nominal value of $500\,rpm$. At the time when the rotational speed equals $80\,\%$ of its nominal value the hydrostatic jacking is turned off. After that moment the bearing operates in a hydrodynamic mode only.

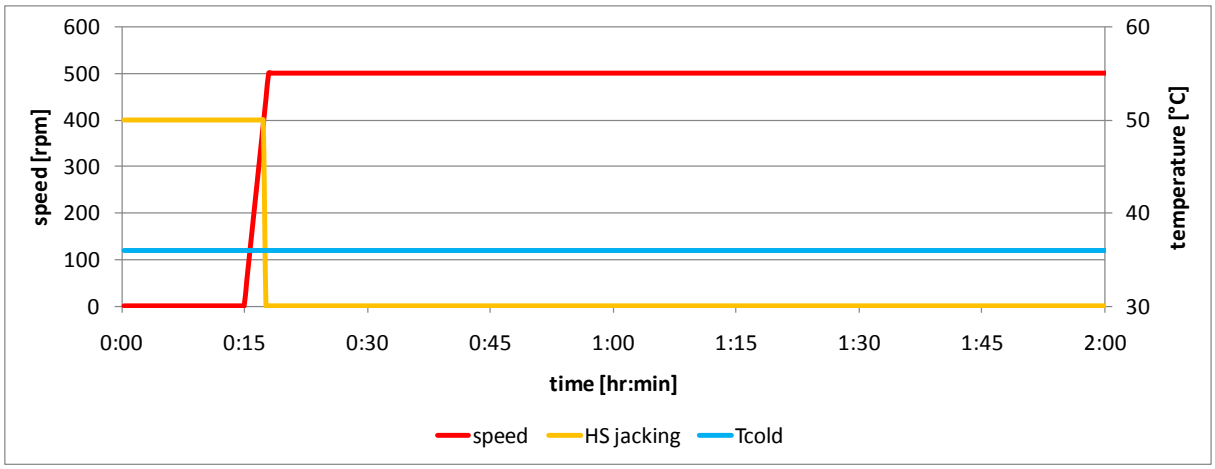

Figure 5.5. Operation parameters assumed for the start up simulation

Other parameters that were not subjected to any changes are listed in Table 5.1. An additional parameter is the startup time which is taken into consideration in the further part of this chapter.

Table 5.1. Input parameters for the simulation

No.	Parameter	Symbol	Value	Unit
1	Nominal speed	n	500	rpm
2	Load	F	3512000	N
3	Specific pressure	p	1.55	MPa
4	Cold oil temperature	T_{cold}	36	°C
5	Start-up time	$t_{startup}$	180	s

5.2.2 Comparison with measurements

The main data registered during measurements in case of Kopswerk II hydro generator were the temperature of the pads. Each pad is equipped with two sensors placed symmetrically relative to the supporting point in order to measure temperatures in both directions of rotation. This gives also a better information about temperature field in the bearing pad. The relative sensor locations are given in Table 5.2. The reference point is located on the inner radius of the oil film inlet edge.

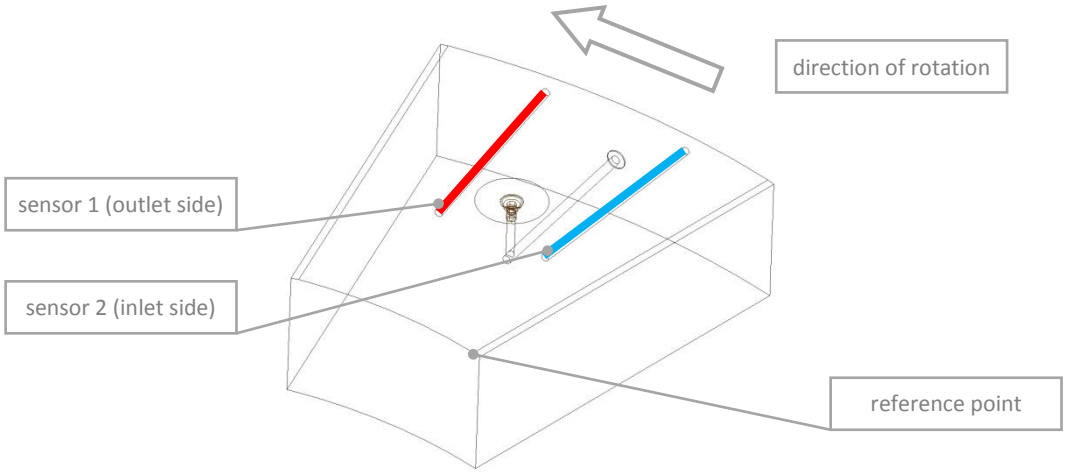

Figure 5.6. Sensor locations and the reference point

For the comparison with measurements counter clockwise direction of rotation is assumed. It means that the sensor 1 is located at the outlet side and the sensor 2 at the inlet.

Table 5.2. The temperature sensor absolute coordinates

No.	Parameter	Sensor 1	Sensor 2
1	Radial position (width)	225 mm (45 %)	225 mm (45 %)
2	Tangential position (length)	17 mm (71 %)	7 mm (29 %)
3	Axial position (height)	25 mm (14.7 %)	25 mm (14.7 %)

Since in the power plant the pads are never equalized perfectly there are some minor differences of the measured temperatures among them. For each measured side of the pad there are two temperature signals in the diagram. They show measured minimum and maximum registered temperature of all the pads. The goal of simulation is to verify if the calculated values fit the measured ones. Since the simulated temperature field is similar to the real one can assume that thermal deformations are also estimated in an appropriate way. Thermal deformations together with accurately estimated load carrying capacity give a realistic oil film gap profile. Properly estimated temperature values indicate also that oil flow and heat generation are calculated properly. On the other hand the temperatures are the most reliable measurements of all that are possible to perform in case of bearing investigations. The pressures can also be measured very precisely but the pressure profile does not give sufficient information since it mainly depends on the external load. Oil film thickness measurements are a great source of data but usually they are very difficult to carry out (especially in case of sensors located in the rotating part) and are also subjected to large measurement uncertainties since many additional effects have to be taken into account (thermal and elastic deformations of bearing parts for example). In case of industrial applications the distance sensors are mounted very rarely. In order to simplify the simulation and interpretation of the results the cold oil temperature is assumed to be at constant level $T_{cold} = 36\,°C$. First of all it helps to interpret the obtained results and makes it possible to compare with other cases that will be analyzed in the later parts of this chapter. Stabilized temperature distribution (time $7200\,s$) on the bearing elements (solid model results) are given in Figure 5.7. Deformations of these elements are magnified 1000 times in order to visualize the true shape. An interesting effect can be noticed on the

inner and outer radii of both parts – these edges are most intensively cooled. Such effect is not observed for models with assumed constant oil film inlet temperature.

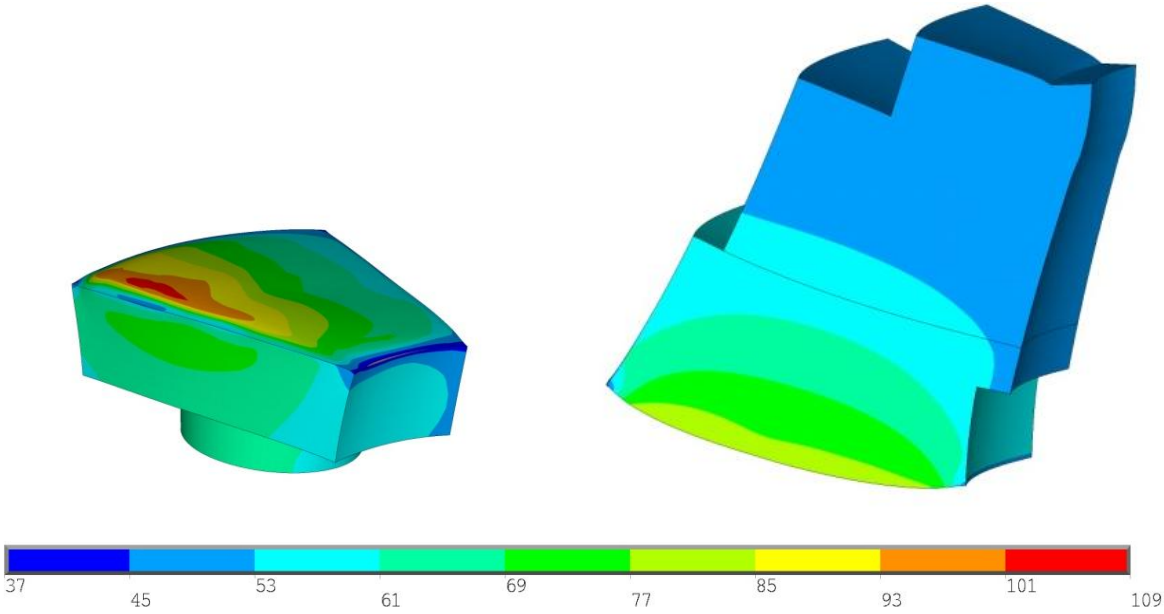

Figure 5.7. Temperature field distribution (steady state solution, time 7200 s) on the thrust bearing elements, deformations magnified 1000 times, temperatures shown in [C]

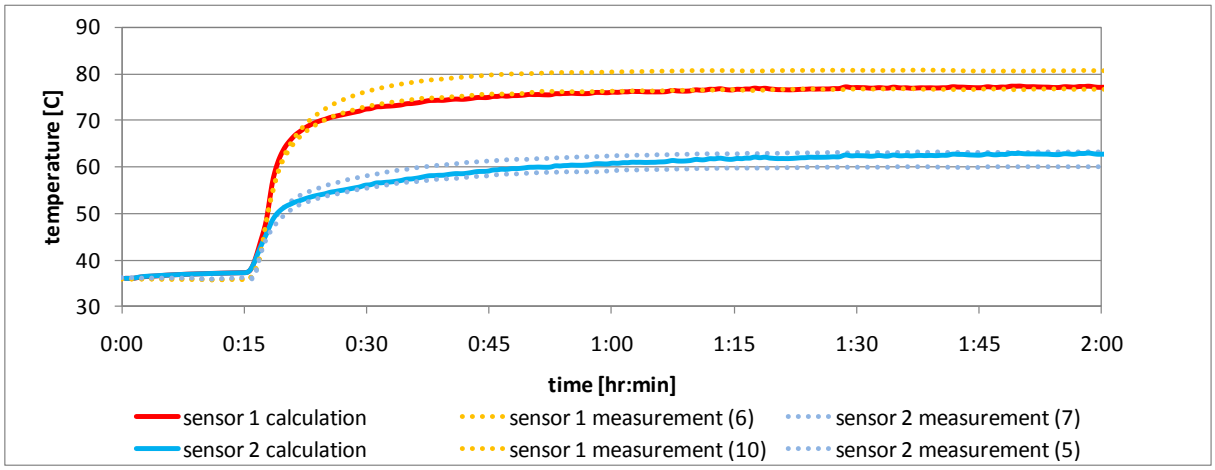

Figure 5.8. Comparison of the measured sensor temperatures with startup simulation

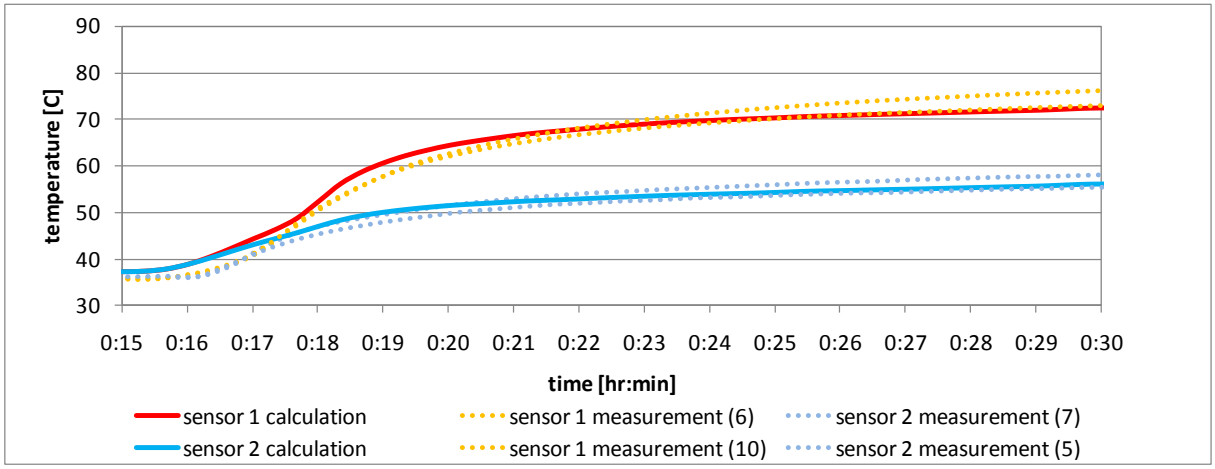

Figure 5.9. Comparison of the measured sensor temperatures with startup simulation

Measured temperature profiles are almost exactly followed by the results of simulation. Also the obtained steady state temperature values are within the range of the measured ones. This indicates that there are no significant errors in the developed model. Thermal dynamics as well as the resulting steady state solution seem to be precisely reflected in the simulation. Good agreement of the calculated temperatures with the measured ones indicates that the physical effects which are the main cause of the temperature increase are simulated properly. The point of hydrostatic jacking turn off ($time = 17.4\ min$, when the rotational speed reaches $80\ \%$ of the nominal speed) is visible on the simulated sensor 1 temperature profile where there is a clear change in the slope of the temperature curve.

5.2.3 Transient results of the simulation

There is a large amount of data gathered about the bearing during simulation. For each time step all results are stored and can be later reviewed for post processing purposes. During simulation several parameters are monitored in order to visualize the progress and to justify the quality of the solution. The simulation process is presented in the following figures (Figure 5.10, Figure 5.11, Figure 5.12, Figure 5.14 and Figure 5.15). Movements of the bearing elements are treated as an average displacement of the whole sliding surface in order to monitor the tendency of movement. These rough information is not used in any calculations and is shown only for information purposes during simulation. In this way the progress and convergence of the solution can be visualized and judged. The average movement of both pad (x - radial, y - tangential and z - axial coordinate) and runner (z - axial coordinate) is monitored during simulation. This information has rather an informative character which can show the tendency of the movements of the bearing parts.

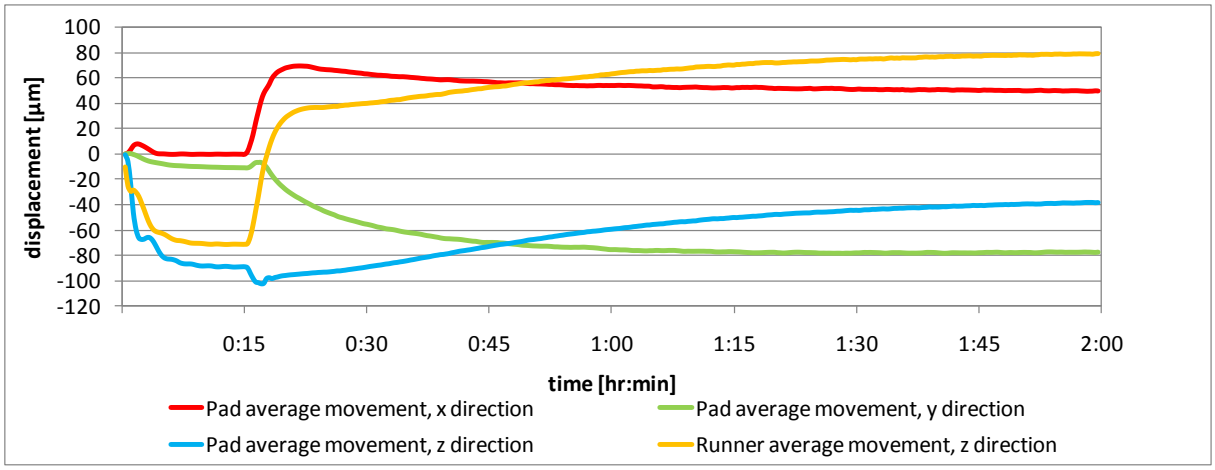

Figure 5.10. Movements of the bearing elements

Velocities of the elements are evaluated on the basis of the time step length $t_{step} = 20\ s$ and the relative difference between positions in the current and previous time step as follows:

$$v_{x_i} = \dot{x}_i = \frac{dx_i}{dt} = \frac{x_i - x_{i-1}}{t_{step}}$$

$$v_{y_i} = \dot{y}_i = \frac{dy_i}{dt} = \frac{y_i - y_{i-1}}{t_{step}}$$

$$v_{z_i} = \dot{z}_i = \frac{dz_i}{dt} = \frac{z_i - z_{i-1}}{t_{step}}$$

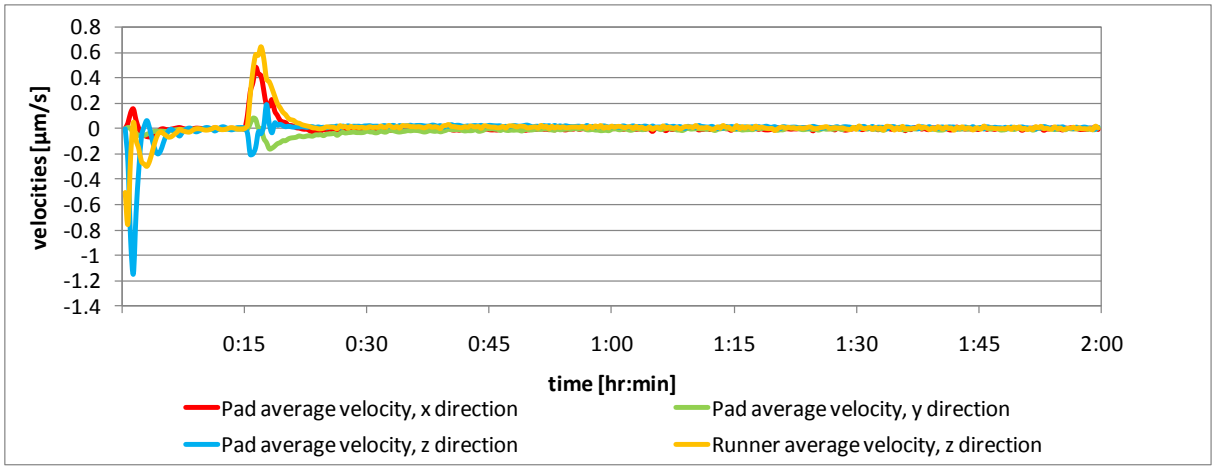

Figure 5.11. Velocities of the bearing elements

Temperatures monitored during simulation:

- maximum oil temperature in the oil film (red),
- average shaft temperature (orange),
- average oil temperature in the oil tank (green),
- minimum oil temperature in the oil tank (blue),

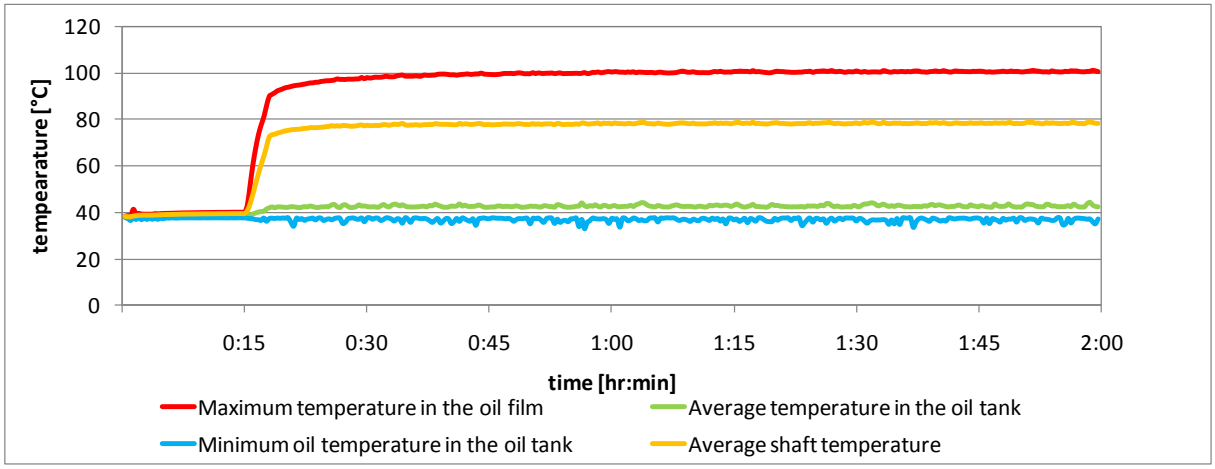

Figure 5.12. Temperatures

The maximum oil pressure in the oil film and the calculated force acting on the runner surface (for a single pad) are given in Figure 5.14. Pressure profile is integrated on the runner surface A in order to check if it equals to the applied thrust load. Where A stands for the area of the runner sliding surface per single pad (see Figure 5.13).

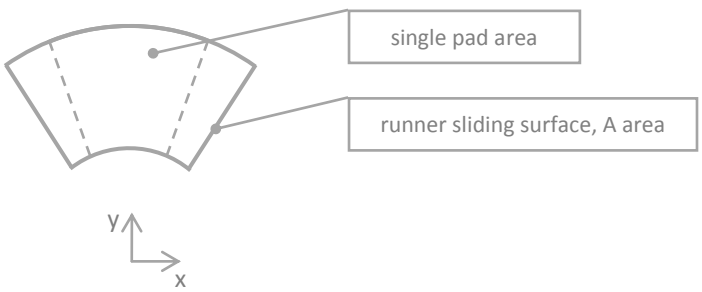

Figure 5.13. Definition of the area of the runner sliding surface A for integration purposes

$$F = \int_A p \, dA$$

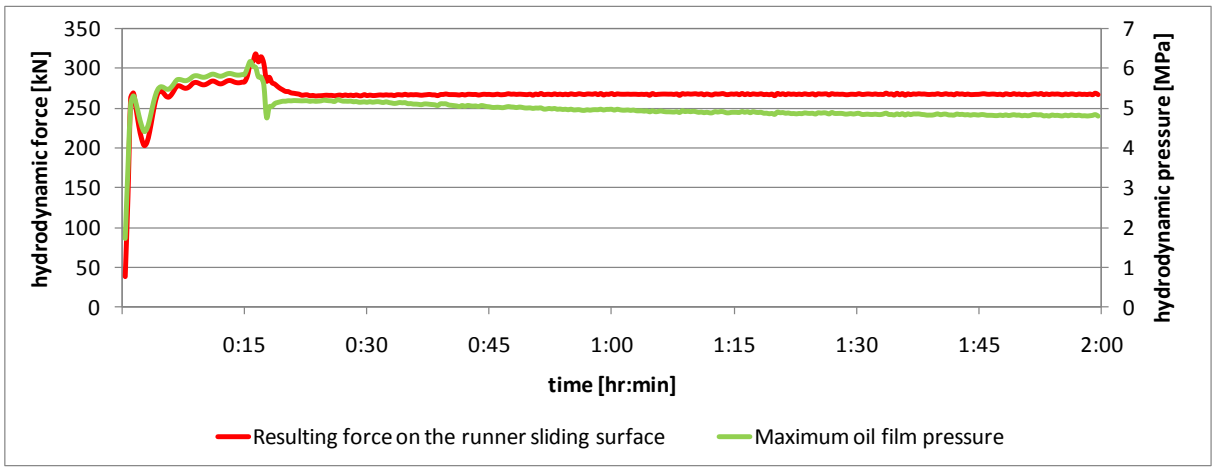

Figure 5.14. The oil film maximum pressure and the resulting force acting on the runner sliding surface

The shear stress that acts on the runner surface is monitored during simulation so the friction torque $\boldsymbol{\tau}$ and the power loss P_{loss} can be evaluated in the following way:

$$\boldsymbol{\tau} = \int_A \tau_{runner} \cdot r \, dA$$

The number of pads has to be taken into account in order to estimate the total bearing power losses:

$$P_{loss} = \boldsymbol{\tau} \cdot \omega \cdot n_p = \boldsymbol{\tau} \cdot \frac{\pi \cdot n}{30} \cdot n_p$$

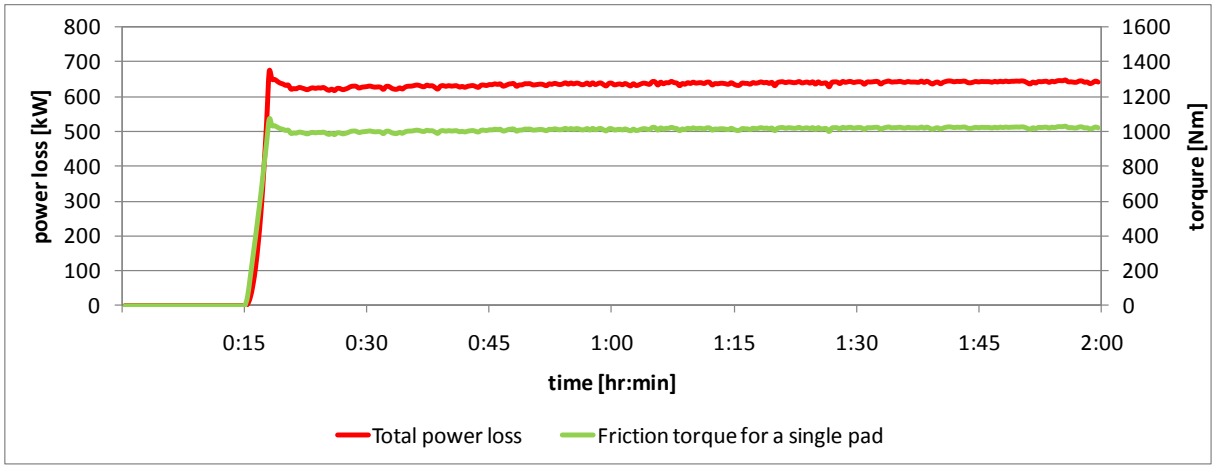

Figure 5.15. Total power losses and friction torque for a single pad

Slightly higher power losses can be observed shortly after startup. This effect can be explained by low temperature of the oil in the bearing and the oil film. Higher viscosity automatically causes higher heat generation and the power loss finally stabilizes at the lower level.

One very interesting result from the simulation model is the transient behavior of the thermoelastic deformations and relative movements of the bearing parts. These results are shown in the following figures (Figure 5.16, Figure 5.17, Figure 5.18, Figure 5.19, Figure 5.20 and Figure 5.21) as a function of time. Radial deformation of the pad shows a clear maximum shortly after the unit obtains its nominal speed. The maximal value is equal to $43\ \mu m$ and the steady state value to $27\ \mu m$ (ratio 1.59).

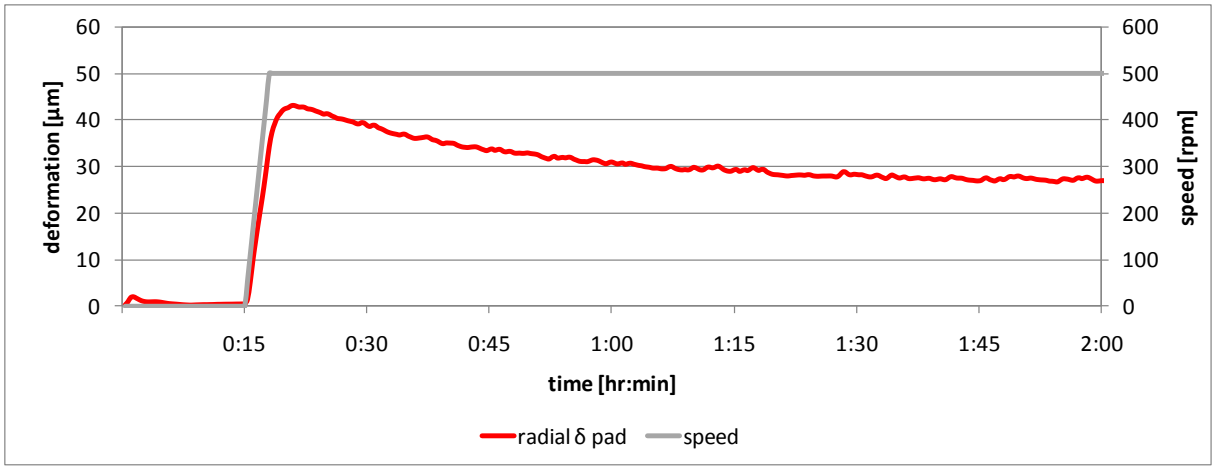

Figure 5.16. Pad radial deformations

The radial tilt angle of the pad is the reaction of the thermal bending of the runner (see Figure 5.21). These two parameters are almost equal – it means that in radial direction both sliding surfaces remain almost parallel. In comparison to Michell type (edge supported) this is the main advantage of the Kingsbury point pad support method. Radial tilt angle of the runner can be compensated by the radial tilt of the pad.

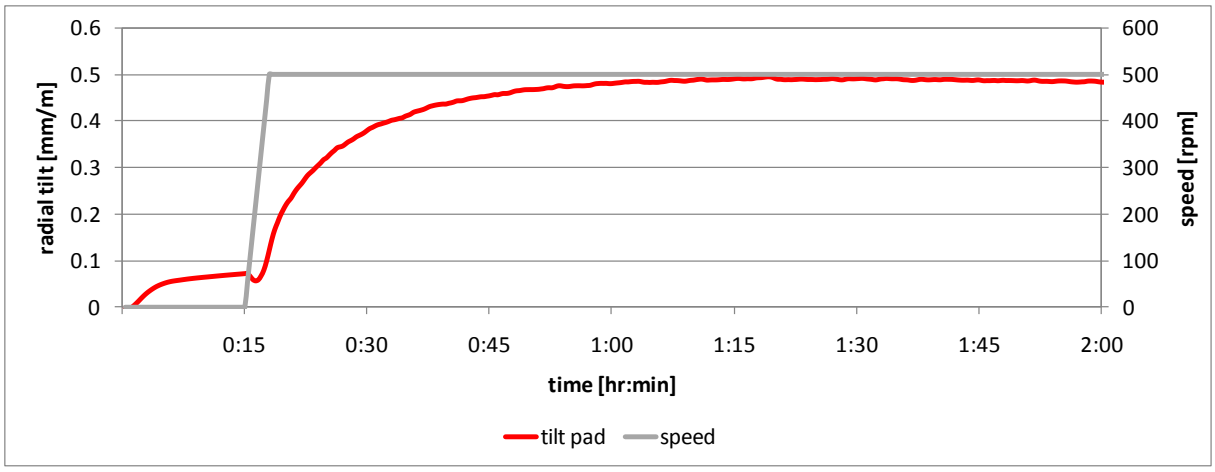

Figure 5.17. Pad radial tilt angles

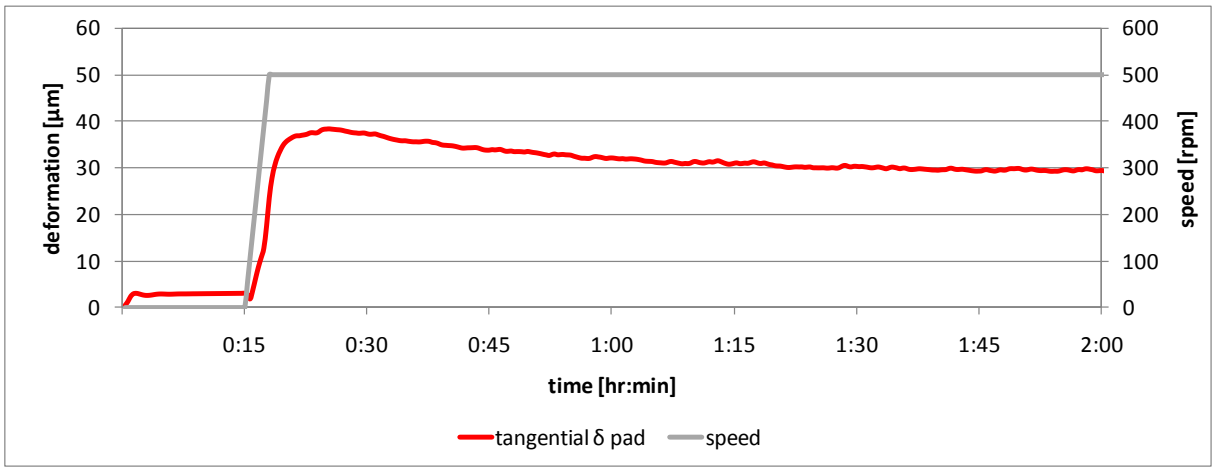

Figure 5.18. Pad tangential deformations

Deformation of the pad in the tangential direction is smaller than the one in radial direction. This is mainly caused by the proportion of the pad dimensions ($B/L = 1.326$). The maximaum value is

equal to $38\ \mu m$ and the steady state value to $29\ \mu m$ (ratio 1.31). Tangential tilt angle shows hydrodynamic inclination of the pad. Almost direct response on the rotational speed can be observed in this case. Later slow relaxation is most probably caused by changes of the pad deformations.

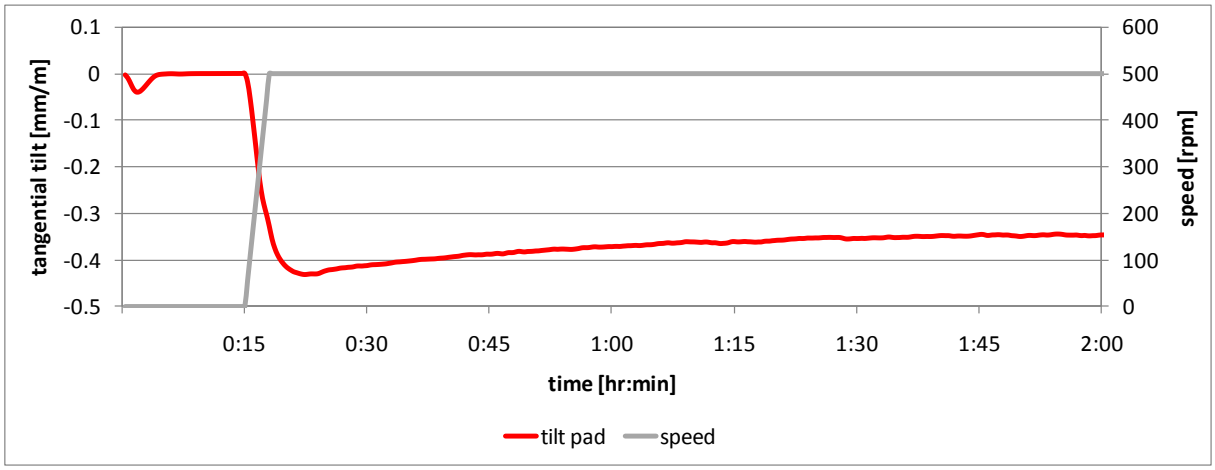

Figure 5.19. Pad tangential tilt angles

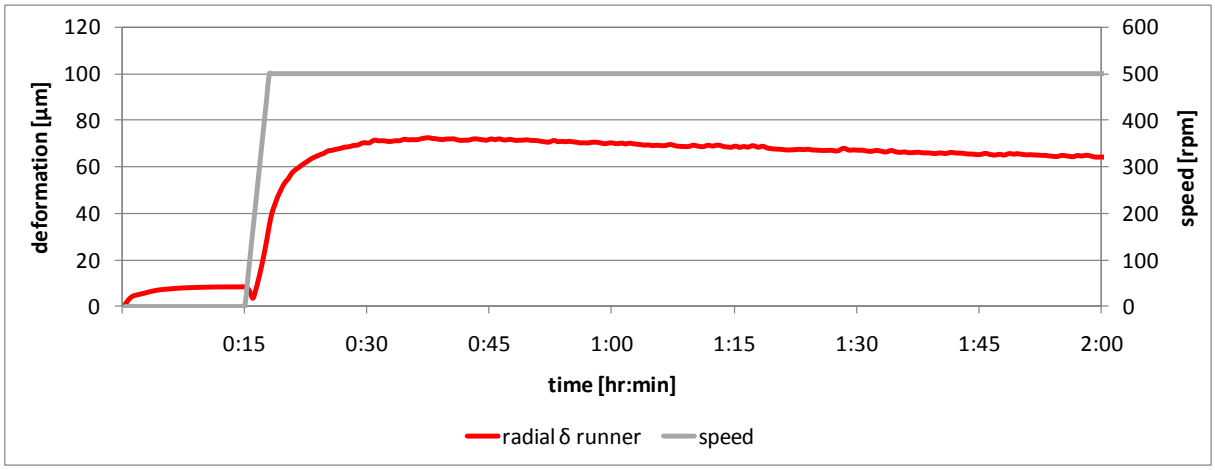

Figure 5.20. Runner radial deformations

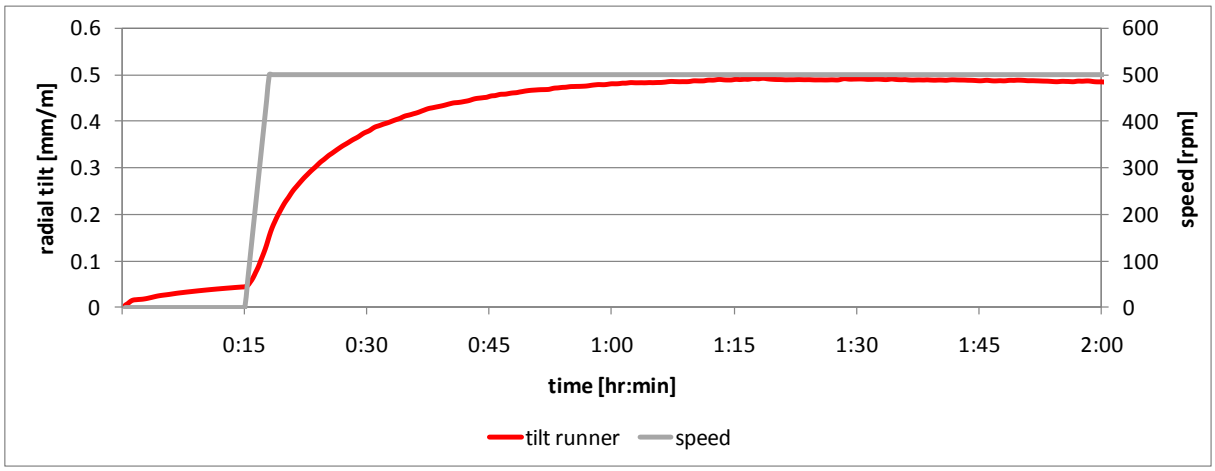

Figure 5.21. Runner radial tilt angles

Runner reaction on startup is much slower than the response of the pad. In this case one can observe a small thermal peak of deformation approximately $30\ min$ after startup. Later very slow relaxation occurs – even $2\ hr$ of simulation time are not enough to obtain a fully stabilized deformation. The

value of runner deformation is significant. It is approximately twice as large as that calculated for the bearing pad. This is an important information since this deformation should not be neglected in the calculation. A peak of pad deformation can be noticed shortly after obtaining nominal rotational speed. Peak values are significantly higher than the steady state ones. The observed ratios are 1.59 for radial and 1.31 for tangential deformation.

5.2.4 Temperature and velocity distributions on the oil film cross sections

In the following figures (Figure 5.22, Figure 5.23, Figure 5.24, Figure 5.25, Figure 5.26, Figure 5.27, Figure 5.28 and Figure 5.29) steady state (time $7200\ s$) oil film temperature and velocity profiles (fluid model results) are presented on the marked cross sections through the thickness of the oil film. The location of the cross section is symbolically presented in the right sketch of the pad. The curved arrow at the bottom represents the direction of rotation of the shaft.

Oil film inlet

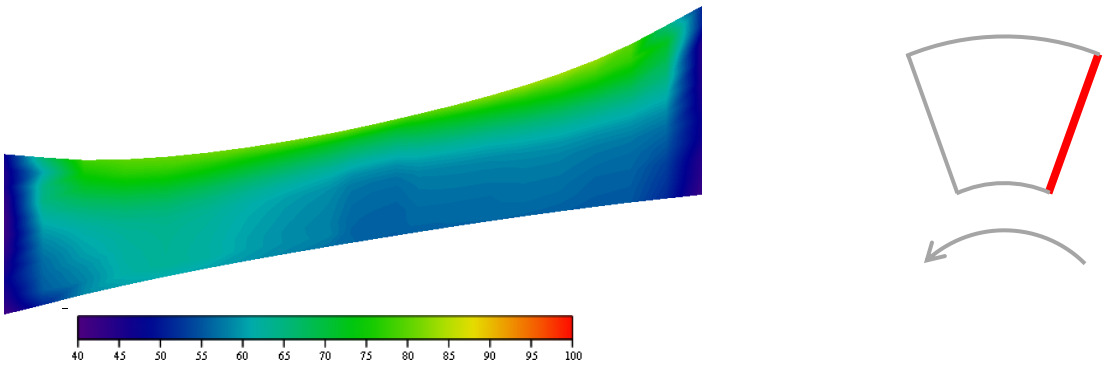

Figure 5.22. Oil film inlet shape and temperature distribution [C]

Oil film outlet

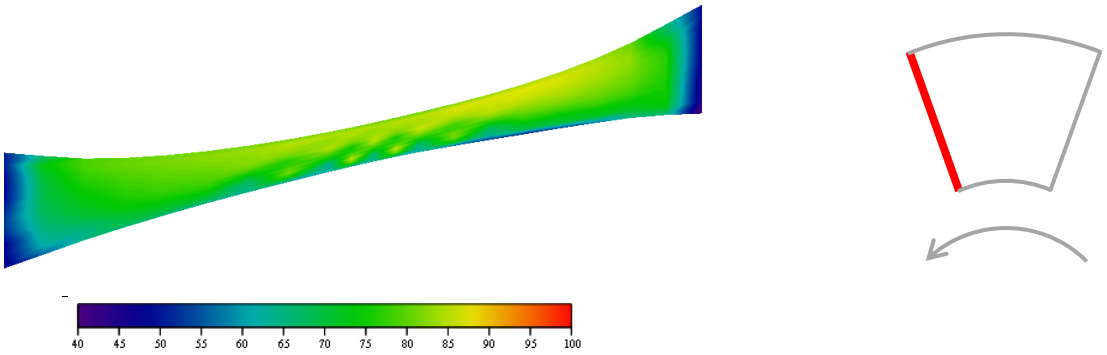

Figure 5.23. Oil film outlet shape and temperature distribution [C]

Oil film 0.75 B tangential cross section

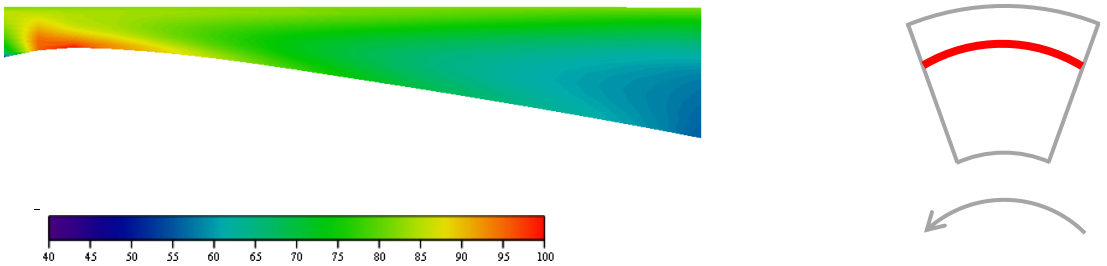

Figure 5.24. Oil film 0.75 B shape and temperature distribution [C]

Oil film inlet tangential velocity profile

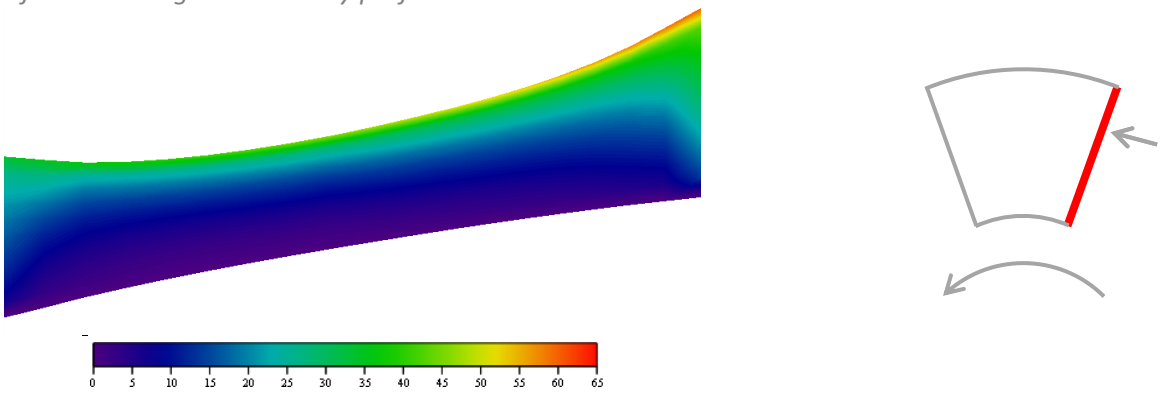

Figure 5.25. Oil film inlet shape and tangential velocity distribution [m/s]

Oil film outlet tangential velocity profile

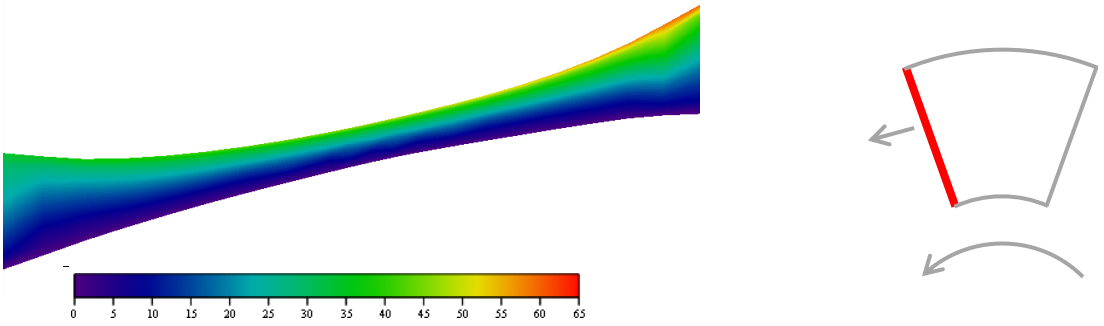

Figure 5.26. Oil film outlet shape and tangential velocity distribution [m/s]

Oil film outer diameter tangential velocity profile $R = 1.15\ m$

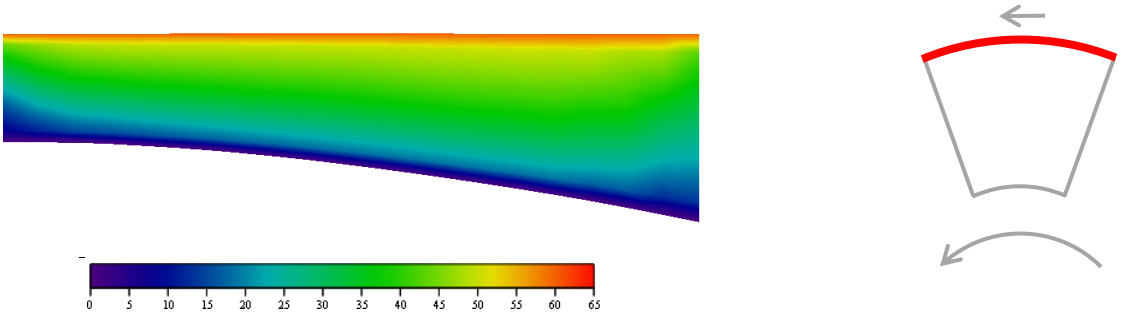

Figure 5.27. Oil film outer diameter shape and tangential velocity distribution [m/s]

Oil film 0.75 B tangential cross section tangential velocity profile $R = 1.025\ m$

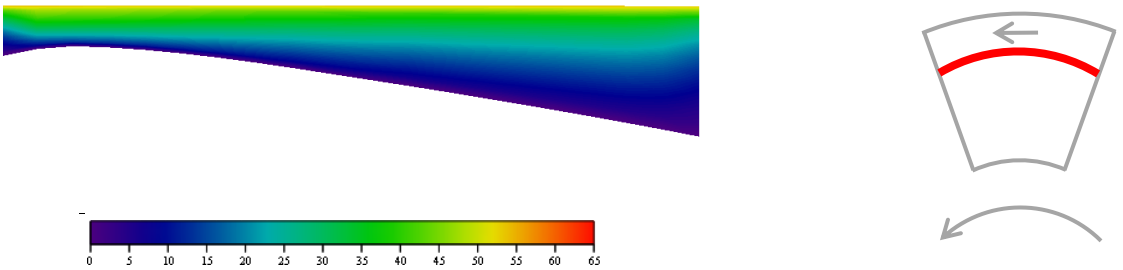

Figure 5.28. Oil film 0.75 B shape and tangential velocity distribution [m/s]

Oil film inner diameter tangential velocity profile $R = 0.65\ m$

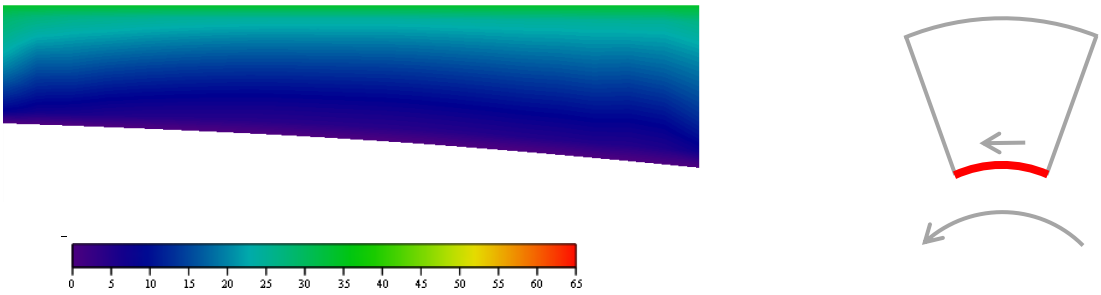

Figure 5.29. Oil film inner diameter shape and tangential velocity distribution [m/s]

Temperature and velocity distributions supply a lot of interesting information about the resulting oil film. The three dimensional temperature profile can be noticed not only at the cross section through the tangential length of the oil film (Figure 5.24) but also at the inlet and outlet of the oil film. In many simpler bearing calculation programs the oil film inlet temperature is assumed as a constant value.

5.2.5 Oil film thickness analysis

Transient analysis of the oil film thickness is shown for six points of the pad sliding surface (three on the leading L1, L2, L3 and three on the trailing edge T1, T2, T3). Distribution of these points is marked in Figure 5.30. Additionally, the overall minimum oil film thickness is given in Figure 5.31.

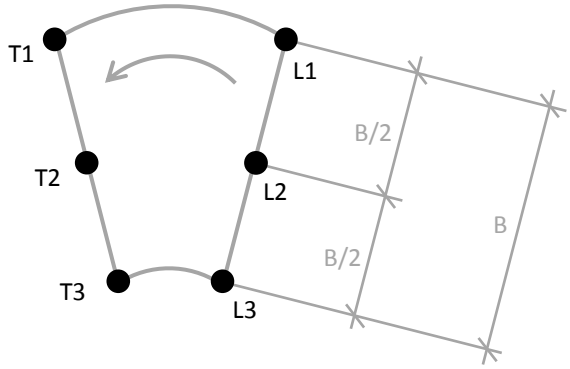

Figure 5.30. Leading and trailing edge points for the oil film gap observation

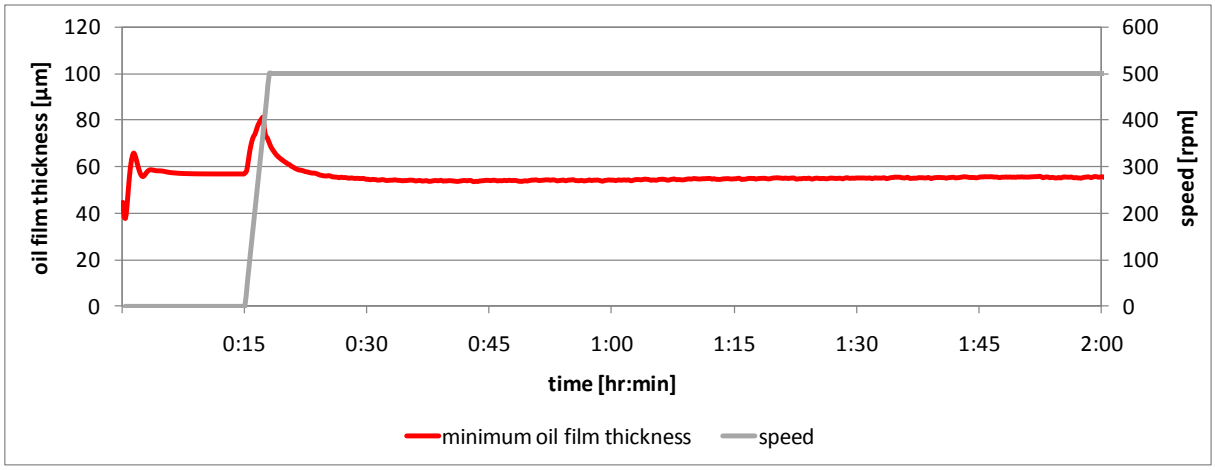

Figure 5.31. Calculated minimum oil film thickness

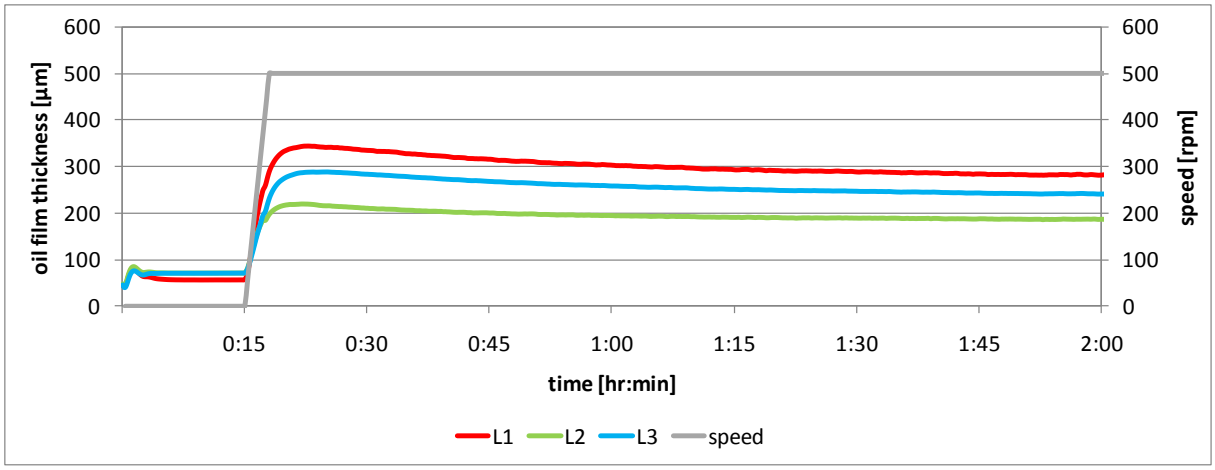

Figure 5.32. Calculated leading edge oil film thickness

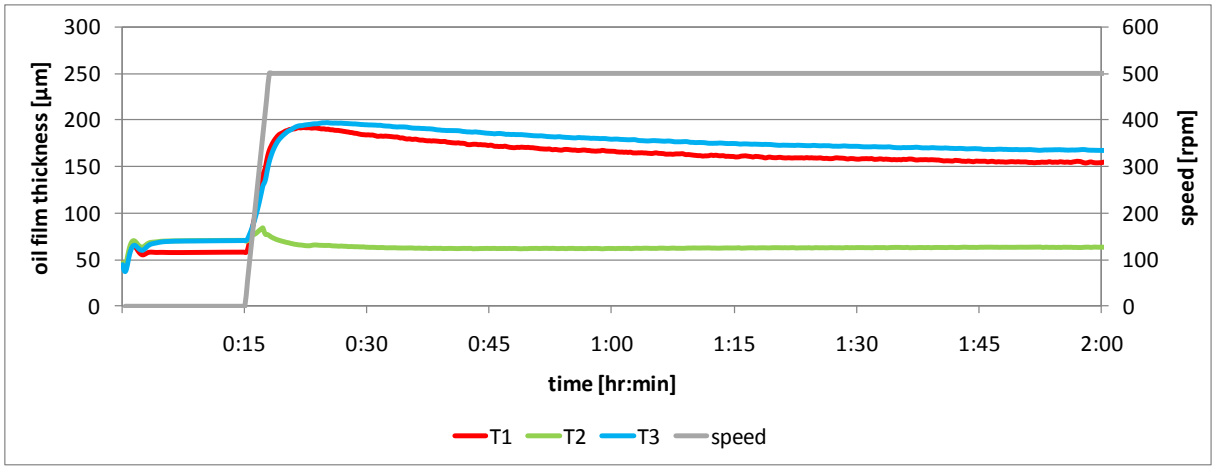

Figure 5.33. Calculated trailing edge oil film thickness

Course of changes of the oil film thickness is similar to the example given in Figure 2.45 (registered in a power plant). For the thrust bearing taken under investigation (Kopswerk II) such oil film thickness measurement data was not available. Calculated distributions of the oil film thickness are shown in Figure 5.34 for two different time points. Minimum and maximum values are listed in Table 5.3.

Table 5.3. Minimum and maximum calculated oil film thickness at different simulation times

No.	Parameter	Symbol	Value (time 00:20)	Value (time 02:00)	Unit
1	Minimum oil film thickness	h_0	62.09	54. 41	μm
2	Maximum oil film thickness	h_1	313.24	267.54	μm

A very interesting fact can be noticed that measurement of the oil film thickness at the trailing edge gives no relevant information about the minimum oil film thickness. The overall calculated minimum value in steady state is $54.4\ \mu m$ whereas the minimum value in the middle of the trailing edge is $63.3\ \mu m$. This difference is caused by significant deformations of the bearing elements. Similar effect can be seen in Figure 5.34 where oil film gap profiles are given at two different time points – minimum oil film thickness is not located on the trailing edge.

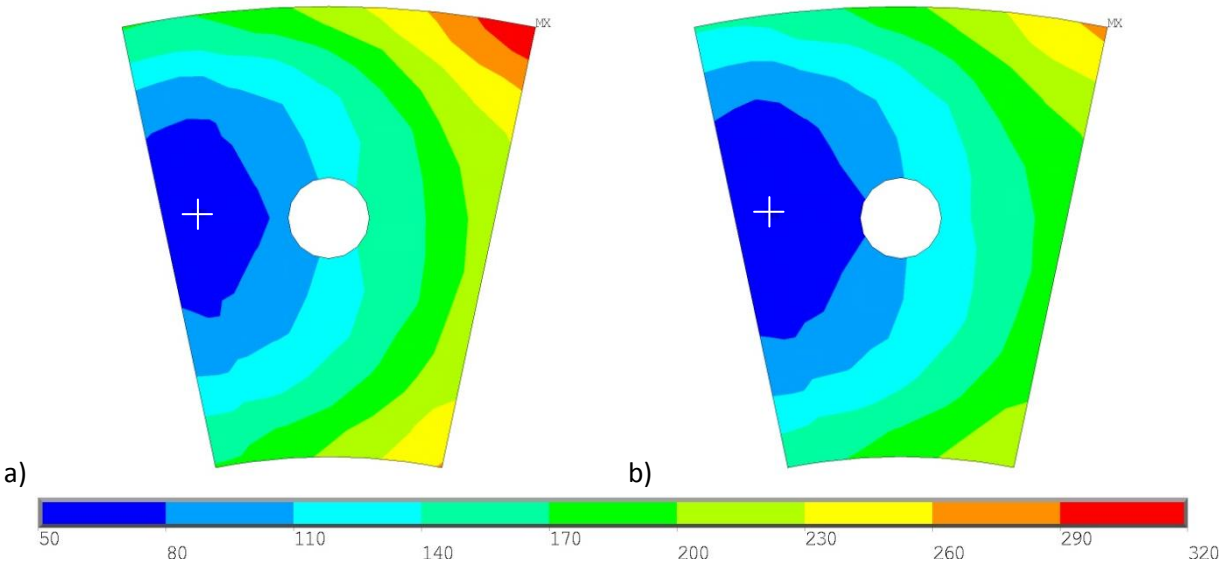

Figure 5.34. Calculated oil film thickness at different simulation times: a) 00:20 hr:min, b) 02:00 hr:min

From this point of view oil film gaps in large bearings should be monitored by distance sensors mounted in the runner. In this way, the whole gap profile can be captured. In order to obtain the whole oil film gap shape such measurement needs to be performed at several different radii, which seems difficult complex in practice.

In hydrostatic mode (Figure 5.35), the oil film gap is much flatter but one can notice elastic deformation of the bearing pad – contours are adjusted in order to cover the range of oil film gap for this particular case. Minimum oil film gap in this case is observed at the outer edge of the pad. Maximum oil film thickness is located close to the high pressure oil recess. Due to elastic deformation of the pad, oil film gap forms sort of a pocket that decreases lateral leakages.

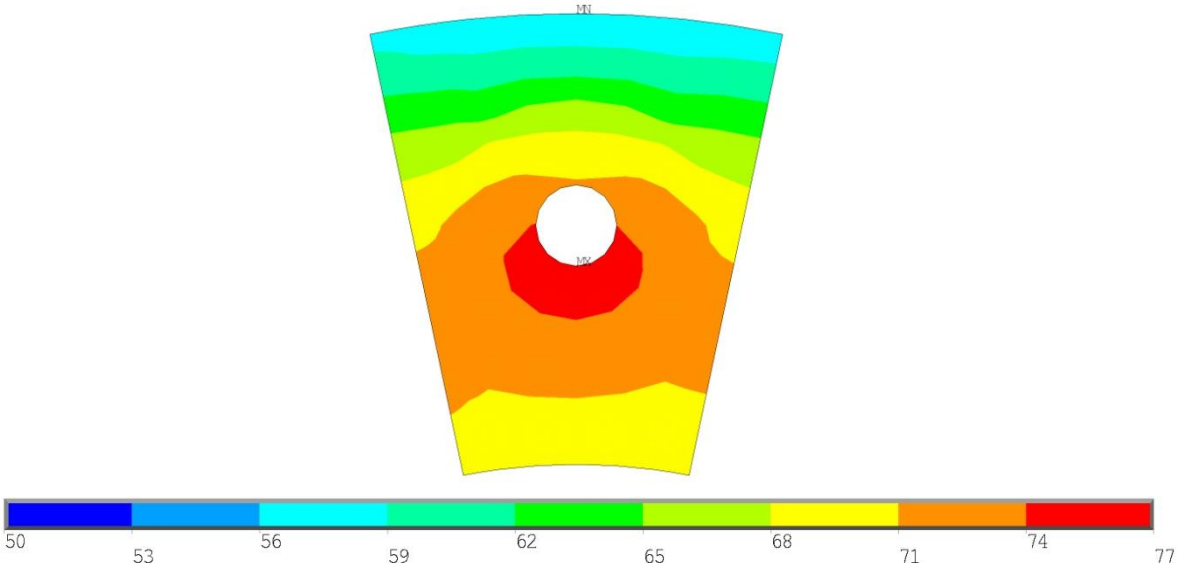

Figure 5.35. Calculated oil film thickness in hydrostatic mode, time 00:15 hr:min

Deformed sliding surfaces and oil film shape are presented in Figure 5.37 and Figure 5.37 in form of the 3D diagrams. In this way oil film thickness can be scaled and is better visible. Presented results illustrate the stabilized solution (steady state).

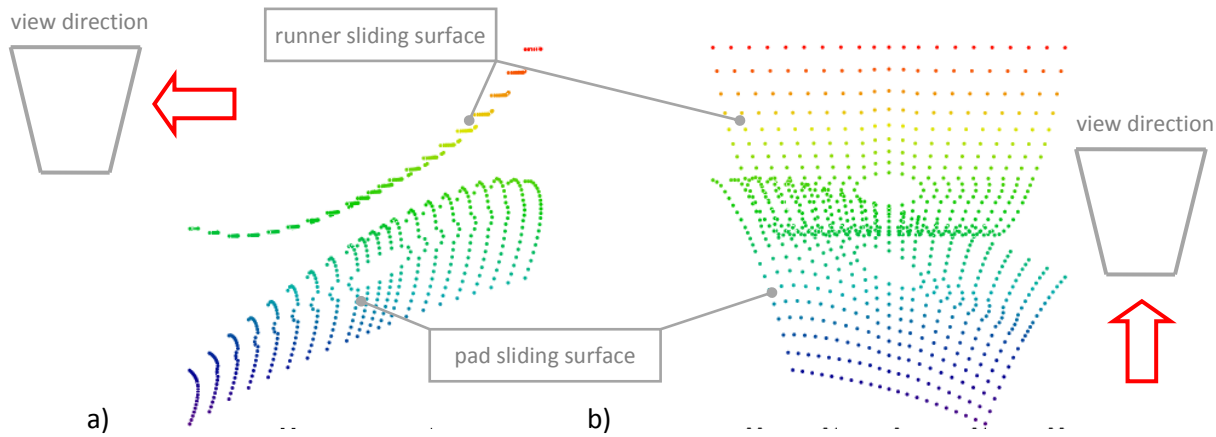

Figure 5.36. Deformed sliding surfaces, a) tangential view, b) radial view

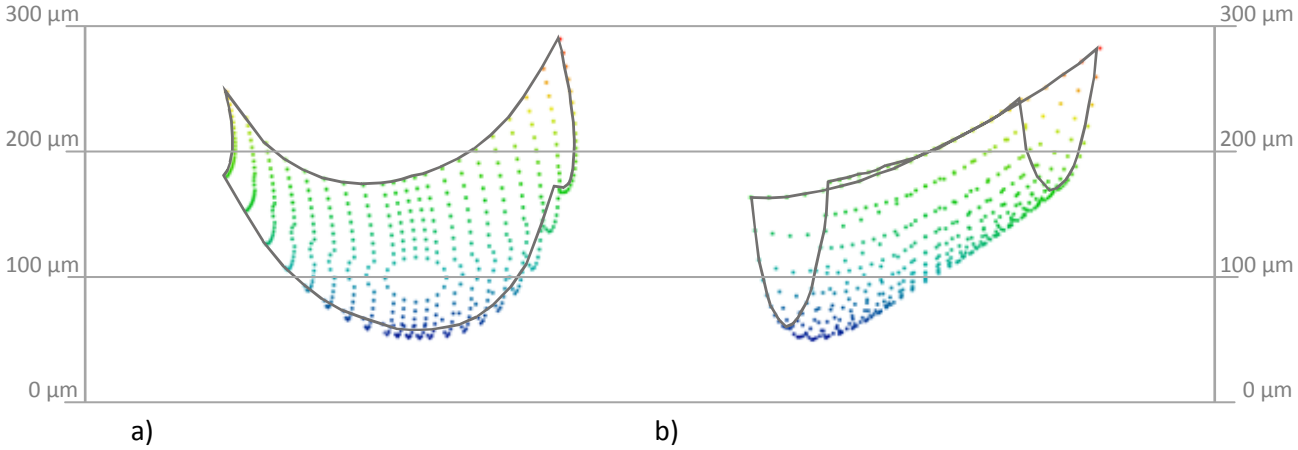

Figure 5.37. Oil film shape and thickness, a) tangential view, b) radial view

In these figures one can notice the three dimensional character of the oil film geometry. Precise estimation of these shapes has an fundamental influence on the calculated bearing parameters. At the left hand side (tangential view) radial tilting of the runner and the pad can be seen – both parts remain almost parallel. At the right hand side (radial view) hydrodynamic inclination of the pad is noticeable.

At the three dimensional sliding surface profiles one can notice that in radial direction both surfaces remain almost parallel. Deformation of the runner surface is more significant than that of the pad. Minimum oil film thickness is not located at the trailing edge but because of the pad deformation it is located slightly before. From these figures it is also visible that tangential inclination (~ 3.2) of the pad is mainly caused by pad tilting and not only by its tangential deformation. It means that variable viscosity ($\mu = \mu(T)$) has a significant influence on the tilt angle also in case of the symmetrically supported bearing pads.

5.2.6 Resulting warm oil mixing coefficient

The fluid model contains the oil film and the space between the pads. Comparison of the oil film inlet and outlet temperatures allows to calculate the resulting warm oil mixing coefficient in steady state (time $7200\ s$). The result of these calculations can be used in simpler bearing calculation models as input parameter. Oil film inlet (see Figure 5.22) and outlet temperatures (see Figure 5.23) are the result of the CFD simulation and vary across these fields. In order to simplify the calculation, average values are taken into account. Warm oil mixing coefficient is calculated according to formula 5.1 given by Ettles [**14**].

$$T_{in} = T_{cold} \cdot \left(\frac{1-k}{1-0.5\,k}\right) + T_{out} \cdot \left(\frac{0.5\,k}{1-0.5k}\right) \tag{5.1}$$

If all temperatures are known one can evaluate the value of the warm oil mixing coefficient

$$k = \frac{2T_{in}-2T_{cold}}{T_{in}+T_{out}-2T_{cold}}$$

FSI simulation results are given in Table 5.4. Oil film inlet and outlet temperatures are calculated as the average value of fields given in Figure 5.22 and Figure 5.23.

Table 5.4. Resulting averaged oil temperatures for warm oil mixing calculation

No.	Parameter	Symbol	Value	Unit
1	Cold oil temperature	T_{cold}	36	$°C$
2	Oil film inlet temperature	T_{in}	61.3	$°C$
3	Oil film outlet temperature	T_{out}	71.8	$°C$
4	Warm oil mixing coefficient	k	0.83	-

The resulting warm oil mixing factor is equal to $k = 0.83$. According to the diagram presented by Ettles for this specific bearing (distance between the pads $94\,mm$ and average sliding speed $47.1\,m/s$) this value is significantly higher than the expected (from the diagram) value of 0.5 – which is the lowest possible value – oil film inlet temperature has an average value of the cold oil and oil film outlet temperatures. Both values of the warm oil mixing factor (expected and calculated) are marked in Figure 5.38.

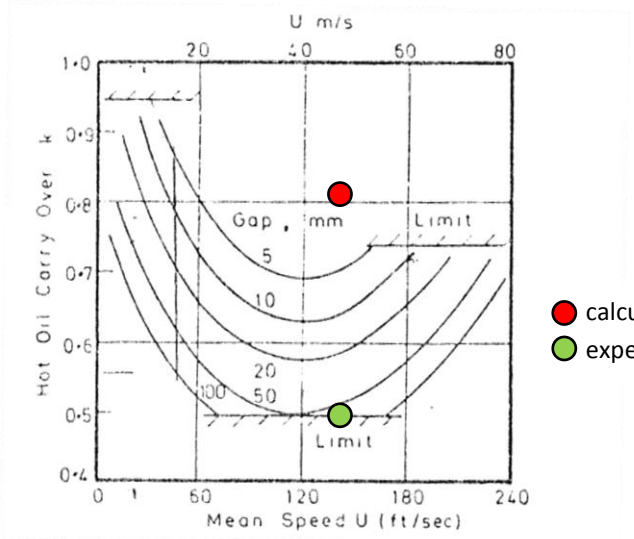

calculated warm oil mixing coefficient from the FSI model

expected warm oil mixing coefficient from the diagram

Figure 5.38. Warm oil mixing coefficient according to [14] and the resulting value from FSI model

The obtained higher value of the warm oil mixing coefficient can be caused by several reasons. First of all, the above diagram is based on measurement data but values of warm oil mixing coefficient are evaluated with the use of a bearing calculation program that calculates 2D temperature fields only. Uniform oil film inlet temperature distribution and triangular velocity profile are assumed whereas all these parameters are calculated in CFD model.

Another reason can be the pumping plate between the pads. This design feature can cause worse exchange of the warm and cold oil between the bearing pads. Oil is heated up by passing the radial channel in the way presented in Figure 5.39. For such a bearing design, the warm oil mixing coefficient can be higher. On the other hand one can notice that the temperature increase between inlet and outlet does not exceed $3 - 5\ °C$ in radial direction. Thus the pumping plate cannot be the only reason for a higher warm oil mixing coefficient.

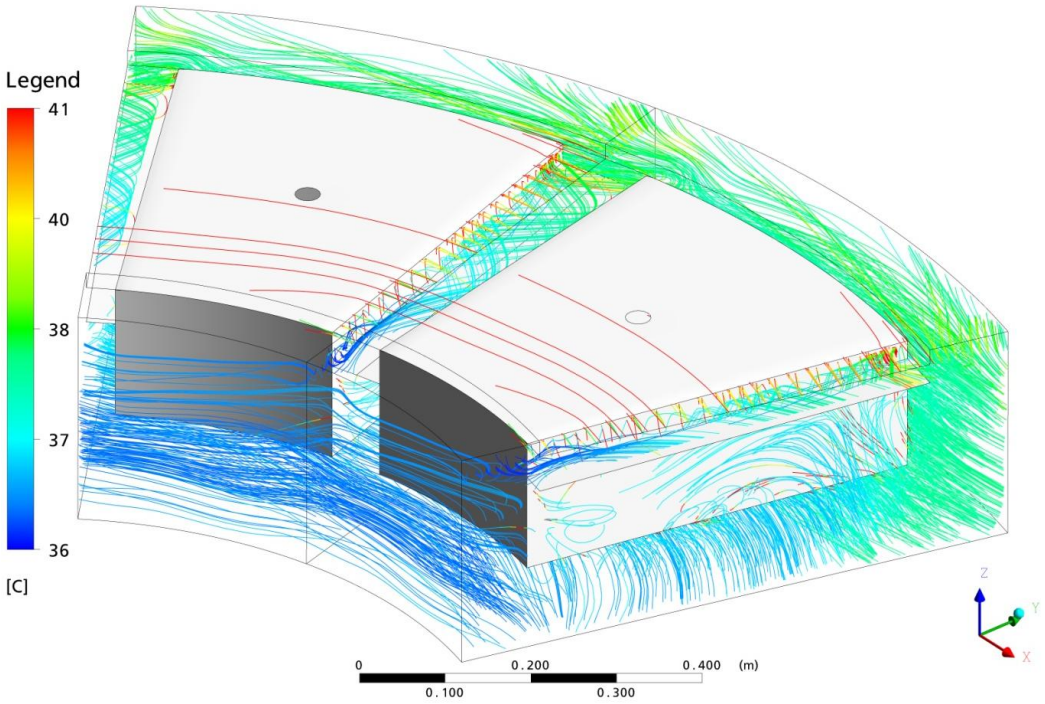

Figure 5.39. Radial oil flow between the bearing pads, contour scale represents temperature of the oil [C]

For the resulting oil film inlet and outlet temperatures it is possible to obtain a warm oil mixing coefficient equal to $k = 0.5$ under assumption of a cold oil temperature $T_{cold} = 56\ °C$. This could indicate higher oil temperature between the pads than the one delivered from the cooler but $20\ °C$ difference is rather an impossible value to obtain.

The difference between both models can be caused by the tangential position of the pivot point. The diagram in Figure 5.38 was most probably developed for thrust bearings with a single direction of rotation but there is no information available in the paper. In the presented example, the bearing is supported symmetrically thus the pad tilt angle is significantly smaller. This can cause lower oil film inlet height and finally higher warm oil mixing coefficient. In order to check this possibility FSI analysis has been performed with the use of modified bearing model. In this analysis the tangential pivot point position has been shifted to $60\ \%$ of the pad length ($pivot_{tan} = 0.6$). This value is a standard pivot position for thrust bearings with a single direction of rotation. In Figure 5.40 a comparison between both (bidirectional and unidirectional) thrust bearings is presented. Unidirectional bearing has significantly lower sensor temperatures ($18\ °C$ at sensor 1 and $13\ °C$ at sensor 2). Bidirectional bearing is generally warmer and additionally temperature difference between the sensors is higher.

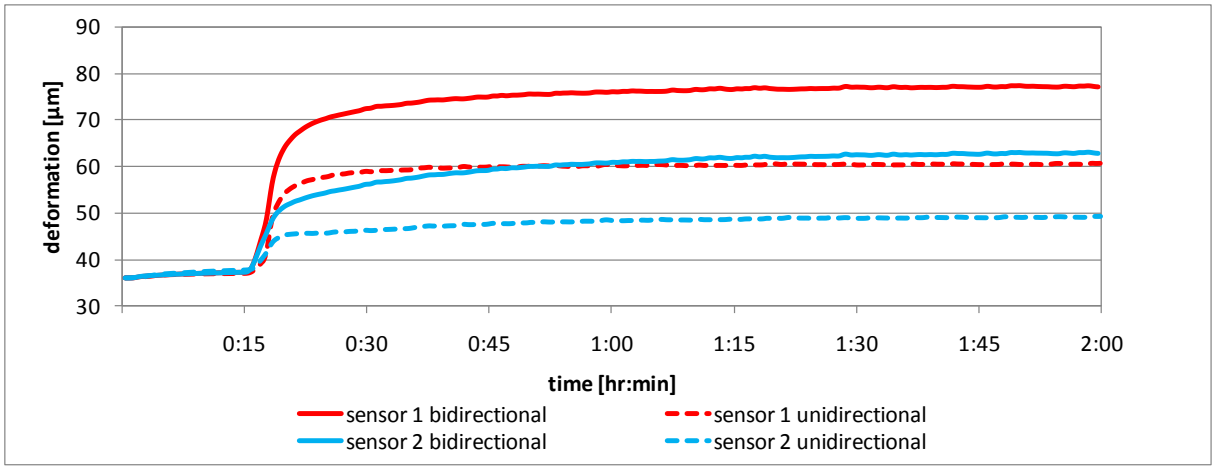

Figure 5.40. Comparison of calculated sensor temperatures, bidirectional versus unidirectional thrust bearing

From Figure 5.41 one can see that the tangential tilt angle of a unidirectional bearing pad is almost twice as large as this for the bidirectional bearing.

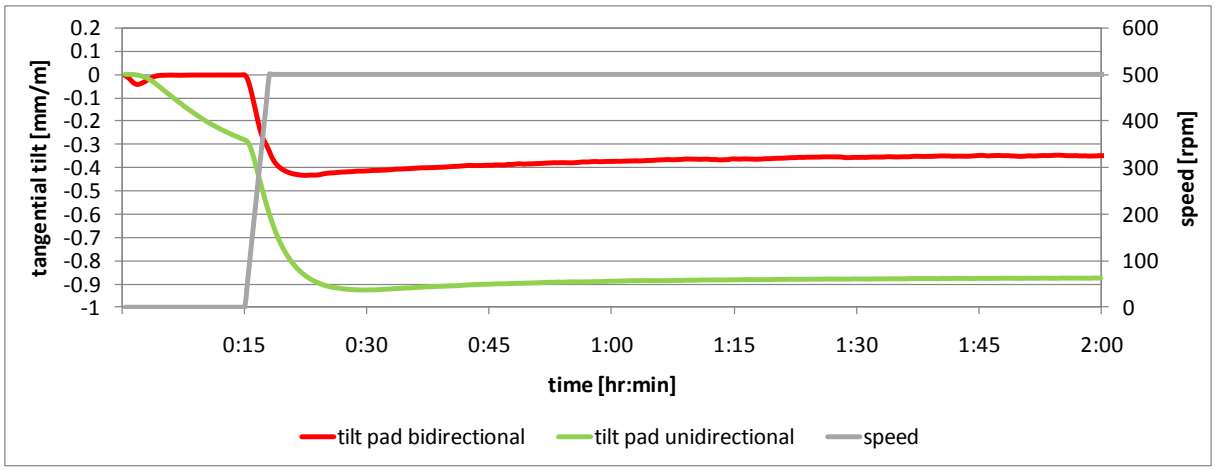

Figure 5.41. Pad tangential tilt angles, bidirectional versus unidirectional thrust bearing

From this comparison one can see significantly lower bearing temperature with single direction of rotation. The only difference between both bearings is the pivot point position. The tangential tilt angle of the pad is responsible for higher temperatures of the bidirectional bearing.

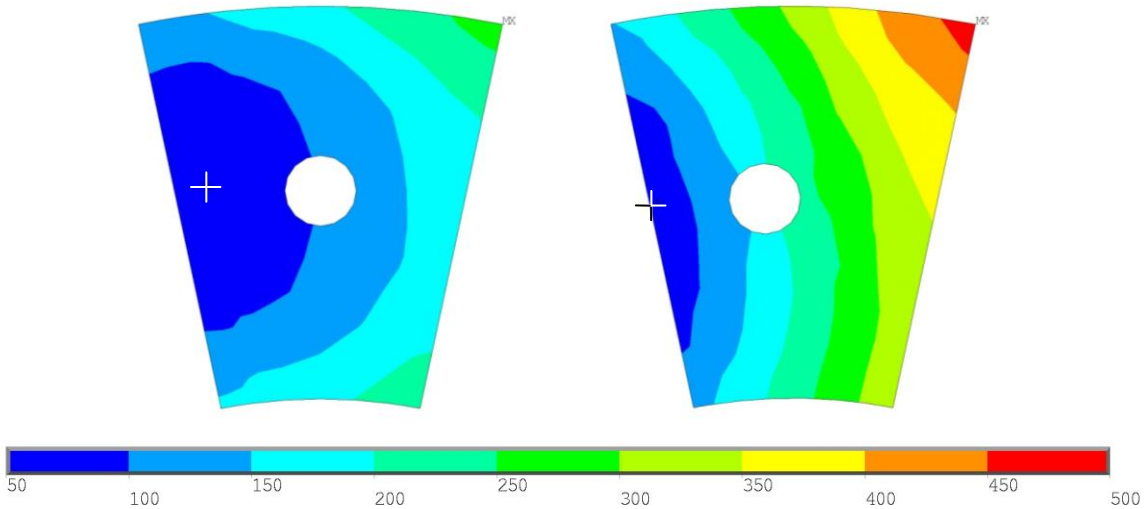

Figure 5.42. Calculated oil film thickness [µm] in steady state (time 7200 s), a) bidirectional, b) unidirectional

The minimum oil film thickness is similar in both cases. It is only $5\,\mu m$ higher in case of the unidirectional bearing (Figure 5.42 and Figure 5.43). In this case, the minimum value can be observed on the trailing edge whereas for the bidirectional pad, the minimum oil film thickness is located before the trailing edge. This pad also has a significantly stronger deformation.

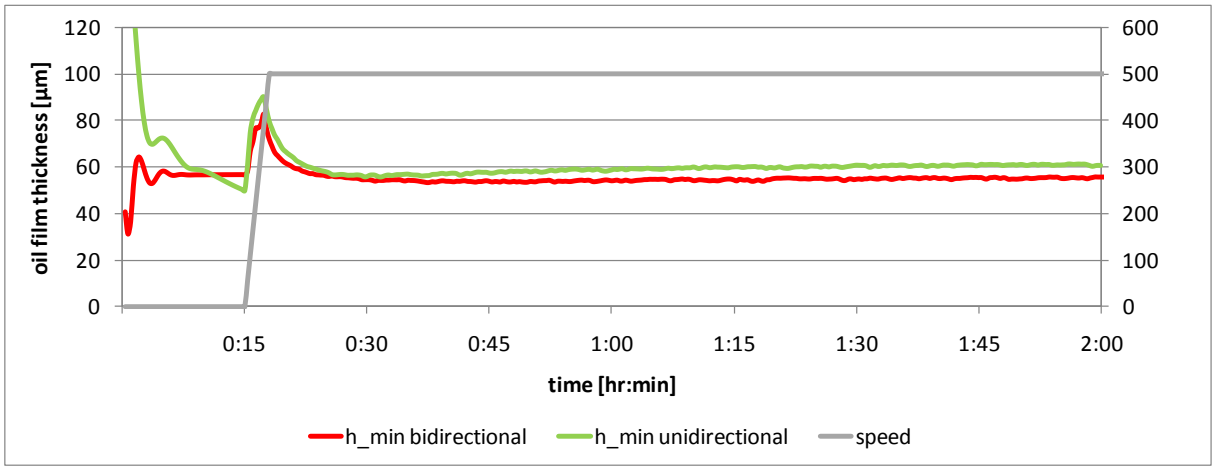

Figure 5.43. Calculated minimum oil film thickness, bidirectional versus unidirectional thrust bearing

It is worth to mention that stabilization of the position of the pad in hydrostatic mode was not possible to obtain (see Figure 5.41 and Figure 5.43). In the hydrostatic mode neither the stabilization of the tangential pad inclination nor the minimum oil film thickness was possible to obtain. This fact can confirm information about unstable hydrostatic operation of the unidirectional bearing pads due to unsymmetrical position of the chamber.

Table 5.5. Resulting averaged oil temperatures for warm oil mixing calculation for unidirectional bearing

No.	Parameter	Symbol	Value	Unit
1	Cold oil temperature	T_{cold}	36	$°C$
2	Oil film inlet temperature	T_{in}	52	$°C$
3	Oil film outlet temperature	T_{out}	69	$°C$
4	Warm oil mixing coefficient	k	0.65	-

The resulting warm oil mixing coefficient for such a bearing is 0.65. It means that symmetrically supported thrust bearings have higher warm oil mixing coefficients and this is one of the reasons of higher operating temperatures. This high value of the warm oil mixing coefficient is caused by smaller tangential inclination of the bearing pad and smaller area of oil inlet cross section.

Velocity and temperature boundary layers are presented on a cross section through the oil film and the bearing groove (see Figure 5.44) for the $75\,\%$ of the radial width of the pad. Scale factor in axial direction is multiplied 100 times in order to show the oil film thickness. Hydrodynamic boundary layer is given in Figure 5.45 and thermal in Figure 5.46 for both analyzed cases (bidirectional and unidirectional).

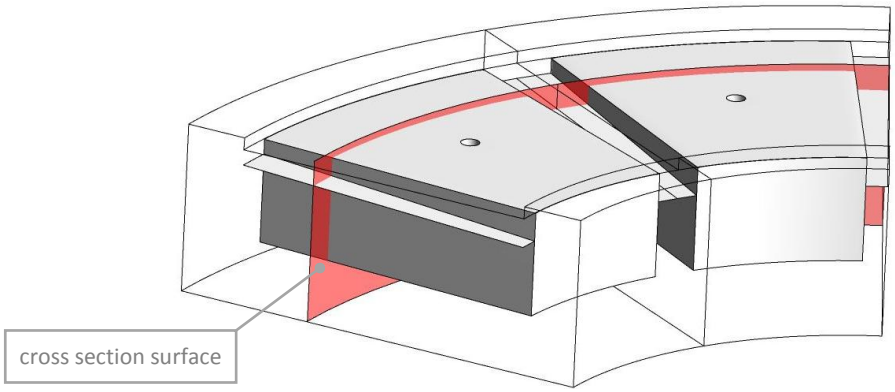

Figure 5.44. Cross section through the oil film and bearing groove for 0.75 of the radial width of the pad

In Figure 5.45 one can see the growth of the hydrodynamic boundary layer between the pads. Final thickness of this layer is rather insignificant ($\sim 1\ mm$) while the growth is interrupted by the following pad.

a)

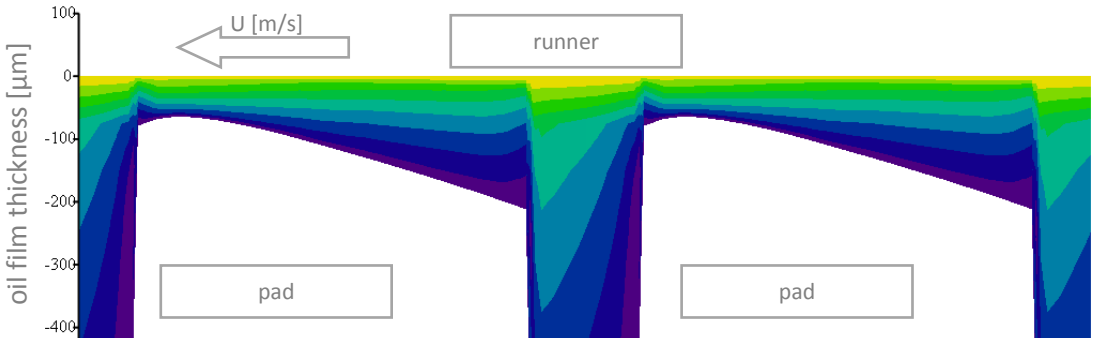

b)

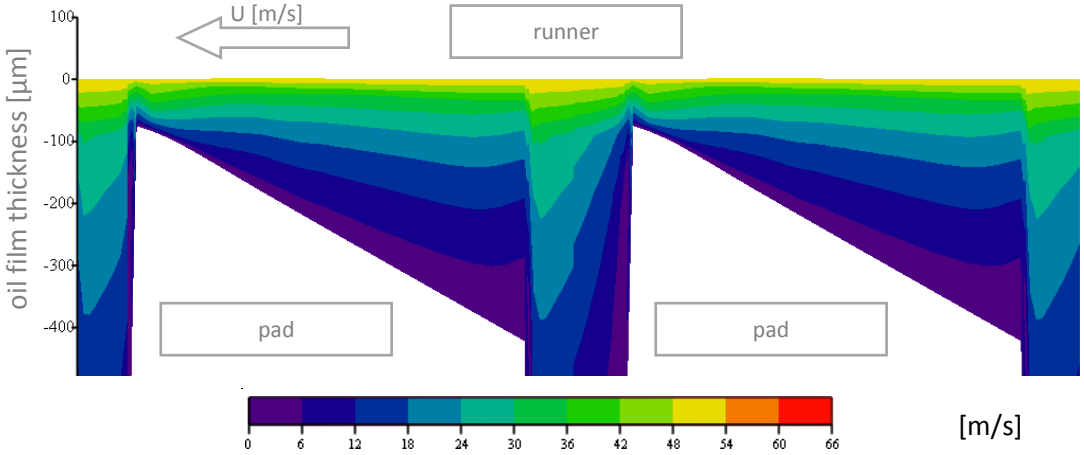

Figure 5.45. Velocity boundary layer [m/s] in steady state (time 7200 s), a) bidirectional, b) unidirectional

As expected for high Prandtl numbers, the fluids thermal boundary layer is significantly thinner. In this case it is even thinner than the oil film inlet (approximately $66\ \%$ of its height). This comparison shows that the thickness of the thermal boundary layer in this case is only $150\ \mu m$ thick. It leads to a conclusion that warm oil mixing effects can be only influenced if the very thin (several tens of microns) thermal boundary layer is affected.

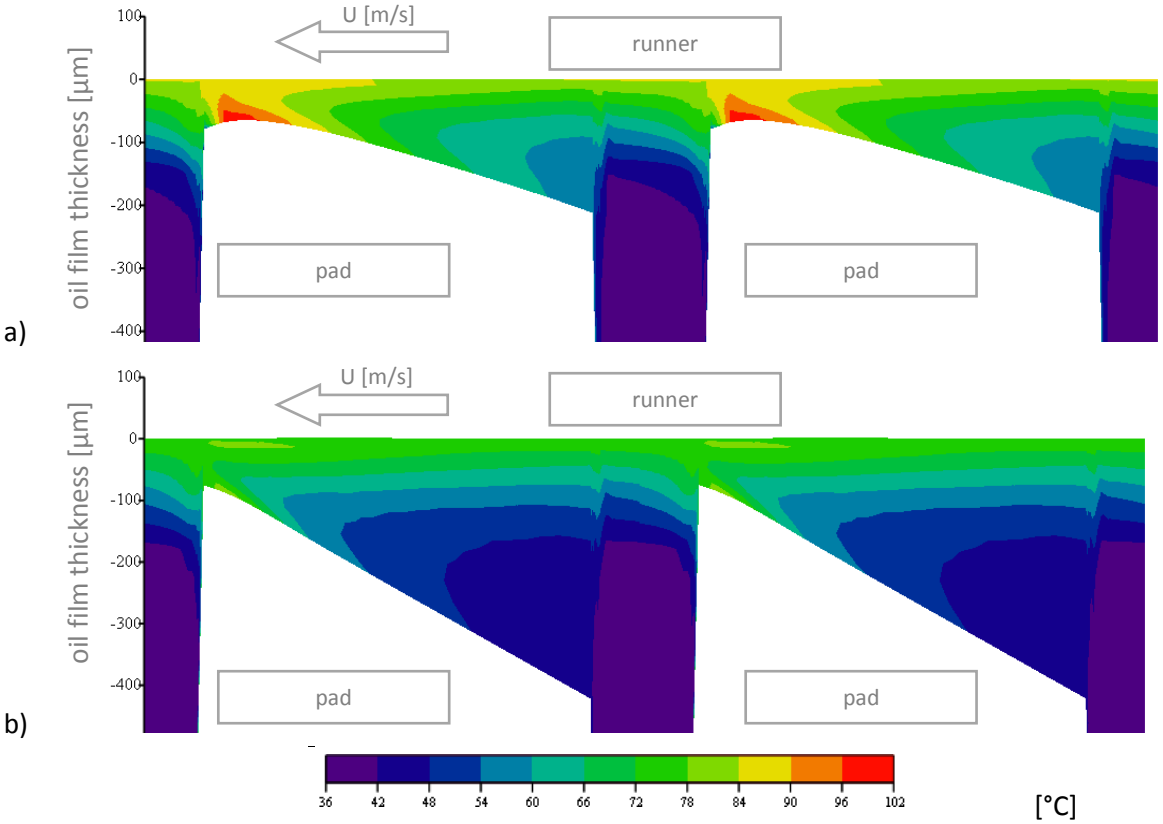

Figure 5.46. Temperature boundary layer [C] in steady state (time 7200 s), a) bidirectional, b) unidirectional

The above investigation shows in a clear way one of the main advantages of the CFD approach. Warm oil mixing and all effects that take place between the pads (beyond the oil film) are calculated inside the model. Warm oil mixing is the result of the computation and not an arbitrary assumed input parameter. Additionally an interesting relationship has been indicated. Tangential pivot point position has influence not only on the inclination of the pad during hydrodynamic operation but also on the warm oil mixing effect.

5.2.7 Heat flow through the sliding surfaces and the heat balance

The calculated power loss in the bearing is the result of the friction losses in the oil film and oil mixing between the bearing pads. Heat generated in the oil film can be divided into three parts. The main part of the heat is taken away by the flowing oil. The rest of the heat is transported by means of convection and conduction through the bearing pad and runner. These heat flows are responsible for warming up these elements. Analysis of the obtained results shows the dependence of these components on the generated power loss.

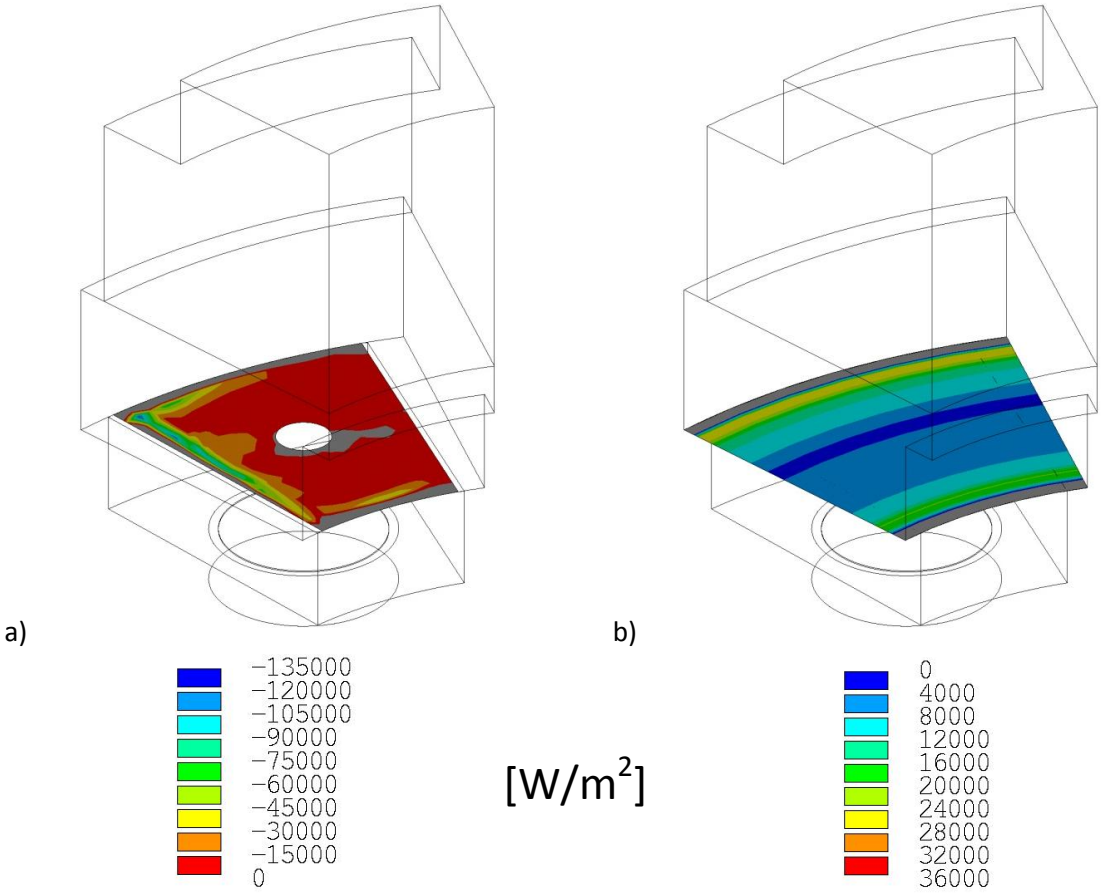

Figure 5.47. Heat flow through the both sliding surfaces, a) pad, b) runner

In order to show not only the amount of the heat flux but also its direction, the axial component is presented in Figure 5.47. For this reason, heat flux into the pad sliding surface is negative and for the runner is positive. Contours are adjusted in order to show variability of these fields. Values at the trailing edge reach approximately $120\ kW/m^2$!!! Grey color indicates regions where heat flux changes its direction to the opposite one. In these regions pad and runner are cooled instead of being heated. Such an effect can be observed at the inner and outer edges of both parts and additionally in the middle of the pad sliding surface – close to the hydrostatic chamber. Integration of the heat flux density on the whole sliding surface area gives the total heat transfer through these surfaces (estimated in kW). The results are given in Table 5.6.

Table 5.6. Heat flow through the sliding surfaces

No.	Parameter	Symbol	Value	Unit
1	Total power loss	P_{loss}	652	kW
2	Heat transfer through the pads	q_{pad}	14.7	kW
3	Heat transfer through the runner	q_{runner}	16.6	kW

From the above table one can notice that the amount of the heat transfer through the pad sliding surface is only $2.25\ \%$ and through the runner sliding surface it is $2.54\ \%$ of the total power loss generated in the bearing. The rest of the heat is transferred by the oil flow and exchanged in the coolers. Such low heat transfer means that for this particular bearing one does not make a significant

error assuming adiabatic boundary condition on both sliding surfaces. This is a quite common assumption made in simpler bearing calculation programs.

5.2.8 Calculated convection coefficients of the pad walls

Many different and interesting results can be collected during post processing of the obtained fluid model results. One of the most interesting information are the resulting convection coefficients on the walls of the bearing pad.

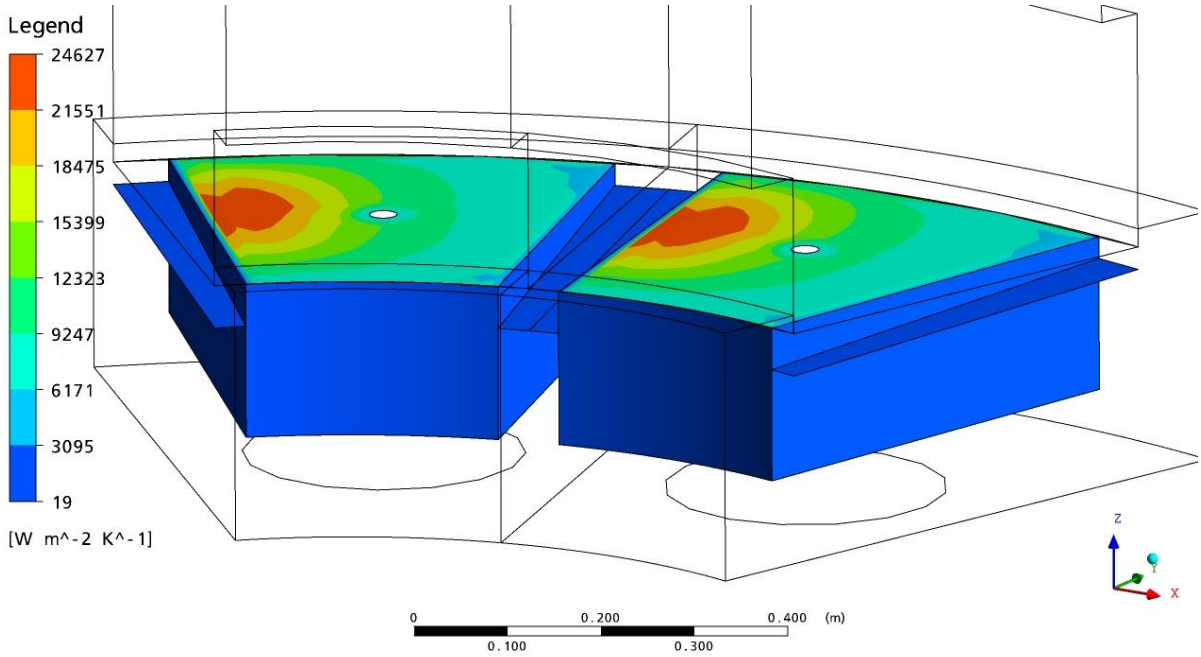

Figure 5.48. Convection coefficients on the sliding surface

In Figure 5.49 strong separation between the two oil flow can zones be noticed. Intensive flow between the pads exists only above the pumping plate whereas underneath the pumping plate convection coefficients are much lower.

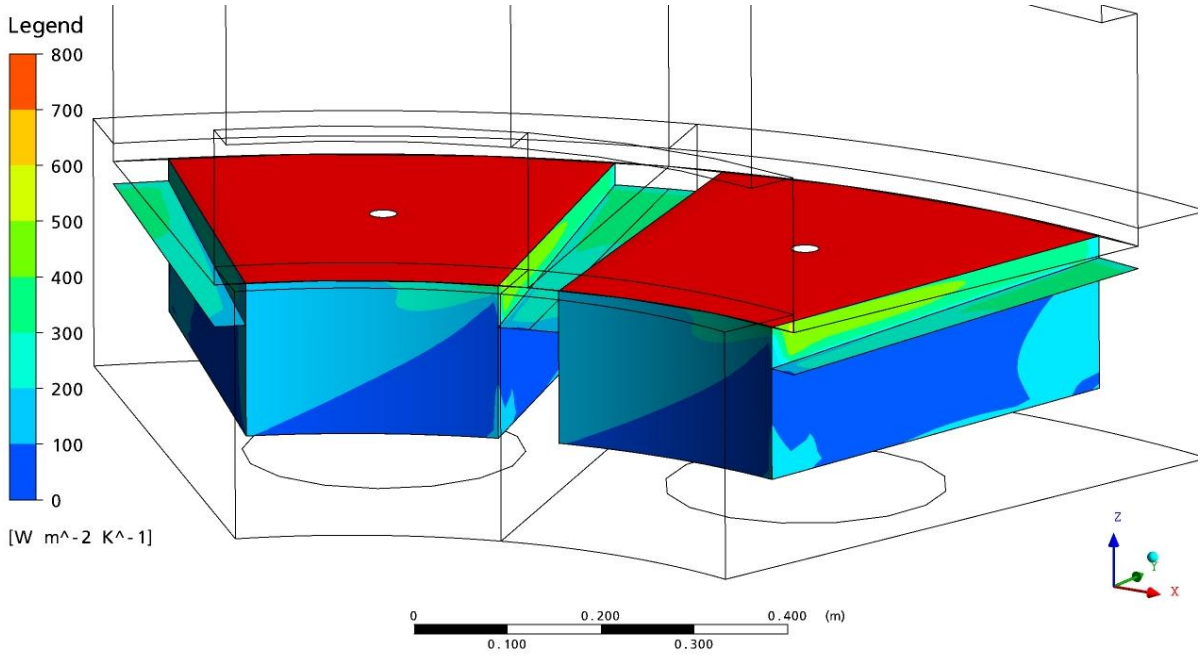

Figure 5.49. Convection coefficients between the pads

Convection coefficient at the sliding surface is several orders of magnitude higher than this on the remaining wall of the pad. On the leading edge its value reaches up to 500 W/m^2 K. Lowest values can be noticed on the bottom of the pad. The convection coefficient on this wall does not exceed 100 W/m^2 K. The obtained convection coefficients can be used as input parameters for the simpler bearing calculation models. It is worth to notice that their values are not constant but vary on the walls of the pad. Convection coefficients will also change for a different rotational speeds of the bearing.

5.2.9 Calculated pressure distributions

The calculated pressure profiles for both modes (hydrostatic and hydrodynamic) are presented in Figure 5.50. Regardless of the fact that in both cases bearing load is the same the maximum oil film pressure is significantly higher in case of hydrostatic lubrication.

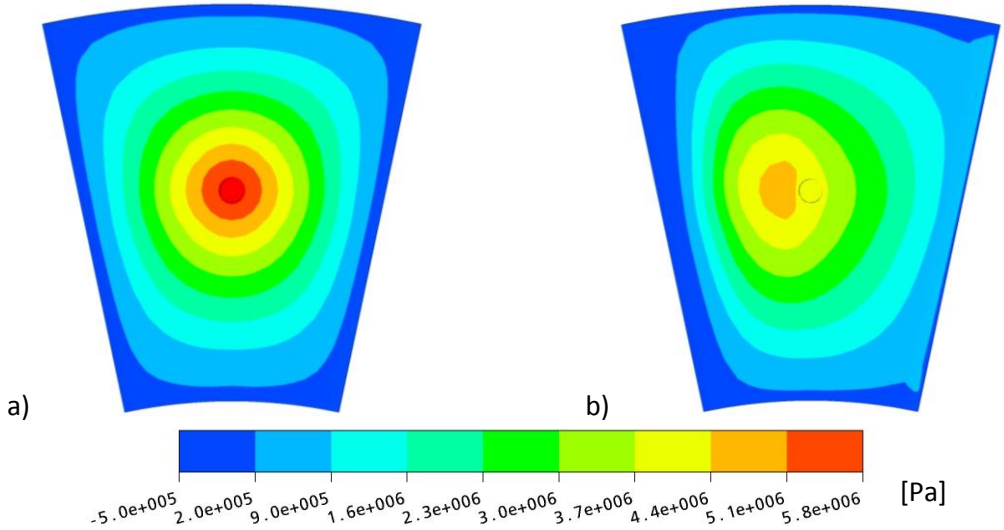

Figure 5.50. Calculated pressure distribution, a) hydrostatic mode, b) hydrodynamic mode

5.2.10 Conclusions

Although the temperature profiles are not exactly the same as the measured ones the overall trend is followed. The main differences are caused by dissimilar operating conditions (assumed constant cold oil temperature). It proves that the overall conservative quantities are estimated properly. Convection and mixing effects also have to be predicted accurately in order to obtain such convergence with measured values.

A small overload during startup of the bearing due to modeling of the damping elements is a reason for faster temperature increase. Further improvements in this field are necessary in order to obtain smaller influence on the transient bearing behavior.

Observation of the deformation profiles may lead to the following operational advice. Since the maximum of deformation appears always later than the nominal speed is obtained – the hydrostatic jacking system assistance should last longer than the acceleration of the unit. In this simple way operating conditions during startup of the thrust bearing may become less severe. The thermal peaking effect could be reduced and the load carrying capacity not affected at all. This idea is investigated further in this chapter.

Many different detailed results have been presented. Some of them like warm oil mixing or convection coefficients can be used as input parameters for simpler bearing calculation programs. In this way application of FSI model could be extended.

5.3 Influence of chosen parameters on the results of simulation

In this subsection the influence of several parameters on the obtained results is checked. Main model features were taken under investigation in order to verify its functionality.

5.3.1 Model validation with DIN bearing calculation guidelines

In order to verify the fundamental ability of the developed model to calculate bearing behavior the validation with the use of DIN standard [**52**] has been performed. This comparison allows to verify if the pad tilting and load carrying capacity are estimated in an appropriate way. Bearings supported symmetrically ($pivot_{tan} = 0.5$) cannot be calculated because of the limitations of the used Reynolds theory. In case of isothermal flow without influence of deformations, the load carrying capacity of bidirectional bearings is equal to zero. For this reason unsymmetrical version of Kopswerk II bearing support was investigated. In the Table 5.7 input parameters are listed.

Table 5.7. Input parameters for isothermal model validation

No.	Parameter	Symbol	Value	Unit
1	Radial support position	$pivot_{rad}$	0.51	-
2	Tangential support position	$pivot_{tan}$	0.55, 0.6, 0.65	-
3	Load	F	6777	kN
4	Specific pressure	p	3.0	MPa
5	B/L ratio	B/L	1.326	-
6	Average oil temperature	T_{cold}	80	°C
7	Oil grade	ISO	$VG32, VG46$	-
8	Oil viscosity	η	0.00073, 0.00113	Pa s

The calculation for three different support positions has been performed and the results are listed in the following tables (Table 5.8 and Table 5.9).

Table 5.8. Tilt parameters and load capacity calculated with the use of the developed tool, ISO VG32

No.	Parameter	Symbol	Value	Value	Value	Unit
1	Support position	a_F^*	0.55	0.6	0.65	-
2	Min oil film thickness (av. diameter)	h_0	60.7	62.1	59.3	μm
3	Max oil film thickness (av. diameter)	h_1	106.3	157.2	260.9	μm
4	Tilt parameter	h_1/h_0	1.75	2.53	4.4	-
5	Tilt parameter relative difference	(FSI-DIN)/DIN	1.33	0.62	0.43	%
6	Load capacity	F^*	0.085	0.089	0.081	-
7	So relative difference	(FSI-DIN)/DIN	-3.05	-1.35	-16.64	%
8	h_0 difference	FSI-DIN	0.9	0.4	5.1	μm
9	h_0 relative difference	(FSI-DIN)/DIN	1.50	0.64	9.41	%

Table 5.9. Tilt parameters and load capacity calculated with the use of the developed tool, ISO VG46

No.	Parameter	Symbol	Value	Value	Value	Unit
1	Support position	a_F^*	0.55	0.6	0.65	-
2	Min oil film thickness (av. diameter)	h_0	74.7	80.8	72.6	μm
3	Max oil film thickness (av. diameter)	h_1	129.3	217.5	320.3	μm
4	Tilt parameter	h_1/h_0	1.73	2.69	4.41	-
5	Tilt parameter relative difference	(FSI-DIN)/DIN	1.07	1.84	0.45	%
6	Load capacity	F^*	0.071	0.083	0.067	-
7	So relative difference	(FSI-DIN)/DIN	15.19	4.4	0.61	%
8	h_0 difference	FSI-DIN	-5.4	-1.7	-0.2	μm
9	h_0 relative difference	(FSI-DIN)/DIN	-6.74	-2.06	-0.27	%

Comparison of the obtained FSI results and DIN standard procedure is given in Figure 5.52 and Figure 5.52

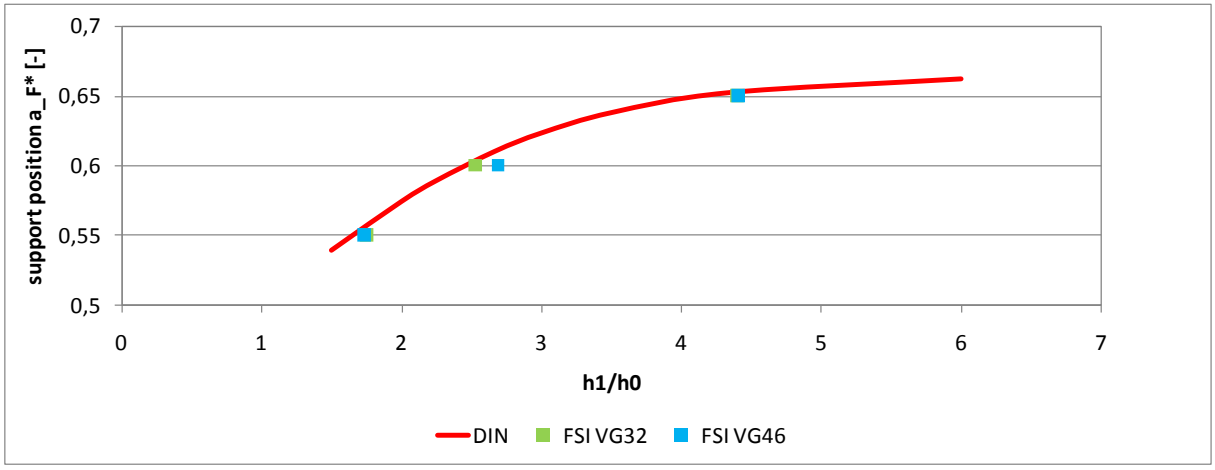

Figure 5.51. Comparison between DIN standard and FSI simulation model results for isothermal flow without influence of the deformations

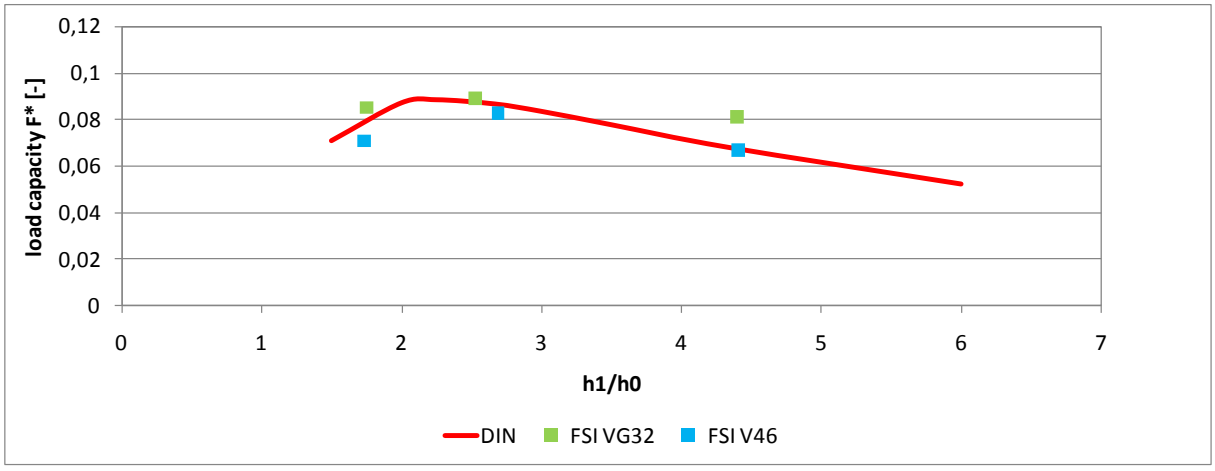

Figure 5.52. Comparison between DIN standard and FSI simulation model results for isothermal flow without influence of the deformations

The comparison showed that the pad tilt angle in tangential direction is estimated with a quite good accuracy. The pad tilts slightly more than it should according to the analytical solution. This small difference can be caused by the following differences between the models:

- point support, tilting in both tangential and radial directions,
- variable tangential speed along the pad width,
- flow action on the pad side walls (especially at the inlet),
- shear stress of the flow acting on the pad sliding surface,
- other minor influences like flow inertia forces, etc.

Load capacity differences were larger (relative difference up to $16\,\%$ - see Figure 5.52) since it depends on the squared minimum oil film thickness. The minimum oil film thickness was usually calculated within the range of $1\ \mu m$ (in the worst cases not larger than $5.4\ \mu m$) in comparison with the DIN standard.

5.3.2 Influence of the boundary condition on the runner

The boundary condition on the rotating surfaces of the runner is one of the most important unknowns in the bearing model. In this chapter a comparison of the obtained results is shown with different combinations of these conditions. The initial assumption for the convection is that the runner rotates in the oil with a certain temperature and the heat transfer occurs into the oil and air according to Figure 4.16 in Chapter 4. The standard calculation is made with the assumption that the runner rotates in the warm oil ($T_{cold} + 12° = 48°$). These values are specified for Kopswerk II power plant bearing. For the comparison there was a simulation performed with the assumption that the runner rotates in the cold oil ($T_{cold} = 36°$). The second assumption might be correct for some specific designs of the bearing housings, for example the one with the internal cooler where the oil bath has the temperature of the cold oil. In case of the forced oil flow the oil that is coming inside the bearing housing is always colder than the oil bath temperature while the oil bath is a mixture of the warm and cold oil. The convection coefficient on the walls is also difficult to estimate since it depends strongly on the sliding speed and the bearing housing arrangement. In the Figure 5.53 one can find a comparison of the runner deformations. For comparison the convection coefficient was increased three times (from the initial value $\alpha = 350\ W/m^2K$) in order to check its influence. For this case its value equals $\alpha = 1050\ W/m^2K$. Summary of the input parameters for these 3 simulations is shown in the Table 5.10.

Table 5.10. Runner boundary condition input parameters

No.	Variant	T_{cold}	T_{runner}	α
1	A	$36\ °C$	$T_{cold} + 12\ °C = 48\ °C$	$350\ W/m^2K$
2	B	$36\ °C$	$T_{cold} = 36\ °C$	$350\ W/m^2K$
3	C	$36\ °C$	$T_{cold} + 12\ °C = 48\ °C$	$1050\ W/m^2K$

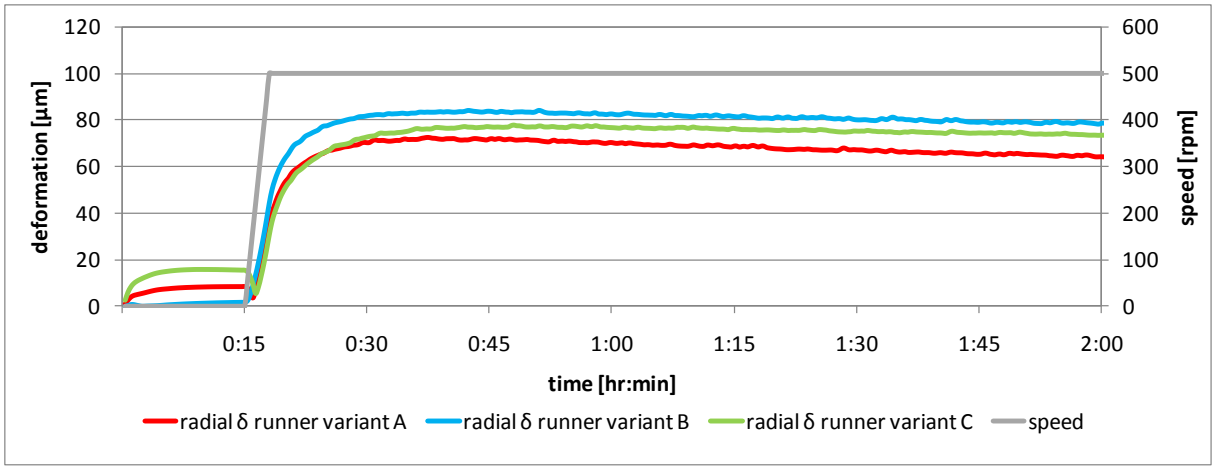

Figure 5.53. Influence of the runner boundary condition on runner deformations, first 120 minutes after startup, T_{cold} = 36°C

It has been shown that boundary conditions applied to the runner's free walls has a strong influence on the obtained results. This influence can also be noticed in the hydrostatic part of the simulation (initial $15\ min$ of operation). Increased wall temperature causes deformation of the runner sliding surface. However, the deformation of the runner varies within the range of 25 % depending on the calculation case the other results of simulation (bearing temperatures, oil film gaps) are influenced in a significantly weaker way. This influence (for steady state results) is presented in Table 5.11.

Table 5.11. Influence of the runner boundary condition on the bearing calculation results

No.	Variant	Minimum oil film gap	Maximum oil film temperature
1	A	$54.4\ \mu m$	$101.6\ °C$
2	B	$51.9\ \mu m$	$102.3\ °C$
3	C	$53.0\ \mu m$	$102.1\ °C$

The general trend is consistent with the expectations. Higher bending of the runner sliding surface causes lower load carrying capacity of the oil film. This results in lower oil film thickness and higher maximum oil film temperature. Above investigation indicates that relatively large error in calculation of the runner sliding surface deformation has a rather small influence on the general bearing calculation result. Nevertheless one of the ways of further development could be extension of the existing fluid model in a way that the oil flow and convection on these walls can also be calculated automatically within the same model without need of any additional assumptions.

5.3.3 Influence of damping coefficients

Damping coefficients described in Chapter 4 are investigated in this subsection. Two sets of damping coefficients were calculated in order to illustrate the influence on the obtained results. The first task was calculated with constant values of damping coefficients whereas in the second one coefficients were decreased to $20\ \%$ of their initial values. These coefficients are decreased after first $15\ min$ of the simulation (see Figure 4.19 in Chapter 4).

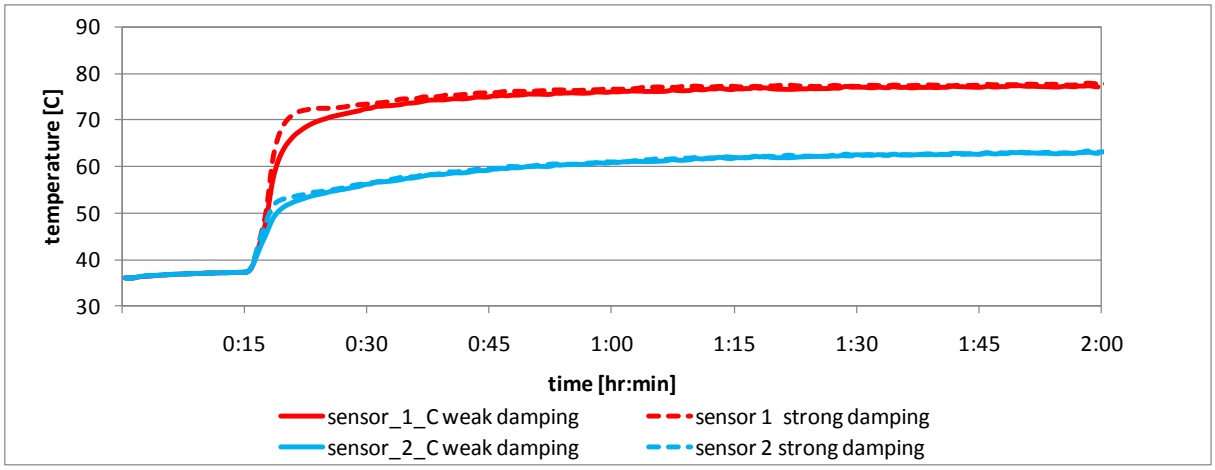

Figure 5.54. Comparison of calculated sensor temperatures for different damping coefficients

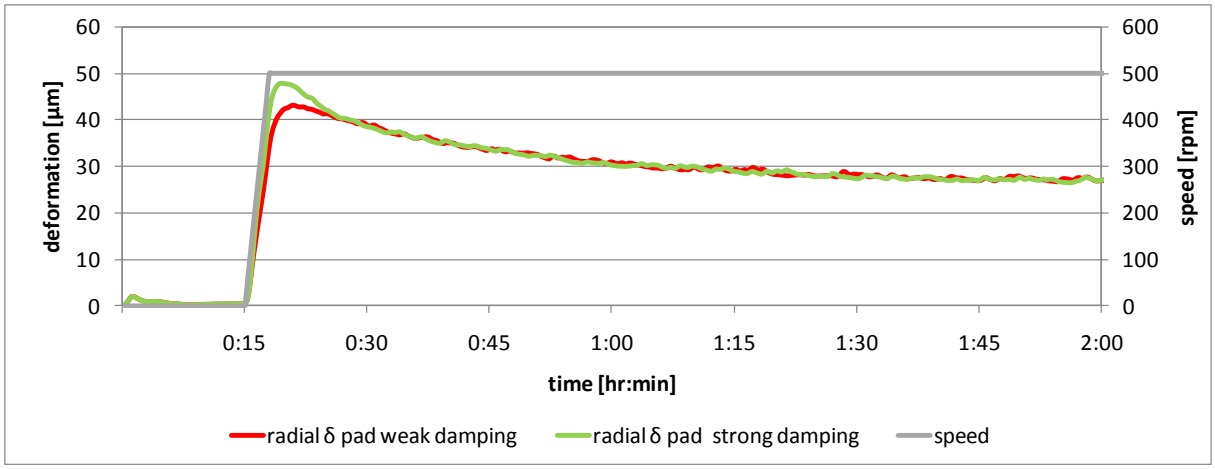

Figure 5.55. Pad radial deformations for different damping coefficients

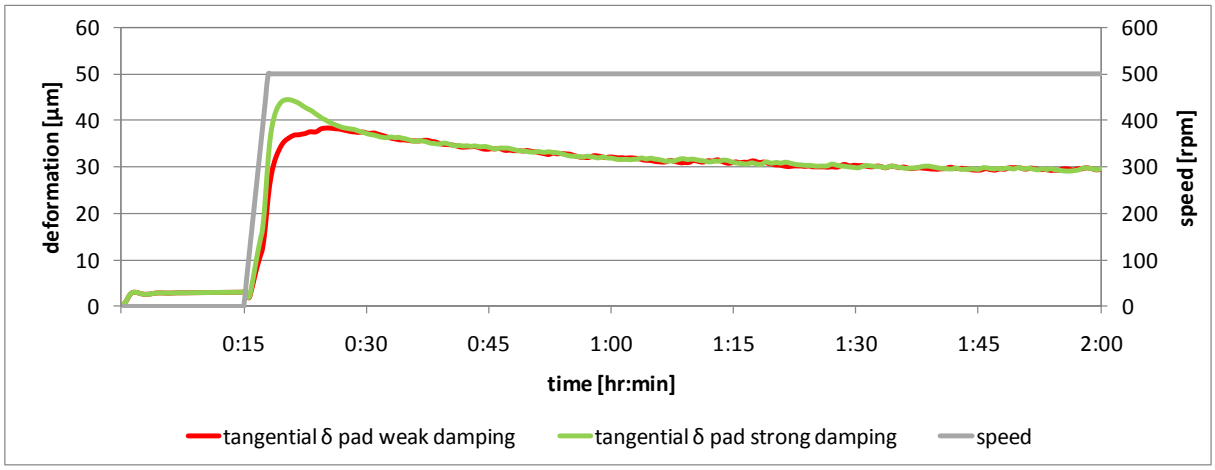

Figure 5.56. Pad tangential deformations for different damping coefficients

Negative influence of the exaggerated damping coefficients can be observed only for periods of increased movement velocities of the bearing elements – directly after startup. The rest of the profiles is not influenced at all. However in order to obtain valuable transient bearing calculation result for each time step it is necessary to assure good accuracy within the whole analyzed time range. Increased velocities produce high damping forces which create an additional load for the bearing. These velocities have two sources. First of them is the quick movement of the bearing parts and the second one is the rapid thermal expansion during startup. Force profiles in Figure 5.57 are

the result of the hydrodynamic pressure integration on the pad sliding surface. The bearing is overloaded directly after startup. One can notice that the force in the hydrostatic mode (time below $15\ min$) is not exactly equal to the force in the hydrodynamic mode (time over $15\ min$). This is caused by inaccuracies in pressure integration over the bearing sliding surface. This difference can be improved by better mesh density in both models.

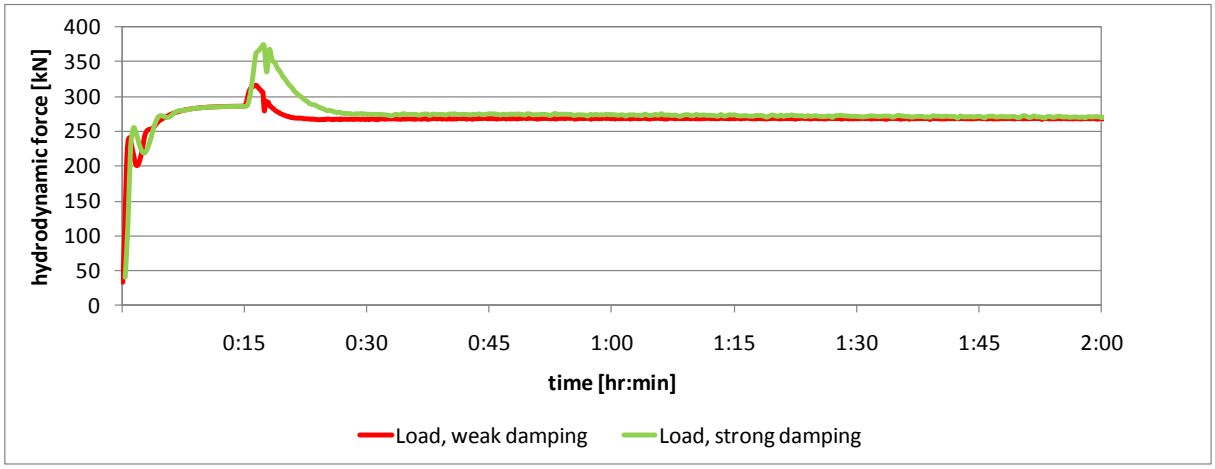

Figure 5.57. Influence of damping coefficients on the resulting bearing load for different damping coefficients

Further consequences of the artificial load of the bearing are increased temperatures and deformations of the bearing elements – see Figure 5.58.

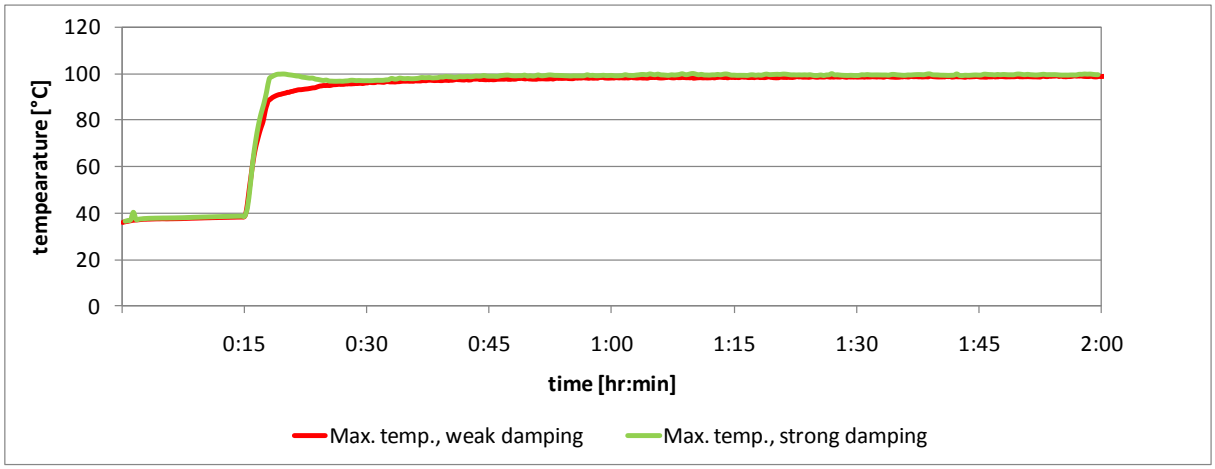

Figure 5.58. Influence of damping coefficients on the bearing maximum temperature for different damping coefficients

It has been shown that exaggerated damping coefficients influence the bearing behavior during startup. The main problem is overloading of the bearing caused by increasing oil film thicknesses and thermal expansion of the bearing elements after startup. These effects cause quick movement of the top surface of the runner model which is attached to the damping elements (see Figure 4.17). This influence can easily be monitored during simulation by observation of the resulting load and bearing temperatures. Therefore appropriate changes can be introduced to the system. It is worth to notice that steady state values are not affected by the damping elements at all. Further development of the mode could introduce more sophisticated control of the damping coefficients than the simple step function. This could for example be variable damping coefficients as a function of the bearing parts movement velocities or as a function of the resulting axial load.

5.3.4 Transient vs. steady state simulation

In this subsection a comparison between steady state and transient state results is presented. Steady state results are obtained with the use of BearOpt program. This is a standard bearing calculation tool used in ALSTOM Hydro company for thrust bearing design. The solver is described in a detailed way in [**77**]. It is a bearing calculation program that calculates oil film parameters in the oil film with the use of the $10x10$ nodes grid. Temperature is assumed to be constant through the oil film thickness so the adiabatic boundaries are placed on the both sliding surfaces. The program assumes constant oil film inlet temperature which calculation is based on the energy balance in the bearing groove and the assumed value of the warm oil mixing coefficient. The bearing calculation program is coupled with FE models of pad and runner in order to estimate thermal and elastic deformations of these elements. Steady state calculations were performed for different rotational speeds (from 200 to $500\ rpm$) in order to simulate startup of the bearing as a quasi steady state analysis. Since the simulations are performed with two different procedures, the final steady state solutions for both of them are different. Pad radial deformations is shown in Figure 5.59 and Figure 5.60 but in the second case time axis is limited to $15\ min$ after startup only. In similar way tangential deformations of the pad are presented in Figure 5.61 and Figure 5.62. In cases of the shorter timescale steady state values reached with the use of transient simulation model are marked by arrows.

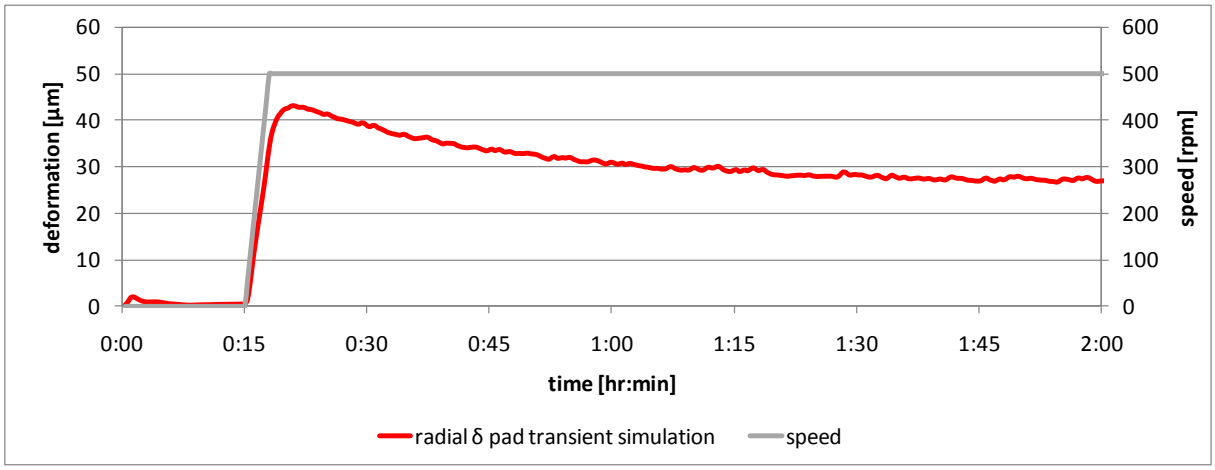

Figure 5.59. Pad radial deformations, transient result

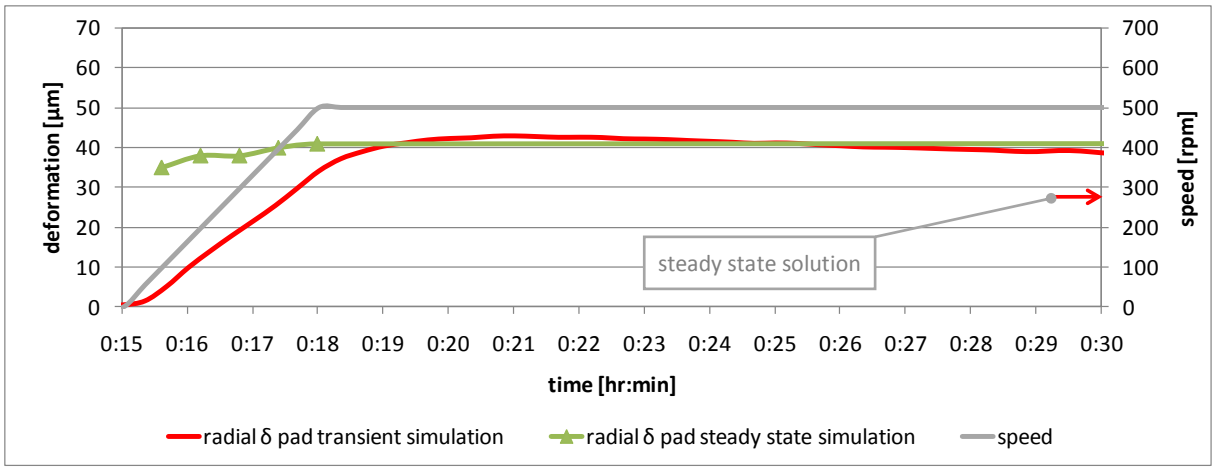

Figure 5.60. Pad radial deformations, transient and steady state result

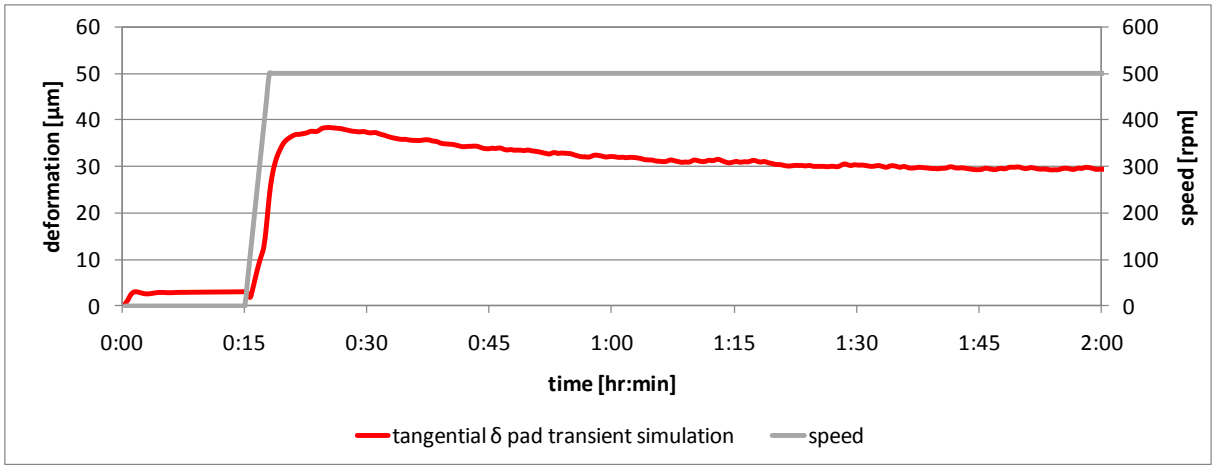

Figure 5.61. Pad tangential deformations, transient result

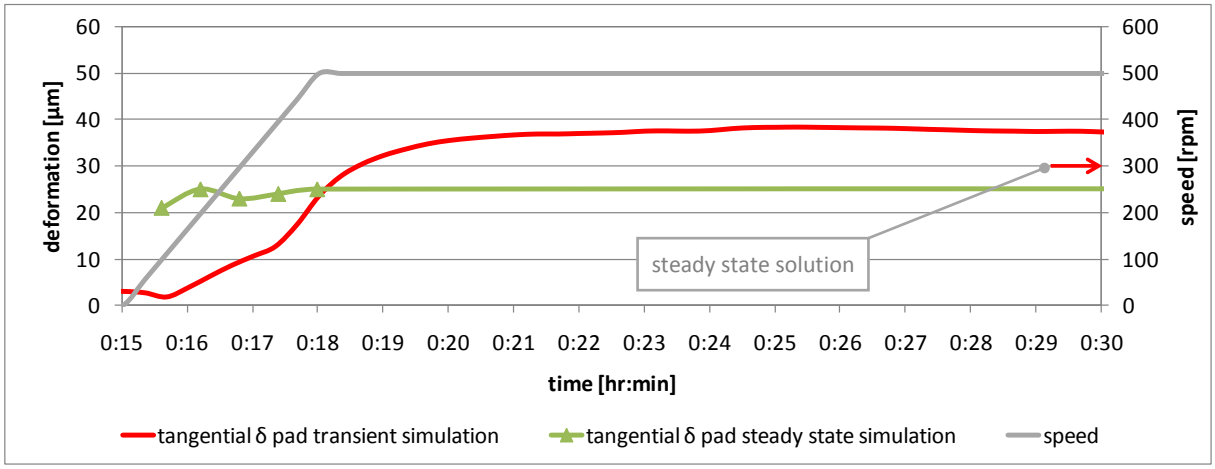

Figure 5.62. Pad tangential deformations, transient and steady state result

The maximum of the radial pad deformation occurs in $21st$ minute of the startup simulation ($43\ \mu m$), the steady state value is obtained at time $1{:}45$ and equals to $28\ \mu m$.

The maximum of the tangential pad deformation occurs in $25th$ minute of the transient simulation ($38\ \mu m$). Tangential deformations in case of the steady state solution are overestimated in comparison with transient state calculation. Steady state value is obtained at time $1{:}15$ and equals to $30\ \mu m$.

Table 5.12. Comparison between steady state and transient state simulation

rotational speed [rpm]	radial δ [µm] (steady state simulation)	radial δ [µm] (transient state simulation)	tangential δ [µm] (steady state simulation)	tangential δ [µm] (transient state simulation)
200	55	10	33	4
300	62	20	37	10
400	63	27	38	15
500	65	34	40	24
500 (peak value)	65	43	40	38
500 (steady state)	65	28	40	30

The comparison of the minimum oil film gaps and sensor temperatures is presented in Figure 5.63 and Figure 5.64. Both diagrams are limited to first $15\,min$ of operation after startup. Steady state values obtained by transient model are marked with arrows.

Minimum oil film thickness calculated by the steady state tool increases almost linear with the rotational speed. This model does not take into account hydrostatic lubrication, so for the rotational speed equal to zero there is no load carrying capacity.

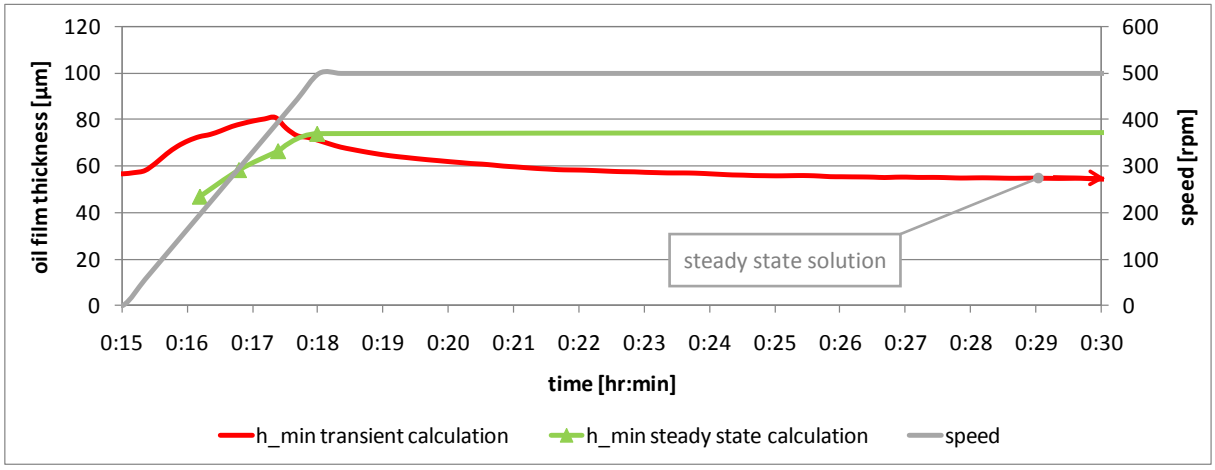

Figure 5.63. Minimum oil film thickness, transient and steady state result

The steady state tool calculates for each speed fully developed temperature field so one cannot observe the warming up process of the bearing pad.

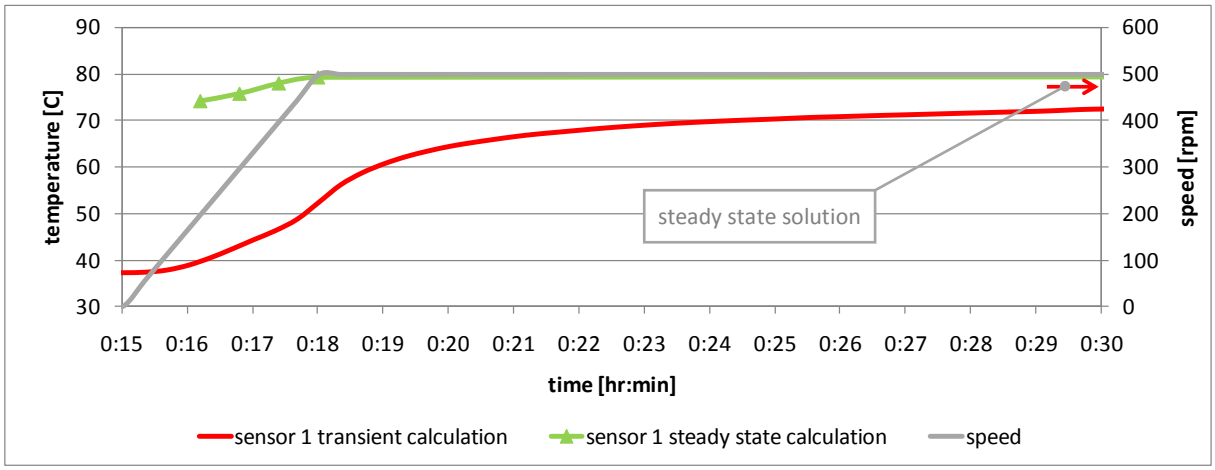

Figure 5.64. Sensor temperature, transient and steady state result

The performed investigation proved that the steady state calculation tool is not able to simulate the startup procedure in a realistic way. In order to simulate startup of the bearing, the steady state calculation tool can be applied only in case of the extremely slow acceleration of the bearing (several tens of minutes). Only in a such case the thermal state of the bearing can accommodate to the actual speed (there is enough time for stabilization of the temperature field). In order to fulfill this condition startup procedure should last several tens of minutes. In other cases transient state simulation is necessary. In industrial reality generators are usually started very quickly – startup time does not exceed a couple minutes.

5.3.5 Higher load case 2.43 MPa

During operation of the hydro generator, thrust load can oftentimes reach higher values than the nominal one. In order to check the bearing operational parameters in case of overload, which can occur during operation, the additional simulation has been performed. The additional $2000\ kN$ of the axial load have been added. Such additional load is applied to the bearing during acceleration of the hydraulic coupling. The load was kept at a constant level during the whole simulation time range. Both analyzed cases are listed in Table 5.13.

Table 5.13. Analyzed thrust loads

No.	Variant	Thrust load	Specific pressure
1	rated load	$3512\ kN$	$1.55\ MPa$
2	higher load	$5512\ kN$	$2.43\ MPa$

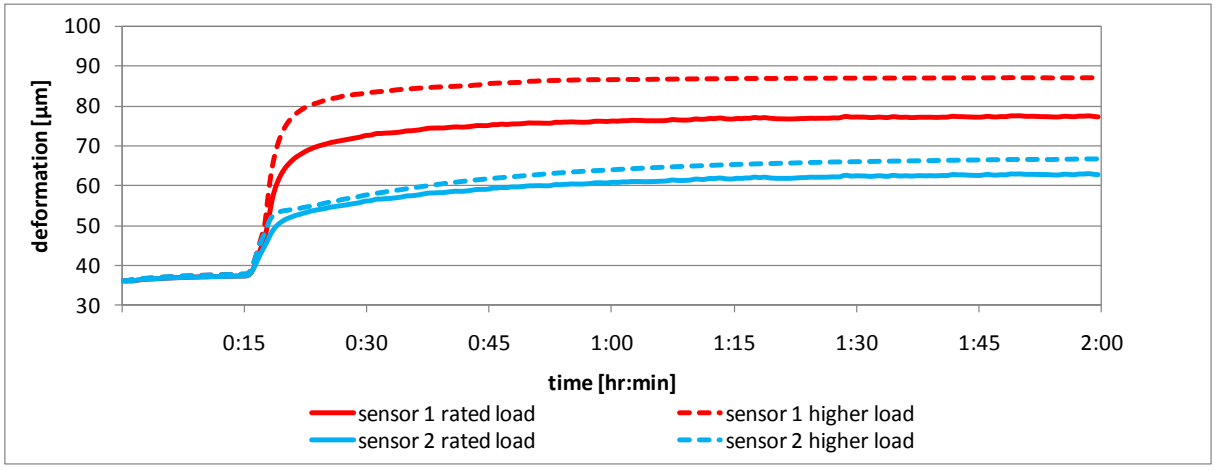

Figure 5.65. Comparison of calculated sensor temperatures for two load cases

One can notice a significantly higher temperature difference between the pad sensors. While the cold sensor shows almost the same temperature for both cases the warm sensor indicates an increase of approximately $10\ °C$ in case of the higher load case. This results in stronger thermal crowning of the bearing pad – see Figure 5.66.

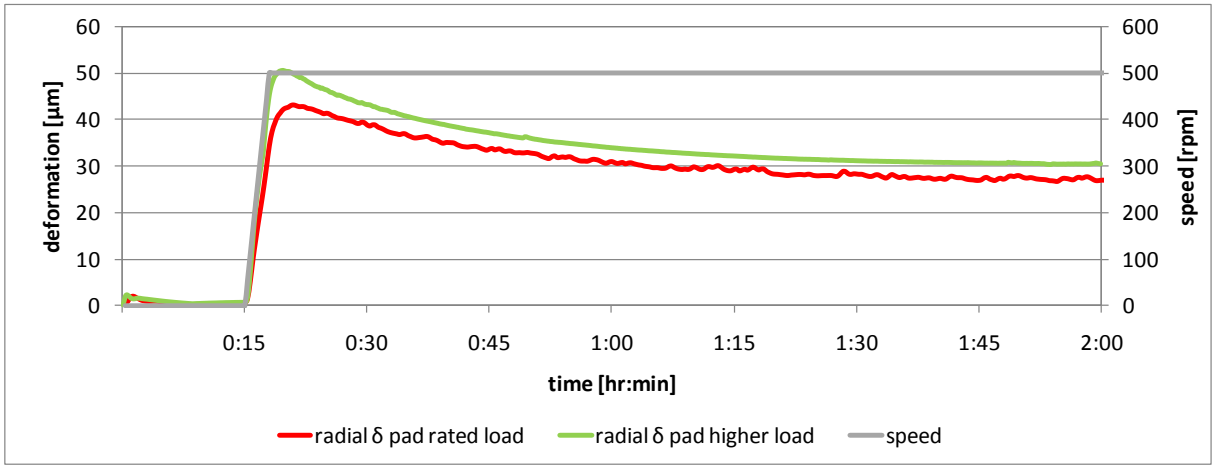

Figure 5.66. Pad radial deformations for two load cases

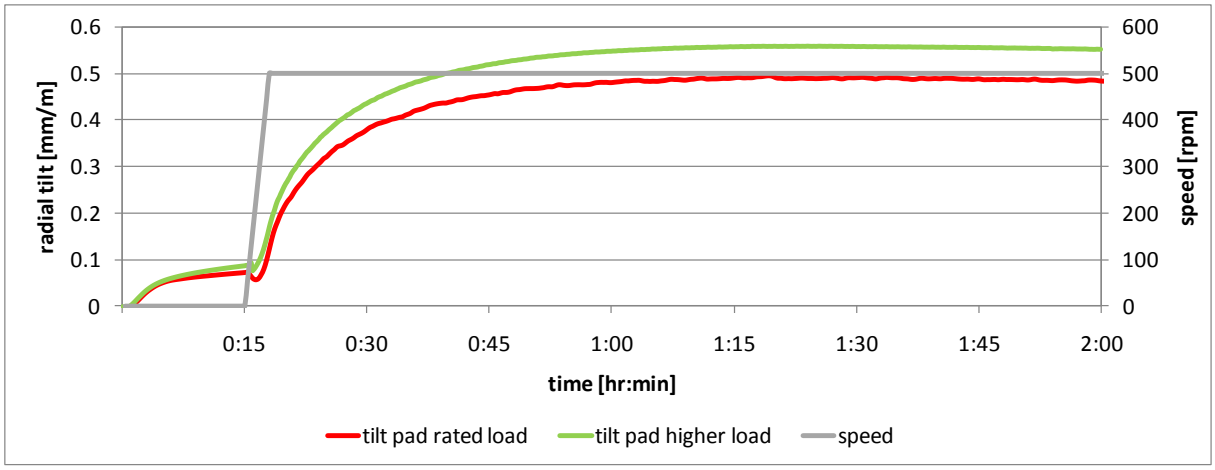

Figure 5.67. Pad radial tilt angles for two load cases

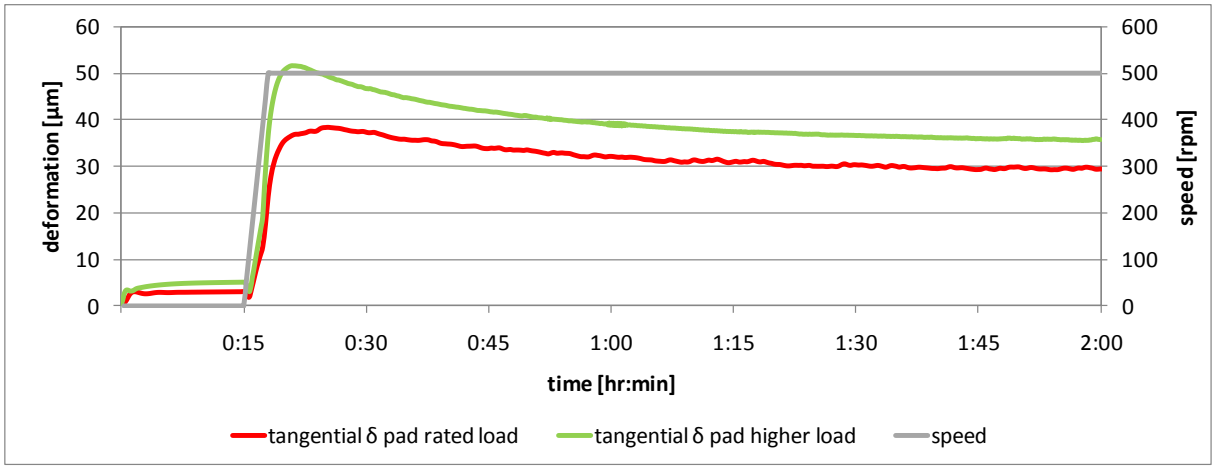

Figure 5.68. Pad tangential deformations for two load cases

Higher load causes more significant thermal distortion of the pad and at the same time decreases its tangential inclination. This can be an additional reason for higher bearing temperature. As shown in subsection 5.2.6 tangential inclination of the bearing pad has a significant influence on the operating temperature of the bearing.

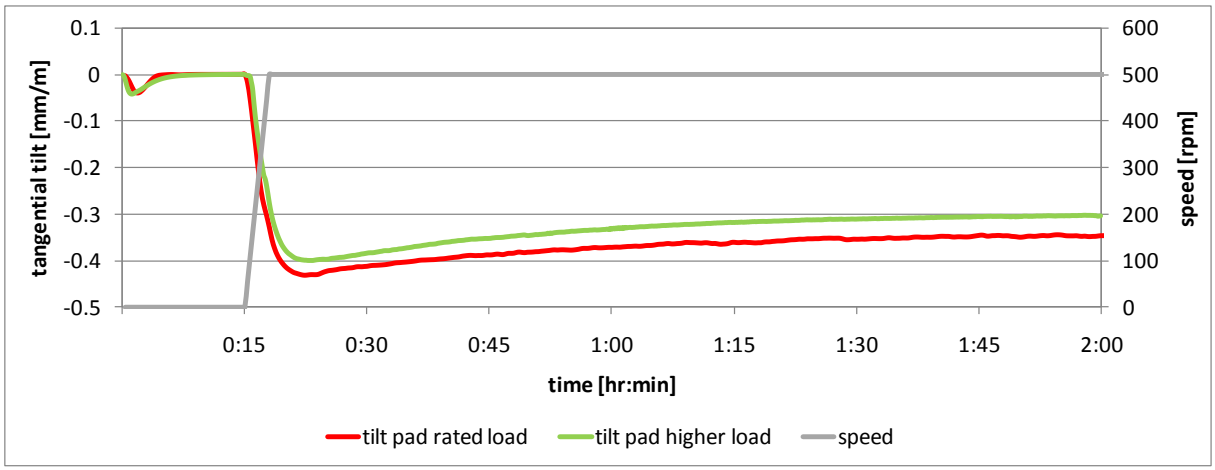

Figure 5.69. pad tangential tilt angles for two load cases

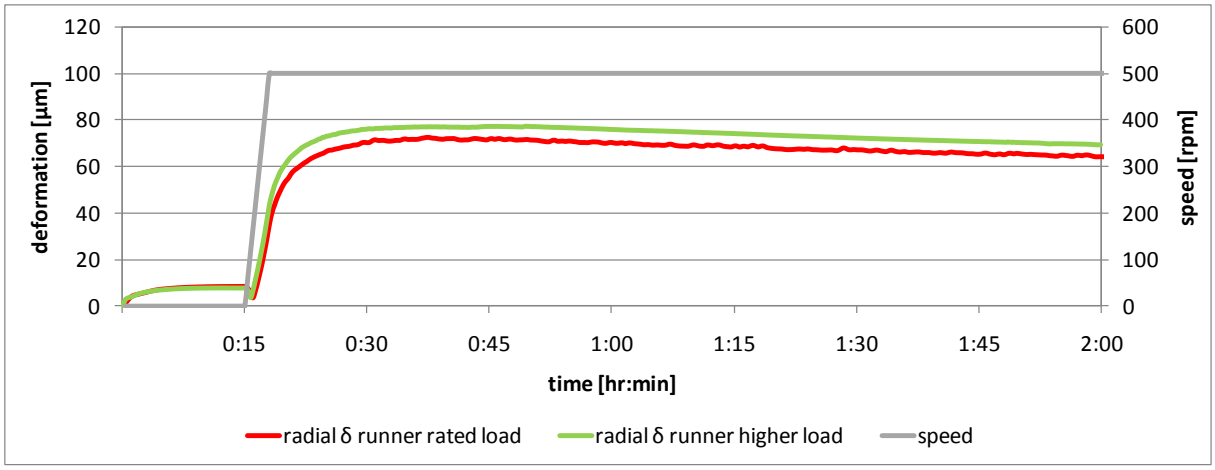

Figure 5.70. Runner radial deformations for two load cases

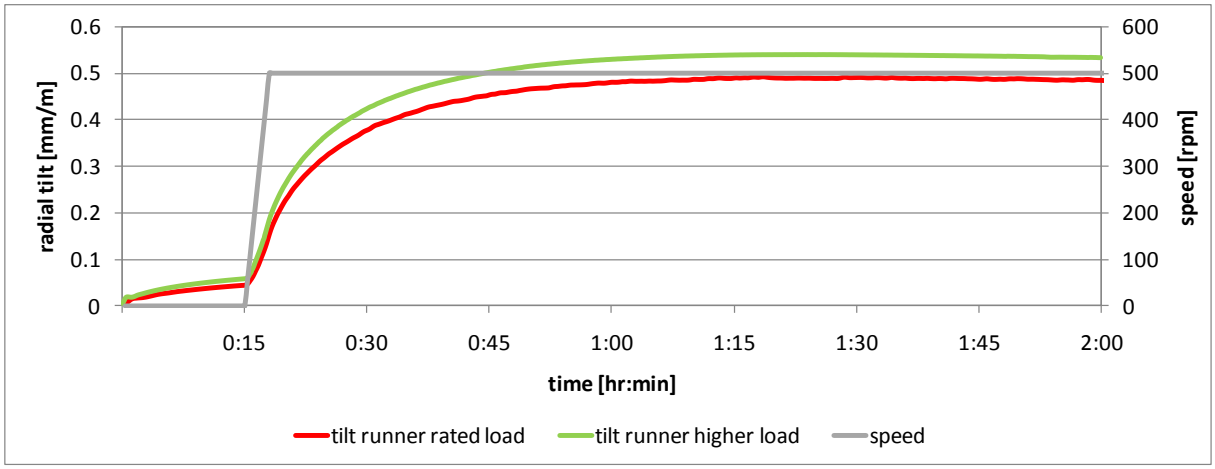

Figure 5.71. Runner radial tilting for two load cases

Oil film gap shapes for both simulations (steady state solution) are presented in Figure 5.72.

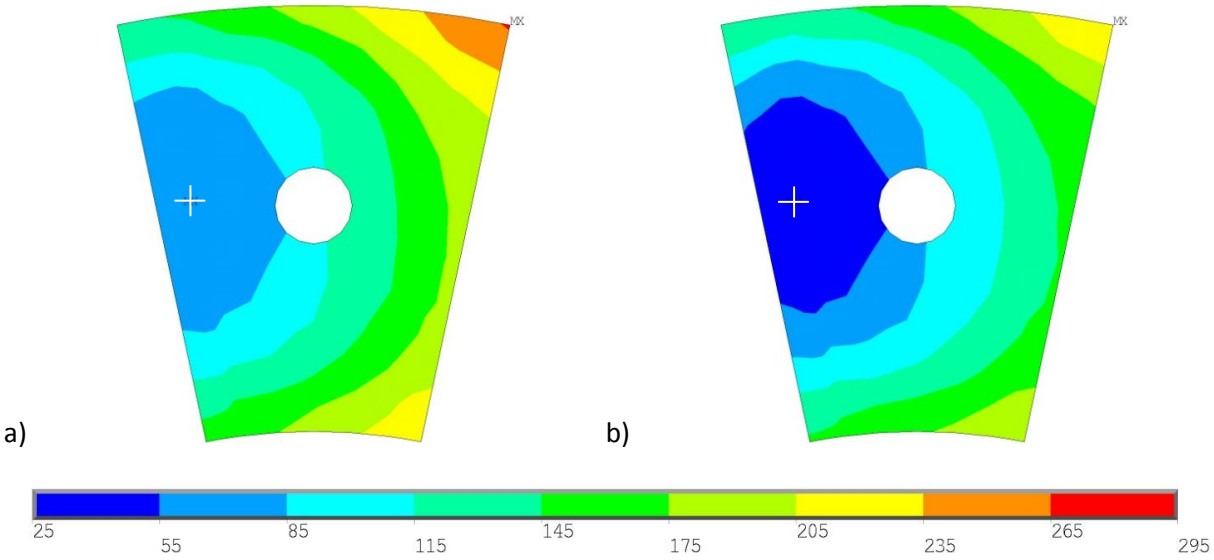

Figure 5.72. Calculated oil film thickness [µm], a) rated load, b) higher load

Minimum and maximum oil film thickness profiles are presented as a function of time in Figure 5.73 and Figure 5.74. One can notice very fast response on the changing operating conditions (rotational

speed). This indicates that bearing dynamic characteristics are not strongly affected by additional damping elements.

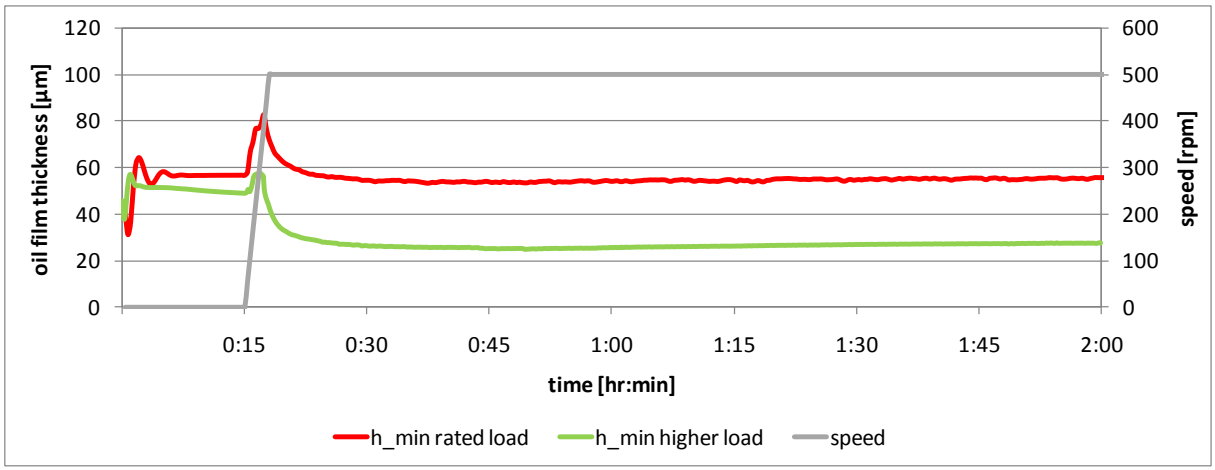

Figure 5.73. Minimum oil film thicknesses for two load cases

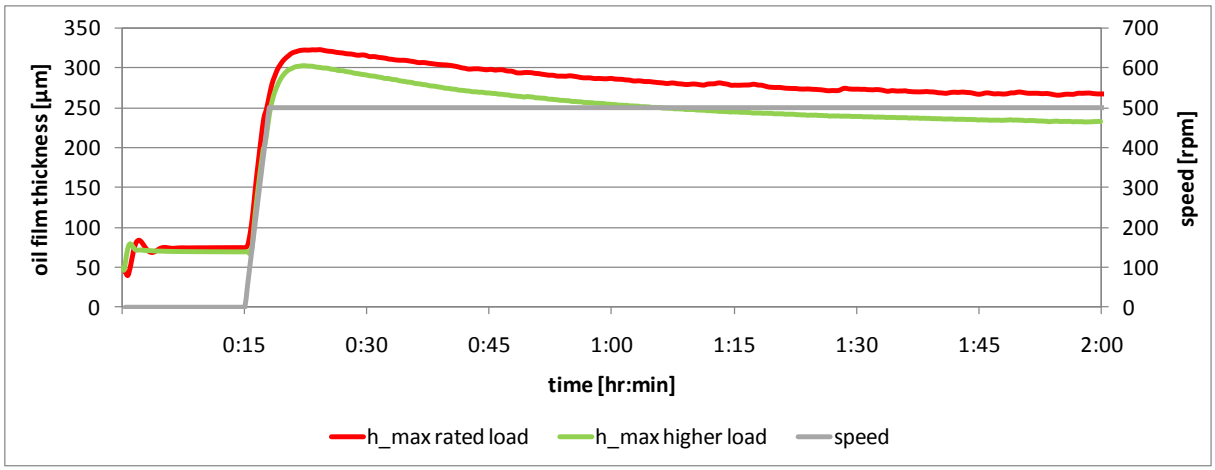

Figure 5.74. Maximum oil film thicknesses for two load cases

Higher bearing load causes an decrease of the minimum oil film thickness. A further reaction is the increase of the operational temperature. Change of the axial load from 3512 to $5512\ kN$ causes higher thermal peak of deformation during startup. Steady state calculations do not reflect the effect of overload on the pad deformations (see Figure 5.68). During operation one can observe slight increase of the minimum oil film thickness. This indicates that it is necessary to perform transient bearing analysis in order to see such an effect. Simple steady state analysis would show that higher thrust load is less critical than it is in the reality.

5.3.6 Influence of the startup time on the bearing deformations

In case of bearings that experience troubles during operation, one can try to make their operating conditions less severe through some minor operational modifications. The easiest from the unit operator point of view is to change the length of the startup and/or hydrostatic system assistance times. In this chapter startup conditions are being investigated. According to the literature [**9**] hydro generators (pump storage especially) are brought to the operation as quickly as possible. This can lead to high thermal gradients in the bearing elements and their unusual distortions. Additionally it can cause lower bearing load carrying capacity and consequently lower oil film thickness. The process may become unstable due to higher heat generation which finally results in bearing seizure [**9**].

Thanks to the ability of the developed model to simulate transient states it is possible to check the influence of the generator startup time on the bearing behavior. In this part mainly transient deformations are analyzed. For the comparisons the Kopswerk II power plant thrust bearing was chosen which has already been described in Chapter 3. Its bidirectional design makes it more sensitive to deflection effects during startup and operation. Standard startup time during commissioning was set to $3\,min$ but according to the contract it is possible to accelerate unit also within a shorter time (approximately $1\,min$). Six startup procedures A – F are compared in this chapter. In Table 5.14 analyzed startup variants are listed.

Table 5.14. Different startup procedures

No.	Variant	Startup time	Hydrostatic operation
1	A	3 min	up to 80% nominal speed
2	B	3 min	30 min after 100% nominal speed
3	C	1 min	up to 80% nominal speed
4	D	5 min	up to 80% nominal speed
5	E	30 min	up to 80% nominal speed
6	F	30 min	30 min after 100% nominal speed

Comparisons of the sensor temperatures and transient behavior of the bearing parts for all 5 analyzed alternatives are presented in the following diagrams (Figure 5.75, Figure 5.76, Figure 5.77, Figure 5.78, Figure 5.79, Figure 5.80 and Figure 5.81).

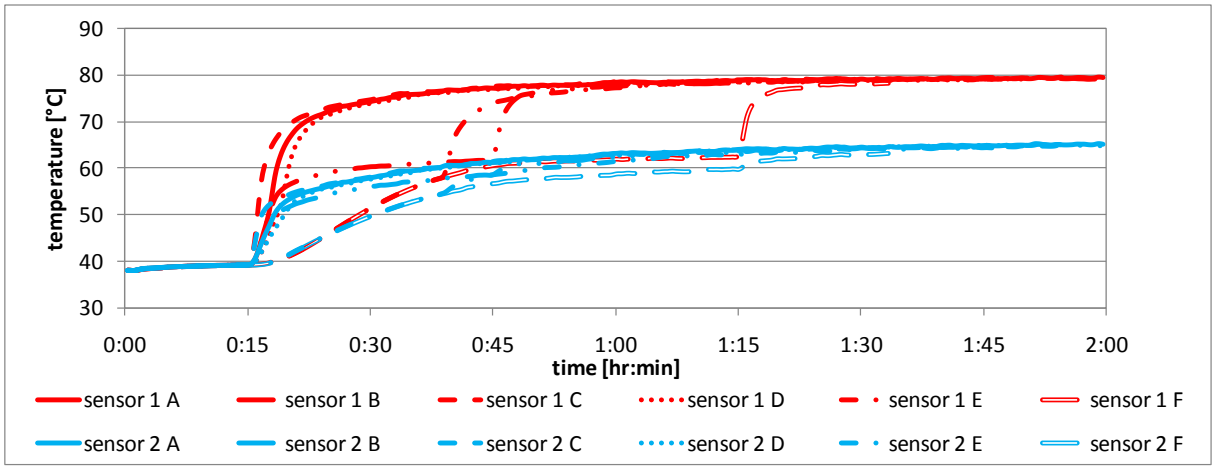

Figure 5.75. Comparison of calculated sensor temperatures for different startup procedures

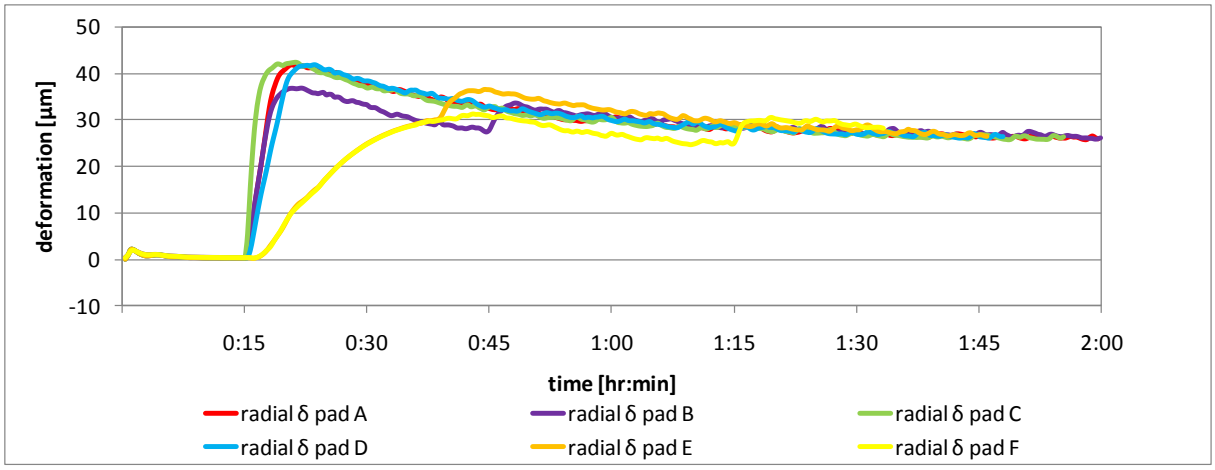

Figure 5.76. Pad radial deformations for different startup procedures

Radial deformation of the pad can be reduced by 25 % for the slower startup procedure. Thermal peaking of the pad deformation can be almost eliminated in this way.

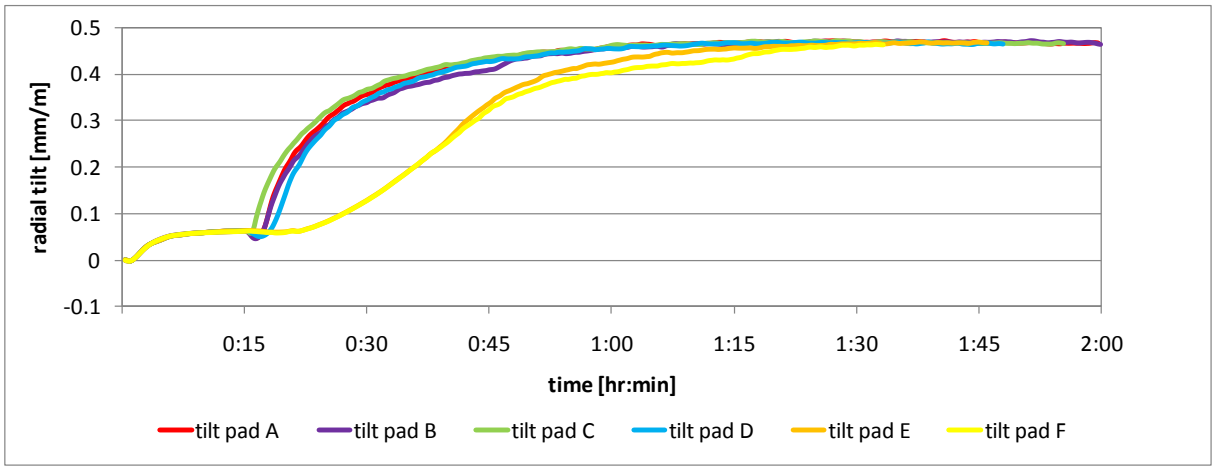

Figure 5.77. Pad radial tilt angles for different startup procedures

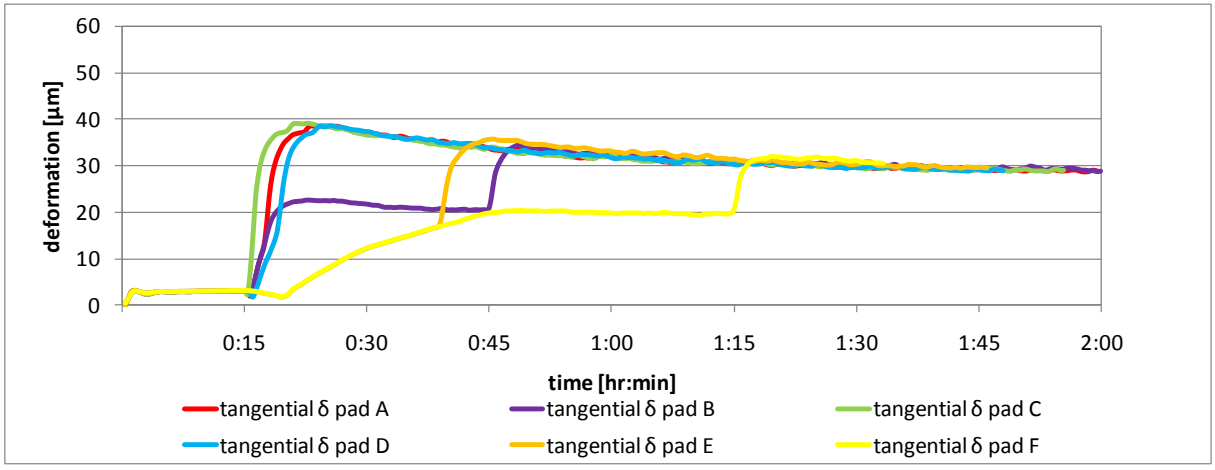

Figure 5.78. Pad tangential deformations for different startup procedures

Turning off hydrostatic jacking system can be observed very well on the tangential pad deformation profiles. There is direct response in form of rapid increase of the shape of the pad. Pad tangential tilt angle is strictly connected with the assumed profile of the rotational speed. One can observe that there is no significant delay of the tangential inclination of the pad.

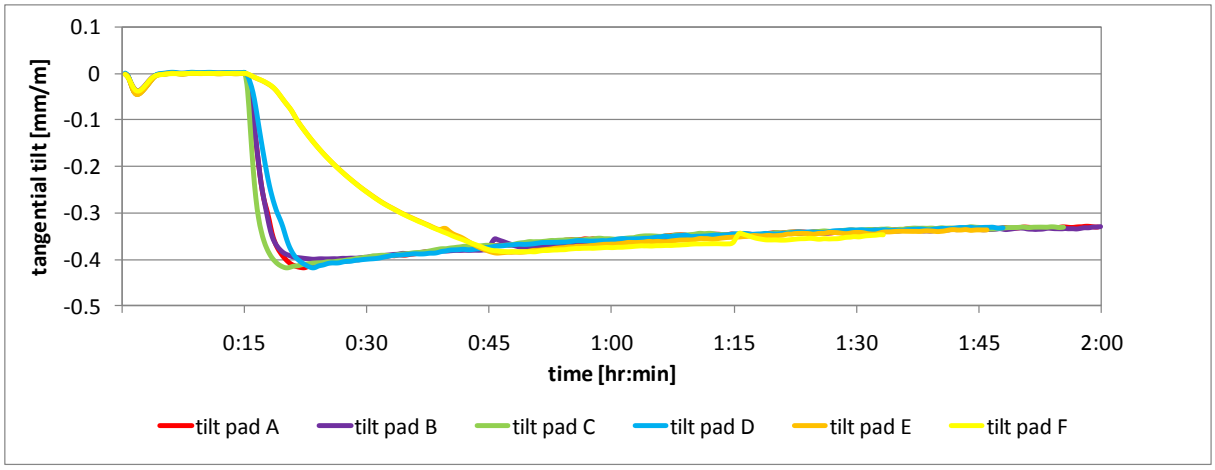

Figure 5.79. Pad tangential tilt angles for different startup procedures

Longer time of hydrostatic system operation has almost no influence on the runner deformation – for both variants D and E deformation of the runner has very similar profile.

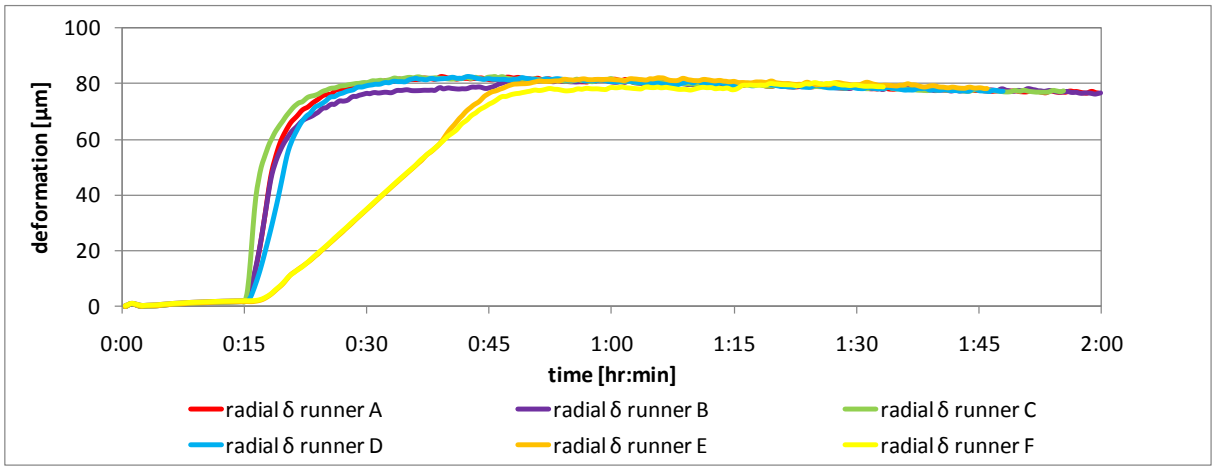

Figure 5.80. Runner radial deformations for different startup procedures

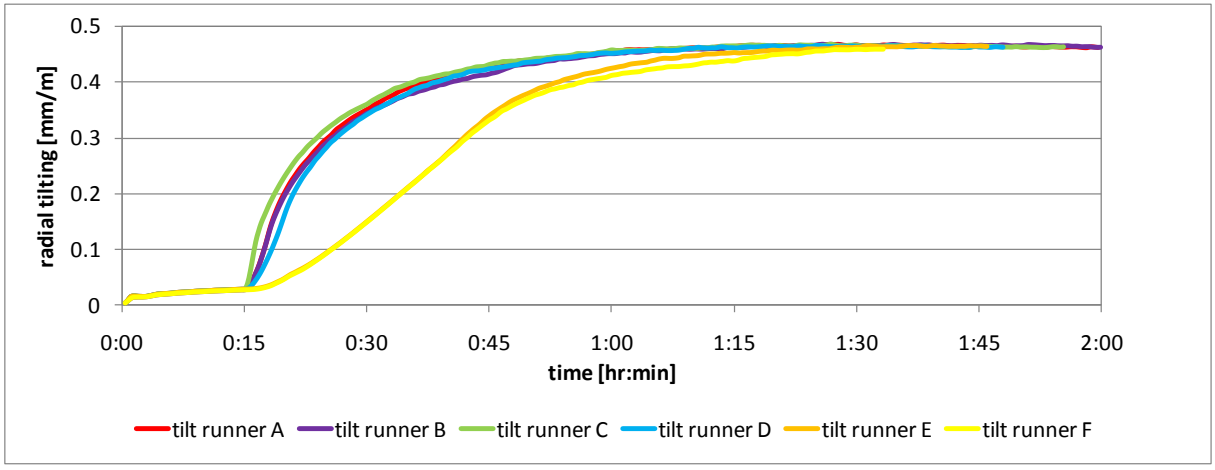

Figure 5.81. Runner radial tilt angles for different startup procedures

It is possible to avoid pad thermal peaking after startup. Bearing operation needs to be supported by the hydrostatic jacking system for a longer time in order to bridge the critical time after startup. Although steady state values of all parameters are equal for all analyzed startup procedures, the peak of the thermal deformation of the bearing pad can be significantly reduced when the startup

procedure takes more time. The longer operation of the hydrostatic jacking system, the better the resulting effects. This could also be easily implemented on the existing power plants without need of introduction of any additional changes into the bearing design.

Above investigation shows again the advantages of the transient analysis of the thrust bearing. Steady state calculation procedure is not able to take the history of operation into account and such investigation could not be performed.

5.4 Comparison of the cold and warm startup simulations

Since the thermal gradients and in consequence the thermal deflections of the bearing elements are essential parameters of the bearing operational conditions, it is very important to ensure an appropriate cold oil temperature in the bearing housing also during startup. Such effect occurs because the sliding surface reaches its maximum very quickly (within several seconds after startup) and the cold pad backing causes even larger crowning than normal. In winter, oil temperature in the housing and tanks can reach very low values which can be dangerous for the bearing. It is the bearing designer's responsibility to define the lowest cold oil temperature that is safe. This can be done, for example, with the use of the developed model that is able to predict the bearing behavior during startup procedure. If the minimum safe cold oil temperature is higher than the existing one (for example $30\ °C$) oil has to be heated up while the generator waits, in a standby mode, for the start order from the network controls. Obviously unnecessary oil heating during winter causes additional costs and reduces overall efficiency of the unit. The purpose of the simulation is to check the influence of the cold oil temperature on the bearing operational parameters like minimum oil film thickness, oil film gap shape, pad deformations and tilt angles and oil film thickness profiles.

5.4.1 Input parameters

In case of this simulation the most important parameter is the cold oil temperature. Two simulations have been performed with two different values of cold oil temperature ($15\ °C$ and $36\ °C$). Material properties, for both models, were defined like those described in Chapter 3. In both cases hydrostatic jacking was turned off at $80\ \%$ of the nominal speed ($400\ rpm$).

Table 5.15. Input parameters for the both simulations

No.	Parameter	Symbol	Value	Unit
1	Nominal speed	n	500	rpm
2	Load	F	3512000	N
3	Specific pressure	p	1.55	MPa
4	Cold oil temperature (warm start)	T_{cold}	36	°C
5	Cold oil temperature (cold start)	T_{cold}	15	°C
6	Initial temperature	$T_{initial}$	T_{cold}	°C
7	Runner temperature	T_{runner}	T_{cold}	°C
8	Startup time	$t_{startup}$	180	s

Transient input parameters for the simulation of the warm and cold startup are given in Figure 5.82.

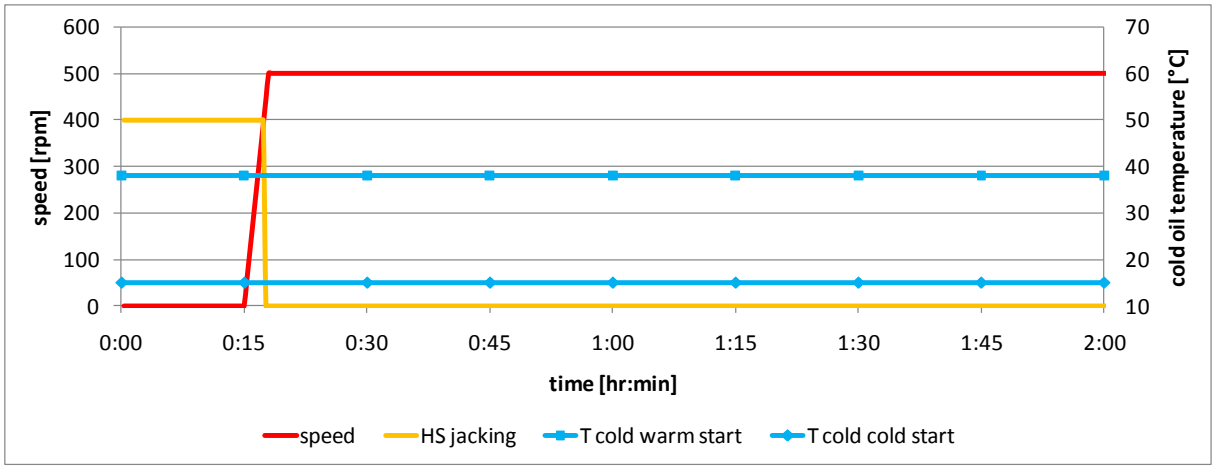

Figure 5.82. Transient input parameters for the both simulations

5.4.2 Comparison of the results

Obtained results of calculations are presented in the following diagrams (Figure 5.83, Figure 5.84, Figure 5.85, Figure 5.86, Figure 5.87, Figure 5.88 and Figure 5.89).

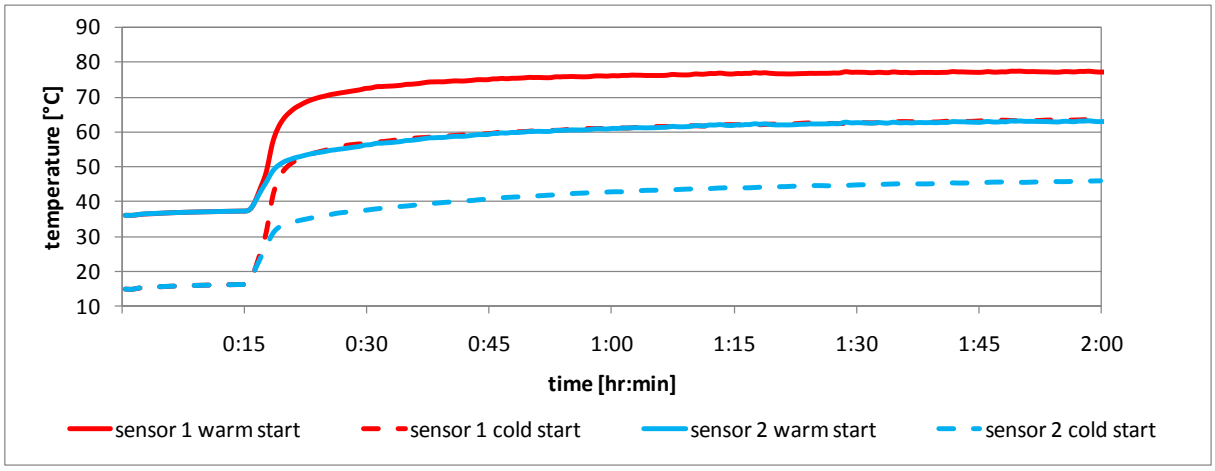

Figure 5.83. Comparison of calculated sensor temperatures for warm and cold start

One can notice slightly larger difference between the cold oil temperature and sensor 1 temperature values in case of the cold startup. This increased temperature difference causes larger pad thermal deformations in steady state.

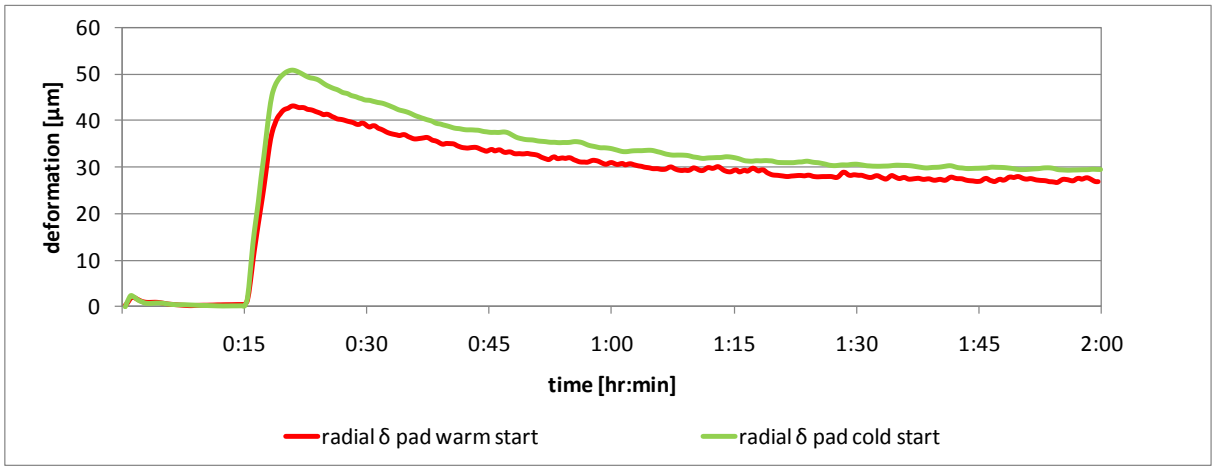

Figure 5.84. Pad radial deformations for warm and cold start

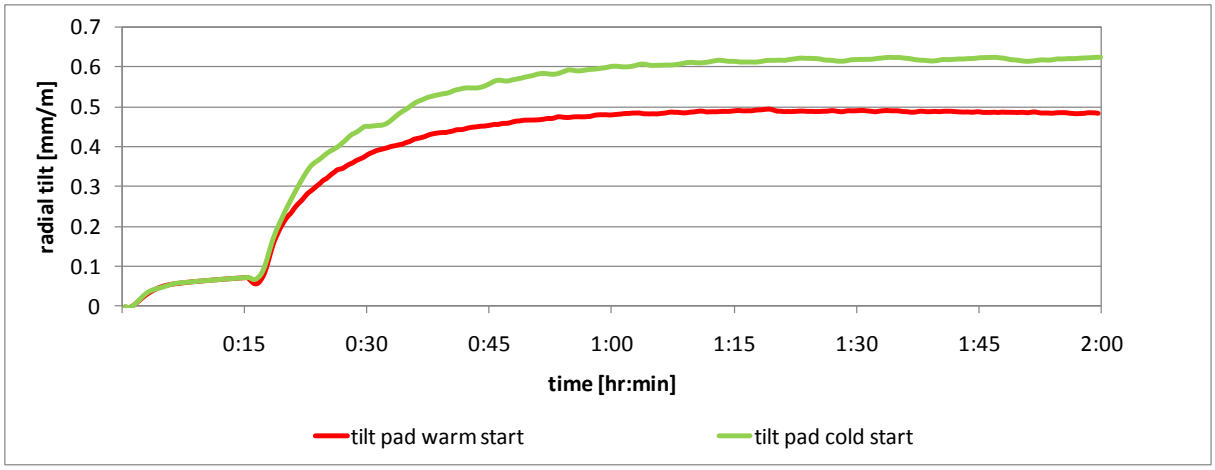

Figure 5.85. Pad radial tilt angles for warm and cold start

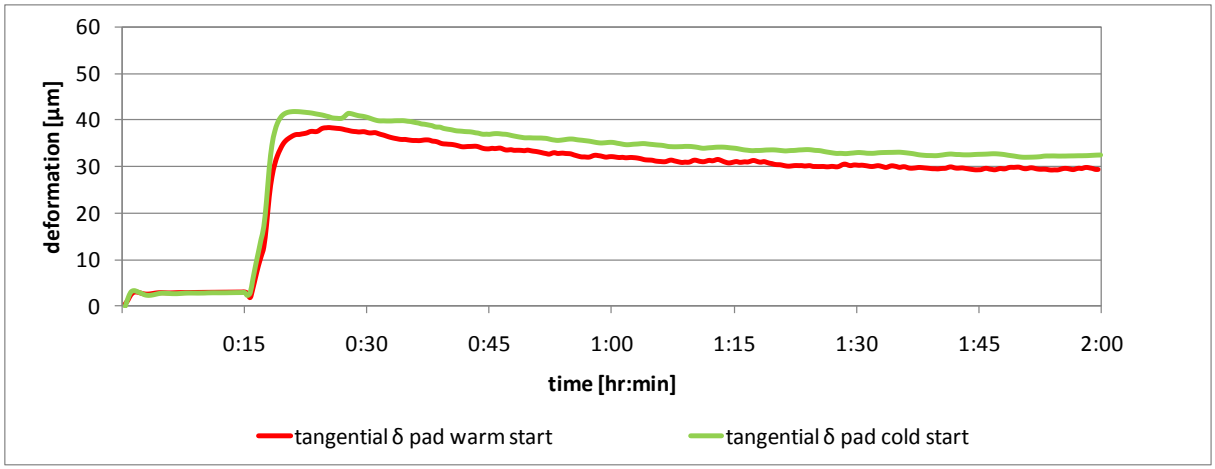

Figure 5.86. Pad tangential deformations for warm and cold start

Pad tilt angle in circumferential direction is significantly ($\sim 0.1\ mm/m$) higher in case of the cold start. This effect is caused by higher oil viscosity in case of the cold startup.

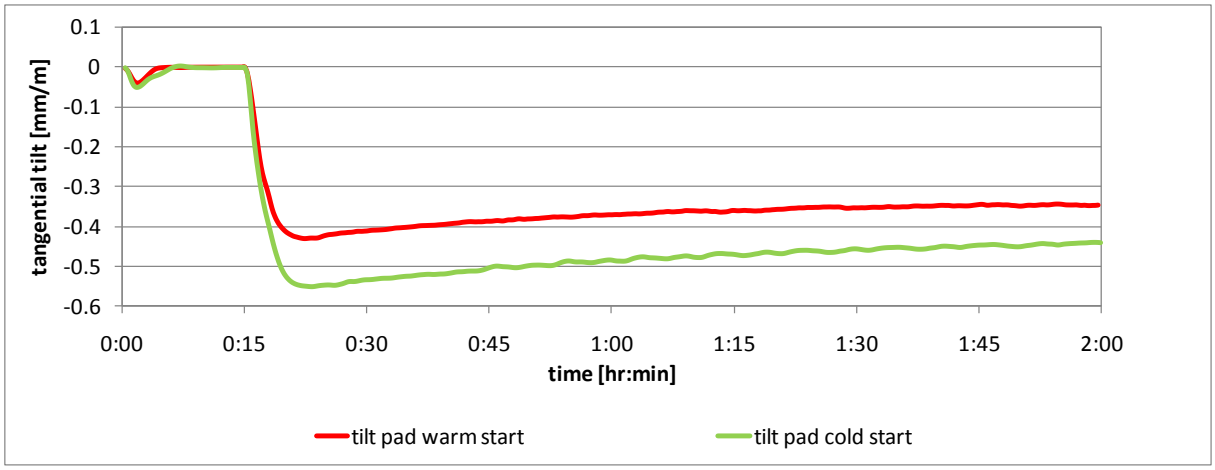

Figure 5.87. Pad tangential tilt angles for warm and cold start

Thermal deformation of the runner is significantly stronger ($\sim 30\ \%$) in case of the cold startup. This is an effect of higher temperature difference. Thermal peak of the deformation is also better visible for that case.

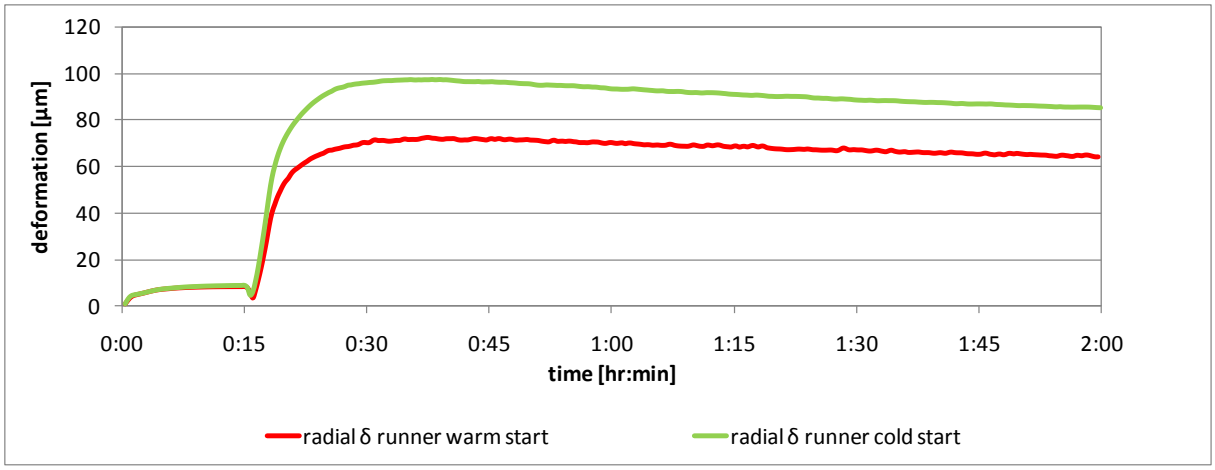

Figure 5.88. Runner radial deformations for warm and cold start

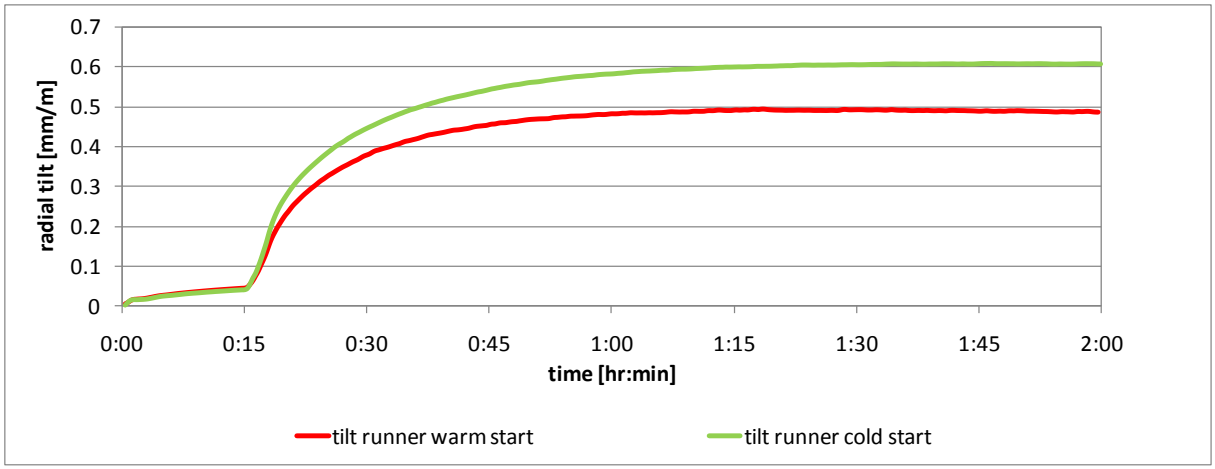

Figure 5.89. Runner radial tilt angles for warm and cold start

Minimum oil film thickness reaches similar values in both cases. It means that favorable influence of the higher viscosity of the oil in case of the cold start is reduced by more disadvantageous oil gap profile. In the analyzed case both effects are almost equal thus there is almost no change in the minimum oil film thickness.

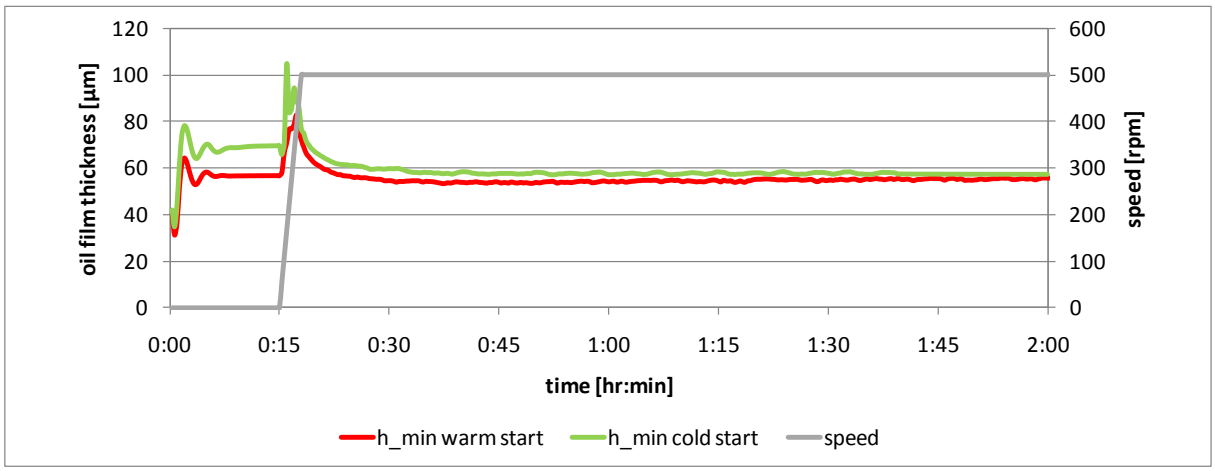

Figure 5.90. Minimum oil film thicknesses for warm and cold start

Maximum oil film thickness is slightly higher in case of the cold start what is caused by higher tangential inclination of the pad.

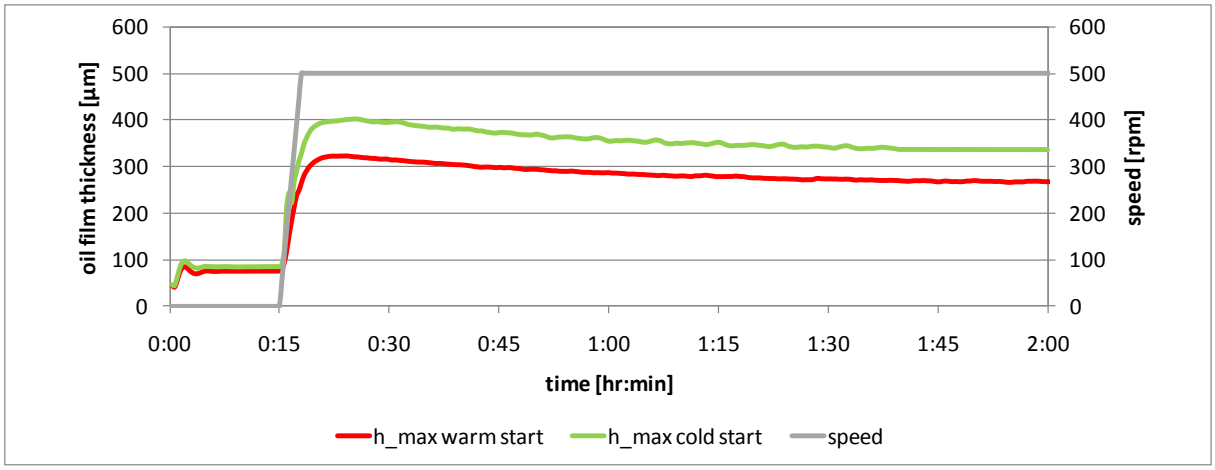

Figure 5.91. Maximum oil film thicknesses for warm and cold start

Oil gap profiles at two chosen time points are presented in the following figures (Figure 5.92 and Figure 5.93). Marked cross sections (A, B, C, D) are presented in Figure 5.94.

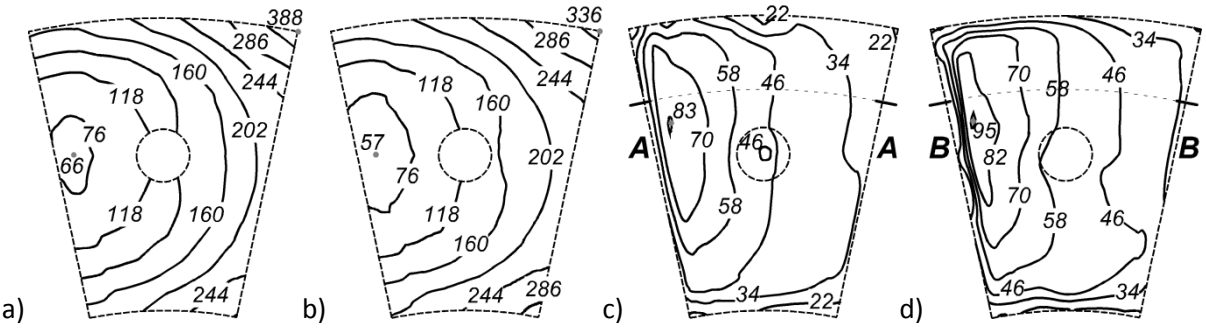

Figure 5.92. Results of simulation – cold start, a) oil film gap [µm], time 00:20 [hr:min], b) oil film gap [µm], time 01:40 [hr:min], c) sliding surface temperature [°C], time 00:20 [hr:min], d) sliding surface temperature [°C], time 01:40 [hr:min]

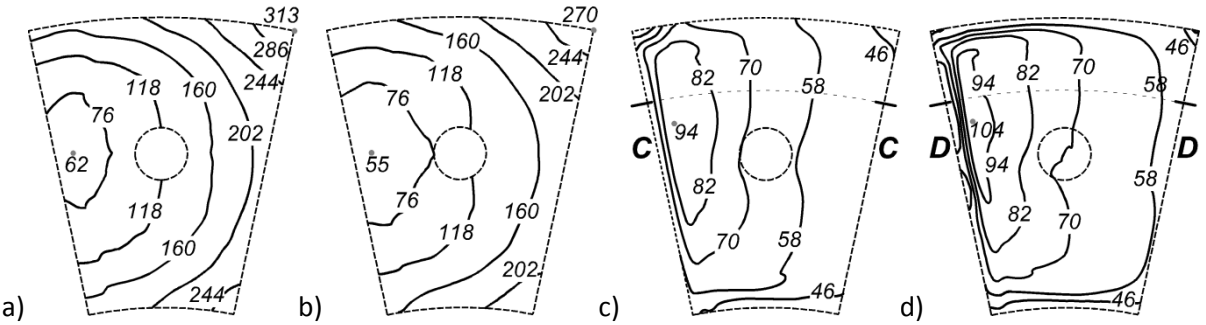

Figure 5.93. Results of simulation – warm start, a) oil film gap [µm], time 00:20 [hr:min], b) oil film gap [µm], time 01:40 [hr:min], c) sliding surface temperature [°C], time 00:20 [hr:min], d) sliding surface temperature [°C], time 01:40 [hr:min]

Temperature profiles in the oil gap through the marked cross sections are shown in Figure 5.94. Two different time points are presented for both cases. The first time point ($00{:}\,20\ hr{:}\,min$) shows the oil film gap shape almost directly after startup. The second one ($01{:}\,40\ hr{:}\,min$) shows the oil film gap in steady state. Contours show the distribution of the temperature fields through the oil film.

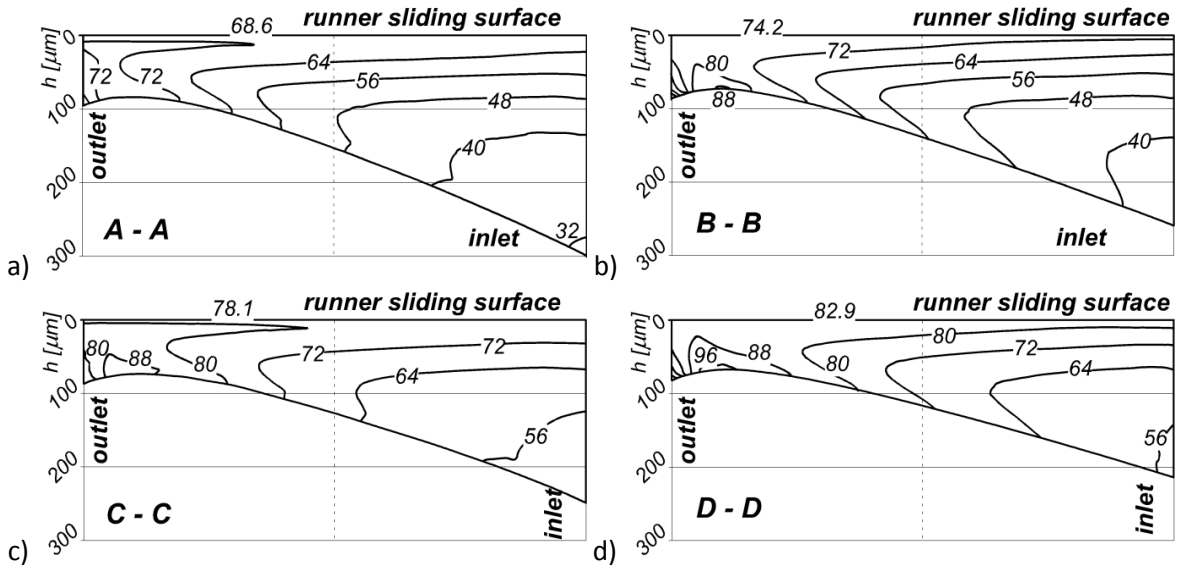

Figure 5.94. Temperature profiles across the oil film, a) cold start, time 00:20 [hr:min], b) cold start, time 01:40 [hr:min], c) warm start, time 00:20 [hr:min], d) warm start, time 01:40 [hr:min]

5.4.3 Conclusions

Although the whole bearing was colder in case of cold start (maximum oil film temperature, oil film thickness profiles and sensor temperatures) thermal gradients in the bearing elements caused larger thermal deflections. The differences reach up to 25 % in comparison to the warm start conditions.

The ability of transient simulation of large thrust bearing assemblies has been shown. It has been indicated that during cold start, the bearing is subjected to higher deformations that are caused by larger temperature differences. On the other hand however, the less advantageous oil film profile is compensated by a higher viscosity of the oil and the resulting load carrying capacity is similar in both cases.

5.5 Comparison of three different support systems

One of the great advantages of the developed model is its flexibility. Taking into account many geometrically complicated cases would not be possible with many calculation programs with closed code. The FEM model connected to the CFD flow simulation can easily be adjusted or completely be rebuilt in order to calculate different bearing design cases. In this chapter a comparison of different support systems is presented in order to show the flexibility of the tool and to check if the supporting system can affect the bearing itself. Three of the most representative support systems were chosen: pivot support, membrane support and spring bed support.

5.5.1 Analyzed supporting systems

The most common support system is the one known from the Kingsbury's bearing with the pivoted pads. This system has many advantages (compensation of runner radial tilting for example) but does not allow for uniform load distribution among all bearing pads during operation. This issue is very important in case of large bearings where it is very difficult and expensive to assure assembly tolerances in the range of microns without any compensating devices. Sometimes it is even impossible because of deflections of housings and foundations. Differences in pad heights larger than several tens of microns may lead to serious bearing problems. There are designs that allow to setup an appropriate pad loading but only during bearing assembly with the use of the so called spindle support. Its elastic deformation can be measured and thus the load of each pad can be estimated.

Since the spindle is supported by the means of a threaded connection the height of each pad can be adjusted with high accuracy. Elastic deformation of the supporting spindle is the measure of the axial load. Other solutions make use of the polymer discs located below the pads in order to increase axial elasticity and in this way to decrease influence of the assembly uncertainties [**27**].

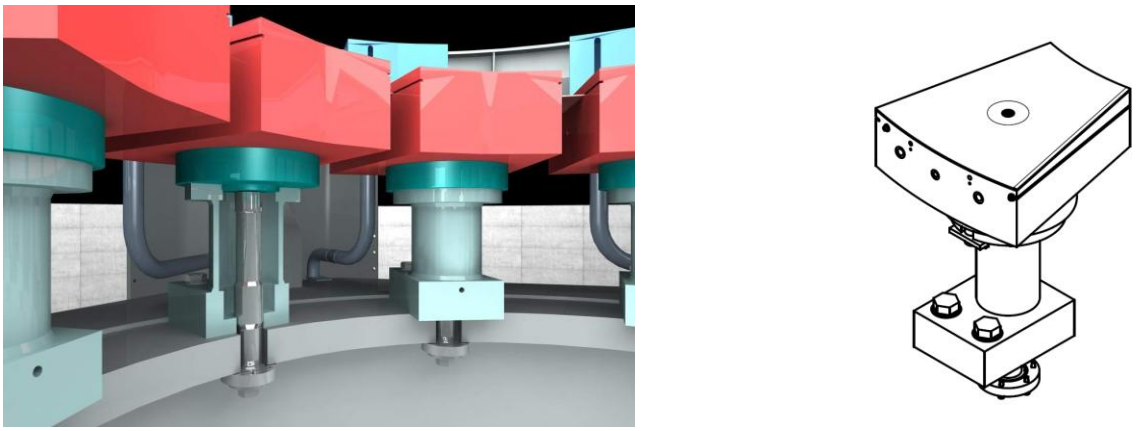

Figure 5.95. The pivoted thrust bearing pad supported on the adjustable spindle (ALSTOM Hydro)

In order to minimize the influence of the manufacturing and assembly inaccuracies the membrane support technology has been developed. The first designs based on this solution were complicated and expensive but the last (third) generation of the membranes is very simplified and robust. The design based on the membrane support allows to equalize load among all the bearing pads also during operation and within the whole bearing lifecycle without any maintenance. Underneath each pad, a flexible membrane is located. From the bottom, the membranes are supported by pressurized oil. Since all the oil chambers are connected with each other, supporting oil pressure is equal for all the bearing pads. In this way all bearing pads are loaded with equal forces. The manufacturing and assembly misalignments are compensated by the membrane deformations.

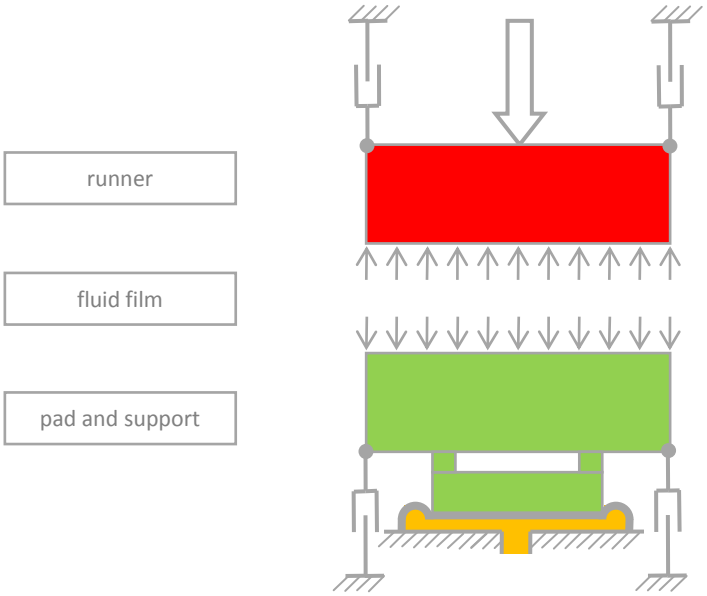

Figure 5.96. Sketch of the membrane support

Relatively small bending stiffness of the membrane should not affect the bearing characteristics but in order to check the influence of its reaction moment on the pad inclination the additional simulation has been performed.

a) 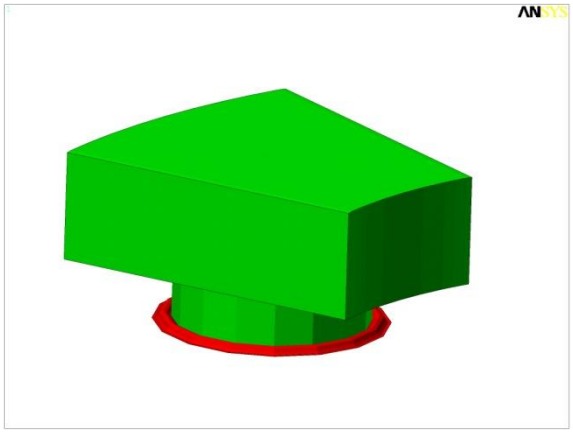 b) 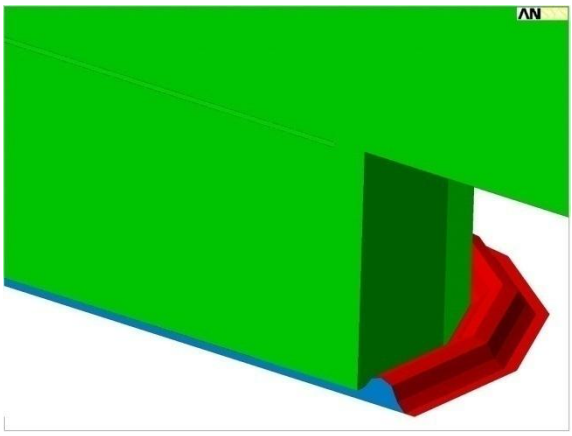

Figure 5.97. The membrane support FE model, a) view, b) cross section

On the model cross section (Figure 5.97) one can notice the pad and the disc with the supporting ring (green) that compensates pad thermal crowning due to elastic deformations, membrane (red) and pressurized oil under the membrane (blue). Since the hydrostatic pressure of the fluid is calculated during simulation it equalizes the load applied to the runner and transferred through the oil film. Under the assumption of evenly distributed load among the pads, the model can be reduced to a single pad thus the membrane is closed at the bottom and there is no flow possible. The membrane is made of $1.5\,mm$ thick spring steal so its bending stiffness may cause an additional reaction moment that will resist the tilt movement of the pad. The purpose of this simulation is to verify or disprove these suspicions. The reaction moment has been estimated during the design phase to be equal to approximately $M_R = 200\,Nm$.

Spring bed design is known from many literature sources, e.g. [**23**]. There is no additional supporting disc under the segment in case of the spring bed support but compensation of the pad thermal deformations is assured by uneven deformations of the underlying springs. Thickness of the pad should be relatively small ($\sim 0.1\,B$) in order to assure its bending elasticity but in this investigation all bearings have the same geometry. The springs are symmetrically located underneath the pad. To simplify the structural model the springs are uniformly distributed under the pad (Figure 5.98 and Figure 5.99) but their overall stiffness is equal to the defined value c_{total}. Since the springs have to be distributed symmetrically for a bidirectional bearing such simplification does not have influence on the obtained result. Two sets of springs stiffness have been investigated. Total stiffness of the springs for set A is chosen to obtain axial deformation $1.76\,mm$ under the rated load. This value is taken from similar bearings with spring bed support that operate in the hydro power plants. Set B has four times higher stiffness, so axial deformation equals to $0.44\,mm$. These two sets (see Table 5.16) are investigated in order to check the influence of the stiffness of the supporting springs on the bearing operational parameters.

Table 5.16. Analyzed stiffness of the supporting springs

No.	Variant	Deformation under rated load	Total stiffness of the springs
1	spring bed A	$1.76\,mm$	$0.16629\,MN/mm$
2	spring bed B	$0.44\,mm$	$0.66515\,MN/mm$

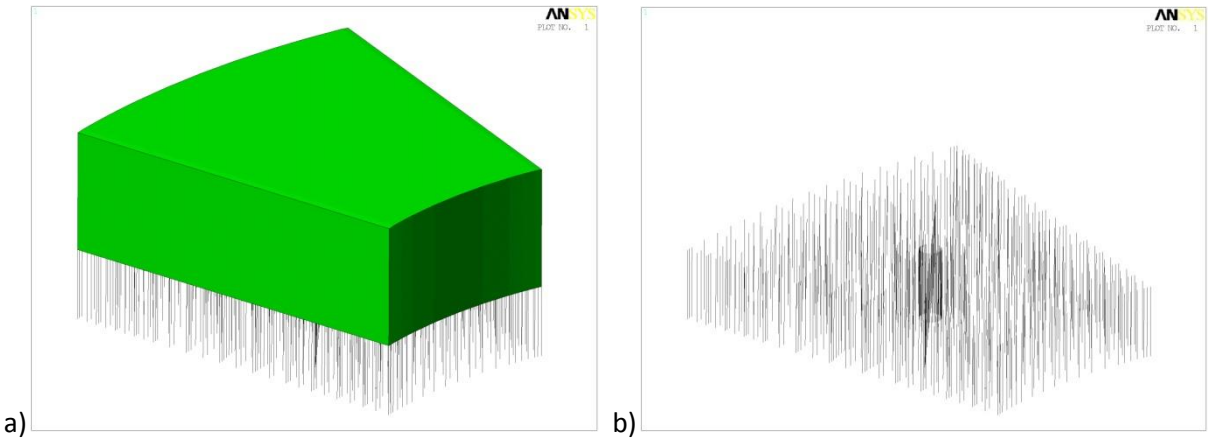

Figure 5.98. The spring support FE model, a) supported pad, b) spring bed

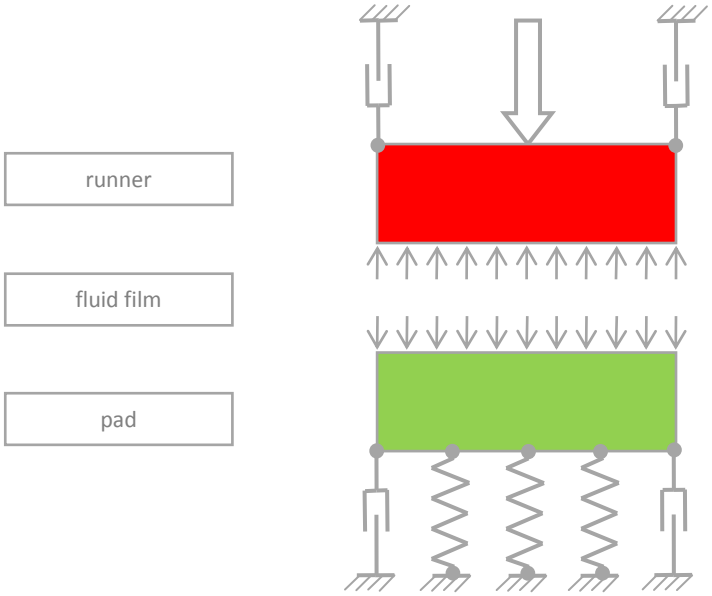

Figure 5.99. The sketch of the spring support

5.5.2 Comparison of the results

For a support system design it is particularly important to ensure that it does not affect the bearing itself in a negative way. It is a well known fact that the optimum bearing parameters can be obtained for pivoted pads. The main purpose to use other systems is to distribute the load between all the pads evenly. In order to check the performance of such supporting system, startup simulations and comparison with pivot support have been performed.

In this simulation the most important parameters were the tilt angles of the pad because only in this way a modified support can affect the bearing itself. Different balance of the pad will result in changed oil film gap and consequently in modified bearing operation parameters. In other words, if the balance of the pad is not affected, the bearing will not “see” the difference between supporting systems. The bearing functionality will not be affected and at the same time the load distribution between the pads will be equalized. In Figure 5.100 one can see a comparison of the calculated sensor temperatures for all 3 analyzed support systems. It can be noticed that sensor temperatures for the spring bed solution are slightly higher than these for the other two designs.

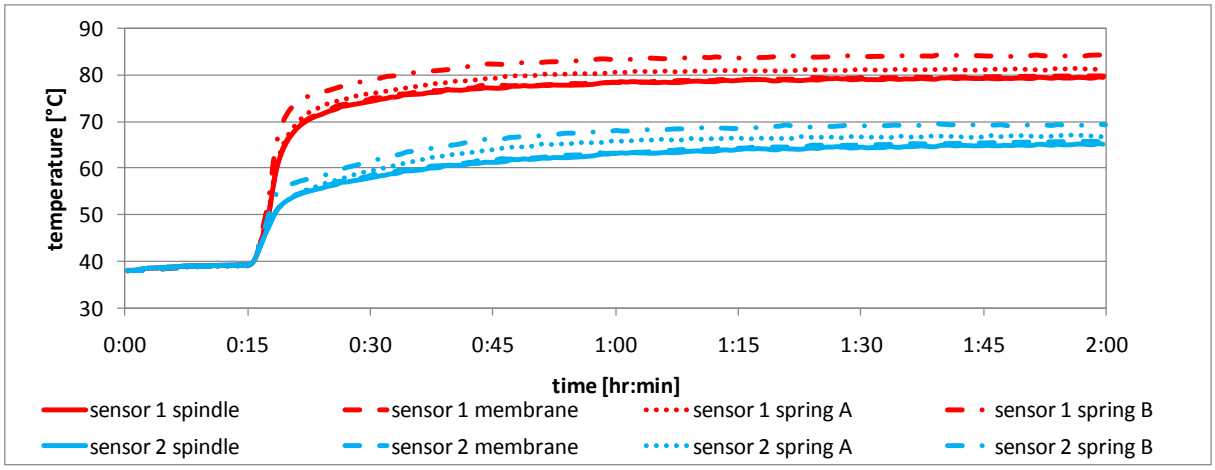

Figure 5.100. Comparison of calculated sensor temperatures for different support systems

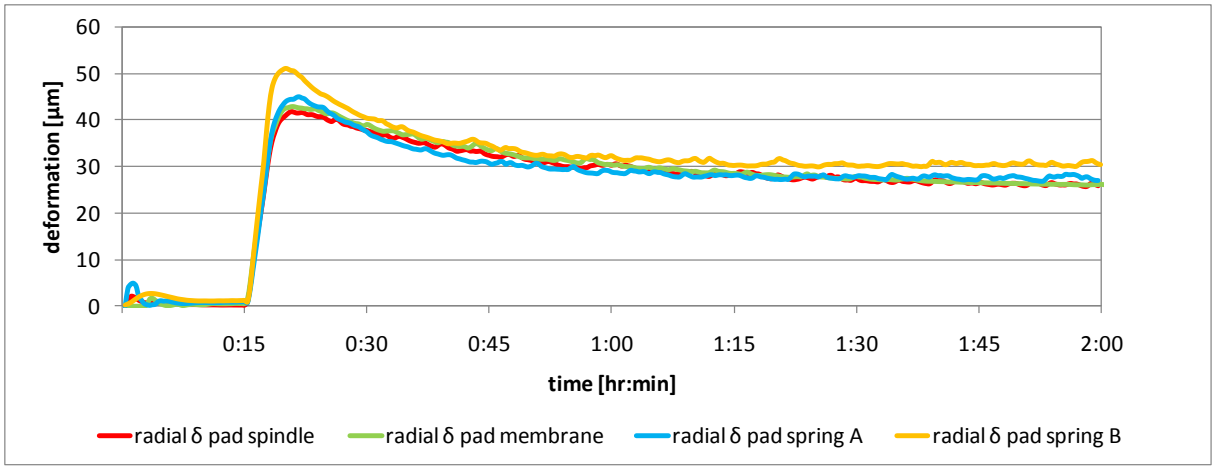

Figure 5.101. Radial pad deformations for different support systems

Radial inclination of the pad is significantly smaller in case of the spring bed design. This effect is caused by the reaction of the springs against tilting. Also in case of membrane support one can notice slightly smaller tilt angles but in this case the difference is much smaller.

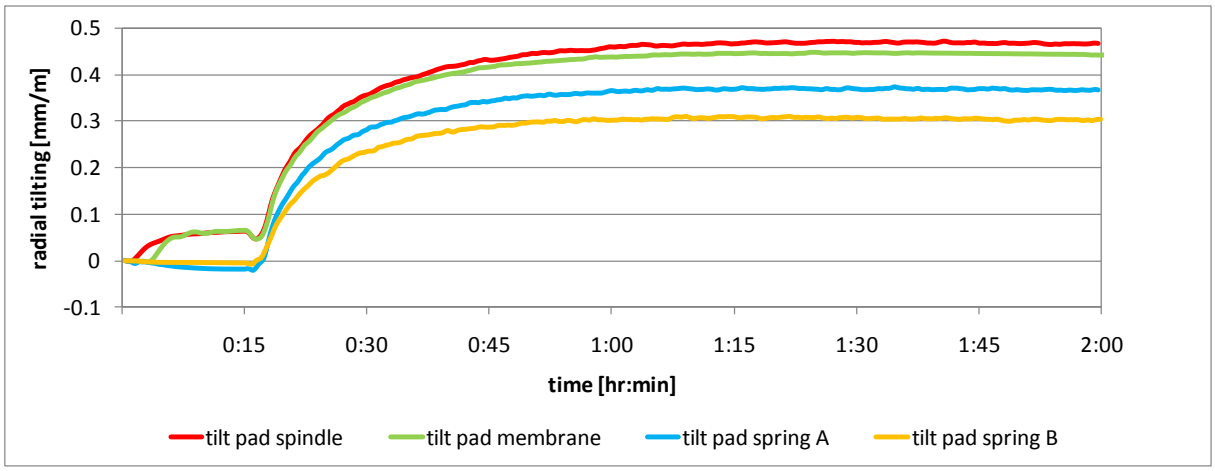

Figure 5.102. Radial pad tilt angles for different support systems

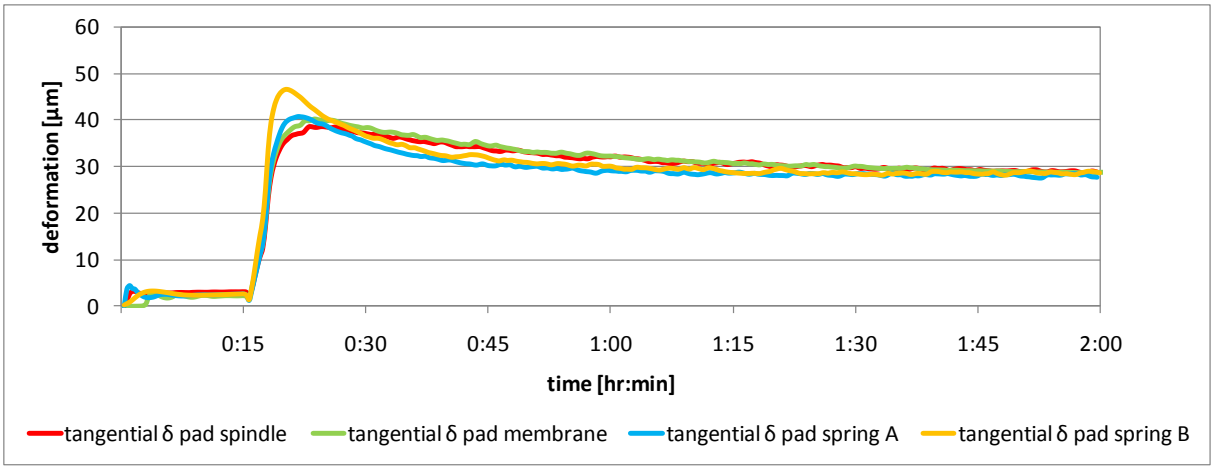

Figure 5.103. Tangential pad deformations for different support systems

The tangential inclination of the pad is smaller in case of the spring bed solution. This is a reason of the higher calculated bearing temperatures.

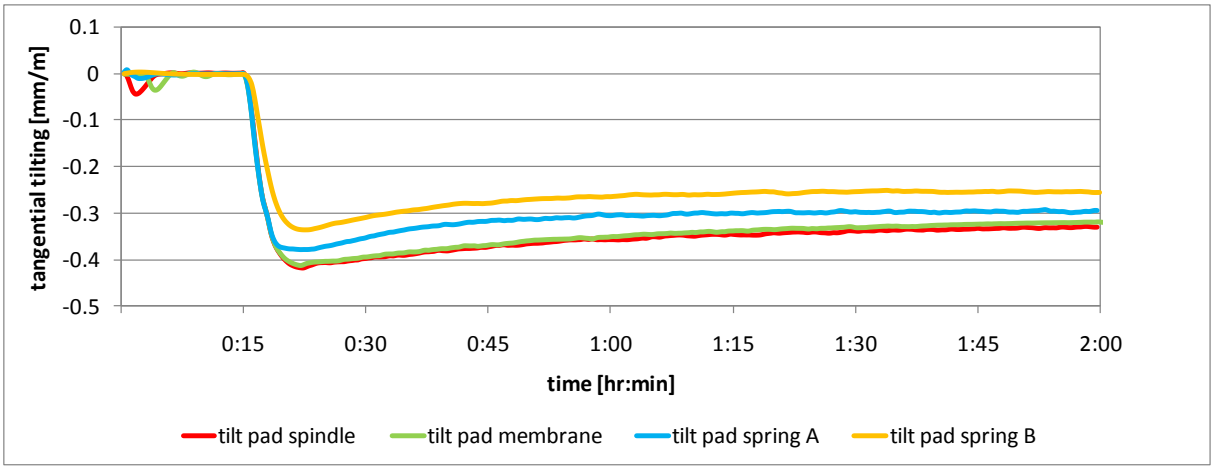

Figure 5.104. Tangential pad tilt angles for different support systems

The support system has hardly any influence on the runner deformation and its tilt angle. Slightly higher deformation is caused by higher oil film temperature in case of the spring bed design but the difference between the supporting systems is very low.

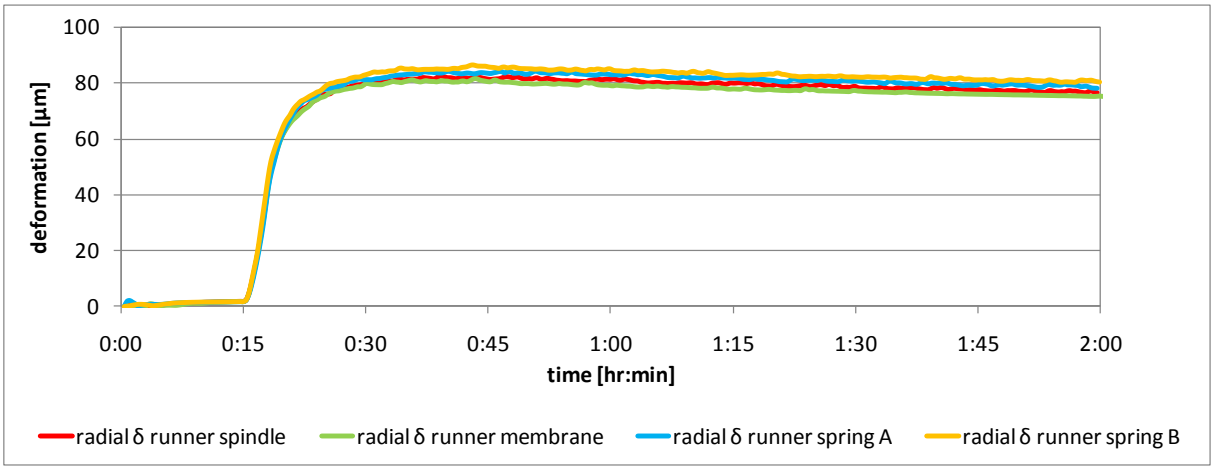

Figure 5.105. Radial runner deformations for different support systems

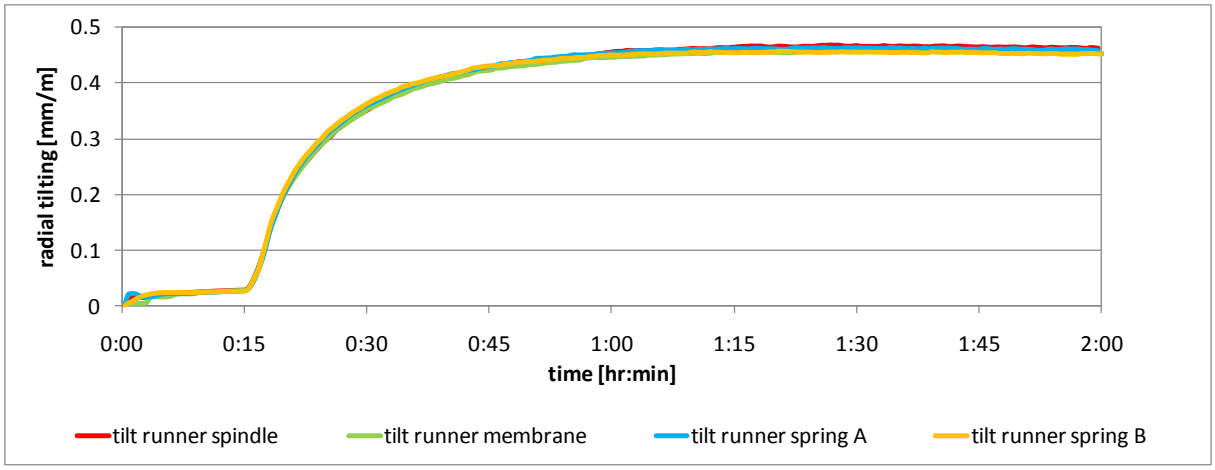

Figure 5.106. Radial runner tilt angles for different support systems

By comparison of the radial tilt angles of the pad and runner for different support systems one can see that the oil film gap remains the most parallel in case of spindle support and the least parallel gap occurs in case of the spring bed design. There is almost no influence of the support system on the behavior of the runner. Radial deformations and tilt angles are very similar in all three analyzed cases.

The tilt angles in both directions in case of spring supported bearings are strongly affected. This is due to the relatively large reaction moment of the support created by the springs deformation. Also pad deformations during startup are slightly larger than those obtained for other supporting systems. As a consequence of this behavior a slight increase of the sensor temperatures ($2-3\ °C$ in case of set A and $5-6\ °C$ in case of set B) can be observed.

Summary of the bearing operating parameters in steady state (time 7200 s) is given in Table 5.17.

Table 5.17. Influence of the supporting system on the bearing calculation results

No.	Variant	Minimum oil film gap	Maximum oil film temperature
1	spindle	$54.4\ \mu m$	$101.6\ °C$
2	membrane	$51.7\ \mu m$	$103.9\ °C$
3	spring bed A	$48.0\ \mu m$	$103.1\ °C$
4	spring bed B	$42.6\ \mu m$	$105.2\ °C$

Generally almost no difference in bearing behavior could be observed between spindle and membrane support systems. In transient as well as in steady state conditions, the pad and runner deformations are almost equal for both designs. Stiffness of the supporting springs has significant influence on bearing operating parameters. Higher value of the stiffness (set B) caused significantly lower minimum oil film thickness and inclination of the pad. Further consequence was higher operating bearing temperature.

5.6 Discussion of the results

In this subsection a summary and a discussion of the main results are given.

Comparison with the measurement data, validation of the model

The comparison between measured and calculated temperatures has shown good agreement within the analyzed time range. The temperature profile is exactly followed during the startup process. This agreement indicates that the effects which take place during hydrodynamic lubrication are also simulated with good accuracy. Comparison of two measured values (sensor 1 and sensor 2) shows that not only temperatures but also temperature increase along the film is estimated in a good way. The temperature field distribution in the bearing pad could be validated more precisely. Additionally it is an information that thermal deformation of the bearing elements are also calculated properly. Transient analysis of the shape of the bearing elements confirmed thermal deformation peaking effects., known from literature.

Good agreement of the calculated temperature profiles with the measurement data indicates that the heat generated in the oil film and its transport through the pad are estimated properly. Heat transfer through the pad is a combination of mainly two effects. First of all, the power loss rate and the heat flux on the sliding surface deliver the heat to the pad. In the presented case total calculated power loss is equal to $652\ kW$ and $2.25\ \%$ of this value is transferred through the pad sliding surfaces. At the same time the pad is cooled on the other walls by the means of convection. It has been found that the convection coefficient varies on the pad surfaces within the range between 100 and $500\ W/m^2$. Both these effects need to be estimated correctly in order to obtain agreement with the measured pad temperatures, which in turn is essential for proper evaluation of deformations.

Observation of the minimum oil film thickness during startup showed reasonable behavior. Turning off the hydrostatic jacking system causes rapid decrease of the minimum oil film thickness. Further on in the simulation, it remains almost on this constant level. During slow relaxation of the thermal deformations of the pad and runner one can even notice a very small increase of the minimum oil film gap ($1 - 2\ \mu m$).

The performed validation of the model with the use of the standardized DIN calculation procedure showed good agreement of the obtained pad tangential inclination and the minimum oil film thickness. The relative difference of the tangential inclination of the pad did not exceed $2\ \%$. The minimum oil film thickness in most of the analyzed cases was also calculated within the range of $2\ \%$ and in the worst case the difference was lower than $10\ \%$. This investigation showed that tilting of the bearing pad is calculated with very good accuracy. Because of some differences between the standardized procedure and the developed model the minimum oil film thickness is estimated with slightly worse accuracy.

Warm oil mixing

Careful analysis of the thermal boundary layer in the oil film and in the bearing groove as well as the comparison of the warm oil mixing coefficients indicated significant differences between bidirectional and unidirectional bearings. Calculation of the warm oil mixing coefficient, based on the obtained results, indicated that the bidirectional bearing has a significantly higher value than the unidirectional one (0.83 and 0.65 respectively). The reason for this difference is the tangential

inclination of the bearing pad ($\sim 0.35\ mm/m$ for the bidirectional and $\sim 0.88\ mm/m$ for the unidirectional case). This result indicated in a clear way that high operating temperatures of bidirectional bearings are caused by a very low oil film inlet height. Further investigation showed that thermal bending of the bearing elements is significantly higher in case of bidirectional bearing. This is a result of clearly higher thermal gradients in a such bearing. Comparison of the calculated minimum oil film thicknesses showed however that there are no significant differences. The oil film gap shape was totally different but the minimum value in case of the unidirectional bearing was only $3\ \mu m$ higher. This shows that despite significantly higher temperatures, the bidirectional bearing still has a safety margin as long as the allowable temperatures are not exceeded. The analyzed case is a clear example of a bearing where the maximum operating temperature is the main limit. It is caused by relatively high sliding speed ($60\ m/s$) and low specific pressure ($1.55\ MPa$).

Boundary condition on the runner

Three different variants of the runner boundary have been calculated. This investigation showed that there is a significant influence of the assumed boundary condition (differences in thermal deformation reach up to $25\ \%$) but the influence on the resulting bearing parameters is rather small. Minimum oil film thickness varied within the range of $5\ \%$ and the maximum oil film temperature within $1\ \%$. Additionally, it has been shown that the developed model responses as expected. Adverse changes of the runner sliding surface shape cause the expected negative influence on the bearing operating parameters.

Damping elements

Damping elements are the artificial part of the bearing model. Their purpose is to reduce oscillations of the bearing elements. It was an important part of the model validation to check whether this artificial damping has a negative influence on the calculated operational parameters. Two different cases were analyzed in order to show this influence. It was indicated that exaggerated damping forces cause overloading of the bearing during startup because of the fast thermal expansion of the bearing elements. This overload could also be visible on the presented temperature profiles and finally on the transient deformations of the bearing elements. It has been shown that properly adjusted damping coefficients have a significantly lower influence on the obtained results. On the other hand it has been indicated that damping coefficients need to be more than three times higher than necessary in order to influence the result significantly. A negative influence of the additional damping elements could be observed only within a very short time directly after startup ($\sim 10\ min$) but it is clear that this is the most important period in case of the startup simulation and therefore needs to be reflected in the simulation with good accuracy.

Transient vs. steady state calculation procedure

A comparison between steady state and transient state results was presented. This investigation showed that a quasi transient approach to the startup simulation can not reflect the transient effects that take place in case of the real bearing startup procedure. Simple graduation of the rotational speed with the use of steady state calculation procedure does not show the most important bearing behavior. Since the temperature field for each of these “steps” is stabilized one cannot observe transient behavior of the thermal deformations of the bearing elements. It has been indicated that the thermal peaking of the bearing elements already occurs after obtaining of the nominal speed and

then gradual stabilization takes place. Steady state calculation procedure is not able to show such behavior.

Startup procedure

Advantages of the transient approach to the bearing calculation have been shown in the investigation of the startup procedure parameters. Five different startup procedures were analyzed. It has been shown that a slower startup and a longer time of operation of the hydrostatic jacking system could helps reducing thermal peaking of the bearing elements. For example radial pad deformation could be reduced by 25% and thermal peak could almost be eliminated in that way.

It has also been shown that the model responses quickly (almost immediate) to the variable input parameters (e.g. rotational speed or mode of the hydrostatic jacking system). Model reaction in each of the analyzed cases was always very rapid and in line with expectations. A certain validation of the developed model was that regardless of the assumed startup procedure the resulting steady state parameters were always the same. This also proves that even if in steady state condition there is no difference in bearing operating parameters, in transient state such differences are possible. If during transient state some disadvantageous effects take place, failure may occur regardless of the fact that in steady state the bearing should operate properly.

Warm/cold startup

Comparison of the warm and cold startup of the bearing confirmed, known from literature, threats of very low oil temperature during startup of the thrust bearing. Thermal deformations of the bearing elements were significantly stronger in case of the cold startup whereas thermal deformation of the runner was even approximately $30\,\%$ higher. The difference in pad deformations was especially noticeable directly after startup, steady state values were similar for both cases. This shows another advantage of the transient analysis of the bearing behavior – even when steady state parameters are affected weakly, in transient state (e.g. during startup) situation may be much more critical.

Even though during cold start simulation oil viscosity was significantly higher, the obtained minimum oil film thickness was very similar to the one obtained during the warm start. This suggests that the favorable influence of the higher oil viscosity in case of the cold start is reduced because of a disadvantageous oil gap profile.

Support systems

Comparison of the three different support systems has shown the flexibility of the developed model and its applicability in the industrial reality where many different bearing designs are present. Three completely different support system designs could be analyzed – spindle support, membrane support and spring bed support. No substantial difference has been found between spindle and membrane supports – regarding the influence on the bearing behavior. Additionally it has been indicated that the spring bed support system is less advantageous than the other two in case of symmetrically supported bearing pads. The reaction moment of the springs against tangential and radial inclination of the bearing pads is the reason for the slightly higher operating temperature of such bearings. This results in approximately $2-3\,°C$ higher sensor temperatures for lower stiffness of the springs and $5-6\,°C$ for the higher stiffness.

6 Summary and final conclusions

6.1 Main conclusions

The flexibility of the model and its ability to perform transient simulations has been shown. The model can be fitted to almost every possible thrust bearing design. This is especially important in case of the hydro generator industry. Many different and not standardized designs are present in the power plants around the globe. Some of them more than one hundred years old. During refurbishment, some parts, as the supporting system, the pad or runner geometry or the bearing housing of the old system oftentimes cannot be changed anymore. With the use of the FSI model every geometrical feature can be modeled in order to check the performance of the old or modified design.

The abilities of the described method have been indicated. It was possible to force a commercial CFD program to simulate performance of hydrodynamic thrust bearings. It is not an easy task mainly because of large discrepancies between dimensions of the bearing elements and the oil film height. Differences of several orders of magnitude cause significant problems with shape of the generated grid and consequently with convergence. Good quality of the mesh has to be assured in order to obtain reliable results. Additionally strong coupling between effects that occur during hydrodynamic lubrication increase the risk of the numerical instability. Together with the use of FEM tools, the entire transient bearing calculation tool has been created which allows to take into account most of the currently identified physical effects that take place during hydrodynamic lubrication.

Detailed conclusions were given together with the presented results. In this subsection a short summary of all obtained results is presented.

The obtained results show good agreement with the measurement data. The temperature profiles are not exactly followed but the differences are relatively small within the simulated time range. The reason for these differences has also been identified so the model can be improved during further work. The obtained temperature profiles and values show that the general bearing parameters are estimated properly (heat generation and transfer, load carrying capacity, etc.). Other presented results can be summarized in the following list:

1. Startup simulation of the thrust bearing could be performed with the use of FSI technology. This feature makes the developed model unique. Previously developed transient bearing calculation programs were only two dimensional with reduced functionality.
2. Thermal pad peaking and runner deformations during startup procedure could be simulated.
3. Hydrostatic and hydrodynamic regime of operation could be simulated simultaneously. This feature gives a possibility of a realistic startup simulation (hydrostatic, hybrid and hydrodynamic mode of operation).
4. Automatic calculation of the warm oil mixing is implemented in the model. It enables full analysis of the effects in the oil film and the bearing groove. Therefore it is capable to calculate realistic oil film inlet boundary conditions. This ability distinguishes the developed model among other bearing calculation tools.
5. It has been indicated that pivot point position has a fundamental influence on the warm oil mixing coefficient. A comparison between bidirectional and unidirectional bearings showed significant differences of this coefficient and finally in bearing operating temperatures. Due to

the larger tangential inclination of the pad in case of a unidirectional support point position the operating bearing temperature is significantly lower than in case of the bidirectional one for the same operating conditions.

6. The developed model allows to calculate convection coefficients on the interface between the fluid and the structural part of the bearing. This new feature is a qualitative change in the research area of bearing simulations. It has been shown that these coefficients have different values on different walls of the bearing pad and that they can also vary across a single wall. This is an especially valuable result which can be used in other bearing calculation programs. According to the models described in literature these coefficients need to be assumed as input parameters. Their values are difficult to guess since they are case dependent parameters.
7. Through comparison of the created model with DIN standard, the fundamental functionality of the model could be confirmed. Pad tangential inclination and load carrying capacity are estimated with good accuracy. Together with the thermodynamic validation made with the use of measurement data it could be proven that the obtained results are reliable.
8. It has been indicated that startup simulation and transient thermal effects cannot be simulated with the use of the standard steady state calculation procedure. A quasi transient analysis is not able to imitate transient thermodynamic effects that take place during startup of the bearing. Advantages of the transient bearing simulation have been indicated in two examples. In the first one the ability of the model to simulate different startup conditions has been shown. Modification of the startup parameters (startup time and hydrostatic jacking system operation) allowed to reduce thermal peaking of the bearing pad. In the second example a comparison between cold and warm startup simulation indicated stronger thermal deformation of the bearing elements for lower cold oil temperature.
9. Comparison of the three different supporting systems showed disadvantages of the spring bed support system regarding bidirectional bearings: the reaction against pad tilting caused slightly higher bearing pad temperatures. Two main conclusions come from this investigation. First of all the flexibility of the developed model could be proven. Additionally it has been shown that the pad support system can influence the bearing operation parameters in a similar way as the pivot point position. The reaction moment against tilting causes smaller tangential inclination of the pad and finally a higher operating temperature.

6.2 Further research

Potential further developments of the model can also be identified. One of them is calculation of the convective boundary condition of the runner cylindrical surfaces. In the described model this boundary condition has been assumed and the parameter study showed its significant influence on the runner deformations. Calculation of the convective heat transfer could on one hand improve the obtained temperature field in the runner and on the other hand the oil rotation power loss calculation would be more accurate. The power loss generated on these walls is currently not taken into account. Though for high speed generators, this can represent a significant component of the total power loss. Another direction of the development can be the analysis of the transient behavior of the bearing during load changes. Variable loads may occur during operation of certain types of turbines. For example in case of PSP power plants significant transient loads occur during emergency shutdown of the unit (power rejection) in pumping mode. In such a situation, the hydraulic load can easily be doubled for a short time. In addition these loads can be applied in a very wide range of operating speeds ($-100\ \%$ to $150\ \%$ including zero). Detailed simulation of the bearing parameters

could improve the design of such bearings and ensure safe operation in case of emergency situations.

A certain disadvantage of the assumed incompressible flow model is the calculation of the low pressures in the diverging zones of the oil film. This effect is not realistic and can have an influence on the obtained pad tilt angle and load carrying capacity. Further development of the model should include implementation of the compressible flow model with estimation of cavitation effects. This requires modeling of the mixture of the oil and air and seems to be out of reach of the commonly used CFD codes. There are algorithms that can take into account cavitation but the main limiting factor in this case is the computing speed of the currently used hardware. Air mixed with the oil also changes the properties of the lubricant.

Long computation time is still an important problem. Therefore the developed model cannot be used to perform parametric studies during design of a particular bearing. Testing of many different parameter configurations would require a very long time and/or a large number of computers. It should rather help to understand the most important phenomena and effects. With this model convection coefficients or oil film inlet boundary conditions can be identified. They can be used later in simpler models as input parameters. However, continuous increase of the computing capabilities of the affordable computers should make the simulation less time consuming. In the further future decrease of the computational times will allow for better quality of the generated grids and finally of the obtained results. From this point of view the model still has large development potential. Use of commercial CFD software ensures also continuous improvement of these codes in the future. Results given by the current version of the model are encouraging for further work.

7 Appendix

The list of files that are attached to this elaboration in an electronic version is presented in Table 7.1.

Table 7.1. List of the attached files

No.	File name	Description
1	text.docx	text of the dissertation in MS Word 2007 format
2	text.pdf	text of the dissertation in pdf format
3	solid.mac	solid model and FSI coupling for ANSYS program
4	fluid.mac	fluid model for ANSYS program
5	fluid.pre	fluid model setup in ANSYS CFX PRE program
6	fluid.cst	post processing layer for ANSYS CFX POST program
7	results.mcd	post processing worksheet for MathCAD program
8	results.xlsx	post processing worksheet MS Excel 2007 program
9	heat.mac	post processing macro for ANSYS program
10	hmin.mac	post processing macro for ANSYS program
11	hmin_plot.mac	post processing macro for ANSYS program
12	hmin_results.mac	post processing macro for ANSYS program
13	hmin_results_2.mac	post processing macro for ANSYS program
14	pad_results.mac	post processing macro for ANSYS program
15	pr_jpg.mac	post processing macro for ANSYS program
16	runner_results.mac	post processing macro for ANSYS program
17	section.mac	post processing macro for ANSYS program
18	sensor.mac	post processing macro for ANSYS program
19	sensor_temp.mac	post processing macro for ANSYS program
20	th_grad.mac	post processing macro for ANSYS program

Bibliography

[1] *International Water Power & Dam Construction*, May 2009.

[2] (2009) Voith Hydro - Products. [Online]. http://www.voithhydro.com/vh_en_pas_products.htm

[3] F. A. Martin, "Tilting Pad Thrust Bearings: Rapid Design Aids," *Proceedings of the Institution of Mechanical Engineers, Tribology Convention*, vol. 184, no. paper 16, 1970.

[4] H. Iliev, "Failure Analysis of Hydro-generator Thrust Bearing," *Wear*, vol. 225-229, pp. 913-917, 1999.

[5] A. J. Leopard, "Tilting Pad Bearings - Limits of Operation," *Lubrication Engineering*, vol. 32, no. 12, pp. 637-644, 1976.

[6] S. B. Glavatskih, "Extending performance limits of tilt pad thrust bearings: a full scale study," *EDF/LMS Workshop*, 2008.

[7] H. Czichos and K. H. Habig, *Gleitlager, Tribologie Handbuch*. Wiesbaden: Vieweg Verlag, 2003.

[8] O. R. Lang and W. Steinhilper, *Gleitlager, Berechnung und Konstruktion von Gleitlagern mit Konstanter und Zeitlich Veränderlicher Belastung*. Berlin, Heidelberg, New York: Springer-Verlag, 1978.

[9] C. M. Ettles, J. Seyler, and M. Bottenschein, "Some Effects of Start-Up and Shut-Down on Thrust Bearing Assemblies in Hydro-Generators," *Transactions of the ASME*, vol. 125, pp. 824-832, 2003.

[10] L. Dąbrowski and M. Wasilczuk, "Analiza warunków pracy łożysk nośnych hydrozespołów HZ-1 i HZ-2 ESP Żar - sprawozdanie z etapu I," 1998.

[11] M. Bottenschein, C. M. Ettles, and J. Seyler, "Calculation of Safety Margin for Hydrogenerator Thrust Bearings," *Tribology Transactions STLE*, vol. 48, no. 4, pp. 450-456, 2005.

[12] "VDI ELEKTRO-THERMIT GMBH catalogue, ELEKTRO-THERMIT GMBH".

[13] M. Fillon, S. B. Glavatskih, and M. Wasilczuk, "Performance peculiarities of PTFE-faced tilting-pad thrust bearings".

[14] C. M. Ettles, "Size effects in tilting pad thrust bearings," *Wear*, vol. 59, pp. 231-245, 1980.

[15] L. Dąbrowski and M. Wasliczuk, "Technical Criteria of Tilting Pad Thrust Bearing Operation (in Polish)," in *XVIII Symposium of Design of Machine Elements Proceedings*, Kielce - Ameliówka, 16-20 September 1997.

[16] A. A. Raimondi, "The Influence of Longitudinal and Transverse Profile on the Load Capacity of Pivoted Pad Bearings," *ASLE Transactions*, vol. 3, pp. 265-276, 1960.

[17] (2009, May) ALSTOM NEWS FLASH. [Online]. www.alstom.com

[18] L. Dąbrowski and M. Wasliczuk, "Evaluation of water turbine hydrodynamic thrust bearing performance on the basis of thermoelastohydrodynamic calculations and operational data," 2004.

[19] (2010, January) Bearing Manufacturer: Industrial Bearings in Fluid, Roller Styles. [Online]. http://www.kingsbury.com/about_us.shtml

[20] W. W. Gardner, "Performance Characteristics of Two Tilting Pad Thrust Bearing Designs," in *Proceedings of the JSLE International Tribology Conference*, Tokyo, 1985.

[21] (2009) Waukesha Bearings, Application Experience. [Online]. www.waukbearing.com/application_experience.html

[22] (2009) Fluid Bearing, EQH Style, from Kingsbury Bearing Engineering. [Online]. www.kingsbury.com/eqh.shtml

[23] C. M. Ettles, "Some Factors Affecting the Design of Spring Supported Thrust Bearings in Hydroelectric Generators," *Transactions of ASME*, vol. 113, pp. 626-632, 1991.

[24] S. Gynt, "Recent Development of Bearings and Lubrication Systems for Vertical Generators," *Allmanna Svenska Elsktrisha AB Journal Vasteras*, vol. 20, pp. 72-87, 1947.

[25] X. Wang, Z. Zhang, and G. Zhang, "Improving the performance of spring-supported thrust bearing by controlling its deformations," *Tribology International*, vol. 32, pp. 713-720, 1999.

[26] Energomachexport, *Wasserkraft-generatoren der UdSSR*.: Wneschtorgizdat, 1975.

[27] (2009) Voith Hydro Brochures. [Online]. www.voithhydro.com/media/t3345e_Bearings_72dpi.pdf

[28] A. Cameron and C. M. Ettles, "Thermal And Elastic Distortions in Thrust Bearings," *Instn. Mech. Engrs. Lubr. Wear Conv.*, no. Paper 7, pp. 60-71, 1963.

[29] D. Eifler et al., *Gleitlagertechnik*. Essen - Mannheim, Germany: Th. Goldschmidt AG, 1992.

[30] M. Wasilczuk, *Studium Problemów Badawczych, Konstrukcyjnych oraz Metod Projektowania Hydrodynamicznych Łożysk Wzdłużnych*. Gdańsk: Politechnika Gdańska, 2004.

[31] ABB Generation AB, "Bearings for large vertical hydro-electric machines," , 2000.

[32] A. Fust and M. Starcevic, "Pumping-Pad Bearings for Vertical Hydro-Electric Generators," *Brown Boveri Review*, vol. 11, 1985.

[33] M. Fillon and S. B. Glavatskih, "TEHD Analysis of Thrust Bearings with PTFE-Faced Pads," *Journal of Tribology*, vol. 128, pp. 49-58, 2006.

[34] M. Fillon and S. B. Glavatskih, "PTFE-faced centre pivot thrust pad bearings: Factors affecting TEHD performance," *Tribology International*, vol. 41, pp. 1219-1225, 2008.

[35] C.A. Mahieux, "Experimental Characterization of the influence of coating materials on the hydrodynamic behavior of thrust bearings: a comparison of Babbitt, PTFE and PFA," *Transactions of ASME*, vol. 127, pp. 568-574, 2005.

[36] R. T. Knox, W. O. Moss, and J. E. L. Simmons, "The devleopement of PTFE (polyetrafluoroethylene)-faced hydrodynamic thrust bearings for hydrogenerator application in the United Kingdom," *Proc Instn Mech Engrs*, vol. 212, pp. 345-352, 1998.

[37] C. M. Ettles, R. T. Knox, J. H. Ferguson, and D. Horner, "Test Results for PTFE-Faced Thrust Pads, With Direct Comparison Against Babbitt-Faced Pads and Correlation With Analysis," *Transactions of the ASME*, vol. 125, pp. 814-823, 2003.

[38] R. T. Knox and W. O. Moss, "The developement of a PTFE faced thrust bearing for Dinorwig pumped storage power station," in *Proc. Hydraulic Machinery and Systems 20th IAHR Symposium, Hydro Technology and Environment for the New Century*, Charlotte North Carolina USA, 2000.

[39] W. O. Moss and R. T. Knox, "PTFE thrust bearings for hydrogenerators and their application to Dinorwig & Ffestiniog Storage Power Plants," in *U. K. Technical Papers, HydroVision '98*, 1998, pp. 595-606.

[40] C. A. Mahieux, "Further Evidences of Advanced Polymer Coating Advantages for Thrust Bearings," in *Hydro 2002 Proceedings 4-7 November 2002*, Kiris Turkey, 2002.

[41] C. A. Mahieux, "Carbon Fiber Thermoplastic Thrust Bearings: Selecting Optimum Coatings for Power Losses Reduction," in *13th International Seminar on Hydro Power Plants*, Vienna, 2004.

[42] C. A. Mahieux, "Carbon fiber/PEEK for use in large hydrogenerator thrust bearings," *JEC composites*, no. 9, pp. 55-56, May 2004.

[43] C. A. Mahieux, "Coating Selection for Thrust Bearing Performance Optimization," in *3rd EDF-LMF Poitiers Wokrshop*, 2004.

[44] C. A. Mahieux, "Field Test for High Performance Thermoplastic Composite Hydrogenerator Thrust Pads," *Hydro Review Worldwide Journal*, 2004.

[45] C. A. Mahieux, "Materials Influence on Hydrodynamic Behavior of Thrust Bearings: a comparison of Babbitt, PTFE and PFA," *Journal of Tribology*, 2004.

[46] *ERCOFTAC Best Practice Guidelines*, 1st ed., 2000.

[47] "ANSYS® Academic Research, Release 12.1, Help System, ANSYS, Inc.".

[48] O. Reynolds, "On the Theory of Lubrication and Its Application to Mr. Beauchamps Tower's Experiments, Including an Experimental Determination of the Viscosity of Olive Oil," *Philos. Trans. R. Soc. London*, vol. 177, pp. 157-234, 1886.

[49] M. B. Dobrica and M. Fillon, "About the Validity of Reynolds Equation and Inertia Effects in Textured Sliders of InfiniteWidth," *Proceedeings of the Institution of Mechanical Engineers, Part J: Journal of Engineering Tribology*, vol. 223, no. 1, pp. 69-78, 2009.

[50] S. B. Glavatskih, D. Markin, and D. M. C. McCarthy, "A FEM approach to simulation of tilting-pad thrust bearing assemblies," *Tribology International*, vol. 36, pp. 807-814, 2003.

[51] G. Rotta, *Wpływ konstrukcji przestrzeni międzyklockowej na charakterystyki wzdłużnego łożyska ślizgowego, doctoral thesis*. Gdańsk, 2009.

[52] "Hydrodynamische Axial-Gleitlager im Stationerem Betrib Teil 1-3," *DIN 31654*, 1991.

[53] J. H. Vohr, "Prediction of the Operating Temperature of Thrust Bearings," *Journal of Lubrication Technology*, vol. 103, no. 1, pp. 97-106, 1981.

[54] Qpedia, Advanced Thermal Solutions, INC. (2008) www.qats.com.

[55] J. H. Lienhard IV and J. H. Lienhard V, *A Heat Transfer Textbook*, 123rd ed. Cambridge, Massachusetts USA: Phloginton Press, 2005.

[56] H. Schlichting, *Grenzschichttheorie*, 5th ed.: Verlag G. Braun, 1965.

[57] W. Bohl, *Kamprath-reihe, Technische Stroemungslehre*, 5th ed. Wurzburg: Vogel-Buchverlag, 1982.

[58] H. Sigloch, *Technische Fluidmechanik*, 2nd ed. Dusseldorf, Germany: VDI-Verlag GmbH, 1991.

[59] M. Tanaka, "Recent thermohydrodynamic analyses," *Proc Instn Mech Engrs*, vol. 214, pp. 107-122, 2000.

[60] J. W. Capitao, "Performance Characteristics of Tilting Pad Thrust Bearings at High Operating Speeds," *Transactions of the ASME, Journal of Lubrication Technology*, pp. 81-89, January 1976.

[61] J. W. Capitao, R. S. Gregory, and R. P. Whitford, "Effects of High-Operating Speeds on Tilting Pad Thrust Bearing Performance," *Transactions of the ASME, Journal of Lubrication Technology*, pp. 73-80, January 1976.

[62] R. S. Gregory and A. M. Mikula, "A Comparison of Tilting Pad Thrust Bearing Lubricant Supply Methodts," *Transactions of the ASME, Journal of Lubrication Technology*, vol. 105, no. 1, pp. 39-47, 1983.

[63] A. Cameron and C. M. Ettles, "Considerations of Flow Across a Bearing Groove," *Transactions of*

ASME, pp. 312-317, 1968.

[64] C. M. Ettles, "The Developement of a Generalized Computer Analysis for Sector Shaped Tilting Pad Thrust Bearings," *Wear*, vol. 59, no. 1, pp. 231-245, March 1980.

[65] J. C, Nicholas, "Tilting Pad Journal Bearings With Spray-Bar Blockers And By-Pass Cooling For High Speed, High Load Applications," in *Proceedings of the 32nd Turbomachinery Symposium*, College Station, TX, USA, 2003, pp. 27-37.

[66] J. C. Nicholas, "Pad Bearing Assembly with Fluid Spray and Blocker Bar," US Patent 5,738,447, 1998.

[67] Y. Hori, K. W. Kim, and M. Tanaka, "A Three Dimensional Analysis of Thermohydrodynamic Performance of Sector-Shaped, Tilting-Pad Thrust Bearings," *ASME Journal of Tribology*, vol. 105, pp. 406-413, 1983.

[68] M. M. Khonsari, "A Review of Thermal Effects in Hydrodynamic Bearings. Part I: Slider and Thrust bearings," *ASLE Transactions*, vol. 30, no. 1, pp. 19-25, 1987.

[69] M. Fillon, J. Frene, and P. Monmousseau, "Transient Thermoelastohydrodynamic Study of Tilting-Pad Journal Bearings – Comparison Between Experimental Data and Theoretical Results," *Journal of Tribology*, vol. 119, pp. 401-407, 1997.

[70] M. Fillon, J. Frene, and P. Monmousseau, "Transient Thermoelastohydrodynamic Study of Tilting-Pad Journal Bearings – Application to Bearing Seizure," *Journal of Tribology*, vol. 120, pp. 319-324, 1998.

[71] M. Fillon and P. Monmousseau, "Transient Thermoelastohydrodynamic Analysis for Safe Operating Conditions of a Tilting-Pad Journal Bearing During Start-up," *Tribology International*, vol. 38, pp. 225-231, 2000.

[72] C. M. Ettles, "Transient Thermoelastic Effects in Fluid Film Bearings," *Wear*, vol. 79, pp. 53-71, 1982.

[73] K. Kawaike, K. Okano, and Y. Furukawa, "Performance of a Large Thrust Bearing with Minimized Thermal Distortion.," *ASLE Trans.*, vol. 22, no. 2, pp. 125-134, 1977.

[74] P. Pajączkowski, A. Schubert, and M. Wasilczuk, "Modeling Transient States of Large Hydrodynamic Thrust Bearings," in *7th EDF-LMF Poitiers Wokrshop*, Poitiers, 2008.

[75] C. A. Pistner, "Some Effects of Start-up Transient Loads on Shoe Bearings for large Hydraulic Pump/Turbines," *Tribology Transactions*, vol. 39, pp. 93-98, 1996.

[76] (2009) Tilting Pad Bearing with LEG Design from Kingsbury. [Online]. www.kingsbury.com/leg.shtml

[77] A. Fust, *Dreidimensionale thermohydrodynamische Berechnung von Axialgleitlagern mit punktformig abgestutzten Segmenten*. Zurich: Institut fur Grundlagen der Maschinenkonstruktion ETH Zurich, 1981.

[78] Qu. Dazhuang, A. Fuerst, S. Liangwei, and D. Schafer, "Investigations Into a 6000 Tons Thrust Bearing with Teflon or Babbitt Layer for the Three Gorges Units," in *Electrical Machines and Systems, ICEMS 2001, Procedeengs of the fifth International Conference on*, Shenyang, China, 2001, pp. 131-136.

[79] H. Vögele, "Design of the Generators for Three Gorges," *Hydropower & Dams*, no. 3, 1998.

[80] (2008) Hydropower Plant Kopswerk II, The new pump storage plant of Vorarlberger Illwerke AG in Gaschurn Partenen. [Online]. www.kopswerk2.at

[81] (2010, January) Encyclopedia Britannica 2010, Encyclopedia Britannica 2010 Online. [Online]. http://www.britannica.com/EBchecked/topic/278236/hydraulic-torque-converter

[82] (2009) Fluid Bearing, VK Style, from Kingsbury Bearing Engineering. [Online]. www.kingsbury.com/vk.shtml

[83] A. J. Rostocki, R. M. Siegoczynski, P. Kielczynski, and M. Szalewski, "High Pressure Changes of the Castor Oil Viscosity By Ultrasonic Method," *Journal of Physics: Conference Series*, vol. 121, 2008.

[84] T. Mang and W. Dresel, *Lubricants and Lubrication*, 2nd ed. Weinheim, Germany: Wiley-VGH GmbH, 2007.

[85] P. W. Gold, A. Schmidt, H. Dicke, J. Loos, and C. Assmann, "Viscosity-Pressure-Temperature Behaviour og Mineral and Synthetic Oils," *Journal of Synthetic Lubrication*, vol. 18, no. 1, pp. 51-79, 2001.

[86] C. W. Wu and G. J. Ma, "Abnormal Behavior of a Hydrodynamic Lubrication Journal Bearing Caused by Wall Slip," *Tribology International*, vol. 38, no. 5, pp. 492-499, May 2005.